NASA/TM—2002-211211

Sixth Microgravity Fluid Physics and Transport Phenomena Conference

Abstracts

August 2002

The NASA STI Program Office . . . in Profile

Since its founding, NASA has been dedicated to the advancement of aeronautics and space science. The NASA Scientific and Technical Information (STI) Program Office plays a key part in helping NASA maintain this important role.

The NASA STI Program Office is operated by Langley Research Center, the Lead Center for NASA's scientific and technical information. The NASA STI Program Office provides access to the NASA STI Database, the largest collection of aeronautical and space science STI in the world. The Program Office is also NASA's institutional mechanism for disseminating the results of its research and development activities. These results are published by NASA in the NASA STI Report Series, which includes the following report types:

- TECHNICAL PUBLICATION. Reports of completed research or a major significant phase of research that present the results of NASA programs and include extensive data or theoretical analysis. Includes compilations of significant scientific and technical data and information deemed to be of continuing reference value. NASA's counterpart of peer-reviewed formal professional papers but has less stringent limitations on manuscript length and extent of graphic presentations.
- TECHNICAL MEMORANDUM. Scientific and technical findings that are preliminary or of specialized interest, e.g., quick release reports, working papers, and bibliographies that contain minimal annotation. Does not contain extensive analysis.
- CONTRACTOR REPORT. Scientific and technical findings by NASA-sponsored contractors and grantees.
- CONFERENCE PUBLICATION. Collected papers from scientific and technical conferences, symposia, seminars, or other meetings sponsored or cosponsored by NASA.
- SPECIAL PUBLICATION. Scientific, technical, or historical information from NASA programs, projects, and missions, often concerned with subjects having substantial public interest.
- TECHNICAL TRANSLATION. English-language translations of foreign scientific and technical material pertinent to NASA's mission.

Specialized services that complement the STI Program Office's diverse offerings include creating custom thesauri, building customized data bases, organizing and publishing research results . . . even providing videos.

For more information about the NASA STI Program Office, see the following:

- Access the NASA STI Program Home Page at ***http://www.sti.nasa.gov***
- E-mail your question via the Internet to help@sti.nasa.gov
- Fax your question to the NASA Access Help Desk at 301–621–0134
- Telephone the NASA Access Help Desk at 301–621–0390
- Write to:
  NASA Access Help Desk
  NASA Center for AeroSpace Information
  7121 Standard Drive
  Hanover, MD 21076

NASA/TM—2002-211211

Sixth Microgravity Fluid Physics and Transport Phenomena Conference

Abstracts

Abstracts of a conference cosponsored by
the NASA Office of Life and Microgravity Sciences and Applications and
the Fluid Physics and Transport Phenomena Discipline Working Group
and hosted by NASA Glenn Research Center and
the National Center for Microgravity Research on Fluids and Combustion
Cleveland, Ohio, August 14–16, 2002

National Aeronautics and
Space Administration

Glenn Research Center

August 2002

The Aerospace Propulsion and Power Program at NASA Glenn Research Center sponsored this work.

Available from

NASA Center for Aerospace Information
7121 Standard Drive
Hanover, MD 21076

National Technical Information Service
5285 Port Royal Road
Springfield, VA 22100

Available electronically at http://gltrs.grc.nasa.gov

PREFACE

The Sixth Microgravity Fluid Physics and Transport Phenomena Conference provides us with the opportunity to view the current scope of the Microgravity Fluid Physics and Transport Phenomena Program and conjecture about its future. The Microgravity Program has become part of the newly established Office of Biological and Physical Research (OBPR), NASA’s fifth Enterprise.

Meanwhile, we commenced the long-awaited and exciting era of conducting Microgravity Fluid Physics experiments on the International Space Station (ISS). We successfully completed the Physics of Colloids in Space (PCS) experiment on ISS and launched the Investigating Structure of Paramagnetic Aggregates of Colloidal Emulsions (InSPACE) experiment that will be conducted later this year.

The excitement of utilizing ISS was tempered, however, by its cost problems that negatively impacted the research budget available for developing flight experiment facilities and hardware. As a result, the Microgravity Fluid Physics discipline took a significant budget reduction that caused deferral/discontinuation of a number of flight investigations that had successfully completed their peer-reviews and received their endorsement. The budget supporting the principal investigators was also negatively impacted, though to a smaller extent. On the positive side, the Fluids Integrated Rack (FIR) that supports much of fluid physics experiments survived these budget reductions. Also the subsequent support of the research community through letters to Congress and to NASA clearly showed how the research community values the Microgravity Fluid Physics and Transport Phenomena Program.

In March, NASA Administrator Sean O'Keefe created the Research Maximization And Prioritization (REMAP) Task Force to perform an independent review and assessment of research priorities for the entire scientific, technological, and commercial portfolio of the Agency's Office of Biological and Physical Research (OBPR) and to provide recommendations on how the office can achieve its research goals. The panel report was released on July 10, 2002. The recommendations of this panel placed almost all of the research content of the Microgravity Fluid Physics Program in Priority 1 or 2 putting the program in an advantageous position as NASA begins to implement the recommendations of the panel.

The program currently has a total of 106 ground-based and 16 candidate flight principal investigators. A look at the collection of abstracts in this document clearly shows both the high quality and the breadth of the ongoing research program. One can easily notice many established world-class scientists as well as investigators who are early in their career poised to achieve that stature. We hope that many of the participants in this conference will perceive microgravity fluid physics as an exciting and rewarding area of research and choose to participate in the NASA Research Announcement released in December 2001. Proposals submitted to the fluid physics research area are due December 2, 2002. More information can be found at the following Web site:
http://research.hq.nasa.gov/code_u/nra/current/NRA-01-OBPR-08/index.html

The content of the Microgravity Fluid Physics and Transport Phenomena Program is well aligned with OBPR’s mission of “conducting basic and applied research to support human exploration of space and to take advantage of the space environment as a laboratory for scientific, technological, and commercial research.” The fluid physics discipline has a major role in the Physical Sciences Division’s goal of developing a rigorous, cross-disciplinary scientific capability, bridging physical sciences and biology to address NASA's human and robotic space exploration goals.

We have implemented a number of changes in the format of this conference based on the inputs received from the participants. We have expanded plenary sessions to include all presentations, eliminated parallel sessions and expanded the exposition session with poster presentations. We hope that this will allow the participants to get a better picture of the overall program through the plenary presentations and promote focused discussion/dialogue through poster presentations. The Discipline Working Group has provided the much-needed guidance in planning the content and the format of this conference. As in the past, we elected to go with a virtual proceedings of the presentation charts that will be available on the World Wide Web at http://www.ncmr.org/events/fluids2002.html. In this regard we acknowledge the support of our principal investigators who have provided us timely inputs of their charts and abstracts and accommodated our format requirements. This cooperation was critical in implementing this and is very much appreciated.

This conference has been organized and hosted by the National Center for Microgravity Research on Fluids and Combustion under the leadership of its Director, Professor Simon Ostrach. I would like to acknowledge the extensive efforts of Ms. Christine Gorecki and other members of the Center in planning, organizing, and hosting the conference and in preparing the proceedings and conference materials. Sincere appreciation is offered to the authors for providing the abstracts and presentation charts in a timely manner and to the members of the Microgravity Fluids Physics Branch of the NASA Glenn Research Center for their many contributions.

Finally, I would like to express my gratitude to all of the conference participants for their contributions to the success of this conference.

Dr. Bhim S. Singh
Fluid Physics Discipline Lead Scientist
NASA Glenn Research Center
21000 Brookpark Road
Cleveland, Ohio 44135
Phone: 216–433–5396
Fax: 216–433–8660
E-mail: bhim.s.singh@grc.nasa.gov

ACKNOWLEDGMENTS

This conference was made possible by the efforts of many people. We acknowledge the contributions of the following individuals:

Fluid Physics and Transport Phenomena Discipline Working Group
G. Paul Neitzel (chair), Georgia Institute of Technology
Bhim Singh (vice-chair), NASA Glenn Research Center
J. Iwan D. Alexander, Case Western Reserve University/National Center for Microgravity Research
Bradley Carpenter, NASA Headquarters
Francis Chiaramonte, NASA Headquarters
Stephen Davis, Northwestern University
Donald Gaver, Tulane University
Joel Koplik, City College of the City University of New York
Matthew Tirrell, University of California Santa Barbara
David Weitz, Harvard University

Session Chairs
Plenary Sessions
J. Iwan D. Alexander, NCMR/Case Western Reserve University
Noel Clark, University of Colorado
Amir Faghri, University of Connecticut
Donald Gaver, Tulane University
R. Glynn Holt, Boston University
Gareth McKinley, Massachusetts Institute of Technology
Simon Ostrach, NCMR/Case Western Reserve University
Ramkumar Parthasarathy, The University of Oklahoma
Jack Salzman, Chief, Microgravity Science Division, NASA Glenn Research Center
Eric Shaqfeh, Stanford University
Mary Silber, Northwestern University
Paul Steen, Cornell University
Theo Theofanous, University of California, Santa Barbara
Eric Weeks, Emory University
David Weitz, Harvard University

National Center for Microgravity Research on Fluids and Combustion
Simon Ostrach, Director
Thomas Labus, Deputy Director
J. Iwan D. Alexander, Fluids Senior Scientist
Christine Gorecki, Conference Coordinator

Conference Team
J. Iwan D. Alexander
Christine Gorecki
Sandra Jones
Beatrix Norton
Cindy Rosenberger
Norman Weinberg
William Yanis

The Logistics and Technical Information Division and its support service contractors, particularly Kristen Easton, Caroline Rist, Lori Feher, Amy Fennell, Diane Furiga, Chris Sanyk, and Gayle DiBiasio.

TABLE OF CONTENTS

Session 1:
Colloids and Soft Condensed Matter

RECENT RESULTS FROM THE PHYSICS OF COLLOIDS IN SPACE

David A. Weitz
Dept. of Physics and DEAS
Harvard University, Cambridge MA 02138

The PCS TEAM
A. Bailey,[1] R. Christianson, S. Manley, and V. Prasad, P. Segre,[2] U. Gasser,[3] L. Cipelletti[4]
Dept. of Physics and DEAS
Harvard University, Cambridge, MA,
1. Current address: Scitech Instruments, Vancouver, BC, Canada
2. Current address: NASA Marshall, Huntsville, AL
3. Current address: University of Konstanz, Germany
4. Current address: Universite' Montpellier II, 34095 Montpellier Cedex 05, FRANCE

A. Schoefield and P. Pusey,
University of Edinburgh, Edinburgh, UK

M. Doherty, and A. Jankovsky
NASA Glenn, Cleveland, OH

T. Lorik, W. Shiley, J. Bowen, C. Kurta, and J. Eggers
ZIN Technologies, Cleveland, OH

ABSTRACT

The Physics of Colloids in Space is an experiment which flew in the ISS. Data on several different samples of colloidal particles were obtained. They provided unexpected information about the behavior of the samples in microgravity. The data are currently being analyzed. The most recent findings will be discussed in this talk.

PHYSICS OF HARD SPHERE EXPERIMENT: SCATTERING, RHEOLOGY AND MICROSCOPY STUDY OF COLLOIDAL PARTICLES

Z-D Cheng, J. Zhu, S-E Phan, W. B. Russel, P. M. Chaikin*
Depts of Physics and Chem. Eng., and Princeton Materials Institute, Princeton University
Princeton, NJ 08544

W. V. Meyer
NCMR, NASA Glenn Research Center, Cleveland Ohio 44135

ABSTRACT

The Physics of Hard Sphere Experiment has two incarnations: the first as a scattering and rheology experiment on STS-83 and STS-94 and the second as a microscopy experiment to be performed in the future on LMM on the space station. Here we describe some of the quantitative and qualitative results from previous flights on the dynamics of crystallization in microgravity and especially the observed interaction of growing crystallites in the coexistance regime. To clarify rheological measurements we also present ground based experiments on the low shear rate viscosity and diffusion coefficient of several hard sphere experiments at high volume fraction. We also show how these experiments will be performed with confocal microscopy and laser tweezers in our lab and as preparation for the phAse II experiments on LMM. One of the main aims of the microscopy study will be the control of colloidal samples using an array of applied fields with an eye toward colloidal architectures. Temperature gradients, electric field gradients, laser tweezers and a variety of switchable imposed surface patterns are used toward this control.

Interaction between growing crystallites. One of the salient features, which has not been emphasized in previous experiments, is the existence of strong interactions between individual crystallites. In Fig1, from t=150s to about 800s, the size of the crystallites increases linearly $L=t^{\alpha}$, $\alpha \sim 1$, while the crystallinity X over this interval increases at a rate considerably less than L^3. Thus the number of crystallites decreases roughly as $N\_c=t^{-\gamma}$, $\gamma \sim 2.6$. This is unusual and contrasts with the classic theory that focuses on the nucleation and the growth in size of isolated crystallites. We identify this process as ``simultaneous coarsening and growth" in which small crystallites shrink and eventually disappear, causing the number of crystallites to decrease, while large crystallites keep growing, causing the measured average crystallites size to increase with time. The growth exponent for the size is about unity, resulting from the combination of normal diffusion limited growth and coarsening with the latter apparently due to direct transport from small to large

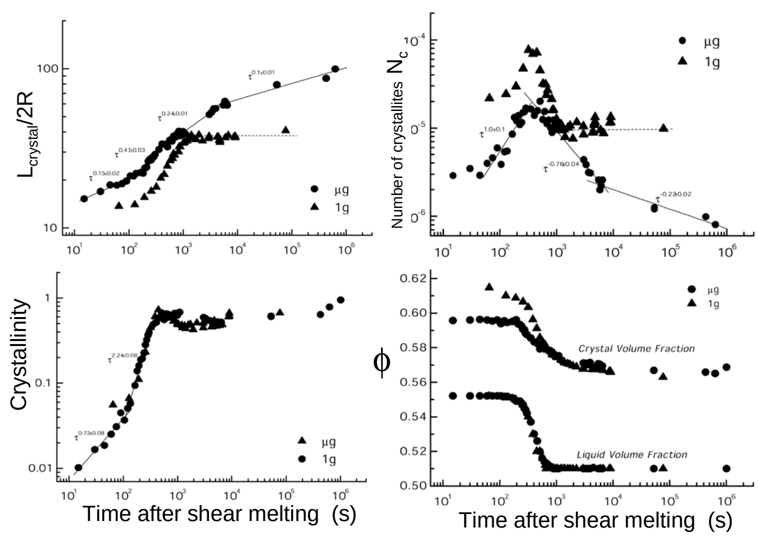

crystallites. Because of the different curvatures of these crystallites,\the smaller crystallites are under higher pressure from the Laplace or surface tension term and hence have a high internal volume fraction value. Therefore, the corresponding equilibrium liquid volume fraction surrounding a small crystallite is relatively higher than that surrounding a large crystallite. Mass transport, via these density gradients in the intervening fluid dispersion, moves particles from the small crystallites to the large ones.

Low Shear Rate Viscosity: For this study we used bare silica spheres with radius 244+/-10nm in index matching, high viscosity ethylene glycol and glycerol and a Zimm-Crother viscometer with shear stress as low as 10^{-5} Pa-S. Figure 2 shows the results plotted in a form consistent with the Doolittle equation: $\eta_0/\mu = (\eta_\infty/\mu)(1 + A\exp[\gamma\phi/(\phi_{max} - \phi)])$ which provides a

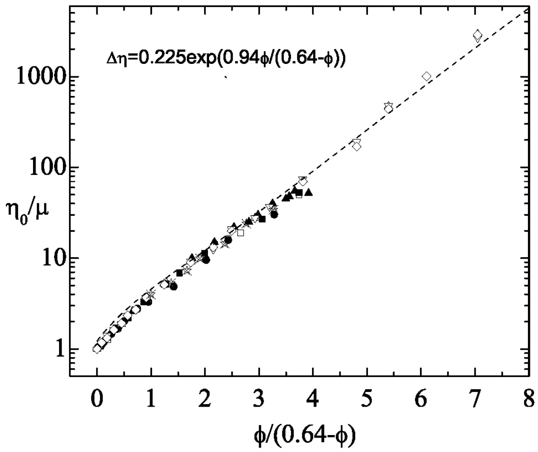

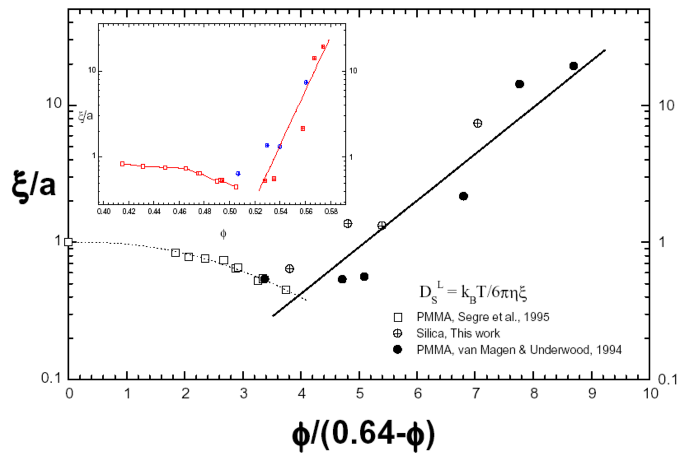

very good fit with γ=0.94, A=0.225 and ϕmax =0.64. For ϕ less than 0.50 there is excellent agreement with previous results on PMMA-PHSA suspensions. The literature suggests defining a dynamical correlation length by $\xi = kT/6\pi\eta(\varphi)D$, where η is the low shear viscosity and D is the long time self diffusion. Figure 3 shows a plot of this length vs ϕ. ξ changes behavior increasing rapidly just beyond the freezing ϕ ~0.5 and does not diverge at the glass transition ϕ=0.58, ξ(ϕ=0.58) =30a but rather appears to head for a divergence at ϕ=0.64 (random close packing). (At ϕ=0.58 ξ crosses the size of a critical nucleus.)

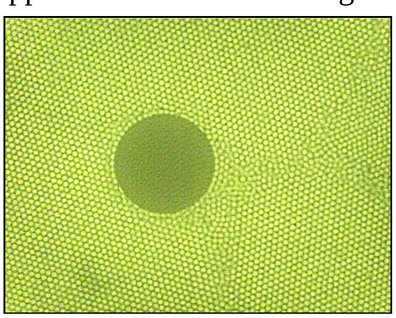

Rheology experiments on LMM will be performed using confocal microscopy and a probe particle whose motion is controlled by a laser tweezer. In Fig. 4 we show a 15μ particle suspended in a dense suspension of flourescently labeled PMMA hard spheres, so that the strain and strain rate can be monitored as the large particle is displaced. We will also discuss ground based experiments with lithographically patterned electric grids, and the effects of electric fields, Fig 5.

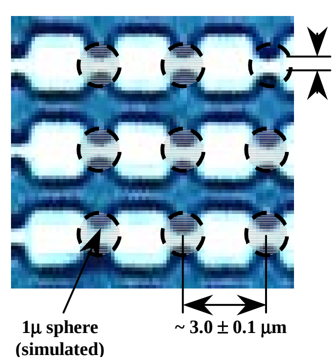

*P.I. chaikin@princeton.edu, 609 258-4338, FAX –6360

1)Z-D Cheng et al. Phys. Rev. Lett. **88**, 015501, (2002)
2) J. Stellbrink et al. Phys. Rev. E. **56**, R3772 (1997)

TWO-DIMENSIONAL STREPTAVIDIN CRYSTALS ON GIANT LIPID BILAYER VESICLES

Pasut Ratanabanangkoon
Department of Chemical Engineering, Stanford University, Stanford, CA

Michael Gropper, Rudolf Merkel
Department of Biophysics, Technical University of Munich, Munich, Germany

Alice P. Gast
Department of Chemical Engineering, Massachusetts Institute of Technology, Cambridge, MA
Phone: (617) 253-1403; Fax: (617)-253-8388; e-mail: gast@mit.edu

ABSTRACT

Two-dimensional (2D) ordering of macromolecules is of particular interest due to their scientific importance as fundamental models for studying phase transitions and self-assembly. It is also a basis for the design and development of many biosensor and bioassay devices and engineered biomaterials. The ability to create and manipulate self-assembled structures of macromolecules requires a thorough understanding and control of the various intermolecular forces involved. In this study, we used 2D streptavidin crystallization as a model system to study 2D protein organization on lipid bilayers and their effect on bilayer properties.

We studied the crystallization of streptavidin on giant lipid bilayer vesicles. Giant Unilamellar Vesicles (GUVs) are composed of a single lipid bilayer membrane with sizes of approximately 10-100 microns in diameter. Due to the sensitivity to ionic species, they remain stable in only extremely low ionic strength solutions. Once bound to the vesicle surface, streptavidin crystallized to form a rigid polycrystalline shell surrounding the vesicle. The ability to create crystals on GUVs provides a means to study many crystals in a single experiment and in a microgravity environment. Transmission Electron Microscopy (TEM) images of negatively-stained vesicles revealed that the crystals are of the lowest-density C222 symmetry, and does not change with solution pH unlike those grown in high ionic strength conditions. The lack of higher density 2D crystal forms is due to the strong electrostatic repulsion. Despite the presence of only one crystal structure, the change in solution pH changed the macroscopic crystal morphology and crystal growth pattern, and the vesicles were distorted into either roughened spheres or football-shaped ellipsoids.

Micropipette aspiration of avidin-coated and streptavidin-coated vesicles revealed the unique mechanical properties of the protein-lipid membrane. Vesicles coated with the noncrystallizable avidin shows relatively similar elastic area expansion modulus to that of uncoated vesicles. The existence of crystalline domains on streptavidin-coated vesicles resulted in various unique mechanical properties. Rapid permanent deformation was observed at low strain, while a slower viscoelastic behavior was observed at higher deformation. Despite their extremely rigid appearance, the presence of an external polycrystalline shell does not increase the toughness of the vesicles beyond that of bare vesicles. The distinctive properties of the protein-lipid

composite membrane can be traced to the unique combination of streptavidin-streptavidin, streptavidin-phospholipid, and phospholipid-phospholipid interactions.

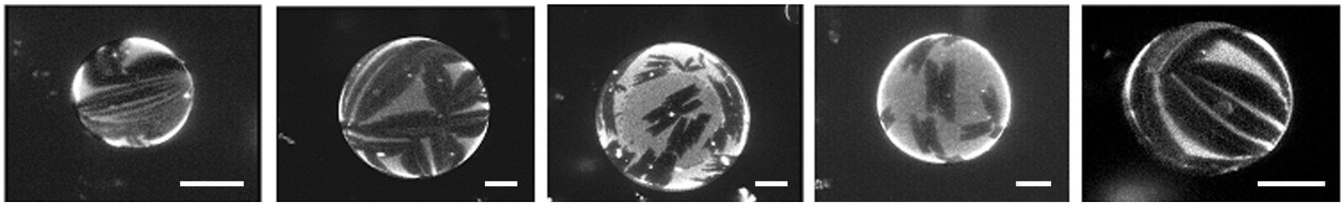

Three-dimensional reconstructed confocal microscopy images of two-dimensional streptavidin crystals (shown in black) on giant lipid bilayer vesicles. Scale bar represents 10 μm.

OPTICALLY-EXCITED WAVES IN 3D DUSTY PLASMAS

John Goree
Dept. of Physics and Astronomy, The University of Iowa, Iowa City, IA 52242

ABSTRACT

Flight experiments are planned for an interdisciplinary study of waves (i.e., phonons) in 3D Coulomb lattices. The experimental system will be a suspension of charged polymer microspheres in a gas-discharge plasma. This so-called "dusty plasma" is a macroscopic system where the microspheres arrange themselves, due to their mutual repulsion, in a lattice. Like a colloidal suspension, this lattice can be in a crystalline or liquid state. The particles are imaged directly using video microscopy.

These experiments are an extension of 2D experiments performed in the laboratory, under gravity conditions. Sedimentation due to gravity causes the microspheres to settle rapidly into a 2D layer that is levitated by the strong electric field near an electrode in a plasma. By eliminating gravity, it is possible to fill a 3D volume with the suspension.

Experiments will focus on the shear acoustic wave in the lattice. This kind of wave has particle motion that is transverse to the direction of wave propagation. Our experiments will exploit the low damping of a dusty plasma as compared to colloidal suspensions. We will excite the waves using a manipulation laser, which applies a radiation pressure on the particles. Particle motion will be measured *in-situ* using direct imaging with video microscopy. After the experiment, we will analyze the video data by computing the particle velocities and then analyzing the wave motion of the particles.

The experiment is to be performed on-orbit in ISS, with accommodation probably in the FIR. Preliminary tests of the experimental procedures will be done in parabolic aircraft flights.

The two experimental tasks for the flight experiments will be:

1. Study the dispersion relation (i.e., phonon spectrum) of sinusoidal waves and the propagation of pulsed waves. These experiments will be performed with plane waves.
2. Study the formation of Mach cones, which are the V-shaped wakes or shocks created by a supersonic disturbance. In this experiment, a moving laser spot is the supersonic disturbance.

These experiments build on our laboratory experience with these waves and Mach cones in a 2D lattice. This earlier work has been carried out as a ground-based project funded by the Fluid Physics discipline of NASA's microgravity program. Some of the results of these ground-based experiments are described below.

A 2D hexagonal lattice sustains two wave modes, for particle motion in the plane of the lattice. These modes are the longitudinal and transverse sound waves. We report experimental results, supported by theory and simulations, demonstrating the properties of these two waves.

The waves, which are observed by measuring the particle velocities, can be excited by two mechanisms in the lab: laser manipulation and thermal particle motion.

Using laser manipulation, we excited both modes. An argon laser beam was directed toward the lattice, where it pushed the particles about with a spatial and temporal variation that we controlled, using scanning mirrors. For low laser power, we verified that both waves obey their linear dispersion relations [1] for a Yukawa inter-particle repulsion. We found that this provides a method of measuring charge and screening length with considerable precision. In contrast to the longitudinal wave, the transverse mode has a dispersion relation with a more linear relationship of f vs. k, i.e., a more dispersionless characteristic over a wide range of k [2]. We found that Mach cones can be excited which consist not only of the longitudinal wave, as reported earlier [3], but also the transverse wave. A Mach cone is excited by a moving laser spot, as shown in the figure. The other waves are excited by a stationary sheet of light that is modulated temporally. By using a higher power for the laser sheet, we excited weakly nonlinear longitudinal waves, which propagated faster than the sound speed for small amplitude waves.

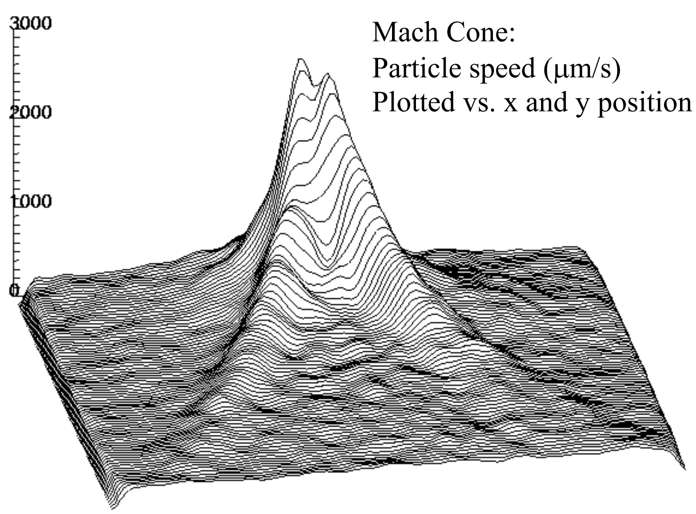

In the absence of external particle manipulation, we found that natural thermal particle motion consists of a spectrum of both kinds of waves, where the wave energy is distributed over values of f and k that satisfy the linear dispersion relation, as shown in the first figure [4].

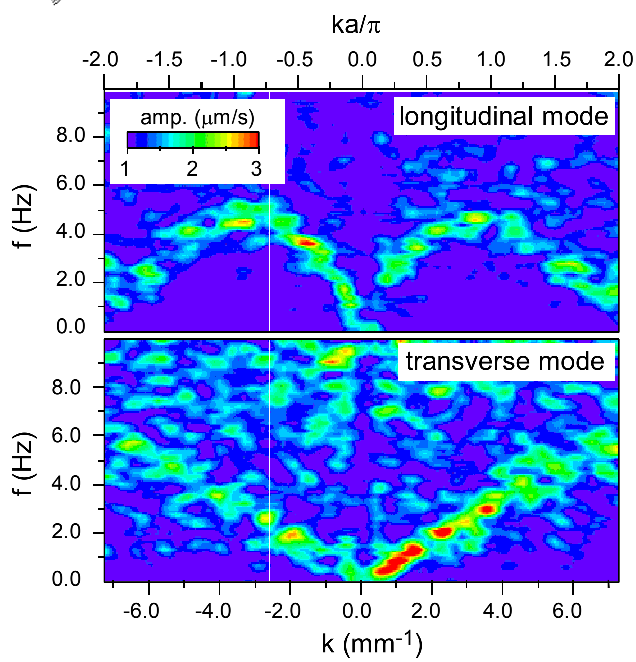

Phonon spectrum in the absence of laser manipulation. The wave amplitude is plotted vs. wavenumber over the first Brillouin zone, for propagation parallel to a primitive lattice vector.

[1] X. Wang, A. Bhattacharjee, and S. Hu, Phys. Rev. Lett. 86, 2569 (2001).
[2] S. Nunomura, D. Samsonov, and J. Goree, Phys. Rev. Lett. 84, 5141 (2000).
[3] V. Nosenko, J. Goree, Z.W. Ma and A. Piel, Phys. Rev. Lett. 88, 135001-1 (2002).
[4] S. Nunomura, J. Goree, S. Hu, X. Wang, A. Bhattacharjee and K. Avinash, Phys. Rev. Lett. (2002).

ELECTRICALLY GUIDED ASSEMBLY OF COLLOIDAL PARTICLES

W. D. Ristenpart, I. A. Aksay, and D. A. Saville
Dept. of Chemical Engineering, Princeton University, Princeton, NJ 08544

In earlier work[1] it was shown that the strength and frequency of an applied electric field alters the dynamic arrangement of particles on an electrode. Two-dimensional ‘gas,’ ‘liquid’ and ‘solid’ arrangements were formed, depending on the field strength and frequency. Since the particles are similarly charged, yet migrate over large distances under the influence of steady or oscillatory fields, it is clear that both hydrodynamic and electrical processes are involved. Here we report on an extensive study of electrically induced ordering in a parallel electrode cell.

First, we discuss the kinetics of aggregation in a DC field as measured using video microscopy and digital image analysis. Rate constants were determined as a function of applied electric field strength and particle zeta potential (Fig.1). The kinetic parameters are compared to models based on electrohydrodynamic and electroosmotic fluid flow mechanisms

Second, using monodisperse micron-sized particles, we examined the average interparticle spacing over a wide range of applied frequencies and field strengths. Variation of these parameters allows formation of closely-spaced arrangements and ordered arrays of widely separated particles (Fig. 2). We find that there is a strong dependence on frequency, but there is surprisingly little influence of the electric field strength past a small threshold.

Last, we present experiments with binary suspensions of similarly sized particles with negative but unequal surface potentials. A a long-range lateral attraction is observed in an AC field. Depending on the frequency, this attractive interaction results in a diverse set of aggregate morphologies, including superstructured hexagonal lattices (Fig. 3). These results are discussed in terms of induced dipole-dipole interactions and electrohydrodynamic flow. Finally, we explore the implications for practical applications.

---

[1] M. Trau, D.A. Saville, I.A. Aksay, *Science* **1996**, 272, 706.

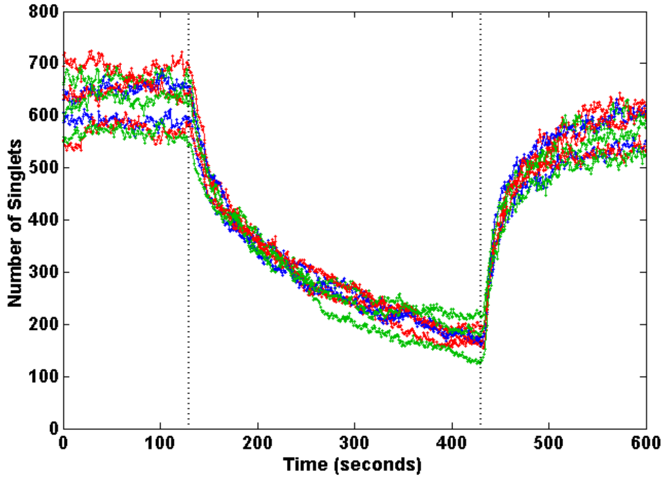

Fig.1 (Above). The concentration of singlets (individual particles) as a function of time for a 10 µA/cm2 applied field. The dashed vertical lines indicate the times at which the field was applied and removed, respectively. Upon application of the field, the concentration of singlets decreases as they join larger aggregates; the concentration increases once the field is removed and the aggregates disperse.

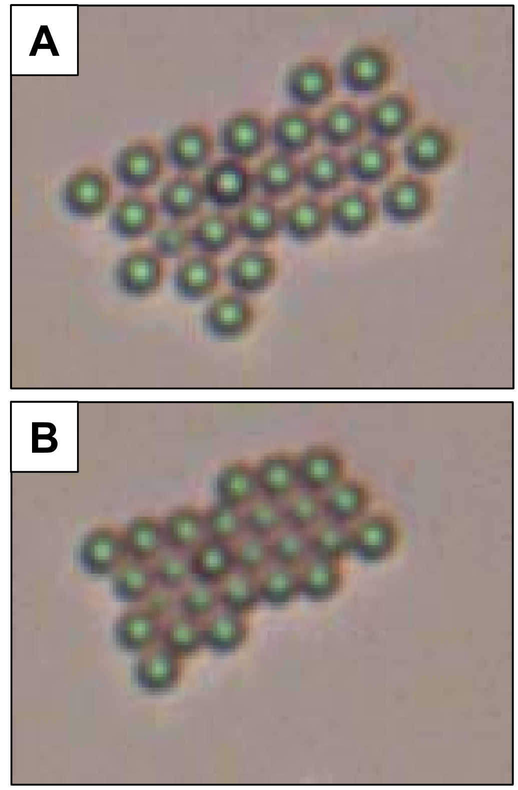

Fig. 2 (Top right). Optical micrographs of 2-µm silica particles on an electrode surface in a 40 V/mm AC field, oriented out of the page. **(A)** At 5 KHz, the particles exhibit simultaneous long-range lateral repulsion and attraction. **(B)** At 2 KHz, the particles come into close contact.

Fig. 3. (Below). Optical micrographs of binary suspensions (light particles are silica, dark particles are polystyrene, both 2-µm diameter) in a 40 V/mm, 2 KHz field. **(A)** Low magnification image of a region with low particle concentration; the particles form clusters typically composed of a silica particle surrounded by six polystyrene particles. **(B)** A higher magnification image of a binary superlattice.

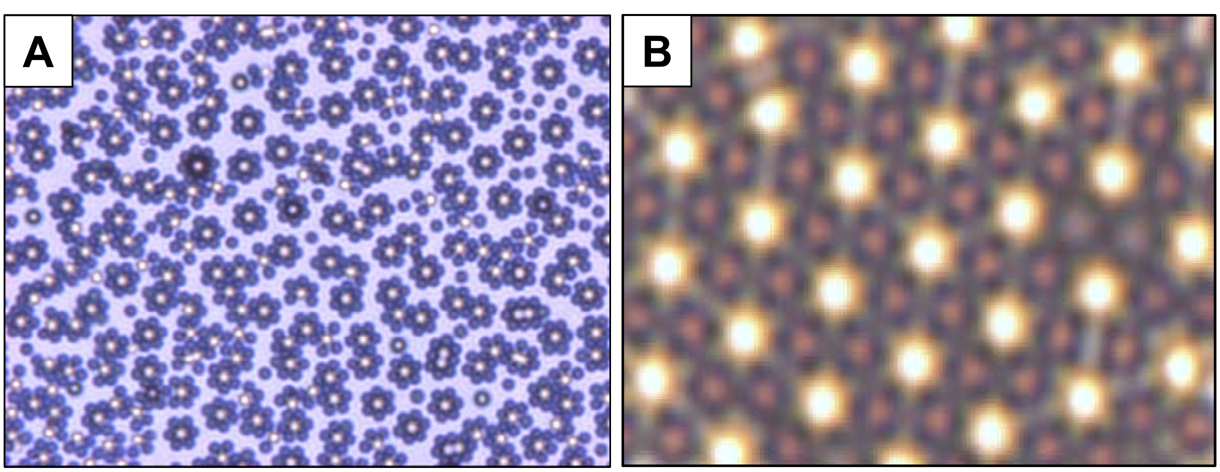

Self-assembly of Colloidal Particles on Template Structures

Arjun G. Yodh
Department of Physics & Astronomy
University of Pennsylvania
Philadelphia, PA 19104-6396
(215)898-6354 (O); x8-2010 (FAX) yodh@dept.physics.upenn.edu

Abstract

I will discuss recent experiments from my lab, which use surface templates to induce ordered colloidal structures. Particle assembly driven by entropic depletion, fluid convection, and sedimentation will be described. Confocal microscopy was used to visualize most of these samples.

Molecular dynamics simulations of crystallization of hard spheres

IGOR VOLKOV[†], MAREK CIEPLAK[§,†], JOEL KOPLIK[‡] & JAYANTH R. BANAVAR[†]

[†] Department of Physics, 104 Davey Laboratory, The Pennsylvania State University, University Park, Pennsylvania 16802

[§] Institue of Physics, Polish Academy of Sciences, 02-668 Warsaw, Poland

[‡] Benjamin Levich Institute and Department of Physics, City College of the City University of New York, New York, NY 10031

Colloidal suspensions exhibit a rich variety of behaviors and are interesting not only from a fundamental scientific viewpoint but also have significant technological applications. It is well-known that such systems self-assemble into a wide range of structures. Thus, they may be thought of as models of atomistic condensed matter systems with the distinct advantage of relevant length and time scales that are more readily accessible to experiments. The use of colloidal particles for engineering new materials is a relatively unexplored field which promises to revolutionize materials synthesis.

On earth, the effects of sedimentation and gravity-induced convection cloud, and sometimes can even radically alter, the intrinsic behavior of certain classes of colloidal systems. Because the binding energies of the crystalline phases are low and comparable to each other, gravity can greatly influence the kinetics of formation and, indeed, the nature of the observed crystal structure.

Colloidal suspensions of hard spheres are model systems for studying the statistical mechanics of structural phase transitions. Such suspensions undergo an entropy-driven phase transition from fluid to crystal as a function of increasing volume fraction. Unlike comparable phase transitions in conventional sytems of condensed matter, the dynamics of such structural phase transitions can be monitored with 'atomic' resolution using conventional light microscopy. In hard sphere systems, at high volume fractions, glass formation competes with the nucleation and growth of the crystalline phase. The Chaikin-Russel experiments on the Space Shuttle have led to the striking result that samples of hard sphere colloids that remain glassy for more than a year on earth crystallize within a few weeks in a microgravity environment.

We have carried out molecular dynamics simulations of the crystallization of hard spheres. Our aim is to study the dynamics of colloidal systems, using microscopic probes which complement conventional earth and space-based measurements and probe the effects of weak gravitational forces, polydispersity and the effect of bounding walls on phase structure. The simulations employed an extensive exclusive particle grid method discussed by Isobe and the type and degree of crystalline order was studied in two independent ways. As in experiments, the structure factor was measured during crystallization and, in addition, the local order was monitored by means of rotational invariants.

We will present quantitative comparisons of the nucleation rates of monodisperse and polydisperse hard sphere systems and benchmark them against experimental results, we will show how the presence of bounding walls leads to wall-induced nucleation and rapid crystallization and we will discuss the role played by gravity in nucleation and crystal growth.

Session 2:
Fluid Physics of Interfaces

Dynamics and Instability of Triple Junctions of Solidifying Eutectics: Flow-Modified Morphologies

S. Davis
Northwestern University

Fluid motions impressed upon a eutectic crystal front during directional solidification result in an increase of the lamellar spacing. This flow-induced change of microstructures is analyzed analytically to show the relationship between spacing and the operating conditions. The resulting system is a set of ordinary differential equations which describe the evolution of triple junctions. In a weak-flow regime lamellar widths at the minimum undercooling have a scaling similar to that of Jackson and Hunt, modified by the flows. When the flows are strong, a new scaling law shows that the width is proportional to one-fourth power of the imposed shear rate. Lamellar phases then tilt into the flow. Only at large morphological numbers does the minimum undercooling point corresponds to the marginal stability limit. Simulations show that the flows promote pinching of unstable lamellae.

ELECTROHYDRODYNAMICALLY DRIVEN CHAOTIC ADVECTION IN DROPS

Thomas Ward & G. M. Homsy*

Department of Mechanical Engineering
Engineering II Building, UCSB
Santa Barbara, CA 93106-5070

ABSTRACT

When a liquid drop of given dielectric constant, resistivity and viscosity is translating in a liquid of different dielectric constant, resistivity and viscosity under Stokes flow conditions in the presence of an electric field, the resulting internal circulation is a superposition of the Hadamard-Rybcynski circulation and the circulation first described theoretically by G. I. Taylor [1]. For sufficiently strong electric field strengths, the quadrapole structure of the Taylor circulation can cause an internal stagnation disk to occur [2]. Our interest is in the situation where a modulation of the electric field causes the stagnation disk to modulate its position, potentially leading to chaotic flows within the drop. The dimensionless electric field strength is characterized by $W = 4V(1+\lambda)/U$, where V is the maximum interfacial velocity of the Taylor circulation, U the translational velocity, and λ the viscosity ratio. The streamfunction for the flow is:

$$\psi = (r^4 - r^2)\sin^2(\theta) + W(t)\,(r^3 - r^5)\sin^2(\theta)\cos(\theta) \quad (1)$$

$$W(t) = W_1 + W_2\cos(\varepsilon t), \quad (2)$$

where ε is the dimensionless frequency, and W_1, W_2 are the amplitudes of the DC and AC components, respectively. We have found it useful to replace these parameters by a secondary set, ε, W_{max}, and $\delta = (1/W_1 - 1/W_2) - (1/W_1 + 1/W_2)$. As shown in Figure 1a, δ is the dimensionless distance the stagnation disk moves over one period of modulation. The advection equations corresponding to the flow in (1) were integrated by standard techniques, and it was found that the trajectories were chaotic over a wide range of parameters [3]. Figure 1b shows a typical Poincaré section, indicating that a large percentage of the drop may become well-mixed asymptotically over a large number of periods.

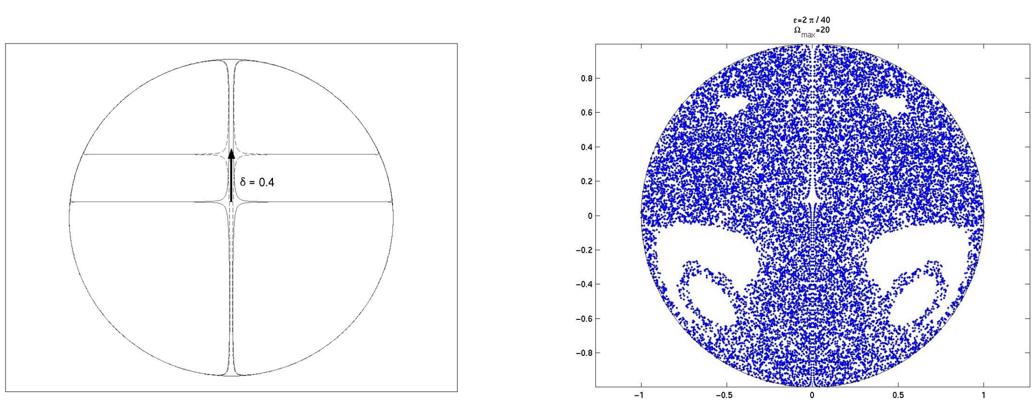

(a) (b)

Figure 1. (a) Schematic of circulation with modulated electric field.
(b) Poincaré section for the parameters: $W_{max} = 20$, $\varepsilon = 10$, $\delta = 0.4$

Experiments were conducted to test the predictions of rapid mixing on convective time scales. Drops of silicon oil were suspended in a small 60 mm x 120 mm x 120 mm test cell filled with castor oil, and subject to time-modulated axial electric fields with a wave form corresponding to eq(2). The drops were typically 5 mm in diameter and settled with typical speeds of O(10^{-1} mm/s). Once formed, the drops were inoculated with small scattering particles and illuminated in an equatorial plane by an Argon-ion laser. Fields of O(10^{-1} kV/mm) and frequencies of O(10^{-2} Hz) resulted in typical values of $W_{max} = 20$, $\varepsilon = 8$, $\delta = 0.4$. The resulting advection of the particles was imaged by a CCD camera, which collected images over a number of modulation periods. In order to make comparisons between these images and the corresponding theory, the trajectories of a large number of particles (typically O(10^4)) were simulated, with initial positions approximately the same as in the experiments.

Figure 2a shows a typical image, recorded after 6 periods of modulation. As can be seen, the particles are not confined to the spherical section in which they began, and the mixing pattern has particular geometric features. The corresponding simulation for the same set of parameters is shown in Figure 2b. As can be seen, there is good qualitative agreement between the two.

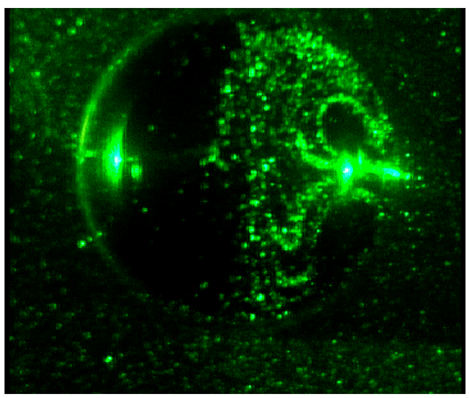

(a)

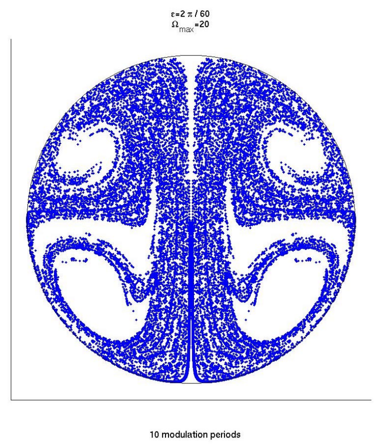

(b)

Figure 2. Results for particle positions after 6 periods for the same conditions as in Figure 2. (a) experimental image. (b) simulation.

In summary, our work has shown that it is possible to drive chaotic advection within drops using time-modulated electrical stresses, and that the resulting mixing is rapid, being achieved over a few modulation periods, and is in good agreement between theory and experiment.

References

1. G. I. Taylor, *Proc. Roy. Soc.* **291A**, 159-166, 1966
2. L. S. Chang, T. E. Carlson, & J. C. Berg, *Int. J. Heat Mass Transfer*, **25**, 1023-1030, 1981.
3. T. Ward & G. M. Homsy, *Phys. Fluids*, **13**, 3521-3525, 2001.

* bud@engineering.ucsb.edu: (805) 893-2704(V) (805)-893-8651(F)

THE EFFECTS OF ULTRATHIN FILMS ON DYNAMIC WETTING

Xia Chen, Stephen Garoff
Dept. of Physics and Center for Complex Fluids Engineering
Carnegie Mellon University, Pittsburgh, PA 15213
Email: sg2e@andrew.cmu.edu
412-268-6877
412-681-0648 (fax)

Enrique Ramé
National Center for Microgravity Research on Fluids and Combustion
NASA Glenn Research Center, MS 110-3, Cleveland, OH 44135

ABSTRACT:

Dynamic wetting, the displacement of one fluid by another immiscible fluid on a surface, controls many natural and technological phenomena, such as coating, printing, spray painting and lubricating. Particularly in coating and spraying applications, contact lines advance across pre-existing fluid films. Most previous work has focused on contact lines advancing across films sufficiently thick that they behave as simple Newtonian fluids. Ultrathin films, where the film thickness may impinge on fundamental length scales in the fluid, have received less attention.

In this talk, we will discuss the effects of ultrathin polymer films on dynamic wetting. We measure the interface shape within microns of moving contact lines advancing across pre-existing films and compare the measurements to existing models of viscous bending for interfaces advancing across dry surfaces and "thick" (in the sense that they behave as liquids) films. In the experiments, we advance a contact line of 10-poise and 1-poise polydimethylsiloxane (silicone oil) across pre-coated films of the same fluid with thickness from a single chain thickness (~10 Å) through a couple of radii of gyration (100-200 Å) to films so thick they are likely bulk in behavior (10^3 Å). All films are physisorbed, i.e. they readily rinse from the surface. Thus, molecules in the film are not anchored to the surface and can move within the film if the hydrodynamics dictate such motion.

For films of the thickness of a single chain (~10 Å), our experiments indicate that the advancing fluid behaves just as it would if it advanced over a dry surface. For the thicker films (10^3 Å), we find behavior indicating that the molecules in the film are acting as a fluid with the bulk properties. In this regime, results for the two different fluids are identical when the experiments are performed at the same pre-existing film thickness and advancing capillary number, Ca. For film of thickness of a few radii of gyration (~100- 200 Å), the behavior depends on Ca of the advancing meniscus. At low Ca, the viscous bending of the interface near the contact line does not behave as it would on a dry surface. It has a lower curvature than expected. However, at higher Ca, the viscous bending is described by the model for spreading over a dry surface. These results show that the fluid flow in the film does behave differently than bulk as the film thickness becomes comparable to molecular length scale. But even more intriguing is the unusual velocity dependence of that behavior where the film behaves more solid-like at higher contact line speeds. We will discuss these results in terms of the properties of confined polymer melts.

PASSIVE AND ACTIVE STABILIZATION OF LIQUID BRIDGES IN LOW GRAVITY

David B. Thiessen, Wei Wei and Philip L. Marston*
Physics Department, Washington State University, Pullman, WA 99164-2814

ABSTRACT

The cylindrical liquid bridge of arbitrary size surrounded by air or vacuum is a fluid configuration that is essentially unique to the zero-gravity environment. An associated technology, which is enhanced in zero gravity, is the float-zone process of crystal growth, which involves a molten liquid bridge between a feed rod and the growing cylindrical crystal. There are several advantages to the crystal growth process in using long molten zones. Unfortunately, long liquid bridges are more susceptible to g-jitter [1]. Also, a cylindrical liquid bridge in zero gravity is unstable if its length exceeds its circumference, or stated in another way, when the slenderness, defined as the length to diameter ratio, exceeds π. This is the well-known Rayleigh-Plateau (RP) instability involving the growth of a varicose mode leading to breaking of the bridge. Stabilization of liquid bridges in air in the low-gravity environment of NASA's KC-135 aircraft has been demonstrated for slenderness values in excess of 4.0 using two techniques, passive acoustic stabilization (PAS) [2] and active electrostatic stabilization (AES) [3]. The PAS method is theoretically capable of stabilizing a bridge of any length, provided a sound field of appropriate dimension is available. The AES method in its current form controls only the (2,0) mode of the bridge, which is the varicose mode that becomes unstable when the slenderness (S) exceeds π. By controlling only the (2,0) mode, the current form of the AES method cannot stabilize cylindrical bridges beyond S=4.493 at which point the (3,0) mode becomes unstable. At present, the longest bridge stabilized on the KC-135 by the AES method had a slenderness of 4.4 [3]. The AES method has the advantage that it can be used to control both the frequency and damping of the (2,0) mode of the bridge. This would be useful in reducing the susceptibility of a long molten zone to g-jitter in that the (2,0) mode frequency could be shifted away from a particularly noisy vibration frequency band of the spacecraft and the response further reduced by control of the damping of the mode.

The principle behind the AES method is to sense the (2,0)-mode amplitude and then apply a mode-coupled feedback stress to control the mode dynamics. Two concentric ring electrodes are used to produce a Maxwell-stress distribution that couples into the (2,0) mode of the bridge. By applying a feedback stress in proportion to the (2,0)-mode amplitude with appropriate gain, the mode frequency can be raised and bridges can be stabilized beyond $S=\pi$. Models show that the stability is affected by the bandwidth of the controller and the (2,0)-mode damping. If the feedback stress is applied in proportion to the velocity of the mode amplitude with appropriate sign, the damping of the mode can be increased. Active control of damping has recently been demonstrated in Plateau-tank experiments. The dynamic response of a bridge to feedback control is predicted to be significantly different for bridges in air compared to those in a Plateau tank

because of the different nature of the viscous damping for the two cases. Boundary-layer damping at the free interface is much more important for the case of a Plateau-tank bridge.

Laboratory experiments: A new fluid system is being used in the Plateau-tank facility to allow for studies of bridge dynamics and active control of damping with the AES system. The bath fluid is a high-density (1.61 g/cc), low viscosity (0.77 cS), low dielectric constant, fluorinated liquid with low water solubility. The bridge liquid is an aqueous solution of CsCl, density matched to the bath (~52.3 wt% CsCl). The Ohnesorge number (ratio of viscous to inertial effects) for bridges with the new fluid system is around 0.003 which is close to that of a pure water bridge in air of the same diameter. The new system is still not dynamically similar to a bridge in air because the dynamics also depend on the density and viscosity ratios between the inner and outer fluids. Dynamics studies involve driving the (2,0) mode by modulating the electrode potentials and then cutting off modulation to allow for a free decay of the mode. Feedback can be active during the entire modulation and free-decay sequence. Results obtained with the new system show that mode damping increases in proportion to the velocity gain as expected. Also, by using negative velocity feedback, damping can be reduced to the point that the bridge spontaneously begins oscillating at the natural (2,0)-mode frequency leading to breakup of the bridge. By using both amplitude and velocity feedback, the mode frequency can be shifted upward and the damping increased.

KC-135 based experiments: KC-135 experiments performed in 2001 concentrated on passive acoustic stabilization. Real-time measurements of transducer power consumption and acoustic pressure were made while stabilizing a bridge. Also, progress was made on confirming the theoretical understanding of PAS by performing experiments with different bridge radii but the same acoustic wavenumber. The theory predicts optimum stabilization for a particular value of the wavenumber-radius product (kR~0.86) [2]. As expected, a bridge with a kR value significantly larger than the predicted optimum could not be stabilized. Because of the limited duration and quality of low gravity, studies of bridge dynamics on the KC-135 using the AES system in the manner described above for the Plateau-tank are very difficult. Some oscillation and free-decay measurements for a bridge in air without feedback were made on the KC-135 in 2000 [3]. The measured frequency and damping of the mode agreed reasonably well with theory [3]. Active damping of bridges in air would be investigated best on the ISS, although a demonstration on the KC-135 may be possible.

REFERENCES

[1] D. Langbein, "Crystal Growth from Liquid Columns," J. Crystal Growth **104**, 47-59 (1990).
[2] M. J. Marr-Lyon, D. B. Thiessen, and P. L. Marston, "Passive stabilization of capillary bridges in air with acoustic radiation pressure," Phys. Rev. Lett. **86**, 2293-2296 (2001); erratum **87** (20), 9001.
[3] D. B. Thiessen, M. J. Marr-Lyon, and P. L. Marston, "Active electrostatic stabilization of liquid bridges in low gravity," J. Fluid Mech. **457**, 285-294 (2002).

* marston@wsu.edu, phone: (509) 335-5343, FAX: (509) 335-7816

MOLTEN-METAL DROPLET DEPOSITION ON A MOVING SUBSTRATE IN MICROGRAVITY: AIDING THE DEVELOPMENT OF NOVEL TECHNOLOGIES FOR MICROELECTRONIC ASSEMBLY

C. M. Megaridis,* I. S. Bayer
Department of Mechanical and Industrial Engineering, University of Illinois at Chicago

D. Poulikakos
Institute of Energy Technology, Swiss Federal Institute of Technology, Zurich, Switzerland

V. Nayagam
National Center for Microgravity Research, Cleveland, Ohio

ABSTRACT

Driven by advancements in microelectronics manufacturing, this research investigates the oblique (non-axisymmetric) impact of liquid-metal droplets on flat substrates. The problem of interest is relevant to the development of the novel technology of on-demand dispension (printing) of microscopic solder deposits for the surface mounting of microelectronic devices. The technology, known as solder jetting, features on-demand deposition of miniature solder droplets (30 to 120μm in diameter) in very fine, very accurate patterns using techniques analogous to those developed for the ink-jet printing industry. Despite its promise, severe limitations exist currently with regards to the throughput rates of the technology; some of these limitations are largely due to the lack of the capability for reliable prediction of solder bump positioning and shapes, especially under ballistic deposition conditions where the droplet impact phenomena are inherently three-dimensional.

The study consists of a theoretical and an experimental component. The theoretical work uses a finite element formulation to simulate numerically the non-axisymmetric (3-D) fluid mechanics and heat transfer phenomena of a liquid solder droplet impacting at an angle α on a flat substrate (Fig. 1). The work focuses on the pre-solidification regime. The modeling of the most challenging fluid mechanics part of the process has been completed successfully. It is based upon the full laminar Navier-Stokes equations employing a Lagrangian frame of reference. Due to the large droplet deformation, the surface (skin) as well as the volumetric mesh have to be regenerated during the calculations in order to maintain the high accuracy of the numerical scheme. The pressure and velocity fields are then interpolated on the newly created mesh. The numerical predictions are being tested against experiments, for cases where wetting phenomena are not important. For the impact parameters used in the example shown in Figs 2, 3 (We = 2.38, Fr = 16300, Re = 157), the droplet rolls along the substrate, but its shape remains practically axisymmetric for all impact angles within the range from 0 to 60 deg. Figure 2 exemplifies the results, showing this rolling motion at an impact angle α=45 deg. Interestingly, the substrate/droplet contact area during the recoiling phase of the impact is not a monotonically decreasing function of time (Fig. 3).

* M/C 251, 842 W. Taylor St., Chicago IL 60607-7022; cmm@uic.edu; fax: (312) 413 0447; tel: (312) 996 3436

The experimental component of the research tests the numerical predictions and provides necessary input data (contact angles) for the theoretical model. The experiments are performed in microgravity (2.2s drop tower of the NASA GRC) in order to allow for the use of mm-size solder droplets, which make feasible the performance of accurate measurements, while maintaining similitude of the relevant fluid dynamic groups (*Re*, *Fr, We, Ste*). Preliminary oblique impact experiments have been performed using water droplets in normal gravity. Figure 4 shows the definition of the two extreme values of contact angle (front θ_F, rear θ_R), as viewed from a direction normal to the plane of impact. Figure 5 compares the measured temporal variations of these two angles for an impact case where α=27deg, We = 11.7, Fr = 20.5 and Re = 1530. It is seen that the oscillatory behavior of the two angles is not in phase, indicating the complex interaction between the bulk fluid motion and the motion of the free surface.

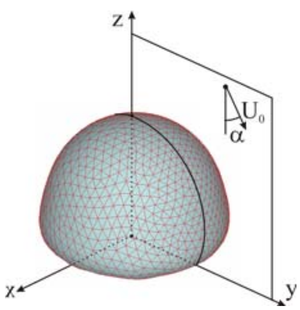

Fig. 1: Problem configuration.

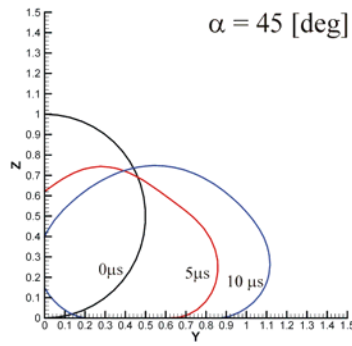

Fig. 2: Time sequence of droplet profiles as predicted by the model.

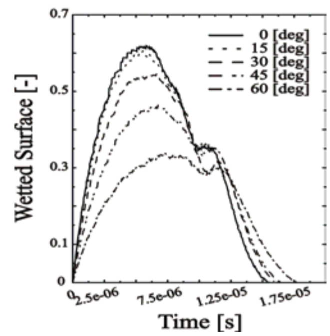

Fig. 3: Evolution of the contact area for various impact angles.

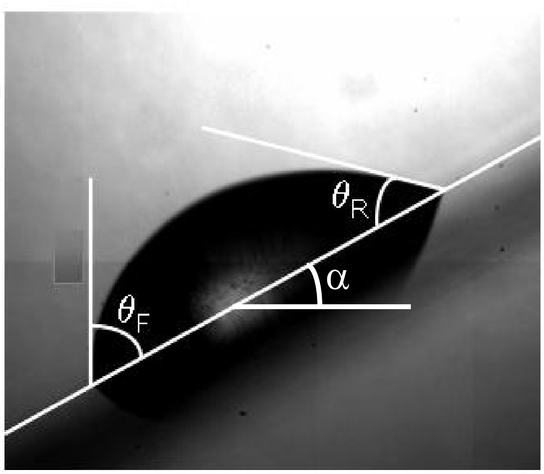

Fig. 4: Definition of front (θ_F) and rear (θ_R) contact angle in the impact of a droplet on an inclined plate.

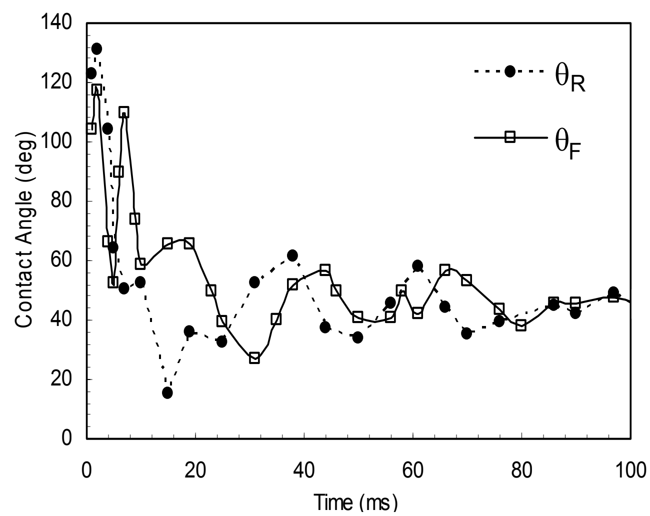

Fig. 5: Temporal variation of front and rear contact angles (Fig. 4) for an experiment with α= 27deg, We = 11.7, Fr = 20.5 and Re = 1530.

NON-COALESCENCE IN MICROGRAVITY: SCIENCE AND TECHNOLOGY

G. Paul Neitzel
The George W. Woodruff School of Mechanical Engineering
Georgia Institute of Technology
Atlanta, GA 30332-0405
paul.neitzel@me.gatech.edu
404-894-3242 (Voice)
404-894-8496 (Fax)

ABSTRACT

In this project we examine non-coalescence and non-wetting phenomena driven by either thermocapillary convection or forced motion of one surface relative to the other. In both cases, the non-coalescence or non-wetting is enabled by the existence of a lubricating layer of gas that exists to keep the two surfaces in question from coming into contact with one another.

Recent progress has been made on several fronts: 1) measurement of the vibrational modes of pinned droplets; 2) development of an apparatus for the measurement of the frictional forces associated with a non-wetting droplet sliding over a solid surface; 3) measurements of the failure modes for non-wetting droplets and the influence of static electric charge on failure; and 4) numerical simulation of a two-dimensional non-wetting droplet revealing a possible explanation for why the phenomenon has not been able to be observed using water as the droplet liquid.

Issue 1) above is of relevance to the use of non-wetting droplets as positioning mechanisms and vibration dampers in a microgravity environment; issue 2) relates to the use of non-wetting droplets as nearly "frictionless" bearings in low-load applications. Understanding of the failure modes identified in 3) is of importance to any potential application and the numerical simulations conducted under 4) allow us to obtain information about these systems that is currently not available through experimentation Each of these topics will be discussed briefly during the presentation.

SHADOWGRAPH STUDY OF GRADIENT DRIVEN FLUCTUATIONS

Gennady Nikolaenko and David S. Cannell
Department of Physics
UC Santa Barbara
Santa Barbara, CA 93106

ABSTRACT

A fluid or fluid mixture, subjected to a vertical temperature and/or concentration gradient in a gravitational field, exhibits greatly enhanced light scattering at small angles [1-3]. This effect is caused by coupling between the vertical velocity fluctuations due to thermal energy and the vertically varying refractive index. Physically, small upward or downward moving regions will be displaced into fluid having a refractive index different from that of the moving region, thus giving rise to the enhanced scattering [4]. The scattered intensity is predicted [5-7] to vary with scattering wave vector $\mathbf{q}$, as q^{-4}, for sufficiently large $\mathbf{q}$, but the divergence is quenched by gravity [8] at small $\mathbf{q}$. In the absence of gravity, the long wavelength fluctuations responsible for the enhanced scattering are predicted to grow until limited by the sample dimensions [9, 10]. It is thus of interest to measure the mean-squared amplitude of such fluctuations in the microgravity environment for comparison with existing theory and ground based measurements.

The relevant wave vectors are extremely small, making traditional low-angle light scattering difficult or impossible because of stray elastically scattered light generated by optical surfaces. An alternative technique is offered by the shadowgraph method, which is normally used to visualize fluid flows, but which can also serve as a quantitative tool to measure fluctuations [11, 12]. A somewhat novel shadowgraph apparatus and the necessary data analysis methods will be described. The apparatus uses a spatially coherent, but temporally incoherent, light source consisting of a super-luminescent diode coupled to a single-mode optical fiber in order to achieve extremely high spatial resolution, while avoiding effects caused by interference of light reflected from the various optical surfaces that are present when using laser sources.

Results obtained for a critical mixture of aniline and cyclohexane subjected to a vertical temperature gradient will be presented. The sample was confined between two horizontal parallel sapphire plates with a vertical spacing of 1 mm. The temperatures of the sapphire plates were controlled by independent circulating water loops that used Peltier devices to add or remove heat from the room air as required.

For a mixture with a temperature gradient, two effects are involved in generating the vertical refractive index gradient, namely thermal expansion and the Soret effect, which generates a concentration gradient in response to the applied temperature gradient. For the aniline/cyclohexane system, the denser component (aniline) migrates toward the colder surface. Consequently, when heating from above, both effects result in the sample density decreasing with altitude and are stabilizing in the sense that no convective motion occurs regardless of the magnitude of the applied temperature gradient. The Soret effect is strong near a binary liquid critical point, and thus the dominant effect is due to the induced concentration gradient. The results clearly show the divergence at low $\mathbf{q}$ and the predicted gravitational quenching. Results obtained for different applied temperature gradients at varying temperature differences from the critical temperature, clearly demonstrate the predicted divergence of the thermal diffusion ratio.

Thus, the more closely the critical point is approached, the smaller becomes the temperature gradient required to generate the same signal.

Two different methods have been used to generate pure concentration gradients. In the first, a sample cell was filled with a single fluid, ethylene glycol, and a denser miscible fluid, water, was added from below thus establishing a sharp interface to begin the experiment. As time went on the two fluids diffused into each other, and large amplitude fluctuations were clearly observed at low $\mathbf{q}$. The effects of gravitational quenching were also evident. In the second method, the aniline/cyclohexane sample was used, and after applying a vertical temperature gradient for several hours, the top and bottom temperatures were set equal and the thermal gradient died on a time scale of seconds, leaving the Soret induced concentration gradient in place. Again, large-scale fluctuations were observed and died away slowly in amplitude as diffusion destroyed the initial concentration gradient.

1. B. M. Law, R. W. Gammon, and J. V. Sengers, Light-scattering observations of long-range correlations in a nonequilibrium liquid, Phys. Rev. Lett. 60, 1554 (1988).
2. P. N. Segrè, R. W. Gammon, J. V. Sengers, and B. M. Law, Rayleigh scattering in a liquid far from thermal equilibrium, Phys. Rev. A 45, 714 (1992).
3. A. Vailati and M. Giglio, Giant fluctuations in a free diffusion process, Nature (London) 390, 262 (1997).
4. D. A. Weitz, Diffusion in a Different Direction, Nature, 390, 233 (1997).
5. T. R. Kirkpatrick, E. G. D. Cohen, and J. R. Dorfman, Light scattering by a fluid in a nonequilibrium steady state. II. Large gradients, Phys. Rev. A 26, 995 (1982).
6. R. Schmitz and E. G. D. Cohen, Fluctuations in a fluid under a stationary heat flux. II Slow part of the correlation matrix, J. Stat. Phys. 40, 431 (1985).
7. P. N. Segrè and J. V. Sengers, Nonequilibrium fluctuations in liquid mixtures under the influence of gravity, Physica A 198, 46 (1993).
8. A. Vailati and M. Giglio, q divergence of nonequilibrium fluctuations and its gravity-induced frustration in a temperature stressed liquid mixture, Phys. Rev. Lett. 77, 1484 (1996).
9. J. M. Ortiz de Zarate, R. Perez Cordon, and J. V. Sengers, Finite-size effects on fluctuations in a fluid out of thermal equilibrium, Physica A 291, 113 (2001).
10. J. M. Ortiz de Zárate and J. V. Sengers, Boundary effects on the nonequilibrium structure factor of fluids below the Rayleigh-Bénard instability, Preprint November, 2001.
11. M. Wu, G. Ahlers, and D. S. Cannell, Thermally induced fluctuations below the onset of Rayleigh-Bénard convection, Phys. Rev. Lett. 75, 1743 (1995).
12. S. P. Trainoff and D. S. Cannell, Physical Optics Treatment of the Shadowgraph, Physics of Fluids, 14, 1340 (2002).

Session 3:
Complex Fluids

PARTICLE SEGREGATION IN A FLOWING SUSPENSION SUBJECT TO HIGH-GRADIENT STRONG ELECTRIC FIELDS

Andreas Acrivos, Zhiyong Qiu
The City College of New York

Boris Khusid, Nikolai Markarian
New Jersey Institute of Technology

PI: Andreas Acrivos, The Levich Institute, The City College of New York, 140th Street & Convent Avenue, New York, NY 10031, Tel: 212-650-8159, Fax: (212) 650-6835; E-mail: acrivos@scisun.sci.ccny.cuny.edu

INTRODUCTION

The widespread use of electro-hydrodynamic devices and processes emphasizes a critical need for developing a comprehensive predictive theory capable of improving our fundamental understanding of the behavior of a suspension subject to an AC electric field and shear, and of facilitating the design and optimization of such devices. The currently favored approach to the qualitative interpretation of the AC-field driven manipulation of suspensions is based on a model which considers only the force exerted on a single particle by an external field and neglects the field-induced and hydrodynamic interparticle interactions both being inversely proportional to the interparticle distance raised to the power three. On the other hand, the purpose of the field-induced separation is to concentrate particles in certain regions of a device. This clearly raises the fundamental question regarding the extent to which we can neglect these slow decaying electrical and hydrodynamic collective interactions and rely on the predictions of a single-particle model. Another important issue that still remains open is how to characterize the polarization of a particle exposed to a strong electric field. The presentation will address both these questions.

EXPERIMENTAL DATA AND COMPARISON WITH SIMULATIONS

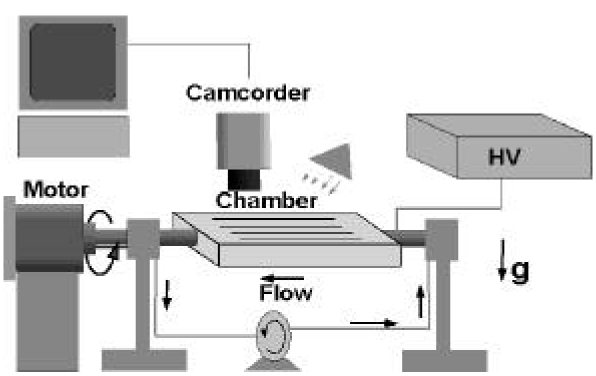

Figure 1. Setup

Experiments were conducted in a parallel-plate channel in which a 10^{-3} (v/v) suspension of heavy, positively polarized Al_2O_3 spheres was exposed to an AC field under conditions such that the field lines were arranged in the channel cross-section perpendicular to the streamlines of the main flow [1, 2]. To reduce the effects of the gravitational settling of the particles, the channel was slowly rotated (4 rpm) around a horizontal axis (Fig.1). Following the application of a high-gradient strong

AC field (~kV/mm), the particles were found to move towards both the high-voltage (HV) and grounded (GR) electrodes and to form "bristles" along their edges (Fig. 2).

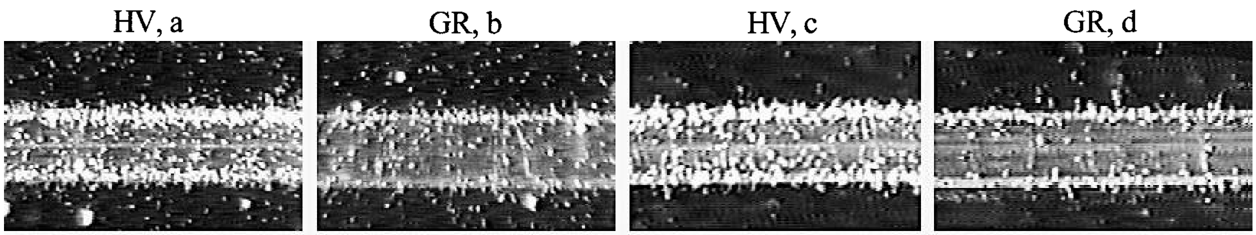

Figure 2. 1kV, 100Hz; (a,b) 20 ml/min, 383s; (c,d) no flow, 314 s. The electrode width is 1.6 mm

The process was modeled by computing the particle motions under the combined action of dielectrophoretic, viscous, and gravitational forces under conditions of negligibly small particle Reynolds numbers and neglecting the interparticle electric and hydrodynamic interactions. The model calculations required no fitting parameters because the particle polarizability was determined independently by measuring the frequency and concentration dependence of the complex dielectric permittivity of a suspension in a low-strength field (~ V/mm).

The predictions of this single-particle model were found to be consistent with the experimental data for the rate of particle accumulation on the electrodes. In particular, Fig. 3 shows the experimental and theoretical data on the kinetics of the particle aggregation on a high-voltage electrode in the middle of the channel for a 10^{-3} (v/v)-suspension following the application of an electric field. The data are plotted against the non-dimensional time, t/τ_d, with τ_d being the characteristic dielectrophoretic time [1, 2]. However, the interparticle interactions, even for initially very dilute suspensions, appear to govern the formation of the. aggregation pattern on the electrodes. The experiments suggested a two-step mechanism for the formation of the arrays of bristles (Fig.2) along the electrode edges, which arose from the interplay of the dielectrophoretic force that confined the particles near the electrode edge and the dipolar interactions of nearby particles.

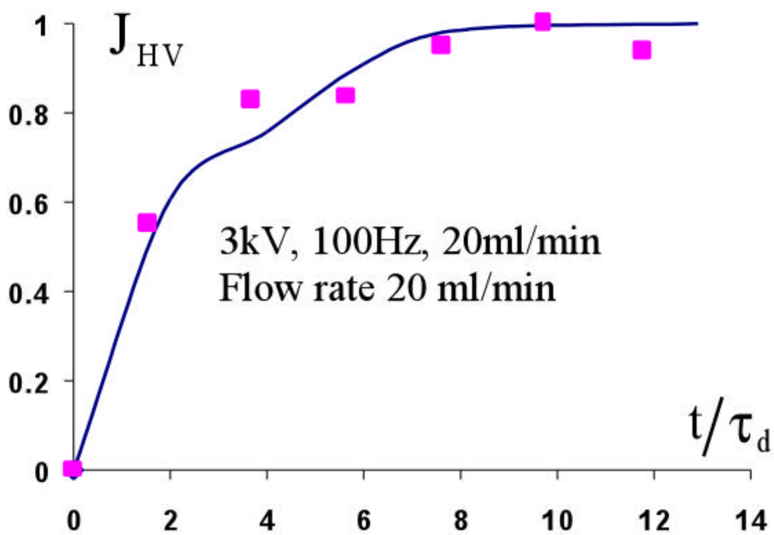

Figure 3. Amount of accumulated particles

REFERENCES

1. A. Dussaud, B. Khusid and A. Acrivos, J. Appl. Phys., 88, 5463 (2000).
2. Z. Qiu, N. Markarian, B. Khusid and A. Acrivos, J. Appl. Phys. (to appear, 2002)

SHEET FLOWS, AVALANCHES, AND DUNE MIGRATION ON EARTH AND MARS

James Jenkins
Department of Theoretical and Applied Mechanics
Cornell University, Ithaca, NY 14853
jtj2@cornell.edu Tel: 606-255-7185, Fax: 607-255-2011

ABSTRACT

We provide an overview of our research on sheet flows and avalanches of granular materials, primarily in terrestrial conditions. Sheet flows are relatively thin, highly concentrated regions of grains that flow near the ground under the influence of a strong turbulent wind. In them grains are suspended by interparticle collisions and the velocity fluctuations of the turbulent gas. Avalanches are flows of dry, cohesionless granular materials that are driven by gravity down inclines against the frictional and collisional resistance of the grains of the bed.

In our study of sheet flows, we have extended existing theories that involve particle-particle and gas-particle interactions to apply to the conditions of a typical terrestrial sand dune during a sandstorm. This has involved the incorporation of both the viscous dissipation of the particle fluctuation energy due to the gas and the turbulent suspension of the grains due to velocity fluctuations of the gas. It has also involved an examination of several different boundary conditions at the bed and a more precise characterization of the conditions that apply at the top of a sheet flow, where the mean-free-path between collisions becomes comparable to the length of a ballistic trajectory. Solutions to the resulting differential equations have been obtained for both steady and unsteady fully-developed flow. The latter solutions provide information on the characteristic time to achieve a steady flow that plays a key role in dune formation.

In support of this modeling effort, experiments have been undertaken to provide a better understanding of the interaction of particles colliding with the bed, and the energy of the rebounding particle and additional ejected particles has been measured in two-dimensional situations.

The research on avalanches has focused on dense, frictional flows. Experiment and numerical simulations indicate that relatively thin dense flows, on the order of ten particle diameters, occur in layers. In these, momentum transfer occurs by rubbing between contacting particles and bumping between particles falling under gravity, rather than in collisions between freely flying particles. Thicker dense flows, on the other hand, do seem to involve collisional transfer of momentum. Theories based on the appropriated mechanisms of momentum transfer predict velocity profiles that are in agreement with those measured in experiment and numerical simulations, some of which have been carried out in the course of the research.

GRAVATIONAL INSTABILITY IN SUSPENSION FLOWS

Ileana C. Carpen and John F. Brady

Division of Chemistry and Chemical Engineering
California Institute of Technology
Pasadena, CA 91125
626-395-4183, 626-586-8743(Fax), jfbrady@caltech.edu

The gravity-driven flow of non-neutrally buoyant suspensions is shown to be unstable to spanwise perturbations when the shearing motion generates a density profile that increases with height. The instability is simply due to having heavier material over light. The wavelength of the perturbation is found to be on the order of the thickness of the suspension layer. The parameters important to the problem are the angle of inclination of the layer relative to gravity, the relative density difference between the particles and fluid, the ratio of the particle size to the suspension layer, and the bulk volume fraction of particles. An example showing the growth rate as a function of wave number is shown below.

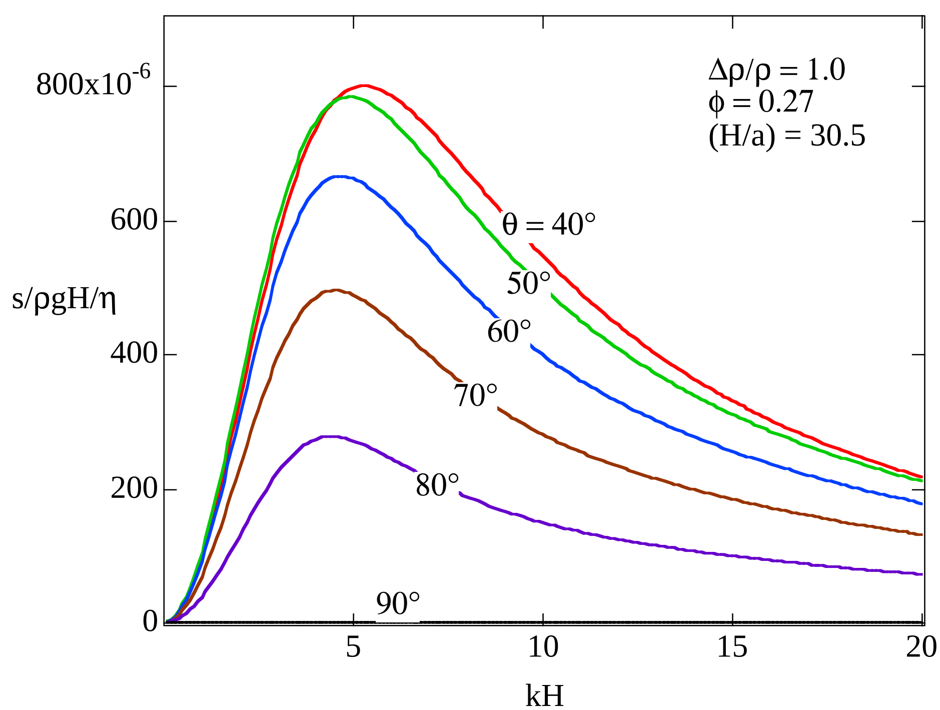

DYNAMICS OF CHARGED DUST NEAR SURFACES IN SPACE

Joshua E. Colwell, Mihály Horányi, Scott Robertson, and Amanda A. Sickafoose
LASP, University of Colorado, Boulder CO 80309-0392, josh.colwell@lasp.colorado.edu,
303-492-6805, Fax: 303-492-6946

ABSTRACT

Objects in plasma, such as planetary bodies in the solar wind, charge to a floating potential determined by the balance between charging currents in the local plasma environment. In cases where secondary electron emission and photoemission are weak, objects will become negatively charged due to electron collection and will be surrounded by a plasma sheath. Solar ultraviolet radiation can produce a photoelectron sheath above the sunlit surface of airless planetary bodies. In both cases an electric field is present near the surface that can accelerate charged dust particles near the surface. Dust may be stably levitated if the electric force balances the gravitational force.

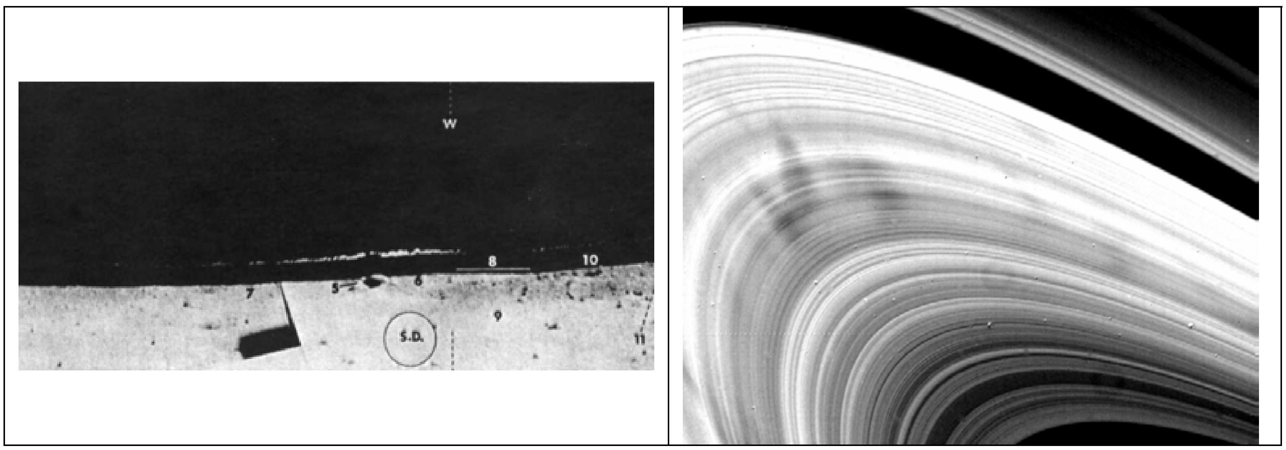

Figure 1: (a) Surveyor photograph of the lunar horizon showing a cloud of small particles suspended 1 m above the surface. The circle labeled "S.D." indicates the apparent size and direction to the Sun [1]. (b) Voyager 2 image of Saturn's rings. The dark smudges are "spokes" of dust particles lifted off the surface of the larger ring particles by electrostatic forces [2].

Experiments in a plasma sheath have shown that particles can be stably levitated with surface potentials consistent with those expected on planetary surfaces [3]. Our experiments have also shown that particles can be lifted off the surface by the electric field without any additional disturbance. This may explain the separation of dust from the surfaces of larger particles in Saturn's rings observed as "spokes" by local plasma presumably generated by an impact (Figure 1). Observations of smooth deposits of regolith in crater bottoms on the asteroid 433 Eros by the NEAR spacecraft suggest a transport mechanism for regolith [4]. Levitation of charged dust and transport in an inhomogeneous electric field is a possible explanation for the distribution of regolith on Eros and other asteroids. More generally, acceleration of charged dust in the near-surface sheath can lead to loss of fine-grained particles from objects with weak gravitational accelerations.

We have carried out experiments on charging, levitation, and transport of dust in plasma and photoelectron sheaths. A tungsten filament beneath the surface plate creates the primary electrons that ionize gas in the chamber. When the surface is biased to a sufficiently high voltage

(-40V to -80V), dust particles are lifted off the surface. Some of these particles, depending on size and mass, become stably levitated a few cm above the surface [3]. On objects with weaker surface gravity the particle size-dependent levitation height is higher.

In addition to levitation our experimental studies show that dust can be transported horizontally over a uniform surface in a uniform plasma sheath. We conducted experiments where a surface is partially covered by dust grains and partially clean. After cycling the plasma on and off, net transport of dust to the initially dust-free portions of the surface is observed. Further experiments will include topographical features on the surface simulating craters and rocks, and we will quantify the horizontal transport of dust in the sheath as a function of grain properties and plasma properties.

Simple numerical simulations also show a net transport of dust when inhomogeneities in the sheath are introduced. We calculate the trajectories of individual dust grains using a numerical integrator that simultaneously solves for the charge on the particle. The forces on the particle are gravity downward and the electric force resulting from the grain charge and the electric field normal to the model surface that is produced by the sheath. Although there are no horizontal forces in our initial simulations, horizontal transport occurs as a result of a combination of initial horizontal velocity components for dust lifted off the surface, the effects of topography, and discontinuities in the photoelectron sheath at the terminator. When dust particles enter shadow the sheath vanishes in this model, and the particle falls to the surface under the effects of gravity. In our simulations this leads to an accumulation of dust at the terminator. Dust also accumulates at the borders of topographical features such as blocks and craters (Figure 3).

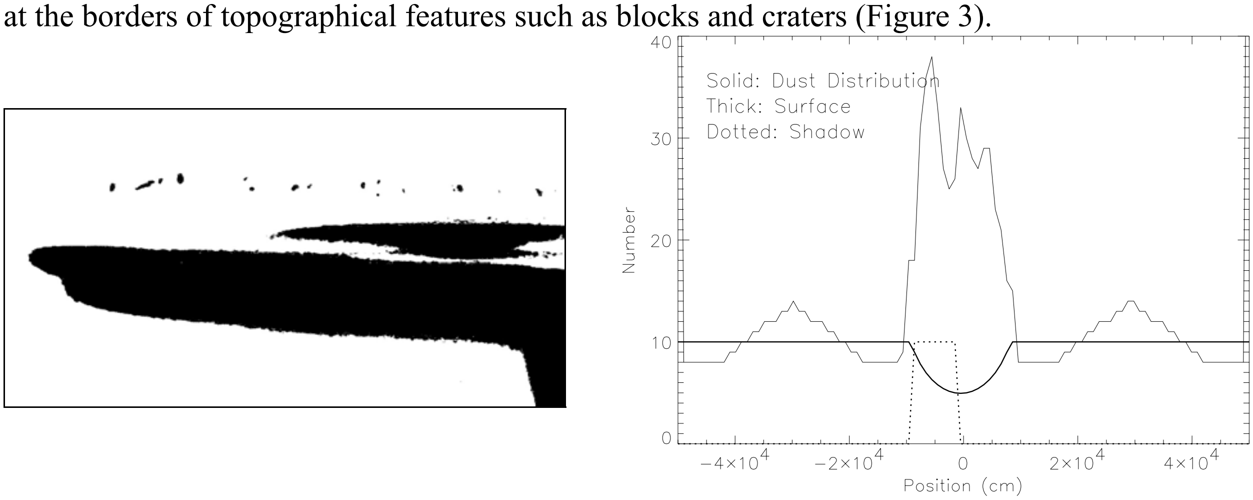

Figure 3: (a) Negative image of levitated dust in our laboratory experiment [3]. (b) Numerical simulation of dust accumulation in a crater on a low-surface-gravity object. Particles accumulate in the shadow where no electric force counteracts gravity. The piles on either side of the crater are edge effects of the simulation.

More realistic modeling of the sheath and the surface at these boundaries are planned, but the basic phenomenon of dust accumulation at shadow and topographical boundaries should persist.

REFERENCES

[1] Rennilson, J. J., and D. R. Criswell, *The Moon*, **10**, 121-142 (1974).
[2] Goertz, C. K., *Reviews of Geophysics*, *27*(2), 271-292 (1989).
[3] Sickafoose, A.A., J.E. Colwell, M. Horányi, and S. Robertson, *J. Geophys. Res.* (sub. 2002).
[4] Robinson, M. S., P. C. Thomas, J. Veverka, S. Murchi, B. Carcich, *Nature*, **413**, 396 (2001).

MICROGRAVITY-DRIVEN INSTABILITIES IN GAS-FLUIDIZED BEDS

Anthony J.C. Ladd
University of Florida

David A. Weitz
Harvard University

A dense pack of solid particles can be fluidized by an upward flow of liquid, which counterbalances the gravitational force on the particles. The resulting suspension is stable for sufficiently small fluid velocities, although the particle dynamics are complex and still not fully understood. A packed particle bed can also be fluidized by a gas flow, but in this case a stable suspension of moving particles cannot be produced in earth's gravitational field. Kinetic theory of gas-fluidized beds predicts that the bed is always unstable to particle inertia, whichis several orders of magnitude larger than fluid inertia in this case. In order to study the onset of this particle-induced instability, the minimum fluidization velocity must be reduced by several orders of magnitude; we believe that this can be most successfully accomplished in a reduced gravity environment. We expect that in a microgravity environment it would be possible to explore the transition between stable and unstable flow regimes in gas-fluidized beds, and contrast the behavior of particle inertia (gas-fluidized) and fluid inertia (liquid fluidized) driven instabilities. However in this preliminary study the investigations of gas-fluidized systems will be done numerically. We will compare and contrast the stability conditions and flow patterns arising from increasing fluid inertia ($Re > 1$, $St \sim Re$) and increasing particle-inertia ($Re < 1$, $St > 1$). Laboratory experiments on liquid-fluidized beds are being used to validate the predictions of the numerical simulations.

In this talk I will summarize results from computer simulations of particles settling in a low-Reynolds number regime. Experimental measurements of the velocity fluctuations in a sedimenting suspension [1, 2] are independent of system size for sufficiently large containers. However, this observation is at odds with theoretical [3] and numerical [4, 5] predictions for a random distribution of particles. I will present new data for suspensions bounded by a rigid container, and compare them with results for homogeneous suspensions with periodic boundary conditions. Velocity fluctuations in vertically*inhomogeneous* suspensions are found to saturate under conditions similar to those found in laboratory experiments, while in vertically *homogeneous* suspensions the velocity fluctuations diverge with increasing container dimension (Fig. 1) [6].

The strikingly different behavior in the velocity fluctuations for the different boundary conditions is caused by the interfaces between the dense pack, the homogenous suspension, and the supernatent fluid. These interfaces are a sink for the fluctuation energy, which drains out of the system at a rate that is roughly proportional to the inverse of the cell height. Random density fluctuations convect to one of these two interfaces and are absorbed by the density gradient at the interface. A scaling argument suggests that convection of density fluctuations to the boundaries at the top and bottom of the suspension leads to a correlation length proportional to the mean interparticle spacing $\alpha^{1/3}$.

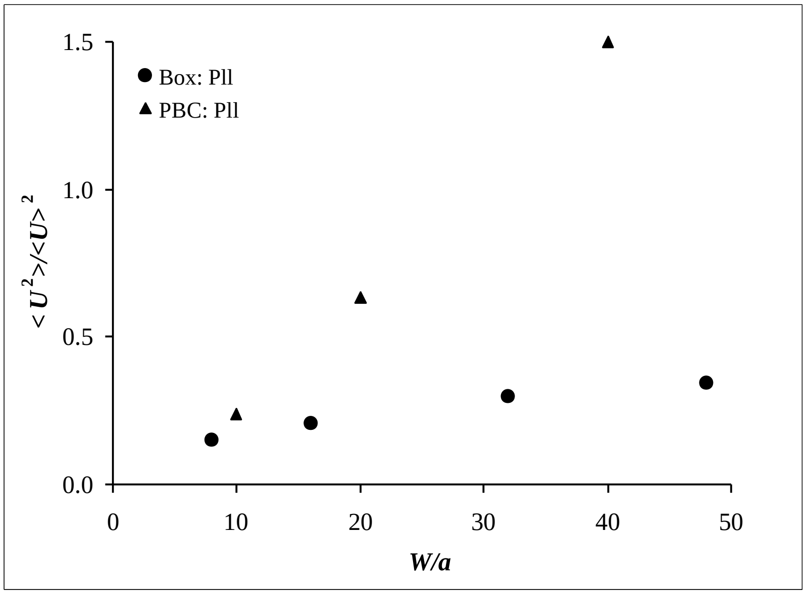

Figure 1. Fluctuations in the settling velocity as a function of container width a cell bounded in all three directions by no-slip walls (Box) and a cell that is periodic in all three directions (PBC). The statistical errors are comparable to the size of the symbols.

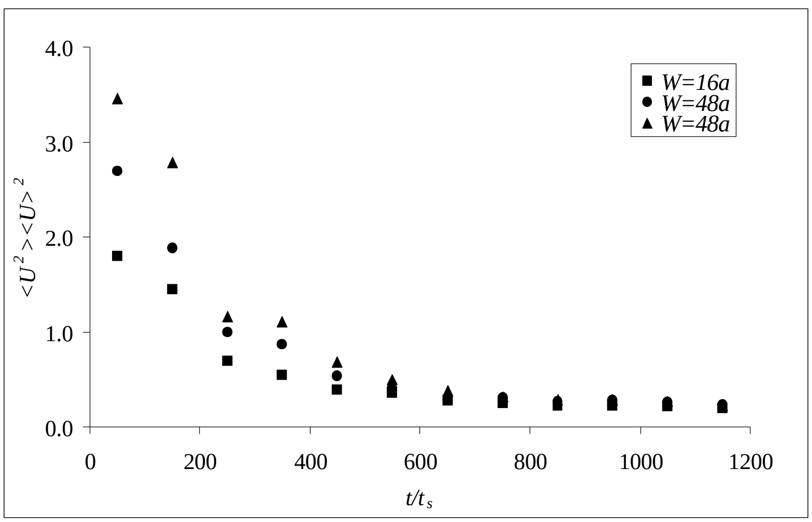

Figure 2. Time dependence of relative velocity fluctuations for different container widths.

1. Segrè, P.N., E. Herbolzheimer, and P.M. Chaikin, *Long-Range Correlations in Sedimentation.* Physical Review Letters, 1997. **79**(13): p. 2574-2577.
2. Nicolai, H. and E. Guazzelli, *Effect of the vessel size on the hydrodynamic diffusion of sedimenting spheres.* Physics of Fluids, 1995. **7**(1): p. 3-5.
3. Caflisch, R.E. and J.H.C. Luke, *Variance in the sedimentation speed of a suspension.* Phys. Fluids, 1985. **28**: p. 759.
4. Ladd, A.J.C., *Hydrodynamic Screening in Sedimenting Suspensions of non-Brownian Spheres.* Physical Review Letters, 1996. **76**(8): p. 1392-1395.
5. Ladd, A.J.C., *Sedimentation of homogeneous suspensions of non-Brownian spheres.* Physics of Fluids, 1997. **9**(3): p. 491-499.
6. Ladd, A.J.C., *Effects of container walls on the velocity fluctuations in sedimenting suspensions.* Phys. Rev. Lett., 2002. **88**: p. 048301.

STUDIES OF GAS-PARTICLE INTERACTIONS IN A MICROGRAVITY FLOW CELL

Michel Y. Louge†, James T. Jenkins, Haitao Xu and Anthony Reeves
Cornell University, Ithaca, NY 14853

ABSTRACT

The NASA-Glenn Research Center is designing a microgravity flow cell in which to study the interaction of a flowing gas with relatively massive particles that collide with each other and with the moving boundaries of the cell. This cell will permit us to study suspensions over a range of laminar, steady, fully developed conditions where viscous forces dominate the gas flow and inertial forces proportional to the gas density are nearly eliminated. Unlike terrestrial flows, where the gas velocity must be set to a value large enough to support the weight of particles, the duration and quality of microgravity on the International Space Station will permit us to achieve suspensions in which the agitation of the particles and the gas flow can be controlled independently by adjusting the pressure gradient along the flow and the relative motion of the boundaries. To do this, we will use an axisymmetric Couette shearing cell permitting the independent control of the speeds of the moving inner and outer boundaries. This apparatus will be configured for two experiments on gas-solid interactions.

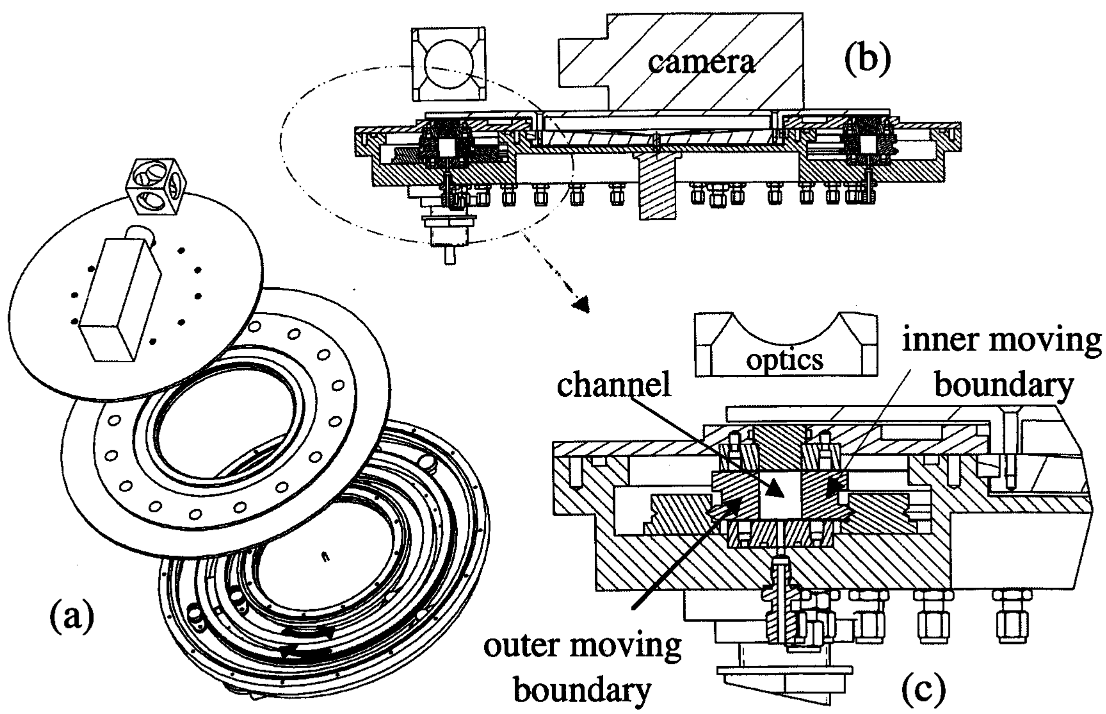

In the first series of experiments, we will characterize the viscous dissipation of the energy of the particle fluctuations when there is no relative mean velocity between gas and solids. We

† Sibley School of Mechanical and Aerospace Engineering, Cornell University, 192 Rhodes Hall, Ithaca, NY 14853, MYL3@cornell.edu, voice: (607) 255 4193, fax: (607) 255 1222.

recall that in the absence of a gas, individual impacts are so fast that the only time scale governing the granular phase is the inverse of , the shear rate imposed by the moving boundaries. At small particle Reynolds numbers, the gas introduces an additional viscous relaxation time $_s = {}_s d^2/18\mu_g$, where $_s$, d and μ_g are, respectively, the density of the spheres, their diameter and the gas viscosity. In simple shear flows, Sangani et al. (1996) calculated values of the limiting Stokes number St = $_s$ at which the particle fluctuation energy is equally dissipated by viscous and collisional interactions. Far above this limit, the shear rate is sufficient to ignore the viscous drag on the spheres.

In contrast, for these Viscous Dissipation Experiments, our intention is to reduce the boundary speed in successive tests until the Stokes number becomes small enough for the gas to affect the balance of fluctuation energy of the spheres. We will control the magnitude of the particle Reynolds number by adjusting the absolute pressure in the cell. At sufficiently low Stokes number, Sangani et al. (1996) showed that the granular fluctuation velocity scales as $\sqrt{T}$ / d μ St /R_{diss}, where R_{diss}( ) is a coefficient characterizing viscous dissipation. In our experiments, we will infer R_{diss} by recording transverse profiles of granular temperature and comparing these with theoretical predictions.

The measurements will be accomplished by observing the flow through side walls and by using computer vision techniques to record transverse profiles of the mean and fluctuation velocities of the solids. In order to evaluate the role of non-continuum lubrication, we will also reduce the pressure of the apparatus and measure R_{diss} at increasing values of the molecular mean free path. Finally, we will perform experiments at Stokes and Reynolds numbers where the present theory is valid and also, in an effort to inform future theoretical work, at values when it is not.

In the second series of experiments, we will impose a gas pressure gradient on the shearing cell. The gradient will induce a relative velocity between the two phases, while the shearing will set independently the agitation of the solids. These Viscous Drag Experiments will be unique in exploring a regime where particle velocity fluctuations are determined by a mechanism other than interactions with the gas. In this regime, we will measure the dependence of R_{diss} and the drag coefficient R_{drag} on the solid volume fraction.

We will do so by recording the following variables and comparing these with theoretical predictions: mean gas volume flow rate through the flow channel, pressure gradient in the gas and transverse profiles of mean granular velocity, granular temperature and volume fraction. By reducing the pressure of the cell, we will also record the effects of particle Reynolds number on R_{drag}. Finally, we will record the cross-sectional mean solid volume fraction at several positions along the channel. This will permit us to monitor the flow development and the approach to steady-state, and it will contribute to measuring the required volume flow rate of gas through all branches of the flow channel.

REFERENCE

Sangani A.S., Mo G., Tsao H.-K., and Koch D.L., "Simple shear flows of dense gas-solid suspensions at finite Stokes number," *J. Fluid Mech.* **313**, 309-341 (1996).

Dynamics of Sheared Granular Materials

Lou Kondic
Department of Mathematical Sciences and Center for Applied Mathematics & Statistics,
New Jersey Institute of Technology, Newark, NJ 07102

Brian Utter and Robert P. Behringer
Department of Physics and Center for Nonlinear and Complex Systems
Duke University, Durham, NC 27708

ABSTRACT

This work focuses on the properties of sheared granular materials near the jamming transition. The project currently involves two aspects. The first of these is an experiment that is a prototype for a planned ISS flight. The second is discrete element simulations (DES) that can give insight into the behavior one might expect in a reduced-g environment.

The experimental arrangement consists of an annular channel that contains the granular material. One surface, say the upper surface, rotates so as to shear the material contained in the annulus. The lower surface controls the mean density/mean stress on the sample through an actuator or other control system. A novel feature under development is the ability to 'thermalize' the layer–i.e. create a larger amount of random motion in the material, by using the actuating system to provide vibrations as well control the mean volume of the annulus. The stress states of the system are determined by transducers on the non-rotating wall. These measure both shear and normal components of the stress on different size scales. Here, the idea is to characterize the system as the density varies through values spanning dense almost solid to relatively mobile granular states. This transition regime encompasses the regime usually thought of as the glass transition, and/or the jamming transition.

Motivation for this experiment springs from ideas of a granular glass transition, a related jamming transition, and from recent experiments. In particular, we note recent experiments carried out by our group to characterize this type of transition (Howell et al. Phys. Rev. Lett. **82**, 5241 (1999)) and also to demonstrate/characterize fluctuations in slowly sheared systems (Miller et al. Phys. Rev. Lett. **77**, 3110 (1996)). These experiments give key insights into what one might expect in near-zero g. In particular, they show that the compressibility of granular systems diverges at a transition or critical point. It is this divergence, coupled to gravity, that makes it extremely difficult if not impossible to characterize the transition region in an earth-bound experiment.

In the DE modeling, we analyze dynamics of a sheared granular system in Couette geometry in two (2D) and three (3D) space dimensions. Here, the idea is to both better understand what we might encounter in a reduced-g environment, and at a deeper level to deduce the physics of sheared systems in a density regime that has not been addressed by past experiments or simulations.

One aspect of the simulations addresses sheared 2D system in zero-g environment. For low volume fractions, the expected dynamics of this type of system is relatively well understood. However, as the volume fraction is increased, the system undergoes a phase transition, as explained above. The DES concentrate on the evolution of the system as the solid volume fraction is slowly increased, and in particular on the behavior of very dense systems. For these configurations, the simulations show that polydispersity of the sheared particles is a crucial factor that determines the system response. Figures 1 and 2 below, that present the total force on each grain, show that even relatively small (10 %) nonuniformity of the size

of the grains (expected in typical experiments) may lead to significant modifications of the system properties, such as velocity profiles, temperature, force propagation, and formation of shear bands.

The simulations are extended in a few other directions, in order to provide additional insight to the experimental system analyzed above. In one direction, both gravity, and driving due to vibrations are included. These simulations allow for predictions on the driving regime that is required in the experiments in order to analyze the jamming transition. Furthermore, direct comparison of experiments and DES will allow for verification of the modeling assumptions. We have also extended our modeling efforts to 3D. The (preliminary) results of these simulations of an annular system in zero-g environment will conclude the presentation.

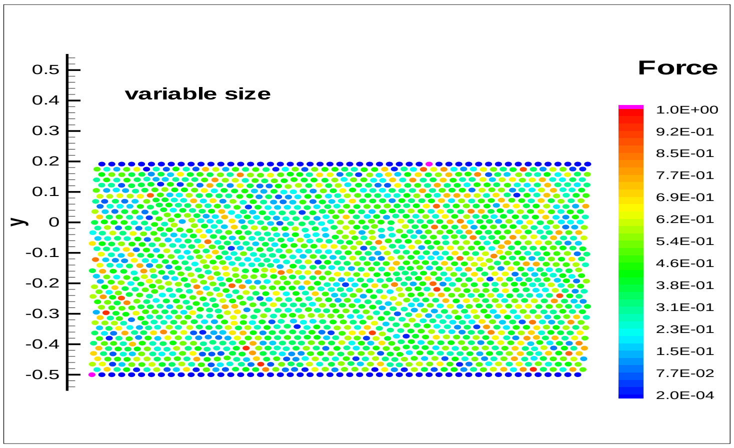

Figure 1: The (instantaneous) force experienced by the variable size particles; the volume fraction at the instant shown is approximately 0.9. The flow is driven by constant velocity motion of the upper wall in the $+x$ direction (left to right).

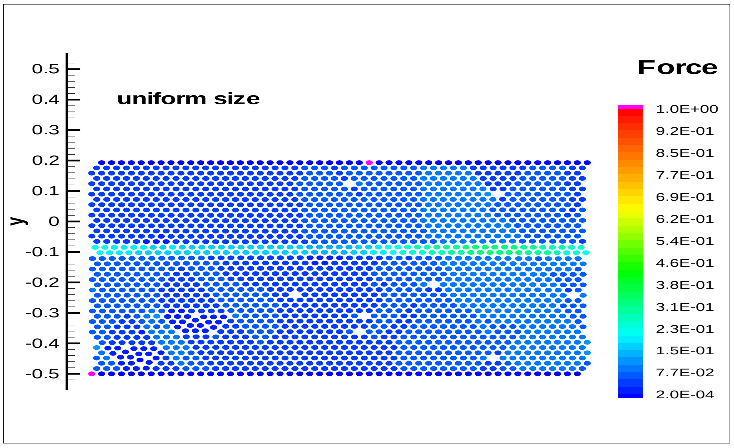

Figure 2: The force in the case of uniform size particles; all the other quantities are the same as in Fig. 1. Note formation of a shear band at $y \approx -0.1$; it should be mentioned that this particular shear band is just one of possible configurations characterizing the flow, and the manner in which the force propagates.

Session 4:
Multiphase Flow and Phase Change

FLUID DYNAMICS OF BUBBLY LIQUIDS

Y. H. Tsang, D. L. Koch
School of Chemical Engineering, Cornell University
Ithaca, NY 14853

A. Sangani
Department of Chemical Engineering, Syracuse University
Syracuse, NY 13244

ABSTRACT

Experiments have been performed to study the average flow properties of inertially dominated bubbly liquids which may be described by a novel analysis. Bubbles with high Reynolds number and low Weber number may produce a fluid velocity disturbance that can be approximated by a potential flow. We studied the behavior of suspensions of bubbles of about 1.5 mm diameter in vertical and inclined channels. The suspension was produced using a bank of 900 glass capillaries with inner diameter of about 100 μm in a quasi-steady fashion. In addition, salt was added to the suspension to prevent bubble-bubble coalescence. As a result, a nearly monodisperse suspension of bubble was produced. By increasing the inclination angle, we were able to explore an increasing amount of shear to buoyancy motion. A pipe flow experiment with the liquid beingrecirculated is under construction. This will provide an even larger range of shear to buoyancy motion. We are planning a microgravity experiment in which a bubble suspension is subjected to shearing in acouette cell in the absence of a buoyancy-driven relative motion of the two phases.

By employing a single-wire, hot film anemometer, we were able to obtain the liquid velocity fluctuations. The shear stress at the wall was measured using a hot film probe flush mounted on the wall. The gas volume fraction, bubble velocity, and bubble velocity fluctuations were measured using a homemade, dual impedance probe. In addition, we also employed a high-speed camera to obtain the bubble size distribution and bubble shape in a dilute suspension.

A rapid decrease in bubble velocity for a dilute bubble suspension is attributed to the effects of bubble-wall collisions. The more gradual decrease of bubble velocity as gas volume fraction increases, due to subsequent hindering of bubble motion, is in qualitative agreement with the predictions of Spelt and Sangani (1998) for the effects of potential-flow bubble-bubble interactions on the mean velocity. The ratio of the bubble velocity variance to the square of the mean is $O(0.1)$. For these conditions Spelt and Sangani predicted that the homogeneous suspension would be unstable and clustering into horizontal rafts will take place. Evidence for bubble clustering is obtained by analysis of video images. The liquid velocity variance is larger than would be expected for a homogeneous suspension and the liquid velocity frequency spectrum indicates the presence of velocity fluctuations that are slow compared with the time for the passage of an individual bubble. These observations provide further evidence for bubble clustering.

Inclination of the channel at angles between 2 to 10 degrees relative to gravity produces a variation in bubble volume fraction across the channel. The resulting buoyancy variation drives a shear flow in the channel and provides a means of observing the effects of weak shear on a bubbly liquid. The bubble velocity and volume fraction gradients increase with channel inclination and exhibit little or no dependence on the mean gas volume fraction. The tendency of buoyancy driven motion to cause the bubbles to accumulate on the upper wall is balanced by lift forces and by an effective bubble-phase diffusivity in the cross-channel direction. The bubble velocity gradient can be understood in terms of a balance of the component of the buoyancy force parallel to the channel walls and an effective viscosity associated with the Reynolds stresses produced by bubble-induced liquid velocity fluctuations. The effective viscosity required to explain the measured bubble velocity gradient is about 1000 times the viscosity of the suspending water. This magnitude is consistent with the liquid velocity fluctuations measured with the hot film anemometer.

In addition, we are studying the Reynolds number dependence of the average properties of the suspension by using a glycerin-water mixture. In a more viscous solution, the boundary layer may become thicker and the wake behind the bubble may become larger. As a result, vorticity may be created. A glycerin solution with a viscosity two times that of water will reduce the Reynolds number based on the bubble radius and the bubble terminal velocity by a factor of four to a value between 40 and 60 which is at the margin of the region for which the potential flow approximation is accurate.

A pipe flow apparatus with recirculation of the liquid has been designed and is under construction. This will provide a larger range of superficial liquid velocities (0.05 to 1 m/s) and liquid velocity gradients than can be achieved in the inclined channel. As a result, a stronger shear can be produced. This apparatus will allow us to study the bubble suspension where the liquid velocities will be of the same order of magnitude as the bubble rise velocity and the shear rates, γ, may approach U_t / a where U_t is the terminal bubble velocity and a the bubble radius. The ratio of the Reynolds number based on the pipe radius, R, to that based on a and γ scales like $(R / a)^2$. In order to study the suspension in the laminar regime and the bubbles being in the ignited state ($Re_a > 30$), and also to ensure a continuum suspension flow, a pipe ID of about 10 bubble diameters will be used. The pipe must have a large height (2.5 m) to ensure fully developed flow. A gas / water separator and a vent will be installed at the end of the test section where the gas will be vented to the atmosphere and the water will be recycled to the pipe entrance. A by-pass section with a pair of quick-closing and opening valves will be inserted between the test section and the separator in order to collect samples of suspension for measurement of the gas hold up. This will be used to calibrate the measurement of the gas volume fraction using the impedance probes. This new experimental setup will allow us to examine how the probes will respond when there is a significant mean liquid velocity.

The ground-based experiments will demonstrate the qualitative phenomenon of shear-induced, bubble-phase pressure that will be measured more quantitatively and in a more ideal setting in the microgravity experiment in which the effects of gravity and lift force will be eliminated.

MEASUREMENTS OF TURBULENCE ATTENUATION BY A DILUTE DISPERSION OF SOLID PARTICLES IN HOMOGENEOUS ISOTROPIC TURBULENCE

John K. Eaton and Wontae Hwang

Department of Mechanical Engineering
Stanford University
Stanford, California 94305
eaton@vk.stanford.edu, (v) 650-723-1971 (f) 650-723-4548

ABSTRACT

This research addresses turbulent gas flows laden with fine solid particles at sufficiently large mass loading that strong two-way coupling occurs. By two-way coupling we mean that the particle motion is governed largely by the flow, while the particles affect the gas-phase mean flow and the turbulence properties. Our main interest is in understanding how the particles affect the turbulence. Computational techniques have been developed which can accurately predict flows carrying particles that are much smaller than the smallest scales of turbulence. Also, advanced computational techniques and burgeoning computer resources make it feasible to fully resolve very large particles moving through turbulent flows. However, flows with particle diameters of the same order as the Kolmogorov scale of the turbulence are notoriously difficult to predict. Some simple flows show strong turbulence attenuation with reductions in the turbulent kinetic energy by up to a factor of five. On the other hand, some seemingly similar flows show almost no modification. No model has been proposed that allows prediction of when the strong attenuation will occur. Unfortunately, many technological and natural two-phase flows fall into this regime, so there is a strong need for new physical understanding and modeling capability.

Our objective is to study the simplest possible turbulent particle-laden flow, namely homogeneous, isotropic turbulence with a uniform dispersion of monodisperse particles. We chose such a simple flow for two reasons. First, the simplicity allows us to probe the interaction in more detail and offers analytical simplicity in interpreting the results. Secondly, this flow can be addressed by numerical simulation, and many research groups are already working on calculating the flow. Our detailed data can help guide some of these efforts. By using microgravity, we can further simplify the flow to the case of no mean velocity for either the turbulence or the particles. In fact the addition of gravity as a variable parameter may help us to better understand the physics of turbulence attenuation.

The experiments are conducted in a turbulence chamber capable of producing stationary or decaying isotropic turbulence with nearly zero mean flow and Taylor microscale Reynolds numbers up to nearly 500. The chamber is a 410 mm cubic box with the corners cut off to make it approximately spherical. Synthetic jet turbulence generators are mounted in each of the eight corners or the box. Each generator consists of a loudspeaker forcing a plenum and producing a pulsed jet through a 20 mm diameter orifice. These synthetic jets are directed into ejector tubes pointing towards the chamber center. The ejector tubes increase the jet mass flow and decrease the velocity. The jets then pass through a turbulence grid. Each of the eight loudspeakers is

forced with a random phase and frequency. The resulting turbulence is highly isotropic and matches typical behavior of grid turbulence.

Measurements of both phases are acquired using particle image velocimetry (PIV). The gas is seeded with approximately 1 micron diameter seeding particles while the solid phase is typically 150 micron diameter spherical glass particles. A double-pulsed YAG laser and a Kodak ES-1.0 10-bit PIV camera provide the PIV images. Custom software is used to separate the images into individual images containing either gas-phase tracers or large particles. Modern high-resolution PIV algorithms are then used to calculate the velocity field. A large set of image pairs are acquired for each case, then the results are averaged both spatially and over the ensemble of acquired images.

The entire apparatus is mounted in two racks which are carried aboard NASA's KC-135 Flying Microgravity Laboratory. The rack containing the turbulence chamber, the laser head, and the camera floats freely in the airplane cabin (constrained by competent NASA personnel) to minimize g-jitter. The floating rack with safety covers removed is shown in Figure 1. In a typical day of flying, we obtain quality data during about 20 of the 40 parabolas flown. Prior to taking off, a measured quantity of solid particles are loaded into the turbulence chamber. During the course of the experiments, there is attrition as particles become stuck in the corners of the box and in the synthetic jet actuators. For this reason, the particle mass loading for each image pair is calculated by the number of particles captured in the images. This increases the uncertainty in the particle loading. We are presently doing calibrations to reduce this uncertainty.

Results for 150 micron diameter particles are shown in Figure 2. The turbulent kinetic energy is reduced by approximately a factor of four for a mass-loading ratio of 0.3. It is interesting to note that the attenuation agrees closely with results from a parallel experiment on the centerplane of fully developed channel flow.

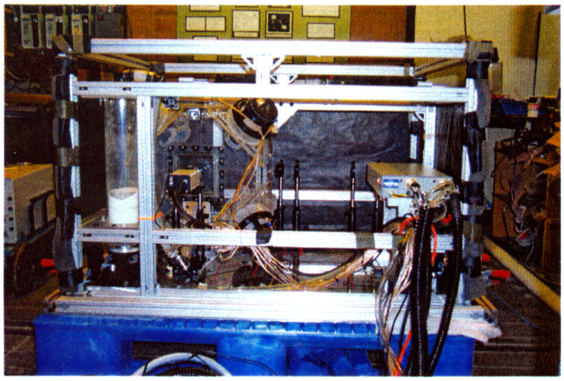

Figure 1. Free-floating rack

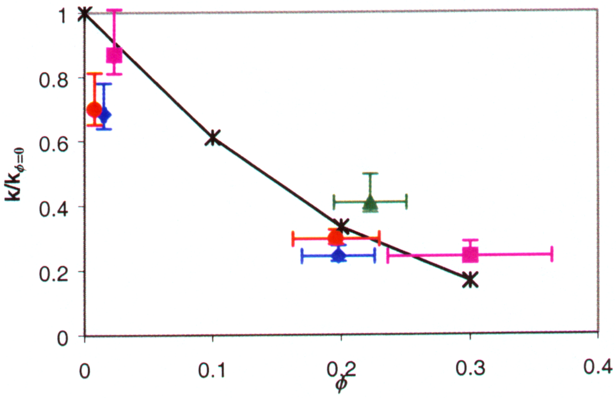

Figure 2. Attenuation of turbulent kinetic energy with 150 micron glass beads

A Mechanistic Study of Nucleate Boiling Under Microgravity Conditions

V. K. Dhir and G. R. Warrier
Mechancial and Aerospace Engineering Department
School of Engineering and Applied Science
University of California, Los Angeles
Los Angeles, CA 90095-1597
Ph: (310) 825-8507, Fax: (310) 206-4830
Email: vdhir@seas.ucla.edu

ABSTRACT

The overall objective of this work is to study nucleate boiling heat transfer under microgravity conditions in such a way that while providing basic knowledge of the phenomena, it also leads to development of simulation models ad correlations that can be used as design tools for a wide range of gravity levels. In the study a building block type of approach is used and both pool and low velocity flow boiling are investigated. Starting with experiments using a single bubble, the complexity of the experiments is increased to two or three inline bubbles, to five bubbles placed on a two-dimensional grid. Finally, experiments are conducted where a large number of prescribed cavities nucleate on the heater and when a commercial surface is used. So far experiments have been conducted at earth normal gravity and in the reduced gravity environment of the KC-135 aircraft whereas experiments on the space station are planned. Modeling/complete numerical simulation of the boiling process is an integral part of the total effort.

Experiments conducted with single bubbles formed on a nucleation site microfabricated on a polished silicon wafer show that for gravity levels (g) varying from $1.5g_e$ to $0.01g_e$, the bubble diameter at departure varies approximately as $(g_e/g)^{1/2}$ and the growth period as (g_e/g). When bubbles merge either inline or in a plane, the bubble diameter at departure is found to be smaller than that obtained for a single bubble and shows a weaker dependence on the level of gravity. The possible reason is that as the bubbles merge they create fluid circulation around the bubbles, which in turn induces a lift force that is responsible for the earlier departure of the bubbles. The verification of this proposition is being sought through numerical simulations. Figures 1a, 1b, and 1c, respectively show the merger of two inline, three inline, and several bubbles in a plane in the low gravity environment of the KC-135 aircraft. After merger and before departure, a mushroom type of bubble with several stems attached to the heater surface is clearly evident. Local heat fluxes during growth and departure of a single bubble were also measured. It was found that during most of the growth period of the bubble, generally the wall heat flux decreased with time because of the increased dry area under the bubble. However, the heat flux increased rapidly just prior to departure of the bubble because of the transient conduction into the cold liquid rushing to fill the space vacated by the

bubble as the bubble base shrinks. The measured heat fluxes at various radial locations are found to be in qualitative agreement with the numerical predictions.

Single bubble studies at earth normal gravity have also been performed on surfaces oriented at different angles to the gravitational acceleration with flow parallel to the surface. It is found that in all cases the bubbles slide along the surface before lift-off from the surface. The lift force generated as a result of the relative motion between the sliding bubbles and the imposed flow is found to play an important role when the normal force due to buoyancy is reduced. An experimental apparatus for the study of the bubble behavior with imposed flow under reduced gravity conditions has been developed and will soon be employed for experiments in the KC-135 aircraft.

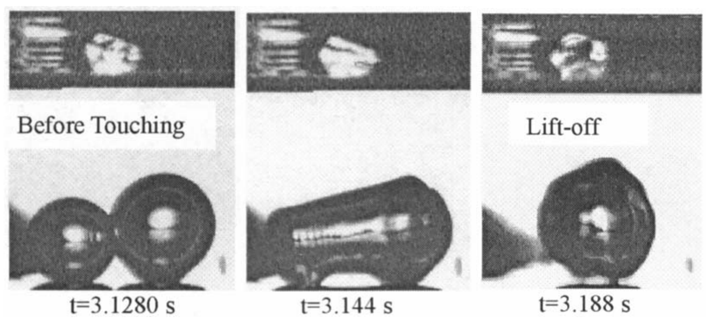

a. Two bubble merger.

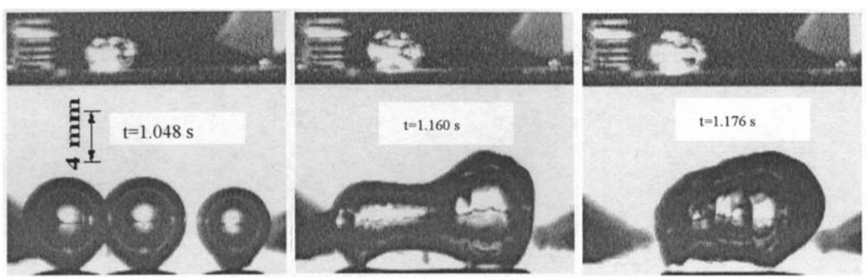

b. Three bubble merger.

c. Multiple bubble merger.

Figure 1. Photographs of bubble merger in the reduced gravity environment of the KC-135 aircraft with saturated water at one atmosphere pressure as the test liquid.

INVESTIGATION OF BODY FORCE EFFECTS ON FLOW BOILING CRITICAL HEAT FLUX

Issam Mudawar and Hui Zhang

Boiling and Two-phase Flow Laboratory
School of Mechanical Engineering, Purdue University
West Lafayette, IN 47907, USA
mudawar@ecn.purdue.edu
Fax: 765-494-0539
Tel: 765-494-5705

and

Mohammad M. Hasan

NASA Glenn Research Center
21000 Brookpark Road
Cleveland, OH 44135, USA

The bubble coalescence and interfacial instabilities that are important to modeling critical heat flux (CHF) in reduced-gravity systems can be sensitive to even minute body forces. Understanding these complex phenomena is vital to the design and safe implementation of two-phase thermal management loops proposed for space and planetary-based thermal systems. While reduced gravity conditions cannot be accurately simulated in 1*g* ground-based experiments, such experiments can help isolate the effects of the various forces (body force, surface tension force and inertia) which influence flow boiling CHF. In this project, the effects of the component of body force perpendicular to a heated wall were examined by conducting 1*g* flow boiling experiments at different orientations. FC-72 liquid was boiled along one wall of a transparent rectangular flow channel that permitted photographic study of the vapor-liquid interface at conditions approaching CHF. High-speed video imaging was employed to capture dominant CHF mechanisms. Six different CHF regimes were identified: Wavy Vapor Layer, Pool Boiling, Stratification, Vapor Counterflow, Vapor Stagnation, and Separated Concurrent Vapor Flow. CHF showed great sensitivity to orientation for flow velocities below 0.2 m/s, where very small CHF values where measured, especially with downflow and downward-facing heated wall orientations. High flow velocities dampened the effects of orientation considerably. Figure 1 shows representative images for the different CHF regimes.

The Wavy Vapor Layer regime was dominant for all high velocities and most orientations, while all other regimes were encountered at low velocities, in the downflow and/or downward-facing heated wall orientations. The Interfacial Lift-off model was modified to predict the effects of orientation on CHF for the dominant Wavy Vapor Layer regime. The photographic study captured a fairly continuous wavy vapor layer travelling along the heated wall while permitting liquid contact only in wetting fronts, located in the troughs of the interfacial waves. CHF commenced when wetting fronts near the outlet were lifted off the wall. The Interfacial Lift-off model is shown to an effective tool for predicting the effects of body force on CHF at high velocities.

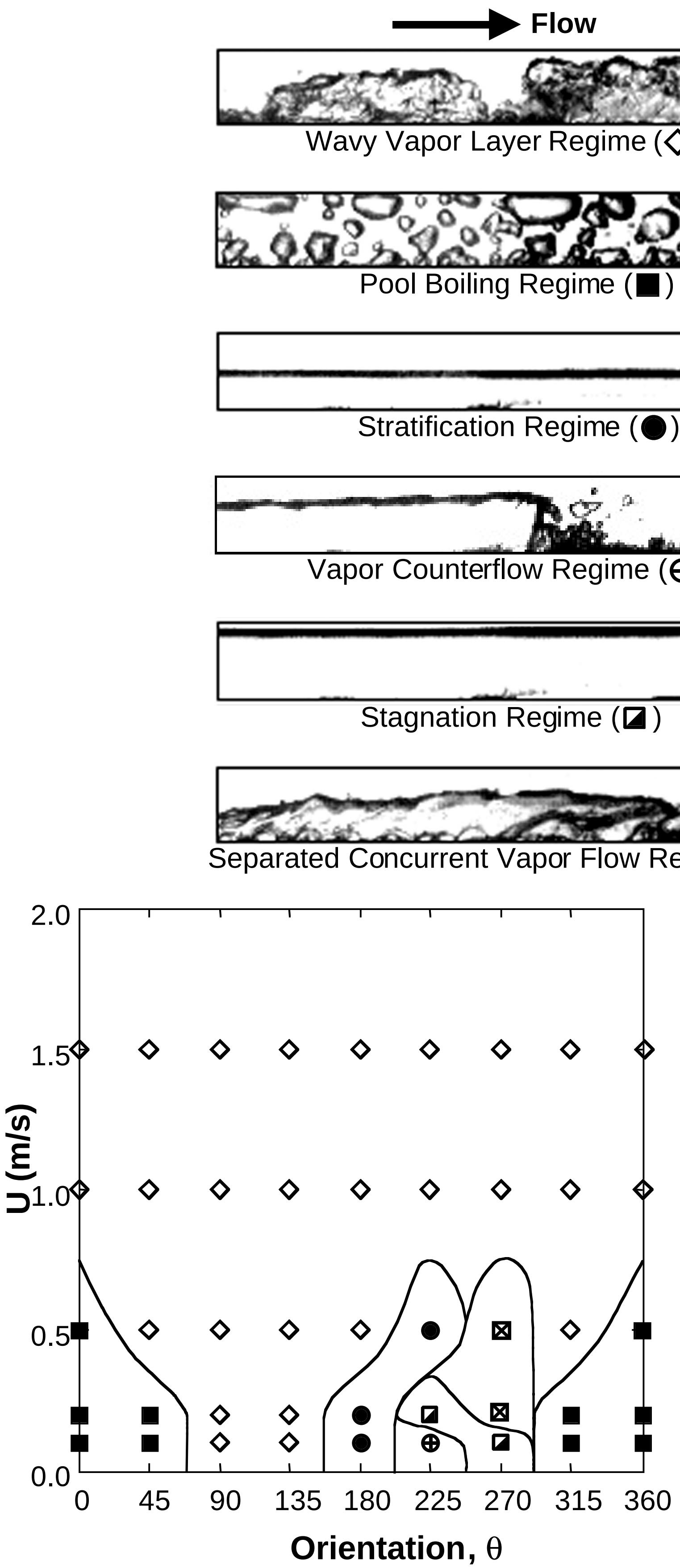

Figure 1 CHF regime map and representative flow characteristics for each regime.

LENGTH SCALE AND GRAVITY EFFECTS ON MICROGRAVITY BOILING HEAT TRANSFER

Jungho Kim and Christopher Henry
University of Maryland
Dept. of Mechanical Engineering
College Park, MD 20742

ABSTRACT

Boiling is a complex phenomenon where hydrodynamics, heat transfer, mass transfer, and interfacial phenomena are tightly interwoven. An understanding of boiling and critical heat flux in microgravity environments is of importance to space based hardware and processes such as heat exchange, cryogenic fuel storage and transportation, electronic cooling, and material processing due to the large amounts of heat that can be removed with relatively little increase in temperature. Although research in this area has been performed in the past four decades, the mechanisms by which heat is removed from surfaces in microgravity are still unclear. In earth gravity, buoyancy is an important parameter that affects boiling heat transfer through the rate at which bubbles are removed from the surface. A simple model describing the bubble departure size based on a quasi-static force balance between buoyancy and surface tension is given by the Fritz [1] relation:

$$Bo^{1/2} = 0.0208\,\theta$$

where Bo is the ratio between buoyancy and surface tension forces. For small, rapidly growing bubbles, inertia associated with the induced liquid motion can also cause bubble departure. In microgravity, the magnitude of effects related to natural convection and buoyancy are small and physical mechanisms normally masked by natural convection in earth gravity such as Marangoni convection can substantially influence the boiling and vapor bubble dynamics.

CHF is also substantially affected by microgravity. In 1-g environments, Bo has been used as a correlating parameter for CHF. Zuber's [2] CHF model for an infinite horizontal surface assumes that vapor columns formed by the merger of bubbles become unstable due to a Helmholtz instability blocking the supply of liquid to the surface. The jets are spaced λ_D apart, where

$$\lambda_D = 2\pi\sqrt{3}\left[\frac{\sigma}{g(\rho_l - \rho_v)}\right]^{1/2} = 2\pi\sqrt{3}L\,Bo^{-1/2} = \sqrt{3}\lambda_c$$

and is the wavelength that amplifies most rapidly. The critical wavelength, λ_c, is the wavelength below which a vapor layer underneath a liquid layer is stable. For heaters with Bo smaller than about 3 (heaters smaller than λ_D), the above model is not applicable, and surface tension effects dominate. Bubble coalescence is thought to be the mechanism for CHF under these conditions. Small Bo can result by decreasing the size of a heater in earth gravity, or by operating a large heater in a lower gravity environment. In the microgravity of space, even large heaters can have

low Bo, and models based on Helmholtz instability should not be applicable. The macrolayer model of Haramura and Katto [3] is dimensionally equivalent to Zuber's model and has the same dependence on gravity, so it should not be applicable as well. The goal of this work is to determine how boiling heat transfer mechanisms in a low-g environment are altered from those at higher gravity levels.

Boiling data using a microheater array was obtained under gravity environments ranging from 1.8 g to 0.02 g with heater sizes ranging from 2.7 mm to 1 mm. The boiling behavior for 2.7 mm at 0.02 g looked quite similar to boiling on the 1 mm heater at 1 g–the formation of a large primary bubble surrounded by smaller satellite bubbles was observed under both conditions. The similarity suggests that for heaters smaller than some fraction of l_c, coalescence and surface tension dominate boiling heat transfer. It also suggests that microgravity boiling can be studied by studying boiling on very small heaters.

[1] Fritz, W. (1935) "Berechnungen des Maximalvolumens von Dampfblasen", Phys. Z., Vol. 36, pp. 379-384.

[2] Zuber, N., (1959) "Hydrodynamics of Boiling Heat Transfer", AEC Report AECU-4439.

[3] Haramura, Y, and Katto, Y. (1983) "A New Hydrodynamic Model of the Ciritical Heat Flux, Applicable Widely to Both Pool and Forced Convective Boiling on Submerged Bodies in Saturated Liquids", Int. J. of Heat and Mass Transfer, Vol. 26, pp. 389-399.

Constrained Vapor Bubble Experiment

Peter C. Wayner, Jr., Joel L. Plawsky, Ling Zheng, and Ying-Xi Wang
Isermann Department of Chemcial Engineering
Rensselaer Polytechnic Institute
Troy, NY 12180

Microgravity experiments on the Constrained Vapor Bubble Heat Exchanger, CVB, are being developed for the International Space Station. In particular, we present results of a precursory experimental and theoretical study of the vertical Constrained Vapor Bubble in the Earth's environment. A novel non-isothermal experimental setup was designed and built to study the transport processes in an ethanol/quartz vertical CVB system.

Temperature profiles were measured using an in situ PC-based LabView data acquisition system via thermocouples. Film thickness profiles were measured using interferometry. A theoretical model was developed to predict the curvature profile of the stable film in the evaporator. The concept of the total amount of evaporation, which can be obtained directly by integrating the experimental temperature profile, was introduced. Experimentally measured curvature profiles are in good agreement with modeling results. For microgravity conditions, an analytical expression, which reveals an inherent relation between temperature and curvature profiles, was derived.

SEPARATION OF CARBON MONOXIDE AND CARBON DIOXIDE FOR MARS ISRU

M. Douglas LeVan and Krista S. Walton
Department of Chemical Engineering, Vanderbilt University
VU Station B 351604, Nashville, TN 37235
m.douglas.levan@vanderbilt.edu
Ph: (615) 322-2441 Fax: (615) 343-7951

John E. Finn
Astrobiology Technology Branch, M/S 239-15
NASA Ames Research Center, Moffett Field, CA 94035-1000

K. R. Sridhar
Department of Aerospace and Mechanical Engineering
The University of Arizona, P.O. Box 210016, Tucson, AZ 85721

ABSTRACT

Human Exploration and Development of Space will require the use of fundamental process technologies for gas storage and separation. These are enabling technologies. In our research, we are designing, constructing, and testing an innovative, robust, low mass, low power separation device that can recover carbon dioxide and carbon monoxide for Mars ISRU (in-situ resource utilization). The work has broad implications for gas storage and separations for gas-solid systems; these are ideally suited for reduced gravitational environments. The work is also important for robotic sample return missions using ISRU and in lunar oxygen production from regolith using carbothermal reduction. This paper describes our overall effort and highlights our results on adsorption equilibrium determination and process design. A second paper will provide details on adsorption equilibrium measurement and adsorbent selection.

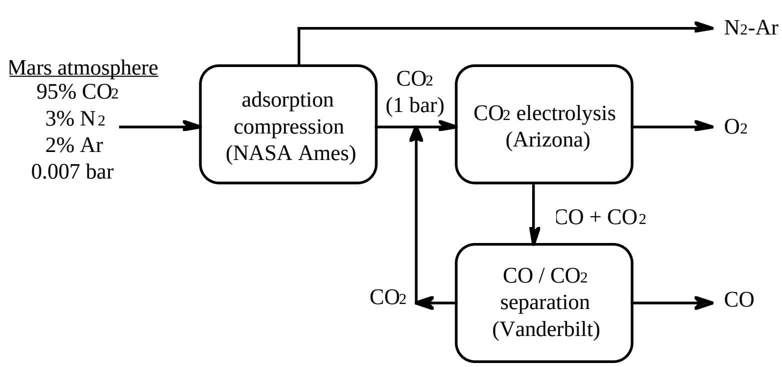

Figure 1: Flow diagram of a chemical system for conversion of Mars atmosphere to a N_2-Ar mixture and high-pressure CO_2, O_2, and CO.

As shown in Figure 1, this work is a collaborative effort involving the integration of an adsorption compressor developed at NASA Ames Research Center, a solid oxide electrolysis cell developed at the University of Arizona, and our separator. Solid oxide electrolyzers, such as electrolysis cells utilizing yttria-stabilized zirconia, can produce oxygen from planetary atmospheric carbon dioxide and reject carbon monoxide and unreacted carbon dioxide in a separate stream. The oxygen-production process is far more efficient if the high-pressure, unreacted carbon dioxide can be separated and recycled back into the feed stream. Additionally, the mass of the adsorption compressor can be reduced. Also, the carbon monoxide by-product is a valuable fuel for space exploration and habitation, with applications from fuel cells to production of hydrocarbons and plastics.

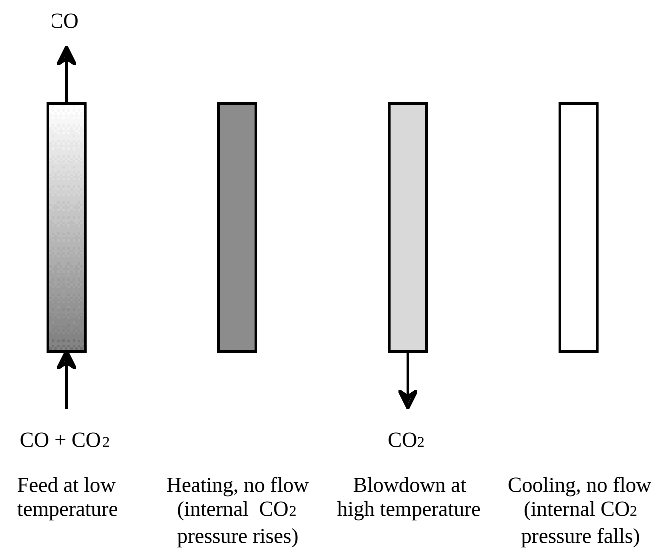

Figure 2: Four-step adsorption cycle for separation of CO and CO_2. CO is produced at the feed pressure (e.g., 1 bar); CO_2 product is expanded to a pressure determined by the zirconia cell's requirements.

Our separations cycle is shown in Figure 2. It combines concepts of temperature swing adsorption, pressure swing adsorption, and adsorption compression. The cycle will separate unreacted CO_2 such that it can be recycled back to re-feed the zirconia cell, permit essentially complete conversion of CO_2 to O_2 and CO in the integrated system, permit essentially complete recovery of CO, and be able to generate CO product at various purities.

With reference to the process steps shown in Figure 2, we seek an adsorbent high in CO_2 capacity and low in CO capacity, but which will release the CO_2 at elevated temperatures as pressure is reduced. We have measured pure component adsorption equilibrium for CO_2 and CO on many adsorbents using a gravimetric system. We have measured binary adsorption equilibrium for CO/CO_2 on the most promising adsorbents over wide temperature ranges using a volumetric system. We have developed process models for the cycle and are constructing the proof-of-concept CO/CO_2 separator. These will all be discussed.

Exposition Session
Topical Area 1:
Colloids and Soft Condensed Matter

Nonlinear Theory of Void Formation in Colloidal Plasmas

A. Bhattacharjee
University of Iowa

A colloidal (or dusty) plasma is an electron-ion plasma containing a dispersed phase of micron-size solid particles. In typical plasma conditions, these particles usually acquire a large negative charge. As a result of the strong Coulomb coupling between the dust particles, a colloidal plasma may undergo phase transitions and exist in a liquid or a crystalline state. Recently, a number of colloidal plasma experiments, in laboratory as well as under microgravity conditions, have shown the spontaneous development of voids. A void is typically a small and stable centimeter-size region (within the plasma) that is completely free of dust particles and characterized by sharp boundaries. In the laboratory, the void is seen to develop from a uniform dust cloud as a consequence of an instability when the dust particle has grown to a sufficient size. The instability is first seen as a so-called filamentary mode, which exhibits a sudden onset. The filaments take the form of beam-like striations in the dust density and glow. The spectrum of the filamentary mode is observed to be broadband, with a peak at about 100 Hz. After onset, the filaments are seen to evolve rapidly (in about 10 ms) to a nonlinear saturated state containing a single void.

Theoretical analyses have confirmed that the ion drag force plays a crucial role in causing the initial instability. These analyses fall into two types: linear stability analyses that include the effect of ion drag, and nonlinear but steady-state analyses that yield void solutions. As yet, there appears to be no nonlinear time-dependent model that describes the spontaneous development of the linear instability and its subsequent saturation to produce a void.

In this paper we propose a basic, time-dependent, self-consistent nonlinear model for void formation in a dusty plasma. This basic model contains three elements: (a) an initial instability caused by the ion drag, (b) a nonlinear saturation mechanism for the instability, and (c) the void as one of the possible nonlinearly saturated states, dynamically accessible from the initially unstable equilibrium. For the initial instability we consider a simple variant of a zero-frequency mode, caused by the ion drag The saturation mechanism we adopt is relevant for collisional voids where ions achieve near-thermal velocities in the void region. In this regime, the ion drag force initially increases with the ion fluid velocity, attains a maximum when the ion fluid velocity equals the ion thermal velocity, and decreases when the ion fluid velocity exceeds the ion thermal velocity. As the linear instability grows, the ions are initially accelerated in the growing electric field, and the ion drag force initially increases. Eventually, as the ions are accelerated to speeds larger than the ion thermal speed, the ion drag force decreases to balance the electric field and thus saturate the instability. We demonstrate by analysis and numerical simulation that in the saturated state, a stable void is formed.

Prediction of Particle Clustering in Turbulent Aerosols

Jaehun Chun[1], *Aruj Ahluwalia*[2], *Donald Koch*[1] *and Lance R. Collins*[3]
[1]School of Chemical Engineering
Cornell University
Olin Hall
Ithaca, NY 14853
[2]Department of Chemical Engineering
Penn State University
102 Fenske Building
University Park, PA 16802
[3]Sibley School of Mechanical & Aerospace Engineering
Cornell University
246 Upson Hall
Ithaca, NY 14853

It has long been recognized that heavy particles in the micron size range embedded in a turbulent flow field are thrown out of regions of high vorticity and collect in regions of high strain. This particle clustering has a profound effect on processes such as collision, coalescence and evaporation/condensation. For example, recent work in the meteorology community suggests this effect may play an important role in the evolution of droplet nuclei in cumulus clouds. A recent study by Reade & Collins (2000) showed that the tendency of particles to cluster continues down to length scales much smaller than the Kolmogorov scale. Indeed, the particle pair correlation function was shown to increase as a power law of the inverse of the particle pair separation distance indefinitely (or at least until the finite particle size cuts it off). The traditional explanation of particle clustering based on the 'centrifuge' effect cannot explain this sub-Kolmogorov scale clustering. Motivated by this observation, we have developed an analytical theory for the pair correlation function for particles with a small but finite Stokes number. The theory treates the particle dynamics as a Markov process, in which a drift is generated by the tendency of particle pairs to occupy regions of higher strain than vorticity. This drift is opposed by turbulent diffusion, which turns out to be a nonlocal process due to the finite correlation length of the fluctuations. The theory predicts a power law for the pair correlation function that is in good agreement with direct numerical simulations and stochastic simulations of the velocity gradient following a particle trajectory. The theory does not predict the Reynolds number dependence of the pair correlation function directly (an important issue in the cloud physics problem), but relates it to the Reynolds number dependence of Lagrangian velocity statistics. These were studied over the limited range of Reynolds numbers that can be achieved in the direct numerical simulations; the results suggest a saturation of the effect at high Reynolds number, in agreement with recent high-Reynolds-number simulations of particle populations (Keswani & Collins 2002).

STUDIES OF ISLANDS ON FREELY SUSPENDED BUBBLES OF SMECTIC LIQUID CRYSTAL

A. Pattanaporkratana, B. Mavel, C. S. Park, J. E. Maclennan, and N. A. Clark

Department of Physics and Ferroelectric Liquid Crystal Materials Center, University of Colorado, Boulder, CO 80309 U.S.A.

We have constructed an optical system for observing the internal structure of freely suspended smectic liquid crystal bubbles using a reflected light microscope. Liquid crystal bubbles can have thicker circular regions (islands) which can easily be generated by shrinking the bubble diameter. The diameter of these islands is ~ 10 μm and they are typically up to five times thicker than the surrounding liquid crystal film (500 Å). In the Laboratory, the location of the islands is strongly influenced by gravity, which causes the majority of islands to migrate to the bottom half of the bubble.

We will describe the size and thickness distributions of islands and their time evolution, and also discuss two-dimensional hydrodynamics and turbulence of smectic bubbles, the shapes of islands and holes affected by bubble vibrations, and the interactions between islands, which we have probed using optical tweezers.

*This research is supported by NASA Grant NAG3-1846

Figure. 1. Islands on Bubble Surface

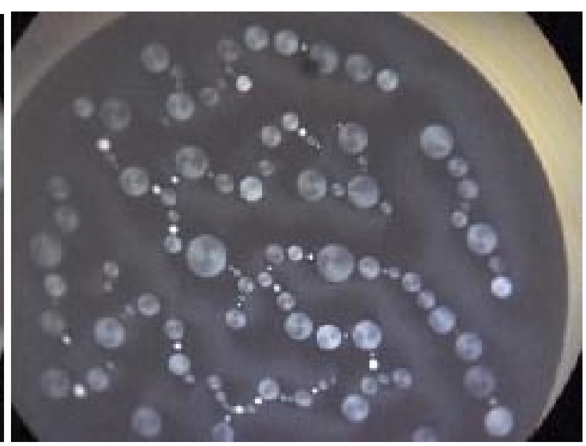

Figure 2. Large Aggregates: a long time after the sample preparation

Compression of Paramagnetic Colloidal Chains

Daniel J. Smith
Department of Chemical Engineering
Massachusetts Institute of Technology
Cambridge, MA 02139

Alice P. Gast
Department of Chemical Engineering
Massachusetts Institute of Technology
Cambridge, MA 02139

Phone: (617) 253-1403
FAX: (617)-253-8388
Email: gast@mit.edu

Abstract

The electric or magnetic field-induced aggregation of polarizable particles produces a rapid rheological transition known as electrorheological (ER) or magnetorheological (MR) response. The ability to tune these interactions with an external field makes them attractive for feedback-controlled devices such as shock absorbers and suspension systems. In response to an applied magnetic field, paramagnetic colloidal suspensions aggregate into anisotropic microstructures that produce the bulk rheological response. The microstructure is composed of chains, columns of chains and chain networks. The deformation and rupturing of this microstructure leads to a finite yield stress for the suspension. In this work, we investigate the strengths and interactions of chains and columns of chains to compression parallel to the applied magnetic field with optical tweezers.

Optical trapping is used to manipulate the microstructure and to measure the forces resisting its distortion. The iron oxide present in the particles prevents us from trapping them directly, so we use a tether-handle system utilizing latex particles attached to the magnetic particles via the biotin-streptavidin binding reaction.

Using optical traps, we explore the response of single chains and columns of chains to compression. We find that chains bend and undergo reorganization processes before their ultimate failure due to rupture. We believe that these reorganization events are key mechanisms of stress reduction. Columns of chains exhibit the same mechanisms, but higher forces are required for both the rearrangements and column failure. This strengthening is caused by the enhanced local field due to additional magnetized particles and the additional strength of the column due to the multiple chain interactions. We show how these studies provide mechanistic explanations of magnetic suspension rheology. We model the microstructures and forces through numerical simulations.

DIFFUSIVE COARSENING OF LIQUID FOAMS IN MICROGRAVITY

Igor N. Veretennikov and James A. Glazier
Department of Physics, University of Notre Dame, Notre Dame, IN 46556

Our main goal is to simulate, to some extent, microgravity conditions in the presence of gravity, to check the stages of a proposed scenario for coarsening of "space" foams, and to determine relations between foam structure and wetness and rheological properties. Our current focus is on preliminary experiments needed for MRI studies of stabilized foam: optimization of the foam's composition, of imaging parameters and the investigation of foam stability against global convection.

To mimic foam behavior under microgravity, we stabilize the foam by supplying extra fluid on the top of the foam head. While this fluid increases the MRI signal, it also creates some extra problems. Although the Plateau borders have no breaks and are well resolved, the image is noisy and difficult to analyze. Noise sources include: 1) higher water content increases the signal from the membranes, which registers as noise since the membranes remain unresolved. 2) The extra flow in the membranes creates ghosts in the images due to phase errors. 3) The weak signal from the Plateau borders is averaged over a large voxel volume. To understand the relative importance of each noise source and to find an effective way to eliminate or reduce it, we conducted several series of experiments with solid gelatin-based foams. We make the foam from a heated gelatin-water solution and cool it immediately after foam generation.

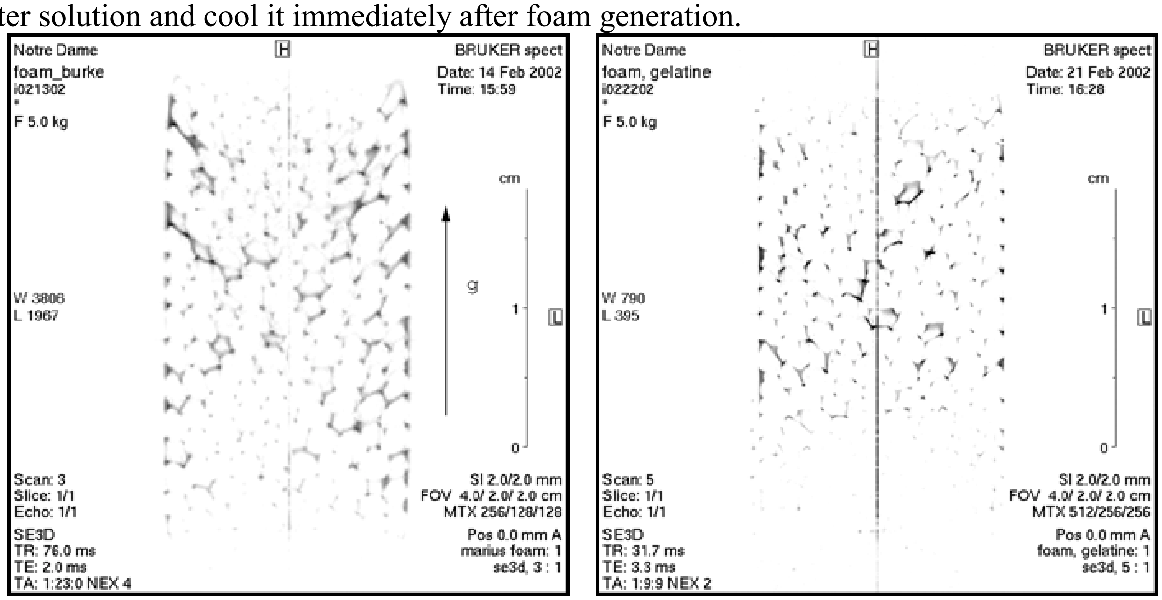

Then we image the resulting motionless foam using various imaging parameters. Figure 1a shows a sample central slice from a 256x128x128 MRI image. Some noise is still present, especially in the central part, where Plateau borders are thinner, suggesting that "partial volume" artifact is important. The 512x256x256 image of the same foam in Figure 1b has twice the spatial resolution (below 100 μm, which is below the Plateau border thickness) and is completely noise-free. We will use such clean images as real test data for our 3D data analysis algorithm.

Another interesting phenomenon in images of solidified foams (especially apparent in Figure 1a) is the presence of "lines" of increased gelatin content, inclined at about 45^{o} from the vertical and directed from the tube axis to the wall. They seem to appear during solidification of the gelatin and are related to the stress distribution in the solidifying foam. In liquid foams, we never see anything similar. Examining this effect in more detail may be important for solid foam production.

"Stabilized" foams are convectively unstable if the flow rate exceeds some critical value. We have carried out extensive experimental studies of these instabilities to avoid convection during MRI imaging. CMC-water solutions with different CMC concentrations and different surfactants were used as basic fluids. Foam was generated in a glass cylinder 50 cm long with an inner diameter of 45 mm. After foam equilibration, we increased the flow rate slowly in small increments until the foam began to move. We define the critical flow rate as the flow rate at which global convection, which affects every bubble, starts. The critical flow drops very fast with increasing viscosity, and remains almost constant when viscosity is higher than about 8 cPoise. It is almost independent of the chemical composition of the surfactant. Figure 2 shows the critical flow rate data. While the physical mechanism of these instabilities remains unclear, the most surprising result was our detection of a compression wave that precedes a melting wave. Foam melting occurs at a local wetness level well below the expected 35%. The flow through membranes is significant, not negligible.

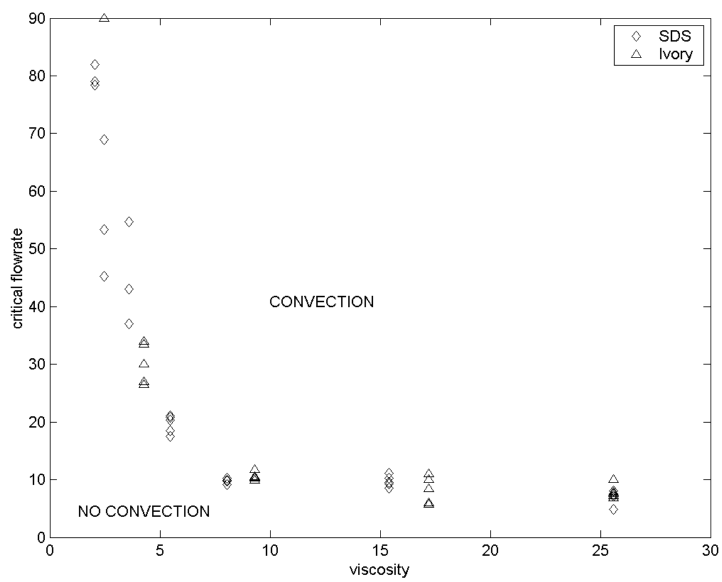

This convective instability may seriously affect our proposed scenario for the aging of "space foam." Our preliminary analysis of experimental data suggests that there are two critical parameters – the membrane thickness (which directly relates to the local foam wetness) and the shear rate (specified by the basic fluid viscosity, bubble size and transverse fluctuations in pressure) determining the instability onset. During the aging of "space foam," we expect both average bubble size and membrane thickness to increase. Hence, at some stage, the pressure fluctuations (caused, for example, by bubble disappearance) may induce global convection. The latter, in turn, should affect the bubble size distribution in a way similar to that observed in our earth-based experiments: strong convection leads to very homogeneous foam.

PI: Prof. James A. Glazier, 225 Nieuwland Science Hall, Department of Physics, University of Notre Dame, In 46556, email: jglazier@rameau.phys.nd.edu, fax: (574)-631-5952, phone: (574)-631-4010

KINETICS AND PERCOLATION IN DENSE PARTICULATE SYSTEMS

Chris Sorensen and Amit Chakrabarti
Department of Physics, Kansas State University, Manhattan, KS 66506-2601

ABSTRACT

Our work involves both experimentation and simulation of aggregating particle systems that form fractal aggregates that eventually fill space to form gels. Our experimental system is soot in diffusion flames. Our simulations model these flames as 3d, off lattice, Brownian motion systems, also known as diffusion limited cluster aggregation (DLCA). We observe in these systems the behavior of the kinetics, cluster size distribution, and cluster morphology as the system evolves from dilute to concentrated and finally to the gel.

With simulations, we find that the dynamical evolution of the system obeys typical DLCA type kinetics at early times when the system is dilute with a constant kinetic exponent z=1 and size distribution exponent λ=0. With increasing aggregation time crowding of clusters occurs and the kinetics can be described by continuously evolving exponents. Both exponents show universal behavior with aggregate volume fraction, independent of the initial volume fraction. Remarkably, the relationship between z and λ maintains it's mean-field nature i.e., mean field kinetics continue to hold when the system is crowded.

Small angle light scattering from heavily sooting flames shows submicron $D \simeq 1.8$ fractal aggregates early in the flame but later, as the soot growth continues, a new supermicron phase appears with a fractal dimension of ca. 2.7. Simulations show essentially the same behavior and allow us to determine that these superaggregates occur when the smaller, $D \simeq 1.8$ DLCA aggregates percolate. With this, we propose the following picture of the sol-to-gel transition: A dilute sol aggregates via DLCA or RLCA kinetics yielding aggregates with fractal dimensions of $D \simeq 1.8$ or 2.15, respectively. Because these aggregate fractal dimensions are less than the spatial dimension, the effective aggregate volume fraction (the occupied volume of the aggregates normalized by the system volume) approaches unity as the aggregation proceeds. Structure factor results for the largest cluster and the entire system imply that the fractal dimension of the aggregates remains 1.8 (or 2.15 for RLCA) right up to the ideal gel point. At the ideal gel point, the aggregates are so crowded that they percolate to form a $D \simeq 2.6$ *superaggregate* made up of $D \simeq 1.8$ (or 2.15 for RLCA) aggregates with an average size of $R_{g,G}$, the ideal gel point radius of gyration.

LOCAL PERTURBATIONS OF JAMMED COLLOIDS

Eric R. Weeks*, Piotr Habdas, David Schaar, and Andrew C. Levitt
Physics Department, Emory University, Atlanta, GA 30322

ABSTRACT

We use confocal microscopy to directly study the microscopic behavior of colloidal glasses and colloidal supercooled liquids. In particular we embed superparamagnetic particles into the system of non-magnetic PMMA colloids and then exert an external magnetic force on these particles to locally perturb the sample in a controlled manner. We investigate the range of these perturbations as a function of magnetic particle size, magnetic force, and colloidal particle concentration, in samples approaching the colloidal glass transition. The results of such studies address broader issues of both a universal description of the origin of the glass transition and also the flow of granular media studied by other groups.

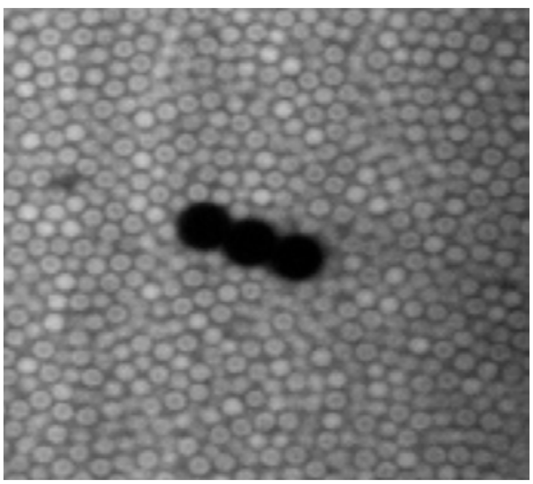

Three superparamagnetic particles stuck together, embedded in a sample of 2 micron diameter colloidal particles. The magnetic chain is rotated using an external magnetic field, and the motion of the other particles is examined. In these pictures, the chain is rotating at 1.25 rev/hr.

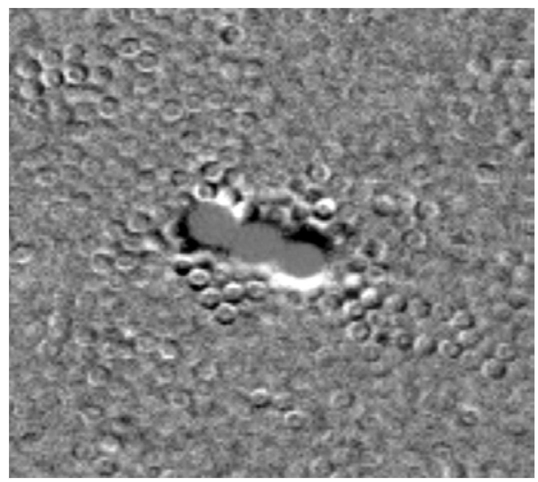

Two images are taken 1 min apart, and subtracted. Black or white regions indicate where the two pictures differ, highlighting the regions where particles are moving.

Movies can be seen at:
http://www.physics.emory.edu/~weeks/lab/

* weeks@physics.emory.edu, phone: 404-727-4479, fax: 404-727-0873

Exposition Session
Topical Area 2:
Fluid Physics of Interfaces

INSTABILITY OF MISCIBLE INTERFACES

R. Balasubramaniam, N. Rashidnia, M.J. Boggess, R.T. Schroer
National Center for Microgravity Research on Fluids and Combustion,
NASA Glenn Research Center, Cleveland, Ohio,
T. Maxworthy
University of Southern California, Los Angeles,
and
R.G. Wilson and J.I.D. Alexander
Case Western Reserve University, Cleveland, Ohio

Abstract

The dynamics of miscible displacements in a cylindrical tube is being studied experimentally and numerically, specifically when a more viscous fluid displaces a less viscous fluid. In the converse situation where a less viscous fluid displaces a more viscous fluid, a fingering instability is known to occur (Petitjeans and Maxworthy, 1996), and a flight experiment proposed by Maxworthy and Meiburg to investigate the interface dynamics in this case is currently being developed by NASA.

From the current theory of miscible displacements, developed for a porous medium satisfying Darcy's law (see review by Homsy, 1987), it can be shown that in the absence of gravity the interface between the fluids is destabilized and thus susceptible to fingering only when a more viscous fluid is displaced by a less viscous one. Therefore, the initial flat interface in the displacement of a less viscous fluid by a more viscous one ought to be stable. However, numerical simulations by Chen and Meiburg (1996) for such displacement in a cylindrical tube show that for a viscosity ratio equal to e, a finger of the more viscous fluid is indeed formed. These calculations were restricted to axisymmetric solutions of the Stokes equations that are valid for negligible values of the Reynolds number.

We report on the experiments that we have conducted to date when a more viscous fluid displaces a less viscous one in a vertical cylindrical tube. The experiments show that not only can a finger form in this instance but also that under certain conditions the advancing finger achieves a sinuous or snake-like spatial pattern. These experiments were performed using silicone oils in a vertical pipette of small diameter. The more viscous fluid also has a slightly larger density than the less viscous fluid. In the initial configuration, the fluids were under rest, and the interface was nominally flat. Both stably and unstably stratified initial configurations were studied. A dye was added to the more viscous fluid for ease of observation of the interface between the fluids. The flow was initiated by pumping the more viscous fluid into the less viscous one. The displacement velocity was such that the Reynolds number is small compared to one, and the Peclet number for mass transfer among the fluids is large compared to one. The gravitational effects are represented by the dimensionless parameter $F = \frac{g\Delta\rho d^2}{\mu U}$ where g is the acceleration due to gravity, $\Delta\rho$ is the density difference between the fluids, d is the tube diameter, μ is the viscosity of the more viscous fluid, and U is the displacement speed.

For the downward displacement of a more viscous fluid resting on the top of a less viscous fluid (*i.e.* an unstably stratified initial configuration), the experiments show that an axisymmetric finger is formed when the value of F is smaller than a critical value F_c. When $F > F_c$, the finger achieves a sinuous spatial pattern. The spatial pattern is not a helical three dimensional pattern, and appears to be two dimensional. Experiments are in progress to obtain F_c as a function of the viscosity ratio of the fluids.

For an upward displacement of the more viscous fluid from an initially stable configuration, only an axisymmetric finger is observed under all conditions. When F is small, the effect of gravity is small and the shape of the finger is qualitatively similar to that observed for downward displacement. For a larger value of F, the finger has a blunt shape. However, a needle shaped spike is seen to propagate from the main finger, similar to that observed by Petitjeans and Maxworthy (1996).

Numerical simulations of the miscible displacement process, starting from an initially flat interface, are in progress. The goal is to identify the conditions when the interface achieves a sinuous shape. When such a shape is computed, we will compare the onset condition and the post onset wavelength to experimental results. The computations will involve time accurate three dimensional simulations of the momentum and mass transport equations. Joseph and Renardy (1993) show that, in general, one must consider the following effects in the mixing region (i) a non-vanishing of the divergence of the velocity field caused by density changes of a fluid element due to diffusion (ii) Korteweg stresses, which accounts for forces in the fluids caused by concentration gradients. We will perform computations without and with these effects, for various values of the system parameters, chiefly the F parameter, the viscosity and density ratio, the Peclet number for mass transport and non-dimensional parameters associated with the Korteweg stresses. The Reynolds number will be small compared to one; however, we will retain the non-linear inertial terms in the momentum equations recognizing that they might be important in predicting the complex interface shapes.

References

Chen, C.H. and Meiburg, E. 1996. Miscible displacements in capillary tubes. Part 2. Numerical simulations. *J. Fluid Mech.*, **326**, 57-90.

Homsy, G.M. 1987 Viscous fingering in porous media. *Ann. Rev. Fluid Mech.*, **19**, 271.

Joseph, D.D. and Renardy, Y. 1993. Fundamentals of Two-Fluid Dynamics. Springer-Verlag.

Petitjeans, P. and Maxworthy, T. 1996. Miscible displacements in capillary tubes. Part 1. Experiments. *J. Fluid Mech.*, **326**, 37-56.

The effect of flow on drop coalescence

Martin Nemer,[1] Xiaohui Chen,[1] Jerzy Bławzdziewicz,[2] and Michael Loewenberg[1]

[1]*Chemical Engineering, Yale University, New Haven, CT 06520*

[2]*Mechanical Engineering, Yale University, New Haven, CT 06520*

Drop coalescence is a complex process due to the nonlinear dynamics of a system with deformable interfaces. In earlier studies the effect of an external flow on near-contact motion of drops was assumed to be equivalent to an external body force [1–3]. Accordingly, the direct coupling between thin-film flow (in the near-contact region) and flow inside the drops was neglected. These assumptions have been used in calculations of collisional efficiencies [4] and analyses of experimental results [5–7].

Our investigations show that for drops with tangentially mobile interfaces the above assumptions do not hold. The velocity field produced inside the drops by the external flow couples to the film motion through tangential stress f_∞ acting on the film interface. For sufficiently thin films (e.g., long times), this stress qualitatively alters the dynamics of the lubrication region by arresting or enhancing film drainage.

Scaling analysis The effect of an external flow on drop motion can be understood by considering the magnitude of the stress f_∞. The external flow varies on the length scale of the drop diameter a and vanishes at the axis of symmetry of the film, thus

$$f_\infty \sim \mu \dot{\gamma} r_\infty / a. \tag{1}$$

Here μ is the drop viscosity, r_∞ is the lateral dimension of the thin film, and $\dot{\gamma}$ is the magnitude of the external flow. For given external flow and force, the pressure gradient in the film p' and lateral dimension r_∞ are nearly independent of film thickness h. It thus follows that

$$f_\infty \sim hp' \tag{2}$$

for sufficiently small h. Hence, external-flow-induced stress f_∞ affects the thin film behavior.

Numerical results These predictions are illustrated in Fig. 1, where results form axisymmetric boundary-integral simulations are shown for two drops with a constant interfacial tension σ. The drops are immersed in an external creeping flow field $\mathbf{u}_{\dot{\gamma}} = \dot{\gamma}(\frac{1}{2} r\hat{\mathbf{e}}_r - z\hat{\mathbf{e}}_z)$ or subjected to body forces $\mathbf{F}_i^{\mathrm{e}} = F_i^{\mathrm{e}} \hat{\mathbf{e}}_z$, where $i = 1, 2$.

For drops in straining flow, the flow-induced stress f_∞ is directed toward the symmetry axis; in this case, at long times a stationary film profile is attained. For drop motion driven by the external forces, f_∞ is directed away from the symmetry axis, and the film drains exponentially with time. In contrast to the above results, in the absence of flow-induced stresses ($f_\infty = 0$) the film has algebraic long-time behavior [8].

Asymptotic analysis For sufficiently weak external flow and force, drops are nearly spherical (except in the near-contact region), and the extent of the thin film is small. In this regime, the hydrodynamic forces F_i^{H} acting on the drops and the interfacial stress f_∞ were calculated by solving the outer problem of two tangential spherical drops in an external flow. The lubrication equations for the inner thin-film region, with boundary conditions

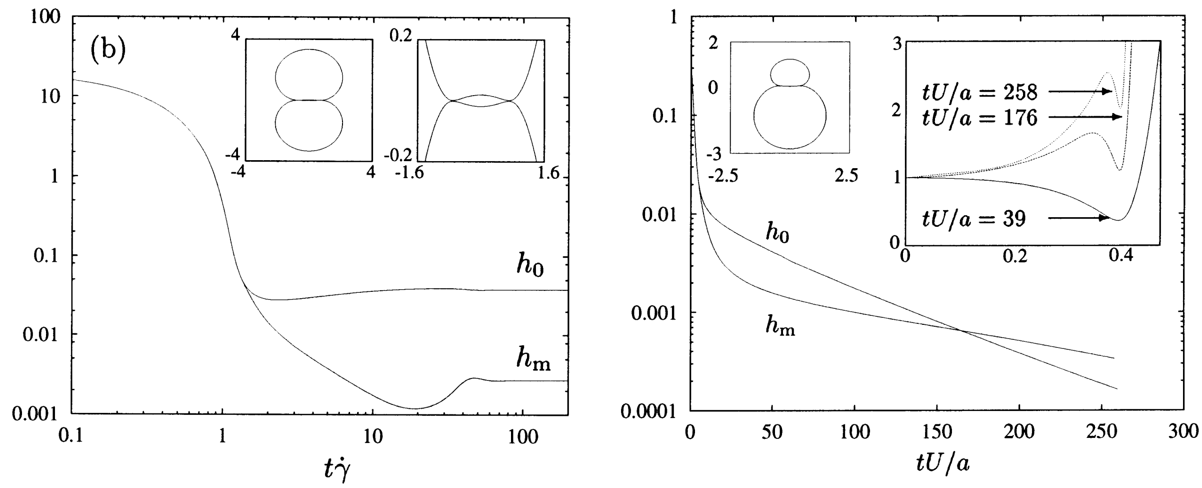

FIG. 1: Central and minimal gap versus time for (a) equal-size drops in straining flow with $\dot{\bar{\gamma}} = 0.02$ and no body force, and (b) drops with size ratio $k = 2$, driven by body forces $\bar{F}_1^e = \frac{1}{3}\pi$, $\bar{F}_2^e = \frac{4}{3}\pi$, and no external flow. Here $\dot{\bar{\gamma}} = \mu\dot\gamma a/\sigma$ and $\bar{F}_i^e = F_i^e/(\sigma a)$.

corresponding to the values of F_i^{H} and f_∞ calculated as described above, were solved by a matched-asymptotics method to obtain the long time stationary film profile. For two drops pushed together by an external flow, our asymptotic solution yields

$$h_0 \sim \dot{\bar{\gamma}}^{3/2}, \qquad h_{\mathrm{m}} \sim \dot{\bar{\gamma}}^3 \tag{3}$$

for the central and minimal stationary gaps.

Conclusions We have shown that external flow can arrest or enhance drainage of a thin film separating drops in near-contact motion. The effect of flow remains finite even for small capillary numbers, provided that the film thickness is sufficiently small. Therefore, this effect needs to be included in predictions of collisional efficiencies and interpretation of experimental data. Our analysis is also applicable to thin-film flows that involve Marangoni or thermocapillary stresses.

[1] A. F. Jones and S. D. R. Wilson, J. Fluid Mech. **87**, 263 (1978).
[2] S. G. Yiantsios and R. H. Davis, J. Colloid Interface Sci. **144**, 412 (1991).
[3] A. Saboni, C. Gourdon, and A. K. Chesters, J. Colloid Interface Sci. **175**, 27 (1995).
[4] M. A. Rother, A. Z. Zinchenko, and R. H. Davis, J. Fluid Mech. **346**, 117 (1997).
[5] X. Zhang, R. H. Davis, and M. F. Ruth, J. Fluid Mech. **249**, 227 (1993).
[6] M. Magna and H. A. Stone, J. Fluid Mech. **300**, 231 (1995).
[7] H. Yang, C. C. Park, Y. T. Hu, and L. G. Leal, Phys. Fluids **13**, 1087 (2001).
[8] M. B. Nemer, X. Chen, J. Bławzdziewicz, and M. Loewenberg, Bull. Am. Phys. Soc. **46**, 140 (2001).

Dynamics of Surfactant-Laden Drops in a Hele-Shaw Cell

Nivedita R. Gupta[1], Ali Nadim[2], Hossein Haj-Hariri[3], Ali Borhan[4]

[1]Dept. of Chem. Eng., Univ. of New Hampshire, Durham, NH 03824
[2]Keck Graduate Inst. & Claremont Graduate Univ., Claremont, CA 91711
[3]Dept. of Mech. Eng., Univ. of Virginia, Charlottesville, VA 22903
[4]Dept. of Chem. Eng., Pennsylvania State Univ., University Park, PA 16802

Buoyancy-driven motion of a liquid drop in a Hele-Shaw cell filled with a second immiscible liquid is considered. In the absence of surfactants, a circle is an exact solution to the depth-averaged Hele-Shaw equations. A circular drop is shown to be linearly stable to infinitesimal shape perturbations provided the interfacial tension is finite. The evolution of the shape of a translating drop subject to finite initial shape deformations is studied by using the boundary integral method to solve the Hele-Shaw equations. Drops that are initially elongated in the direction of motion are found to revert to a circular shape for all Bond numbers considered. The stability of the shape of drops that are initially flattened (elongated normal to the direction of motion) depends on the extent of their initial deformation and the Bond number. Experimental observations of transient drop shapes show good qualitative agreement with the numerical predictions for both symmetric and asymmetric initial shape perturbations. In the presence of adsorbed surfactants, the interface separating the drop from the continuous liquid phase possesses its own distinct rheological properties. As the drop moves, the adsorbed surfactants are constantly redistributed along the interface by advection and diffusion, and give rise to non-uniformities in interfacial tension along the interface. This, in turn, affects the movement of the drop and its shape evolution. Dynamics of translating drops in the presence of bulk-insoluble surfactants are examined using the Langmuir adsorption framework in conjunction with a slip layer model derived for the depth-averaged tangential stress exerted on the two-phase interface. Given the initial shape of the drop and the buoyancy force acting on it, the interfacial distributions of velocity and surfactant concentration are computed, and the evolution of the drop shape is followed in time in order to identify the effect of interface contamination on the critical conditions for drop breakup.

SURFACE COLLISIONS INVOLVING PARTICLES AND MOISTURE (SCIP'M)

Robert H. Davis, Dean A. Rager, Brian T. Good, and Advait Kantak
Department of Chemical Engineering
University of Colorado
Boulder, CO 80309-0424
phone: 303-492-7314; fax: 303-492-4341
email: robert.davis@colorado.edu

ABSTRACT

Collisions of small particles with other particles or surfaces play key roles in industrial and natural processes such as filtration, agglomeration, granular flow, sand blasting, pollen capture, planetary-ring dynamics, and clean-room applications. The surfaces are wet in many cases, which can cause the particles to stick or have reduced kinetic energy due to viscous losses.

Davis *et al.* (1986) first analyzed the problem of a particle colliding with a wet surface, which they called an *elastohydrodynamic collision*, by numerically solving the coupled lubrication equation for the fluid velocity and pressure and the solid-elasticity equation for the Hertzian deformation of the surfaces. They showed that the collision and rebound process is governed by two dimensionless parameters:

$$\text{Stokes number} \qquad St = mv_o \big/ \left(6\pi\mu a^2\right) \quad , \tag{1}$$

$$\text{elasticity parameter} \qquad \varepsilon = 4\theta\mu v_o a^{3/2} \big/ x_o^{5/2} \quad , \tag{2}$$

where $m = 4\pi a^3\rho_s/3$ is the mass of the ball, a is its radius, ρ_s is its density, μ is the fluid viscosity, v_o is the impact velocity starting at a separation x_o between the surfaces, $\theta = (1-\nu_1^2)/(\pi E_1) + (1-\nu_2^2)/(\pi E_2)$, and ν_i and E_i are Poisson's ratio and Young's modulus of elasticity for the ball (i = 1) and plane (i = 2). The same analysis applies for the collision of two spheres, with a and m then equal to the reduced radius and mass, respectively.

The analysis of Davis *et al.* (1986) predicts that no rebound will occur when the Stokes number is less than a critical value ($St < St_c$), due to viscous dissipation of the initial kinetic energy of the sphere. The value of the critical Stokes number for rebound is predicted to depend weakly on the elasticity parameter, increasing from $St_c \approx 1.5$ at $\varepsilon = 10^{-2}$ to $St_c \approx 8$ at $\varepsilon = 10^{-8}$. Rebound is predicted for $St > St_c$, and Davis *et al.* (2002) have used lubrication theory for undeformed spheres and scaling relations for elastic deformation to predict that the coefficient of restitution is then

$$v_r \big/ v_o \equiv e_{wet} = e_{dry}\left(1 - St_c \big/ St\right) \quad , \tag{3}$$

where v_r is the rebound velocity, e_{wet} is the coefficient of restitution for a wet surface, e_{dry} is the coefficient of restitution for a dry surface, and the critical Stokes number for smooth surfaces is

$$St_c = \frac{2}{5}\ln\left(\frac{4\sqrt{2}}{3\pi\varepsilon}\right) \quad . \tag{4}$$

To test the theory, experiments were performed to measure the rebound velocities of small plastic and metal spheres dropped from various heights onto a smooth quartz surface coated with a thin layer of viscous fluid. Similar experiments involving spheres fully immersed in a large body of fluid have been reported recently by Joseph *et al.* (2001) and Gondret *et al.* (2002). The spheres stick without rebounding for low impact velocities, due to viscous dissipation in the thin fluid layer (Figure 1). Above a critical impact velocity, however, the lubrication forces in the thin layer cause elastic deformation and rebound of the spheres. The apparent coefficient of restitution increases with the ratio of the Stokes number to its critical value for rebound (Figure 2). The experimental results show good agreement with the model, except that there is considerable scatter in the data (which may be due to surface roughness).

Additional work is underway on oblique collisions and on slow-speed collisions. The latter will require a low-gravity environment.

Davis, R. H., J.-M. Serayssol, and E. J. Hinch (1986) "The Elastohydrodynamic Collision of Two Spheres," *J. Fluid Mech.* **163**, 479-492.

Davis, R. H., D. A. Rager, and B. T. Good (2002) "Elastohydrodynamic Rebound of Spheres from Coated Surfaces," *J. Fluid Mech.* (in press).

Gondret, P., M. Lance, and L. Pettit (2002) "Bouncing Motion of Spherical Particles in Fluids," *Phys. Fluids* **14**, 643-652.

Joseph, G. G., R. Zenit, M. L. Hunt, and A. M. Rosenwinkel (2001) "Particle-wall Collisions in a Viscous Fluid," *J. Fluid Mech.* **433**, 329-346.

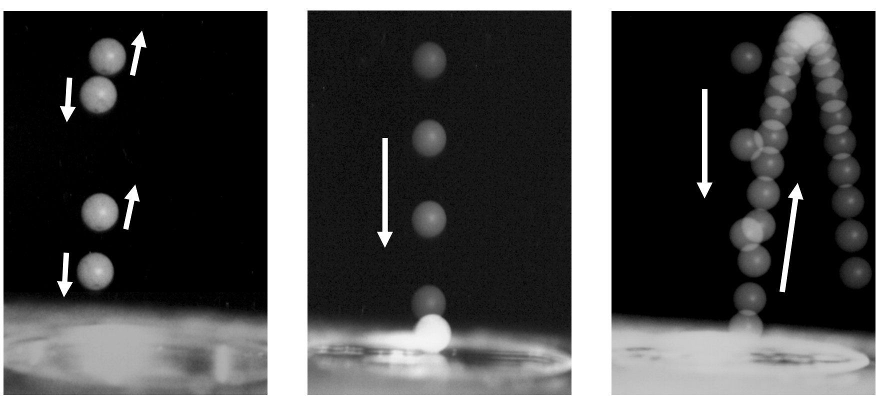

Figure 1. Strobed photographs of a nylon sphere of radius 0.32 cm dropped onto a dry quartz surface from a height of 20 cm (left panel), onto a quartz surface overlaid with a thin layer of fluid with 9.9 g/cm-s viscosity and 80 μm thickness from a height of 20 cm (middle panel), and onto the quartz surface with the same fluid layer from a height of 30 cm (right panel).

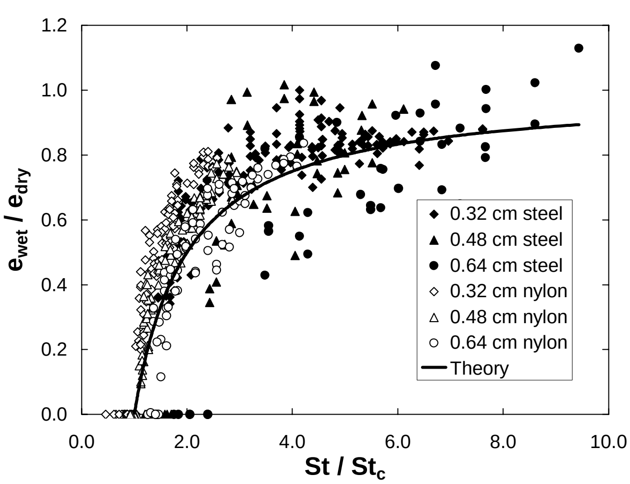

Figure 2. Coefficient of restitution for wet collisions, normalized by that for dry collisions, versus the ratio of the Stokes number to its critical value (determined from Eq. (4)) for nylon (open symbols) and steel (closed symbols) balls impacting a quartz surface overlaid with an 80-250 μm layer of fluid with 9.9 g/cm-s viscosity. The theoretical curve is from Eq. (3).

CRITICAL VELOCITIES IN OPEN CAPILLARY FLOWS

Antje Ohlhoff, Uwe Rosendahl, Michael E. Dreyer, Hans J. Rath

Center of Applied Space Technology and Microgravity (ZARM)
University of Bremen, Am Fallturm, D-28359 Bremen, Germany
e-mail: ohlhoff@zarm.uni-bremen.de, Fax: +49-421 218-2521, Phone: +49-421 218-4788

ABSTRACT

We consider a forced liquid flow in an open capillary channel with free liquid surfaces under low gravity. The channel consists of two parallel plates and is shown in Figure 1. The liquid flows along the x-axis from the inlet to the outlet and forms free surface at the sides between the plates. The flow is maintained by external pumps and the free surface deforms according to the pressure along the flow path. Since the free surface can only withstand a certain difference between the liquid pressure and the ambient pressure the flow rate in the channel is limited. The aim of the consideration is also to determine the shape of the free surface and to find the maximum flow rate without a collapse of the free surface. This critical flow rate depends on the geometry of the channel and the properties of the liquid, specified by the three dimensionless parameters, the OHNESORGE number $\mathrm{Oh} = (\rho\nu^2)/(2\sigma a)$, the aspect ratio $\Lambda = b/a$ and the dimensionless length $\tilde{l}$ (ρ is the density, ν the kinematic viscosity and σ the surface tension of the fluid). The right picture in Fig. 1 shows the cross section area A perpendicular to the flow direction. $k(x) = z(x, y = 0)$ is the observed and computed innermost line of the free surface, $Q^*_{\mathrm{crit}} = Q_{\mathrm{crit}}/A$ the critical volume flux.

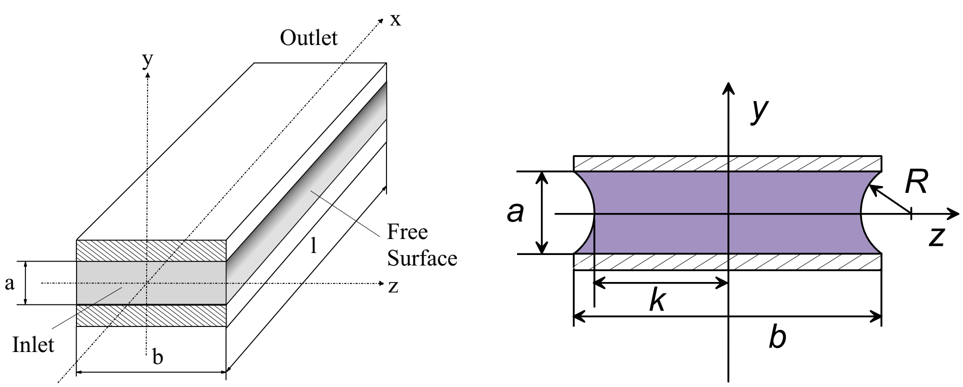

Figure 1: Schematic drawing of the flow channel consisting of two parallel plates. The right picture shows the cross section area A perpendicular to the flow direction.

The experimental investigations were performed in the drop tower Bremen and on board the sounding rocket TEXUS-37. In the TEXUS experiment the volume flux was increased in small steps up to the critical value (quasistatic approach) and the surface collapse was observed by video cameras. The main data are the positions of the liquid surfaces $k(x)$ as function of the adjusted volume flux and the critical flow rate. The results are discussed in [1], [2] and [3].

We developed a one dimensional, stationary mathematical model from the mass and momentum conservation equations. The model contains the pressure gradient caused by the shape of the free surface taking into account both radii of curvature, the convective acceleration due to the change in cross section and the friction losses in the channel. We have to deal with an entrance flow problem, thus the velocity distribution does not obey a simple parabolic profile. The solution of the nonlinear differential system is obtained by a difference schemata (FDM) of second order and the Newton method. This yields the free surface, the mean velocity and the curvature, depending on the parameters. Furthermore we are able to anticipate the critical volume flux in a numerical sense. The numerical results for the free surface position and the critical volume flux shows a very good agreement with the experimental data [3].

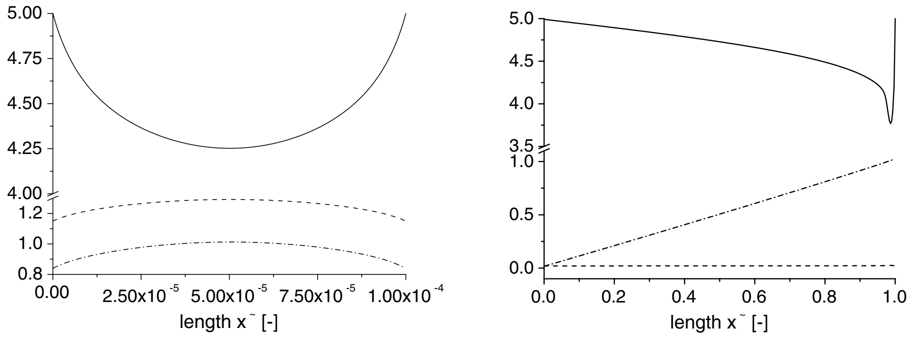

Figure 2: Typical results for convection dominated flow (left: $\mathrm{Oh} = 10^{-4}$, $\Lambda = 5.0$, $\tilde{l} = 10^{-4}$ $Q^* = 1.15$) and friction dominated flow (right: $\mathrm{Oh} = 10^{-2}$, $\Lambda = 5.0$, $\tilde{l} = 1.0$ $Q^* = 0.02$). The contour of the free surface is depicted with a solid line, the velocity with a dashed line and the mean curvature with a dashed-pointed line.

For the interpretation of the results the dimensionless length $\tilde{l} = (\mathrm{Oh} l)/(4a)$ is very appropriate and provides physical insight into the dominant forces. Figure 2 shows typical results from the numerical calculation for the different parts, dominated by convection and dominated by friction. The computations are close to the critical volume flux. The left picture shows the case of low Ohnesorge number and short channel length. The smallest cross section is approximately in the middle of the channel. Especially the mean curvature at the inlet is approximately equal to the curvature at the outlet. The right picture shows the case of large Ohnesorge number and large channel length. The free surface has a strong slope to fit the boundary condition at the outlet. The mean curvature increases nearly linear and the difference between inlet and outlet is very high.

The integration of the momentum equation shows, that the curvature difference between inlet and outlet is a measure for the friction pressure loss in the channel. For small flow lengths $\tilde{l} \leq 10^{-3}$, the pressure loss between inlet and outlet is small, thus the flow is dominated by convective momentum transport. In the other extreme of a very long channel, $\tilde{l} \geq 10^{-1}$, the flow is dominated by viscous momentum transport and the curvature difference tends to unity. This limit can be taken to predict the maximal volume flux for a pure friction dominated flow by $Q^*_{\mathrm{crit}} = 1/(48\tilde{l})$.

1. M. E. Dreyer, U. Rosendahl, H. J. Rath, Experimental Investigation on Flow Rate Limitations in Open Capillary Vanes, AIAA 98–3165, 1998.

2. U. Rosendahl, A. Ohlhoff, M. E. Dreyer, H. J. Rath, Investigation of Forced Liquid Flows in Open Capillary Channels, to appear in Microgravity Sci. Technol.

3. U. Rosendahl, B. Motil, A. Ohlhoff, M. E. Dreyer, H. J. Rath, Critical Velocity in Open Capillary Channel Flows, AIAA-2001–5021, 2001.

Microscale Investigation of Thermo-Fluid Transport In the Transition Film Region of an Evaporating Capillary Meniscus Using a Microgravity Environment

K.D. Kihm
Department of Mechanical Engineering, Texas A&M University
College Station, Texas 77843-3123
E-mail: ken-kihm@tamu.edu, Tel. 979-845-2143, Fax: 979-862-2418

J.S. Allen
National Center for Microgravity Research

K.P. Hallinan
University of Dayton

D.M. Pratt
Wright-Patterson Air Force Base

ABSTRACT

In low gravity, the solid-liquid inter-molecular surface forces are comparable to capillary and gravitational forces at significantly greater film thickness (1 ~ 10 microns), than is possible in earth's gravity (0.01 ~ 0.1 microns). Therefore, advanced microscale optical techniques to measure the film thickness, heat transport, and liquid velocity fields in the transition film region of an extended meniscus; probing, for the first the thermo-fluid transport inside this very important micro-scale region.

Since the project initiation in the beginning of 2002, a preliminary ground study has been done to implement a Molecular Fluorescence Tracking Velocimetry (MFTV) system (Fig. 1), utilizing caged fluorophores of approximately 10-nm in size as seeding particles, ultimately to measure the velocity profiles in the thin film region. Fizeau interferometry in conjunction with a microscope has been completed to measure the thin film slope and thickness variations.

Although the extension of the thin film dimensions under microgravity will be achieved by using a conical evaporator, a simpler and easy-to-fabricate evaporator has been designed and constructed for the ground test (Fig. 2). Note that the experimental setup is to maintain a constant liquid volume and liquid pressure in the capillary region of the evaporating meniscus so as to insure quasi-stationary conditions during measurements on the transition film region. In addition, the new Confocal Laser Scanning Microscopy (CLSM), available at Dr. Kihm's laboratory, has been tested for its optical sectioning capability allowing a depth-wise resolution for MFTV applications.

A micro-heater array has been fabricated using photo-lithography to etch and vapor deposit platinum films (Fig. 3). The heater array is packaged on a thin silicon substrate and then the upper face of the substrate is planarized to form a smooth contact surface. Individual heater elements (20-μm-wide and 20-mm long) are designed to maintain either a constant surface temperature or a controlled temperature variation. A Wheatstone bridge circuit controls each heater element with the temperature-dependent heater resistance value as a feedback signal.

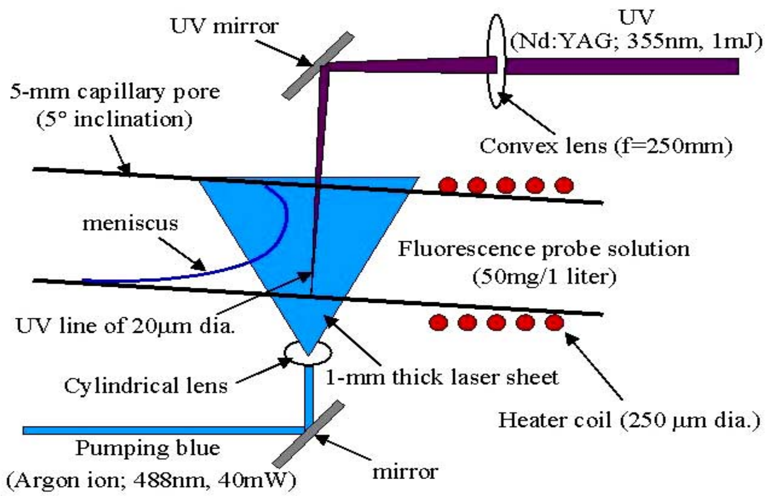

Fig. 1 Molecular Fluorescence Tagging Velocimetry (MFTV)

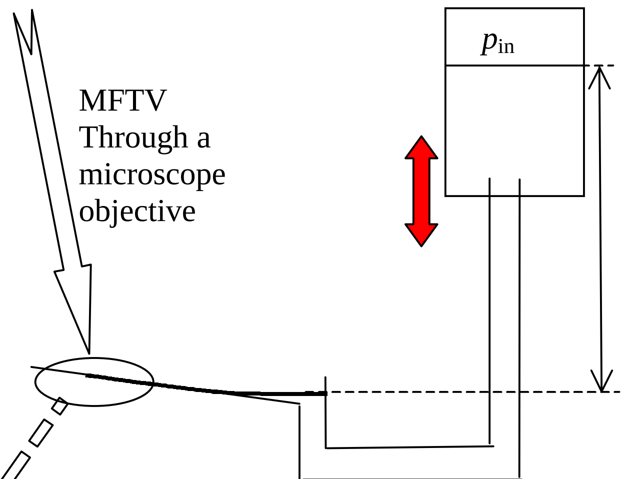

Fig. 2 Evaporating thin film generator

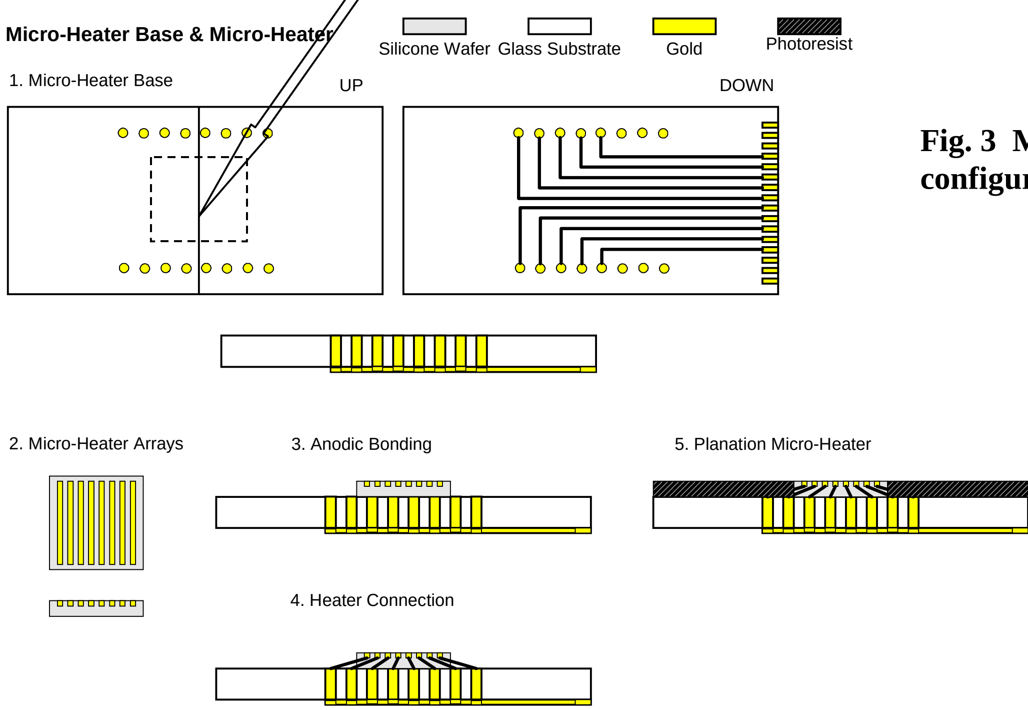

Fig. 3 Micro-heater configuration

DEVELOPMENT OF A NEW MEMBRANE CASTING APPARATUS FOR STUDYING MACROVOID DEFECTS IN LOW-G

Hanyong Lee, Sun-Tak Hwang and William B. Krantz
Department of Chemical Engineering, University of Cincinnati, Cincinnati, Ohio, 45221-0171

Alan R. Greenberg, Vivek Khare and Jeremiah Zartman
Department of Mechanical Engineering, University of Colorado, Boulder, Colorado 80309-0427

Paul W. Todd
Space Hardware Optimization Technology, Inc. Greenville, Indiana 47124-9515

ABSTRACT

A new membrane-casting apparatus is developed for studying macrovoid defects in polymeric membranes made by the wet- and dry-casting process in low-gravity. Macrovoids are large (10-50 μm), open cavities interspersed among the smaller pores in the substructure under the gelled skin surface layer of the cast membrane [1]. Although their occurrence is considered endemic to the wet- and dry-casting process since they can lead to compaction or skin rupture in the membrane process [2], recent studies suggest several useful applications such as transdermal and osmotic drug delivery systems [3,4], miniature bioreactors [5], etc. However, lack of knowledge about the macrovoid formation mechanism is an obstacle to further development of applications using them. An on-going debate is the role of the surface-tension-driven solutocapillary convection during macrovoid formation. The rapid growth of macrovoids within 1-5 seconds and the high polymer concentration in and near macrovoids make it difficult to explain the mechanism of macrovoid growth by diffusion alone, which is the widely accepted hypothesis proposed by Reuvers et al. [6]. The hypothesis advanced by our research group can explain this rapid growth via a mechanism that involves diffusion from the casting solution in the meta-stable region to the macrovoid enhanced by solutocapillary convection induced by the steep nonsolvent concentration gradient in the vicinity of the macrovoid.

Since macrovoid growth is hypothesized to be the interplay of a solutocapillary-induced driving force counteracted by viscous drag and buoyancy, eliminate the latter provides a means for testing this hypothesis. Moreover, free convection mass transfer in the nonsolvent immersion bath used to cause phase-separation in membrane casting complicates developing a model for both the wet-casting process and macrovoid growth. The low-g environment minimizes gravitationally induced free convection thereby permitting a tractable solution to the ternary diffusion equations that characterize membrane formation.

NASA's Parabolic Flight Research Aircraft provides a small window of low-g (~25 s) that can be used to study macrovoid development in both wet- and dry-cast membranes if an appropriate casting apparatus is used. This casting apparatus should be able to cast the membrane in both low- and high-g in a manner so that essential one-dimensional mass transfer conditions are achieved to insure lateral uniformity in the membrane. The apparatus used in previous research on membrane casting in low-gravity was operated with the plunger driven mechanism. The spring-loaded plunger pushes the bottom block containing the polymer casting solution well

directly under the absorbent chamber located in the upper stationary block [7]. However, membranes made via this casting apparatus often displayed lateral nonuniformities that precluded obtaining quantitative information on the macrovoid growth process. Thus, it was necessary to determine the reason for these structural irregularities observed in the low-g casting apparatus.

Both experimental as well as computer simulation studies of the low-g casting apparatus established that the impulsive action of the plunger caused the undesired structural nonuniformities. The simulation results showed that the width-to-depth aspect ratio of the shallow well that contains the casting solution in this apparatus was not an important factor in minimizing this problem. Even for a 40:1 (width : depth) aspect ratio, any convection induced by the horizontal motion of the interface of the casting solution will be damped out within 6.25×10^{-4} seconds. However, the experimental studies revealed that the impulsive motion of the plunger caused a "sloshing" of the casting solution that had to be eliminated. Therefore, the plunger-driven mechanism was changed to a cam-driven mechanism that did not cause any impulsive motion of the casting solution. Other refinements to this new membrane-casting apparatus include provision for removing the membranes from the casting wells in a less destructive manner. This was accomplished by using a slit geometry for the casting well that permitted disassembly for removal of the cast membrane. The materials used in the construction of this casting apparatus were chosen to insure wetting at the side walls and to maintain precise control of the thickness of the polymer solution in the casting well. An additional provision in this new casting apparatus is the ability to carry out both wet- as well as dry-casting. As such, this apparatus permitted the first studies of the wet-casting of polymeric membranes in low-g. Both wet- and dry-casting experiments on NASA's KC-135 research aircraft employing this new membrane-casting apparatus are scheduled in July 2002. The morphology of the resulting membranes will be characterized using an environmental scanning electron microscope (ESEM). The results of these low-g studies will be reported later.

[1] Konagurthu, S., "Macrovoids in dry-cast polymeric membranes: growth mechanisms, non-invasive detection, and effects on performance." Ph.D. Dissertation. University of Colorado, Boulder (1998)

[2] Kesting, R. E., *Synthetic Polymeric Membranes – A structural Perspective*, 2nd ed. Wiley, New York (1986).

[3] Herbig, S. H., Carinal, J. R., Korsmeyer, R. W. and Smith, K. L., "Asymmetric membrane tablet coating for osmotic drug delivery," J. Control. Release, **35** (1995) 127-136

[4] Smolder, C. A., Reuvers, A. J., Boom, R. M. and Wienk, I. M., "Microstructures in phase-inversion membranes. Part I. Formation of macrovoids," J. Mem. Sci., **73** (1992) 259-275

[5] Jacob, E. P. and Leukes, W. D., "Formation of an externally unskinned polysulfone capillary membrane." J. Mem. Sci., **121** (1996) 149-157

[6] Reuvers, A. J. "Membrane formation –diffusion induced demixing processes in ternary phase separation phenomena." Desalination, **32** (1980) 33-45

[7] Pekny, M. R., "Influence of solutocapillary convection on macrovoid defect formation in dry-cast polymeric membrane" M.S. Thesis. University of Colorado, Boulder (1996)

Using Nonlinearity and Contact Lines to Control Fluid Flow in Microgravity

M. Perlin, W.W. Schultz, X. Bian, and M. Agarwal, University of Michigan

Slug flows in a tube are affected by surface tension and contact lines, especially under microgravity. Numerical analyses and experiments are conducted of slug flows in small-diameter tubes with horizontal, inclined and vertical orientations. A PID-controlled, meter-long platform capable of following specified motions is used. An improved understanding of the contact line boundary condition for steady and unsteady contact-line motion is expected. Lastly, a direct fluid-handling method using nonlinear oscillatory motion of a tube is presented.

I. Quasi-static tube inclination with axial gravitational component

A. *Incipient motion*: Experiments were conducted on quasi-statically inclined, 3.7 mm diameter glass circular cylinders containing fluid slugs. Using a simple force balance, the governing equation is

$$\sin(\theta) = \frac{4\sigma}{\rho d\, \lg}\left[\cos\alpha - \cos\beta\right]$$

where θ = angle of the cylinder measured from horizontal, α = contact-line angle at the lower end of the slug for incipient motion, β = contact-line angle at the upper end of the slug for incipient motion, ρ = mass density of liquid (water), σ = air-water interfacial surface tension, and l = slug length. For a typical slug length of 5.08 cm, $\alpha = 53^0$ and $\beta = 25^0$. The theoretical value of θ was 2.75^0; the measured value of θ was 2.53^0. When the cylinder's inner surface is pre-wetted, α is closer to β, and θ is decreased significantly.

B. *Viscous drag on a fluid slug*: Constant motion of a fluid slug is achieved by inclining the tube. Video is used to capture the subsequent motion. When a constant slug velocity results, equilibrium presumably requires the driving force (i.e. pressure force due to gravity) to equal the sum of the viscous and the contact line forces. The liquid flow field is complicated by the deformation of the ends of the slug. For a slug with a large aspect ratio (length to diameter) and velocity *U*, the pressure decrease due to viscosity should be $p_v = \frac{8l\mu U}{R^2}$ neglecting the flow near the ends. As the retarding force due to the contact lines is vastly different for dry and pre-wetted surfaces, experiments under both conditions are conducted. Again, the contact line force for pre-wetted tubes is much smaller than for the dry tubes. Especially for long cylinders, the effect of air in the tube is considered with this friction comparable to the viscous effects directly on the slug.

II. Resonance analyses and experiments for fixed contact or stick-slip motion

As the eventual objective of this project is to control fluid flow in microgravity by nonlinearity, we investigated the natural frequency of the end surfaces of the slug. Presumably, the natural frequency of the confined slugs should create the largest disturbances of the end caps, thereby producing maximum net flow. The initial analytic solution was based on the simplest model, a zero-dimension (0-D) approximation (i.e. a liquid slug where the center of mass shifts due to the oscillation of its ends). Here the end-cap surface is assumed spherical for the axisymmetric geometry, with the spherical segment set by the contact angle. To solve for the natural frequency and its mode shape, the potential flow problem for a fixed contact line condition is formulated as a generalized eigenvalue problem. The dynamic and kinematic boundary conditions are evaluated at the original equilibrium surface. The surface elevation $z = \eta(r,t)$ (relative to the unperturbed curved surface $z = \zeta(r)$) is expressed as a summation of basis functions (cosine series, Chebyshev polynomials, etc.) and the problem is solved accordingly. In figure 1 the numerical results for the 'slosh mode' are presented with direct comparison to the aforementioned 0-D approximation. Good agreement is observed. An experiment was conducted to verify the analysis. The measured slosh frequency is smaller than the analysis suggests. The deviation may be attributed to viscosity and possible contact line slip. The effect of partial slip was also evaluated by introducing a simple slip parameter γ, defined as a slip coefficient in the contact line stick-slip condition: $\eta + \gamma\eta_r = 0\,(r = R)$. As $\gamma \to 0$, the frequencies converge to the pinned contact-line solution. When $\gamma \to \infty$, the contact line slips on the wall, and the frequency goes to zero as the restoring force of the meniscus vanishes.

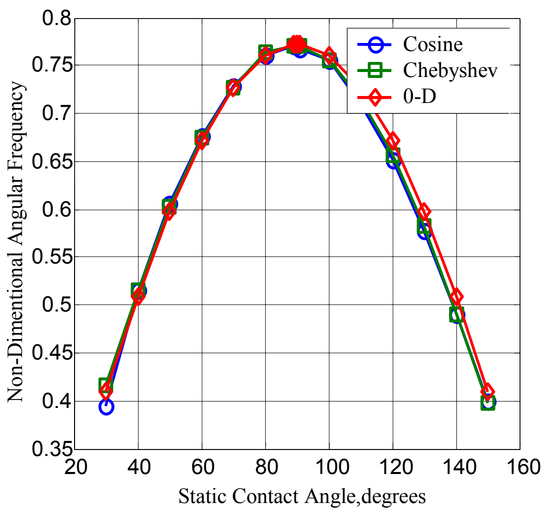

Figure 1. End cap resonance frequency versus static contact angle.

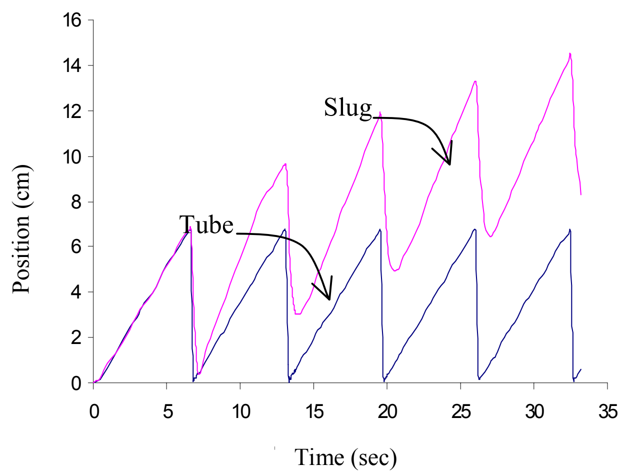

Figure 2. Motion of cylinder and slug showing mean motion generated.

III. Periodic horizontal motion to generate a mean flow

To experimentally achieve periodic motion, an infinite number of motion profiles can be tested. Presented in figure 2 is a cylinder position versus time graph that generates slug mean motion. To qualitatively study the mean motion, three segments of constant cylinder acceleration are chosen that forms a saw-tooth-like velocity profile over each cycle. As shown, a mean motion of the slug is generated with low frequency motion. Motions at higher frequencies will be presented also.

MAGNETIC FLUID MANAGEMENT (MFM)

Dr. Eric Rice, Mr. Robert Gustafson, Dr. John Hochstein,
Mr. Jeff Marchetta, and Dr. Martin Chiaverini
Orbital Technologies Corporation (ORBITEC^{TM})

INTRODUCTION

The difficult problem of cryogenic fluid handling in many aerospace applications in low gravity environments can be solved by employing a new magnetic fluid technology called magnetic fluid management (MFM). The innovative MFM technology has the potential to provide significant advancements over other technologies such as screens, vanes, porous plugs, and no-vent fill processes. MFM technology utilizes the magnetic properties of cryogenic fluids for phase separation. This enables new processes which greatly simplify many critical tasks now encountered, such as gas-free liquid transfer between cryogenic containers, liquid-free gas venting during storage, liquid-free gas venting during tank refill, and use of a self-regulating control system to maintain tank pressure during liquid expulsion.

COMPUTATIONAL MAGNETIC FLUID DYNAMICS (CMFD) MODELING

The magnetic fluid dynamics of the MFM system is being modeled with a modified and enhanced version of the RIPPLE code, originally developed by Los Alamos National Laboratory for modeling the unsteady flow of incompressible, constant property, Newtonian fluids. The ability of the RIPPLE code and its variants to model flows with highly deforming free surfaces in which surface tension forces are significant has been well documented, as has been their fidelity in modeling the propellant reorientation process. Reorientation is determined by the magnet's ability to influence a reasonable portion of the propellant to traverse the tank wall and come in contact with the opposing tank head.

1-G LABORATORY TESTING

A series of ground-based experiments were designed to determine the effect of magnetic fields on ferrofluid and LOX in full gravity. Initial CMFD analyses of both LOX and ferrofluid motion in a cylindrical tank in a 1-g environment have been conducted to support the design of ground-based experiments. The goal of this work is to help identify a reasonable combination of magnetic field strength, tank radius, and ferrofluid volume and concentration that would result in observable fluid deformations in a laboratory environment.

REDUCED GRAVITY AIRCRAFT FLIGHT TESTING

The KC-135 flight testing will involve the construction of two dewar systems: one would be transparent and fully instrumented to be used with ferrofluid for preliminary testing; the other one would be an optimally designed cryogenic dewar that is instrumented as necessary to validate the models. The flight testing will occur during two different weeks. Flight experiments would include:

First Test Series-Transparent Dewars - Ferrofluid
[Rare-Earth Magnet configuration (strong, medium, weak)]
- Acquisition and Stability Testing
- Liquid Expulsion Demonstration
- Liquid-Free, Gas Vent Demonstration
- Fluid Gauging Demonstration .

Second Test Series- Cryogenic Dewar - Liquid Oxygen
[Rare-Earth Magnet Configuration (strong, medium, weak)]
- Acquisition and Stability Testing
- Liquid Expulsion Demonstration
- Liquid-Free, Gas Vent Demonstration
- Fluid Gauging Demonstration
- Heating/Self-Regulating Pressurization.

The following types of measurements must be made to satisfy our scientific objectives: video images via cameras (perhaps with borescopes and light pipes), acceleration in the X-Y-Z axes of the experiment, temperature using cryogenic diodes and thermocouples, pressure in the vessels, fluid position, vent flow rates, liquid levels using cryogenic level sensors, time clock to link all the measurements to flight events, etc. The data would be collected and stored on a laptop PC for analysis.

CURRENT STATUS

The modified RIPPLE code has been enhanced to include fluid magnetic surface tension effects and increase the user friendliness. Ground experiments (performed in 1-g) are being developed and performed as a precursor to the KC-135 flight experiments. ORBITEC has obtained permission to use some of the MAPO (Magnetically Actuated Propellant Orientation) KC-135 flight hardware that was developed and tested by NASA Marshall Space Flight Center. New dewars are being designed for use with the MAPO experiment support structure on upcoming KC-135 flights.

PI CONTACT INFORMATION

Dr. Eric E. Rice
Orbital Technologies Corporation (ORBITEC™)
Space Center, 1212 Fourier Drive
Madison, WI 53717
(608) 827-5000
(608) 827-5050 *fax*
ricee@orbitec.com

MOTION OF DROPS ON SURFACES WITH WETTABILITY GRADIENTS

R. Shankar Subramanian*, John B. McLaughlin, Nadjoua Moumen, and Dongying Qian
Box 5705, Department of Chemical Engineering, Clarkson University, Potsdam New York 13699

ABSTRACT

A liquid drop present on a solid surface can move because of a gradient in wettability along the surface, as manifested by a gradient in the contact angle. The contact angle at a given point on the contact line between a solid and a liquid in a gaseous medium is the angle between the tangent planes to the liquid and the solid surfaces at that point and is measured within the liquid side, by convention. The motion of the drop occurs in the direction of increasing wettability. The cause of the motion is the net force exerted on the drop by the solid surface because of the variation of the contact angle around the periphery. This force causes acceleration of an initially stationary drop, and leads to its motion in the direction of decreasing contact angle. The nature of the motion is determined by the balance between the motivating force and the resisting hydrodynamic force from the solid surface and the surrounding gaseous medium.

A wettability gradient can be chemically induced as shown by Chaudhury and Whitesides (1992) who provided unambiguous experimental evidence that drops can move in such gradients. The phenomenon can be important in heat transfer applications in low gravity, such as when condensation occurs on a surface. Daniel et al. (2001) have demonstrated that the velocity of a drop on a surface due to a wettability gradient in the presence of condensation can be more than two orders of magnitude larger than that observed in the absence of condensation. In the present research program, we have begun to study the motion of a drop in a wettability gradient systematically using a model system. Our initial efforts will be restricted to a system in which no condensation occurs.

The experiments are performed as follows. First, a rectangular strip of approximate dimensions 10 x 20 mm is cut out of a silicon wafer. The strip is cleaned thoroughly and its surface is exposed to the vapor from an alkylchlorosilane for a period lasting between one and two minutes inside a desiccator. This is done using an approximate line source of the vapor in the form of a string soaked in the alkylchlorosilane. Ordinarily, many fluids, including water, wet the surface of silicon quite well. This means that the contact angle is small. But the silanized surface resists wetting, with contact angles that are as large as 100^{o}. Therefore, a gradient of wettability is formed on the silicon surface. The region near the string is highly hydrophobic, and the contact angle decreases gradually toward a small value at the hydrophilic end away from this region. The change in wettability occurs over a distance of several mm.

---

* PI e-mail address: subramanian@clarkson.edu, fax: (315) 268-6654, phone: (315) 268-6648

The strip is placed on a platform within a Plexiglas cell. Drops of a suitable liquid are introduced on top of the strip near the hydrophobic end. An optical system attached to a video camera is trained on the drop so that images of the moving drop can be captured on videotape for subsequent analysis. We have performed preliminary experiments with water as well as ethylene glycol drops. Results from these experiments will be presented in the poster.

Future plans include the refinement of the experimental system so as to permit images to be recorded from the side as well as the top, and the conduct of a systematic study in which the drop size is varied over a good range. Experiments will be conducted with different fluids so as to obtain the largest possible range of suitably defined Reynolds and Capillary numbers. Also, an effort will be initiated on theoretical modeling of this motion. The challenges in the development of the theoretical description lie in the proper analysis of the region in the vicinity of the contact line, as well as in the free boundary nature of the problem. It is known that continuum models assuming the no slip condition all the way to the contact line fail by predicting that the stress on the solid surface becomes singular as the contact line is approached. One approach for dealing with this issue has been to relax the no-slip boundary condition using the Navier model (Dussan V., 1979). Molecular dynamics simulations of the contact line region show that for a non-polar liquid on a solid surface, the no-slip boundary condition is in fact incorrect near the contact line (Thompson et al., 1993). Furthermore, the same simulations also show that the usual relationship between stress and the rate of deformation breaks down in the vicinity of the contact line. In developing continuum theoretical models of the system, we shall accommodate this knowledge to the extent possible.

References

Chaudhury, M.K., and Whitesides, G.M. 1992 How to make water run uphill. Science **256**, 1539-1541.

Daniel, S., Chaudhury, M.K., and Chen, J.C. 2001 Fast drop movements resulting from the phase change on a gradient surface. Science **291**, 633-636.

Dussan V., E.B.. 1979 On the spreading of liquids on solid surfaces: static and dynamic contact lines. in Ann. Rev. Fluid Mech., ed. M. Van Dyke, J.V. Wehausen, and J.L. Lumley (vol. 11, pp. 371-400). Palo Alto, CA: Annual Reviews, Inc.

Thompson, P.A., Brinckerhoff, W.B., and Robbins, M.O. 1993 Microscopic studies of static and dynamic contact angles. J. Adhesion Sci. Technol. **7**, No. 6, 535-554.

MICROCHANNEL PHASE SEPARATION AND PARTIAL CONDENSATION IN NORMAL AND REDUCED GRAVITY ENVIRONMENTS

Ward E. TeGrotenhuis and Victoria S. Stenkamp
Battelle Memorial Institute, Richland, Washington

ABSTRACT

Microtechnology was conceived as a means of shrinking the length scales of heat and mass transfer to 100 microns or less so that orders of magnitude increases in throughput can be realized in chemical processes. The subsequent reduction in size and mass lends itself well to space applications. Using proprietary sheet architecture, Battelle has created such devices with micro chemical and thermal systems (MicroCATS) for gas phase reactions, heat transfer and solvent extraction. Figure 1 depicts a device cross section with micrometer size channels used in such devices.

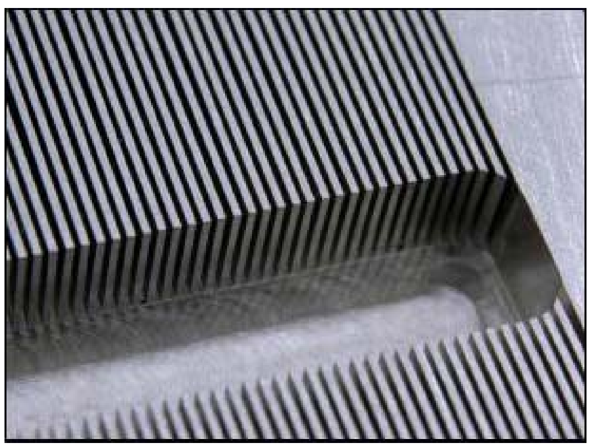

Figure 1. Cross section of microchannels

In this work, Battelle has extended the technology to include phase separation and partial condensation with phase separation in channels between 100 microns and a few millimeters at the smallest dimension. These length scale channels are advantageous for all reduced gravity applications involving two-phase flow since hydrodynamic, interfacial and capillary forces dominate over gravitational forces. By controlling the wettability and porosity of the materials within the device, separation occurs spontaneously thus allowing high throughputs and easy recovery from process upsets. Enhanced heat transfer in the case of condensation is obtained through reduction of the narrowest channel dimension. Scale up is achieved by simply increasing the number of layers. Potential space applications for phase separation and condensation include water management in environmental control and life support and thermal systems involving phase change (heat pipes, vapor compression cycles). These devices are also well suited for in-situ resource utilization or "living off the land" since they are compact and efficient. Applications include phase separation and condensation of water during in-situ propellant production.

The performance is reported for a single channel phase separator in both normal and microgravity environments and for a multi channel condenser in normal gravity. A schematic of a single channel device is presented in Figure 2. In the case of phase separation, a gas/liquid mixture is fed to the device and no cooling channel is present. Liquid is moved through the capture structure to the wicking or pore throat structure via capillary and hydrodynamic forces, then towards the appropriate outlet. The gas is allowed to move freely through the device and exit through its outlet. In the case of partial condensation with phase separation, vapor and non-condensable gas is fed to the device and a cooling channel is present. Vapor condenses on the wall nearest the cooling channel so that liquid must be moved to the liquid exit via capillary forces. A multichannel device consists merely of alternating layers of cooling and condensing channels.

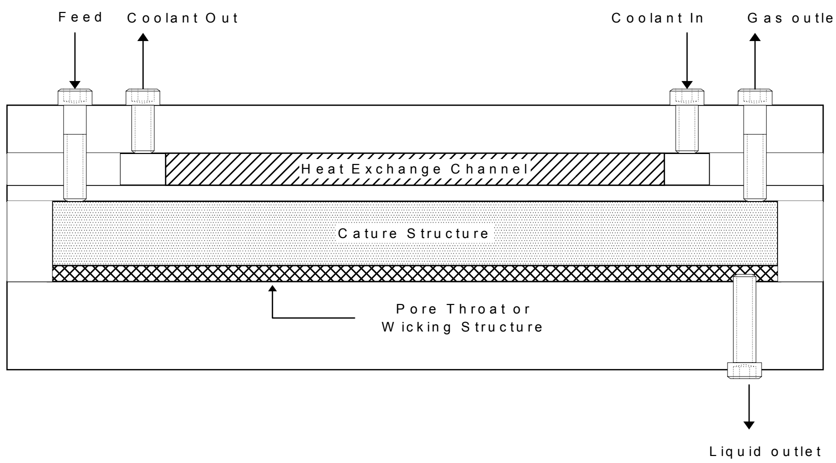

Figure 2. Single channel separator shown in co-current flow.

Complete separation has been obtained during phase separation in both normal and microgravity environments with gas residence times of hundredths of seconds. Liquid fractions tested ranged from 0.0005 to 0.14. In the case of condensation with phase separation, an air-cooled multi-channel device has been operated in normal gravity with complete separation of the gas and liquid phases. Water recovery was essentially 50%, with the difference accounted for by humidification of the air. The overall heat transfer coefficient has been calculated as high as 3300 W/m^2.K with a specific power of over 1200 W/kg.

CAPILLARY FLOW IN INTERIOR CORNERS

Mark M. Weislogel
P.O. Box 751-ME, Portland State University, Portland, OR 97207
Email; mmw@cecs.pdx.edu, Fax; 503-725-4292, Ph; 503-725-8255,

ABSTRACT

Capillary flows in interior corners have an established place in fluids-handling operations in reduced gravity environments. A quantitative understanding of corner flows is essential for the myriad fluid management tasks in space including flows in liquid-fuel tanks, thermal control systems, and life-support systems. Though low-g fluid system designs are 'largely successful,' current techniques for predicting system performance are primarily limited to order of magnitude estimates, delicately guided by the experience of the designer, or direct numerical simulation which can be prohibitively time consuming. Highly reliable and quantitative design tools serving between these extremes are welcome contributions to the low-g fluids management community.

In this research effort, an asymptotic analysis developed and benchmarked for capillary flows in simplified containers possessing interior corners [1] is generalized and broadly applied to flows in containers and/or corner geometries of increasing complexity. Closed form solutions to important problems such as interior corner transient flow rates, local and global flow characteristics, interface profiles, and stability are determined for a variety of container types and boundary conditions. A partial list of problems addressed includes flows in corners of infinite extent [2], regular and irregular polygonal cylinders [3], and complex 'vaned' containers modeling propellant management devices in liquid fuel tanks [4]. Other complicating conditions such as nonplanar corners, out-of-plane corners, helical corners, background accelerations, heat and mass transfer, and interfacial shear are addressed. Applications of the results to low-g fluid system design and analysis are manifold and an excellent example is provided by way of a post-analysis of NASA's Vented Tank Resupply Experiment performed on the shuttle in 1996.

Extensive drop tower and low-g aircraft experiments are performed to guide and/or support the development and application of the most fundamental aspects of the theory. For the special case of steady capillary driven flow the analysis is readily extended to complex corner networks modeling macroscale flows within intricately vaned containers in space as well as microscale flows on rough surfaces on Earth.

References

[1] Weislogel, M.M., Lichter, S., Capillary Flow in Interior Corners, *J. Fluid Mech*., 373:349-378, November 1998.
[2] Weislogel, M.M. Capillary Flow in Containers of Polygonal Section, *AIAA J*., 39(12), 2320-2326, 2001.
[3] Weislogel, M.M. Capillary Flow in Interior Corners: the Infinite Corner, *Phys. of Fluids*, 13(11):3101-3107, Nov., 2001.
[4] M.M. Weislogel, S.H. Collicott, Analysis of Tank PMD Rewetting Following Thrust Resettling, 40th AIAA Meeting, AIAA 2002-0757, Reno, Jan. 14-17, 2002.

Two-Dimensional Turbulence in the Presence of a Polymer

Yonggun Jun and X.L. Wu
Department of Physics and Astronomy
University of Pittsburgh, Pittsburgh, PA 15260

Polymers of sufficient length are known to quench turbulence [1]. However, the fundamental mechanism of quenching, namely the interactions between the polymer and turbulence, is not well understood. In this experiment, we examine the effect of a polymer additive to turbulence in a freely suspended film. The experimental geometry is two-dimensional due to the fact that films are very thin, confining the flow velocity to the plane of the film. The turbulence in the film is created by electromagnetic convection as delineated in the figure below.

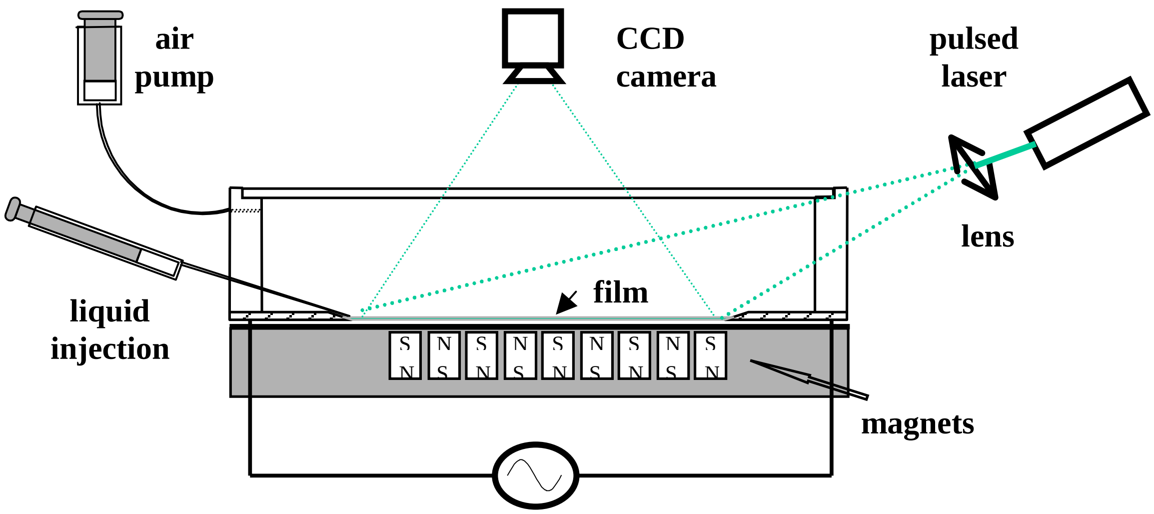

Here a uniform electric current is injected into a salt-doped film, and the ionic current in the film couples to an externally imposed magnetic field, giving rise to a set of vortices. Various convection states can be achieved depending on the magnitude of the current, but in this study we are interested in a large applied current so that flow in the film is spatiotemporally chaotic, or turbulent. The flow velocity field can be interrogated by a particle imaging velocimeter, which consists of a CCD camera and a pulsed laser. For more information on the experimental setup, see Ref. [2].

Since we are ultimately interested in studying polymer conformational fluctuations in the presence of turbulent velocity field, large λ-DNA molecules are used in the experiment. The λ-DNA has a contour length of 16 μm which folded into a globular form of radius ~1 μm in diameter. Preliminary observations show that there exist two different flow regimes depending on the DNA concentrations. For low DNA concentrations (<50 ppm), the 2D film is homogeneous and the turbulent velocity field is similar to those without polymers. For higher DNA concentrations, the film develops inhomogeneities when the turbulent intensity becomes large, with v_{rms}>10 cm/s. Tenuous filaments spontaneously appear and are sometimes discernible to naked eyes. The thin filaments appears to be due to aggregation of DNA molecules, since no such aggregates are present in the bulk suspension, or in the absence of strong turbulence. It remains an intriguing possibility that quenching of turbulence may be a collective effect rather than due to single polymers as suggested by different theories [3,4]. Our current work concentrates on optical microscopy to visualize individual DNAs will put this question to rest.

References:

[1] J.L. Lumley and I. Kubo, The Influence of Polymer Additives on Velocity and Temperature Fields, ed. G. Gampert (Springer, Berlin, 1984).
[2] M. Rivera and X.L. Wu, External Dissipation in Driven Soap Film Turbulence, Phys. Rev. Letts., **85**, 976 (2000).
[3] M. Tabor and P.G. de Gennes, *A Cascade Theory of Drag Reduction*, Europhys. Lett., **2**, 519 (1986).
[4] M. Chertkov, et al., *Polymer Stretching by Turbulence*, Phys. Rev. Letts., **84**, 4761 (2000).

Exposition Session
Topical Area 3:
Complex Fluids

MICROGRAVITY IMPACT EXPERIMENTS: RESULTS FROM COLLIDE-2

Joshua E. Colwell, Larry W. Esposito, and Mihály Horányi
LASP, University of Colorado, Boulder CO 80309-0392, josh.colwell@lasp.colorado.edu,
303-492-6805, Fax: 303-492-6946

ABSTRACT

Protoplanetary disks, planetary rings, the Kuiper belt, and the asteroid belt are collisionally evolved systems. Although objects in each system may be bombarded by impactors at high interplanetary velocities (km/s or higher), they are also subject to repeated collisions at low velocities (v ~ 1-100 m/s). In some regions of Saturn's rings, for example, the typical collision velocity inferred from observations by the Voyager spacecraft and dynamical modeling is a fraction of a centimeter per second [1]. These interparticle collisions control the rate of energy dissipation in planetary rings and the rate of accretion in the early stages of planetesimal formation. Dust on the surface of planetary ring particles and small (1 cm – 10 m) planetesimals helps dissipate energy in the collision, but may also be knocked off, forming dust rings in the case of ring particles and slowing or inhibiting accretion in the case of planetesimals.

The Collisions Into Dust Experiment (COLLIDE) is a self-contained autonomous microgravity experiment that made its second flight in the payload bay of space shuttle Endeavour on flight STS-108 in December 2001. COLLIDE-2 (Figure 1) performed 6 impact experiments into powder in microgravity at speeds between 1.2 and 108 cm/s, simulating the collisions that occur in some astrophysical systems.

(a)

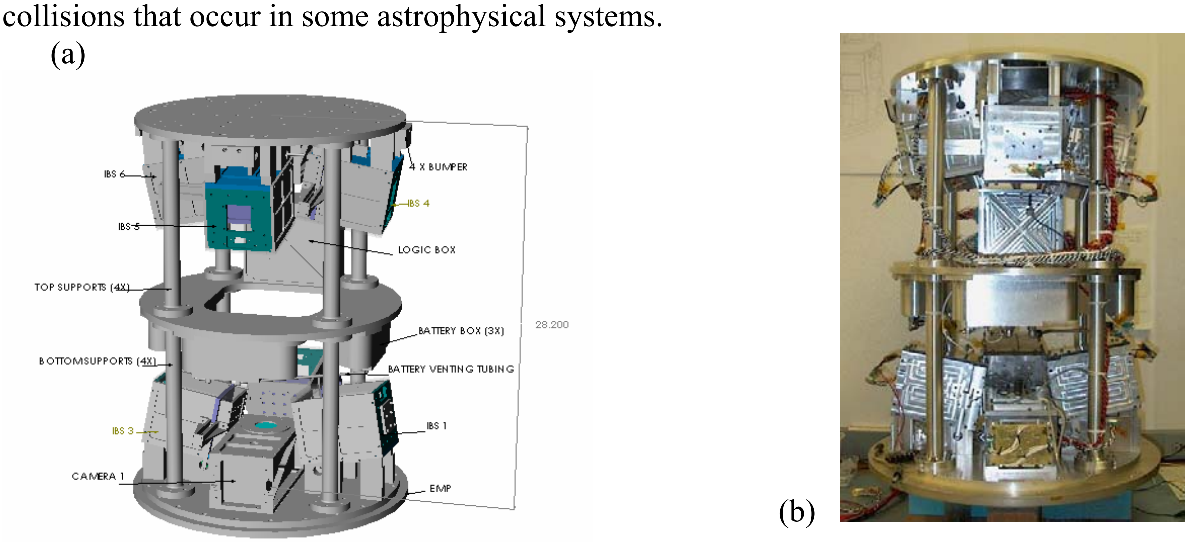

(b)

Figure 1: (a) Schematic of the COLLIDE-2 payload indicating major experiment components. Three impact experiment boxes are mounted to each end plate around a sealed camera container. The camera images the three boxes on the opposite end plate through a hole in the central plate which also serves as the mounting point for electronics and batteries. (b) Image of COLLIDE-2 prior to flight in a similar orientation to the schematic in (a).

Impactors were quartz spheres approximately 1.9 cm in diameter. The target material was quartz sand sieved to a size range of 75-250 µm in 5 of the 6 experiments and JSC-1, a ground basaltic mineral sieved to the same size range in the sixth experiment. The experiment took place in an evacuated standard space shuttle Hitchhiker container fourteen hours after launch. The temperature of the samples at the time of the experiment was 17°C. Digital video recordings of the impacts were made using two consumer-grade camcorders, each one recording three impacts in sequence. Analysis of the video data provides an accurate measure of the impactor velocity before and after impact, velocity of the fastest ejecta produced (if any), and a qualitative measure of the amount of ejecta produced. A single video frame from one impact experiment is shown in Figure 2.

On the first flight of COLLIDE on STS-90 in 1998 experiment malfunctions prevented data from being returned for 3 of the 6 impact experiments. Those experiments used JSC-1 as a target material for all impacts, and included the sub-75 μm portion of the size distribution. Impacts at 15 cm/s and 17 cm/s resulted in virtually no ejecta, and rebound coefficients of restitution were <0.03. A similar coefficient of restitution was found for a third impact at 90 cm/s [2]. The broad size-distribution JSC-1 used in COLLIDE compacted during launch vibrations resulting in a cohesive surface and little or no ejecta production. The quartz sand used in COLLIDE-2 has rounder grains which do not interlock with each other as much as the semi-angular JSC-1 grains. On COLLIDE-2 we found significant ejecta produced at impact speeds above 20 cm/s and no rebound of the impactor at impact speeds below that level. A summary of the findings from COLLIDE-2 is shown in Table 1.

V (cm/s)	Target	Ejecta	Rebound
1.3	SiO_2 sand	0	No
3.9	SiO_2 sand	$M_{ej}<M_{imp}$	No
28	SiO_2 sand	$M_{ej}\geq M_{imp}$	Yes
81	SiO_2 sand	$M_{ej}>M_{imp}$	Yes
108	SiO_2 sand	$M_{ej}>M_{imp}$	Yes
12	JSC-1	$M_{ej}<M_{imp}$	No

Table 1: Summary of results from the 6 COLLIDE-2 impact experiments. A threshold for the boundary between accretion and erosion is between impact speeds of 12 and 28 cm/s for the conditions in this experiment.

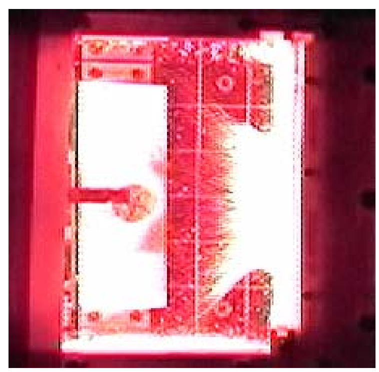

Figure 2: Video frame 0.06 seconds after impact into at 108 cm/s. The reflected image of the projectile is visible in the mirror at left, and the direction of motion of the projectile is left to right. Fiduciary lines are 2 cm apart.

The impact into JSC-1 on COLLIDE-2 was at a speed comparable to two impacts on COLLIDE, but with an impactor that was 9 times more massive. On COLLIDE-2 the impactor remained embedded in the target surface, in contrast to the slow rebound observed on COLLIDE. This difference in behavior is likely due to the absence of small particles in the COLLIDE-2 target, increasing the overall porosity of the target and allowing the surface to deform more in response to the collision.

REFERENCES

[1] Esposito, L. W., *Annu. Rev. Earth Planet. Sci.,* **21**, 487 (1993).
[2] Colwell, J. E., and M. Taylor, *Icarus*, **138**, 241 (1999).

MICROGRAVITY IMPACT EXPERIMENTS: THE PRIME CAMPAIGN ON THE NASA KC-135

Joshua E. Colwell, Stein Sture, and Andreas R. Lemos
LASP, University of Colorado, Boulder CO 80309-0392, josh.colwell@lasp.colorado.edu,
303-492-6805, Fax: 303-492-6946

ABSTRACT

Low velocity collisions ($v < 100$ m/s) occur in a number of astrophysical contexts, including planetary rings, protoplanetary disks, the Kuiper belt of comets, and in secondary cratering events on asteroids and planetary satellites. In most of these situations the surface gravity of the target is less than a few per cent of 1 g. Asteroids and planetary satellites are observed to have a regolith consisting of loose, unconsolidated material. Planetary ring particles likely are also coated with dust based on observations of dust within ring systems [1]. The formation of planetesimals in protoplanetary disks begins with the accretion of dust particles. The response of the surface dust layer to collisions in the near absence of gravity is necessary for understanding the evolution of these systems.

The Collisions Into Dust Experiment (COLLIDE) performs six impact experiments into simulated regolith in microgravity conditions on the space shuttle [2]. The parameter space to be explored is quite large, including effects such as impactor mass and velocity, impact angle, target porosity, size distribution, and particle shape. We have developed an experiment, the Physics of Regolith Impacts in Microgravity Experiment (PRIME), that is analogous to COLLIDE that is optimized for flight on the NASA KC-135 reduced gravity aircraft. The KC-135 environment provides the advantage of more rapid turnover between experiments, allowing a broader range of parameters to be studied quickly, and more room for the experiment so that more impact experiments can be performed each flight. The acceleration environment of the KC-135 is not as stable and minimal as on the space shuttle, and this requires impact velocities to be higher than the minimum achievable with COLLIDE.

The experiment consists of an evacuated PRIME Impact Chamber (PIC) with an aluminum base plate and acrylic sides and top (Figure 1). A target tray, launcher, and mirror mount to the base plate. The launcher may be positioned to allow for impacts at angles of 30, 45, 60, and 90 degrees with respect to the target surface. The target material is contained in a 10 cm by 10 cm by 2 cm tray with a rotating door that is opened via a mechanical feed-through on the base plate. A spring-loaded inner door provides uniform compression on the target material prior to operation of the experiment to keep the material from settling or locking up during vibrations prior to the experiment. Data is recorded with the NASA high speed video camera. Frame rates are selected according to the impact parameters. The direct camera view is orthogonal to the projectile line of motion, and the mirrors within the PIC provide a view normal to the target surface. The spring-loaded launchers allow for projectile speeds between 10 cm/s and 500 cm/s with a variety of impactor sizes and densities. On each flight 8 PICs will be used, each one with a different set of impact parameters.

(a) (b)

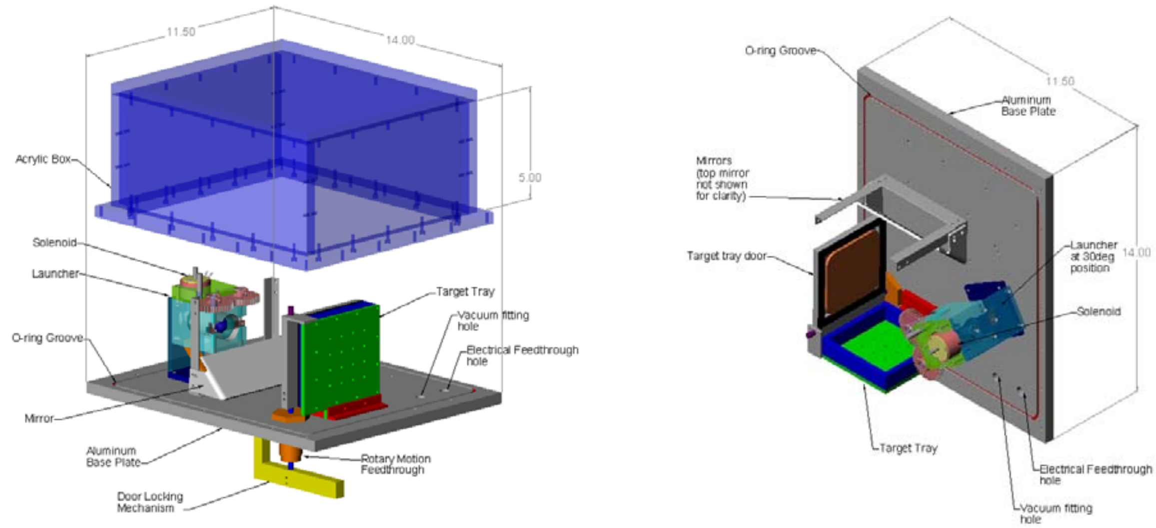

Figure 1: Schematic of PRIME Impact Chamber. (a) The closed target tray at right has vent holes to allow evacuation of pore spaces in the target material. The launcher is positioned for a normal impact onto the target surface. The handle for opening the target tray door is visible below the base plate. (b) The PIC in flight orientation with the target tray door open and the launcher positioned for a 30 degree impact. The acrylic top is not shown for clarity.

The target tray mechanism was tested on the KC-135 in July 2001, and the launchers follow the design of the COLLIDE launchers. The first flight of PRIME is scheduled for the week of July 8, 2002, with repeated flights throughout the year. The anticipated data include the normal and tangential coefficients of restitution for the impactor, the velocity distribution and mass of the ejecta, and the dependence of these quantities on the following parameters: impactor velocity, impactor mass, impactor density, and target particle properties. Initial experiments will be conducted at conditions as close to zero-g as possible, while subsequent experiments will explore the effects of increasing the acceleration to lunar and Martian levels. The range of impact velocities to be studied is 10 cm/s to 500 cm/s. This overlaps the range of impact velocities in the COLLIDE experiment (1 cm/s to 100 cm/s) as well as concurrent ground-based experiments at impact speeds above 100 cm/s [3].

Preliminary results from COLLIDE-2 and ground-based experiments suggest that PRIME will be able to explore the transition regime between accretional impacts (where the impactor sticks to the target and there is little or no ejecta) and erosional impacts (where the impactor rebounds and/or significant ejecta is produced). Results from PRIME will be combined with results from COLLIDE, ground-based experiments at 1 g, and numerical simulations employing discrete element models to develop parameterized models for the outcomes of low velocity collisions in various astrophysical contexts. These models will then be applied to models of planetesimal formation, the evolution of planetary rings, and the production of regolith on asteroids and planetary satellites.

REFERENCES

[1] Esposito, L. W., *Annu. Rev. Earth Planet. Sci.,* **21**, 487 (1993).

[2] Colwell, J. E., and M. Taylor, *Icarus*, **138**, 241 (1999).

[3] Colwell, J. E., and M. T. Mellon, *33rd Lunar Planet. Sci. Conf.*, Abs. #1757 (2002).

MULTIPLE LIGHT SCATTERING USING 3^{RD} ORDER CORRELATION FUNCTIONS

A. S. Gittings, P. A. Lemieux and D. J. Durian*
Department of Physics and Astronomy, University of California, Los Angeles, CA 90095-1547

ABSTRACT

Multiple light scattering provides a non-invasive method for probing the structure of optically opaque materials such as aqueous foam, colloids and sand. Diffusion-wave spectroscopy (DWS) [1-3] examines the intensity fluctuations of the speckle pattern to extract dynamical information about the scattering sites. When many, uncorrelated scattering sites are present, the electric field is a random Gaussian variable, and the dynamics are easily determined from the second order intensity correlation function $g^{(2)}$.

$$g^{(2)}(\tau) = 1 + \beta|<E(0)E^*(\tau)>|^2/|<EE^*>|^2 \qquad \ldots(1)$$

$$g^{(2)}(\tau) = 1 + \beta|\gamma(\tau)|^2 \qquad \ldots(2)$$

This crucial relation relates the measured $g^{(2)}$ with the electric field auto-correlation function $\gamma(\tau)$, which can then be expressed in terms of the scattering site dynamics.

It is not possible, however, to tell whether the Gaussian approximation is valid by inspection of $g^{(2)}$ alone. Recently, a method has been developed to test whether the scattering is Gaussian by measuring higher order intensity correlation functions [3]. In this experiment we measured the third order intensity correlation function $g^{(3)}$ for aqueous foam (Gillette Foamy Regular) and compared it with the Gaussian prediction for $g^{(3)}$.

$$g^{(3)}(\tau_1, \tau_2) = 1 + \beta_1(|\gamma_{01}|^2\,|\gamma_{02}|^2\,|\gamma_{12}|^2) + 2\beta_2 \mathrm{Re}(\gamma_{01}\gamma_{12}\gamma_{20}) \quad \ldots(3)$$

Preliminary data indicate that the scattering is Gaussian to sixth order in the electric field.

REFERENCES

[1] D. Weitz and D. Pine, "Diffusing-wave spectroscopy," *in dynamic light scattering: The Method and Some Applications*, W. Brown, ed. (Clarendon, Oxford, UK, 1993, pp. 652-720.
[2] G. Maret, "Diffusing-wave spectroscopy," Curr. Opin. Colloid Interface Sci. **2**, 251-257 (1997).
[3] P. A. Lemieux and D. J. Durian. "Investigating non-Gaussian scattering processes by using nth-order intensity correlation functions." *Journal Optical Society of America A*, **16**(7):1651-64, (1999).

* P.I. , 2-240A Knudsen Hall, Department of Physics and Astronomy, University of California Los Angeles, CA 90095-1547, USA. E-mail:durian@physics.ucla.edu, FAX: 310-206-5668, Phone: 310-206-2645.

ABSORPTION OPTICS OF AQUEOUS FOAMS

Ranjini Bandyopadhyay, Alex Gittings and D. J. Durian*
Department of Physics and Astronomy, University of California,
Los Angeles, CA 90095-1547

ABSTRACT

Aqueous foams are composed of gas bubbles packed together in a small volume of soapy water. The large number of gas-liquid interfaces in foams results in very strong scattering of light, which explains the opaque nature of conventional aqueous foams such as shaving foams and mousse. For dry foams, the interfaces can take the following three forms : the soap films where two bubbles meet, the triangular plateau borders where three soap films meet and the vertices where four plateau borders meet [1]. Previous experiments have shown that most of the scattering occurs from the plateau borders [2,3] and the transport mean free path of light (l*), the bubble radius (R) and the liquid fraction of foam (ε) is related through the relation $l^*=R/\varepsilon^{0.5}$ [2].

To understand the reflection and scattering of light at the gas-bubble interfaces, we study the absorption of photons in the liquid network as a function of the foam absorptivity. We do this to confirm if the time spent by the photons in the liquid phase is proportional to the liquid fraction of the foam. Our results indicate that for a specific range of liquid fractions ($0.05 < \varepsilon < 0.1$), the photons seem to get *trapped* in the liquid network. This result is independent of the absorptivity of the foam and leads us to conclude that under appropriate conditions, an aqueous foam behaves very much like an optical fiber network.

Aqueous foam is generated in the lab by the method of turbulent mixing [4] of N_2 gas with a jet of alpha-olefin-sulfonate (AOS) solution. The foam has been made absorbing by dissolving small quantities of rhodamine dye ([R] = 0.005 g/l, [R] = 0.01 g/l and [R] = 0.0124 g/l) in the AOS solution. The transmission of photons through the foams of liquid fractions $0.0297 < \varepsilon < 0.35$ has been studied using Diffuse Transmission Spectroscopy (DTS). For each liquid fraction, the transport mean free path l* (the length over which the photon travels before it gets completely randomized) has been estimated from DTS experiments on foams with [R] = 0.0 g/l. The absorption length of foams (l_a^{foam}) of various absorptivities has been estimated by fitting the transmission *vs*. thickness data to the formula [5]

$$T_d = \frac{1+z_e}{[1+(D_o^2+z_e^2)\mu_a'/D_o)\sinh(L'\sqrt{\alpha})/\sqrt{\alpha}+2z_e\cosh(L'\sqrt{\alpha})]} \quad \ldots (1)$$

In Eqn. (1), z_e is the extrapolation length ratio (distance outside the sample, in units of l*, where the photon flux extrapolates to 0), D_o = 0.33 is the dimensionless diffusion coefficient, $\mu_a' = l^*/l_a^{foam}$, $L' = L/l^*$ (L is the thickness of the sample) and $\alpha = \mu_a'\,(1/D_0+\mu_a')$.

Fig. 1 shows a plot of the ratio l_a^{foam}/l_a^{soln} for the liquid fraction range investigated, for all three rhodamine concentrations. l_a^{soln} is the absorption length of the pure rhodamine solution estimated using transmission measurements. In the liquid fraction range $0.05 < \varepsilon < 0.1$, the ratio is found to be lower than the theoretical prediction ($l_a^{foam}/l_a^{soln} \sim 1/\varepsilon$, shown by solid line in Fig. 1). The deviation of the experimental estimates of l_a^{foam}/l_a^{soln} from the solid line leads us to conclude that at $0.05 < \varepsilon < 0.1$, the foam behaves like an optical fiber network with the photons getting trapped in and then channeled through the plateau borders. We believe that our results may be explained quantitatively by relating the reflectance of light at liquid-gas and gas-liquid interfaces to the average angles of incidence at these interfaces.

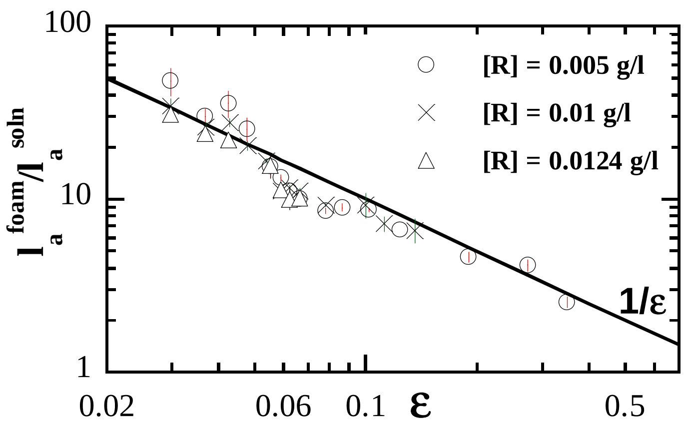

Fig. 1 : Ratio of absorption length of foam to that of the pure rhodamine solution for the liquid fraction range $0.05 < \varepsilon < 0.1$ and [R] = 0.005 g/l (circles), 0.01 g/l (crosses) and 0.0124 g/l (triangles). The solid line ($y = 1/\varepsilon$) is the theoretical prediction assuming that the time spent by the photon in the liquid network is proportional to ε.

REFERENCES

* P.I. , 2-240A Knudsen Hall, Department of Physics and Astronomy, University of California Los Angeles, CA 90095-1547, USA. E-mail:durian@physics.ucla.edu, FAX: 310-206-5668, Phone: 310-206-2645.

[1] D. Weaire and S. Hutzler, *The Physics of Foams* (Oxford University Press, New York, 1999).

[2] M. U. Vera, A. Saint-Jalmes and D. J. Durian, Applied Optics **40**, 4179 (2001).

[3] D. J. Durian, D. A. Weitz and D. J. Pine, Science (USA) **252**, 686 (1991).

[4] A. Saint-Jalmes, M. U. Vera and D. J. Durian, European Physical Jl. B **12**, 67 (1999).

[5] A. Cox and D. J. Durian, Applied Optics **40**, 4228 (2001).

Phase-Shifting Liquid Crystal Interferometers for Microgravity Fluid Physics

DeVon W. Griffin
Microgravity Fluid Physics Branch
NASA Glenn Research Center
21000 Brookpark Road
Cleveland, OH 44135

Kenneth L. Marshall
Laboratory for Laser Energetics
University of Rochester
250 East River Rd
Rochester, NY 14623

Fluid physics investigations frequently need to measure the density of fluids and gases. Ground laboratories typically use interferometry for such measurements. However, interferometry can be difficult to employ in reduced gravity laboratories due to both the path lengths that are typically required and effects of parasitic vibrational noise. While older common path interferometers are relatively compact and are more immune to vibration, thus overcoming these problems, they have not been capable of phase-shifting, which is required for the most accurate data. Recent work demonstrated phase-shifting common-path interferometers based on liquid crystal devices.[1] However, initial interferometers did not operate at video frame rates and suffered from variations in optical density with applied voltage. The initial focus of this project was to eliminate both of these problems in the Liquid Crystal Point-Diffraction Interferometer (LCPDI). Progress toward that goal will be described, along with the demonstration of a phase shifting Liquid Crystal Shearing Interferometer (LCSI) that was developed as part of this work.

Mercer, Creath and Rashidnia[2] demonstrated that the liquid crystal point diffraction interferometer produced data as accurate as that generated using a Mach Zehnder interferometer. While accurate, this device could not operate at video frame rates, presented alignment difficulties due to the large number of microspheres used as spacers and suffered from voltage-dependent fluctuations in optical density.

Figure 1 is a photograph of the latest LCPDI. Other than a lens to focus the light from a test section onto a diffracting microsphere within the interferometer and a collimated laser for illumination, the pink region contained within the glass plates on the rod-mounted platform is the complete interferometer. The total width is approximately 1.5 inches with 0.25 inches on each side for bonding the electrical leads. It is 1 inch high and there are only four diffracting microspheres within the interferometer. As a result, it is very easy to align, achieving the first goal.

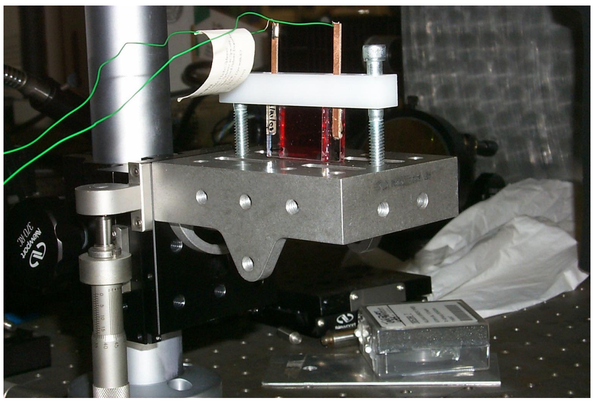

Figure 1 LCPDI

The liquid crystal electro-optical response time is a function of layer thickness, with thinner devices switching faster due to a reduction in long-range viscoelastic forces between the LC molecules. The LCPDI in Figure 1 has a liquid crystal layer thickness of 10 microns, which is controlled by plastic or glass microspheres embedded in epoxy "pads" at the corners of the device. The diffracting spheres are composed of polystyrene/divinyl benzene polymer with an initial diameter of 15 microns. The spheres deform slightly when the interferometer is assembled to conform to the spacing produced by the microsphere-filled epoxy spacer pads. While the speed of this interferometer has not yet been tested, previous LCPDIs fabricated at the Laboratory for Laser Energetics switched at a rate of approximately 3.3 Hz, a factor of 10 slower than desired. We anticipate better performance when the speed of these interferometers is tested since they are approximately three times thinner.

Phase shifting in these devices is a function of the AC voltage level applied to the liquid crystal. As the voltage increases, the dye in the liquid crystal tends to become more transparent, thus introducing a rather large amount of error into the phase-shifting measurement. While that error can be greatly reduced by normalization, we prefer eliminating the source of the error. To that end, we have pursued development of a "blend" of custom dyes that will not exhibit these properties. That goal has not yet been fully achieved as is illustrated by the set of five interferograms in Figure 2. Guardalben, et al, presented a similar set of interferograms in a paper partially funded by this grant.[3]

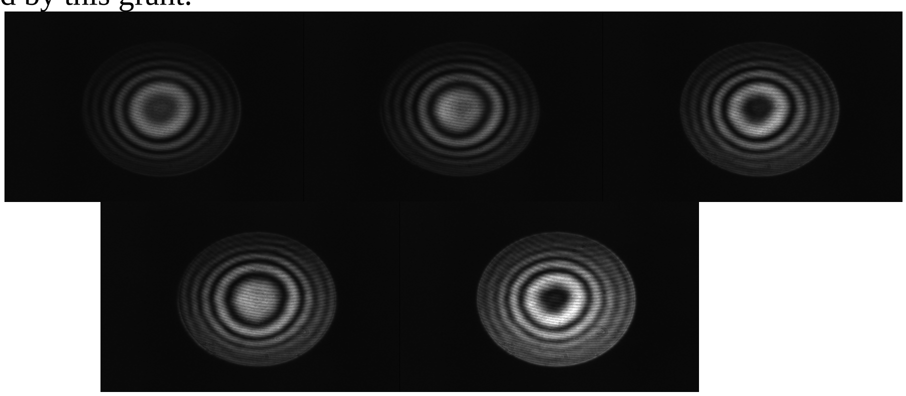

Figure 2 Set of five interferograms shifted by 90 degrees between each image

Shearing interferometers are a second class of common path interferometers. Typically they consist of a thick glass plate optimized for equal reflection from the front and back surface. While not part of the original thrust of the project, through the course of laboratory work, we demonstrated a prototype of a shearing interferometer capable of phase shifting using a commercial liquid crystal retardation plate.[4] A schematic of this liquid crystal shearing interferometer (LCSI) and a sample set of interferograms are in the reference.

This work was also supported by the U.S. Department of Energy Office of Inertial Confinement Fusion under Cooperative Agreement No. DE-FC03-92SF19460, the University of Rochester, and the New York State Energy Research and Development Authority. The support of DOE does not constitute an endorsement by DOE of the views expressed in this article.

References:

1. Mercer, C.R., Creath, K. , "Liquid-crystal point-diffraction interferometer for wave-front measurements," Applied Optics, **35**, 1633-1642 (1996).
2. Mercer, C.R., Rashidnia, N. and Creath, K., "High data density temperature measurement for quasi steady-state flows," Experiments in Fluids, **21**, 11-16 (1996).
3. Guardalben, M.J., Ning, L., Jain, N., Battaglia, D.J. and Marshall, K.L., "Experimental comparison of a liquid-crystal point-diffraction interferometer (LCPDI) and a commercial phase-shifting interferometer and methods to improve LCPDI accuracy," Applied Optics, **41**, 1535-1365 (2002).
4. Griffin, D.W., "Phase-shifting shearing interferometer," Optics Letters, **26**,140-141 (2001).

RHEOLOGY OF FOAM NEAR THE ORDER-DISORDER PHASE TRANSITION

R. Glynn Holt (rgholt@bu.edu) and J. Gregory McDaniel (jgm@bu.edu), Boston University, Dept. of Aerospace and Mechanical Engineering, 110 Cummington St, Boston, MA 02215

INTRODUCTION AND MOTIVATION

Foams are extremely important in a variety of industrial applications. They are widely used in firefighting applications, in flow applications such as enhanced oil recovery, and as trapping, transport and separation agents. The most important quality of a foam in many of these industrial processes is its response to imposed strain, or its *rheological* behavior. There exists little experimental data on the rheological properties of real 3D foams, even though such knowledge would likely enhance the efficacy of current applications and suggest other unique applications. The lack of 3D data is due in large part to the earth-based requirements for contact containment, and to the fact that gravity-induced drainage quickly destroys all but the "driest" foams, those with a very high gas volume fraction α_g. We introduce a unique method to provide non-contact control and manipulation of foam samples. The development of this technique will provide the ability to carry out a set of benchmark experiments in **0g** allowing determination of a foam's yield stress, bulk shear and dilatational moduli and viscosities as a continuous function of gas volume (or 'void') fraction α_g from the dry limit ($\alpha_g \approx 1$) through the order-disorder phase transition to the wet limit ($\alpha_g \ll 1$) of a bubbly liquid.

OBJECTIVES

The goal of the investigation is the determination of the mechanical and rheological properties of foams, utilizing the microgravity environment to explore foam rheology for foams that cannot exist, or only exist for a short time, in **1g**. *The specific objectives of the investigation are:*

1) To refine and utilize a novel, non-contact acoustic technique for experimentally measuring the stress-response of small samples of foam ("foam drops") subjected to both static and time-varying acoustic strain.
2) To experimentally measure the stress-response of foam drops subjected to both static and time-varying strain.
3) To model the response of foam drops to static and time-varying modulation of the acoustic field to extract rheological properties.
4) To define experiments that can be performed in the μg environment, where the effects of drainage, buoyancy and high acoustic fields can be avoided, and α_g can be varied smoothly through the order-disorder transition.

RESULTS

Our ground-based investigations have concentrated on the investigation and analysis of normal-mode oscillations of foam drops. We can organize the presentation of our results to date by void fraction:

Dry limit, effective medium model. In the limit of dry foams (void fraction greater than the critical value, and approaching unity) and small deformations from equilibrium, we model foam as an effective elastic solid medium. In [1] we present a model for the normal modes of oscillation of an effective elastic sphere. By specifying (via measurement) the natural frequency of a specific mode we may infer the effective shear elastic modulus G of the foam via the formula

$$G = \rho \left(\frac{\omega R}{\xi} \right)^2 \frac{1-2\upsilon}{2(1-\upsilon)} \qquad \textbf{(1)}$$

where ρ is the effective density of the foam, ω is the measured modal frequency, R is the measured drop radius, ξ is the computed dimensionless modal frequency from the model, and ν is Poisson's ratio for the foam.

Results for a drop with void fraction of 0.8 yielded a shear modulus $G = 75 \pm 3$ Pa, which is of the same order as several estimates of the shear modulus of foams reported in the literature using contact-based techniques. Importantly, this result was insensitive to the foam's Poisson ratio, which is difficult to independently measure.

Wet limit, bubble dynamics model. In the limit of 'low' void fractions (roughly 0.5 and below) we model foam as a bubbly liquid. In [2] we develop a model for the dynamics of a spherical drop of such a foam which retains fully nonlinear behavior of individual bubbles. The primary advantage of this bubble-based model is that it has predictive power.

In the limit of linear, inviscid motion we obtain approximate analytic expressions for the normal mode frequencies of a spherical foam drop of equilibrium radius R_0 as a function of the equilibrium void fraction α_{g0}:

$$\omega_n^2 \approx \frac{\sigma n(n-1)(n+2)}{\rho_l (1-\alpha_{g0}) R_0^3} = \omega_{n,pureliquid}^2 \cdot \frac{1}{(1-\alpha_{g0})} \qquad \omega_0^2 \approx \frac{\omega_{SB}^2}{\frac{3R_0^2}{\pi^2 a_0^2} \alpha_{g0} \ (1-\alpha_{g0}) + 1 - \alpha_{g0}^{1/3}} \qquad \mathbf{(2)}$$

The shape mode frequencies ω_n of mode number $n \geq 2$ (after a Legendre polynomial expansion) are approximately the mass-corrected Lamb frequencies for a pure liquid drop, where σ is the surface tension, and ρ_l is the liquid component density. The breathing mode frequency ω_0 depends on the frequency ω_{sb} of the individual bubble constituents of radius a_0 as well as the void fraction.

MICROGRAVITY RELEVANCE AND SIGNIFICANCE

All but the driest foams drain in gravity. The liquid component will flow downward, and the bubbles will rise until a pool of liquid with a dry foam cap will form. Gravity will thus prevent the measurement of foam properties as the gas volume fraction is decreased towards the order-disorder transition, because the foam will be destroyed. There is very little experimental data on the rheological properties of 3D foams, primarily because potential experiments are severely hindered by the requirement for contact containment, and draining and thinning due to gravity.

Our experimental technique can provide non-contact control and manipulation of multicomponent and multiphase drops. In comparison with existing experimental techniques for rheological measurements, our technique offers at least four advantages. First, it is a non-contact technique that can nevertheless provide stable positioning and straining manipulation of a sample. Second, we can easily levitate and strain samples of arbitrary void fraction continuously from 0 to 1. Third, we can test small samples of foam with variable number and size of bubbles to investigate limiting cases. Finally, we can simultaneously measure shear and compressional parameters, whereas traditional techniques are restricted to either of these.

REFERENCES

[1] J. Gregory McDaniel and R. Glynn Holt, "Measurement of aqueous foam rheology by acoustic levitation", Phys. Rev. E **61**, 2204 (2000).

[2] J. Gregory McDaniel, Iskander Akhatov, and R. Glynn Holt, "Inviscid dynamics of a wet foam drop with monodisperse bubble size distribution", Phys Fluids **14**, 1886-1894 (2002).

GRANULAR MATERIAL FLOWS WITH INTERSTITIAL FLUID EFFECTS

M. L. Hunt[1] and C. E. Brennen
California Institute of Technology, Pasadena, CA 91125

C.S. Campbell
University of Southern California, Los Angeles, CA

ABSTRACT

In 1954, R.A. Bagnold published his seminal findings on the rheological properties of liquid-solid flows. Over the last fifty years, this work has been cited extensively in studies of granular and debris flows, sedimentation, suspensions, magma flows, sand transport and a range of other multiphase flow processes. We recently completed an extensive reevaluation of Bagnold's work (Hunt, et al. 2002) and our analysis and simulations indicate that the rheological measurements of Bagnold were affected significantly by secondary flows within the experimental apparatus. The concentric cylinder rheometer was designed by Bagnold to measure simultaneously the shear and normal forces for a wide range for solid concentrations, fluid viscosities and shear rates. As presented by Bagnold, the shear and normal forces depended linearly on the shear rate in the `macroviscous' regime. As the grain-to-grain interactions increased in the `grain inertia' regime, the stresses depended on the square of the shear rate and were independent of the fluid viscosity. These results, however, appear to be dictated by the design of the experimental facility. In Bagnold's experiments, the height (h) of the rheometer was relatively short compared to the spacing (t) between the rotating outer and stationary inner cylinder (h/t=4.6). Since the top and bottom end plates rotated with the outer cylinder, the flow contained two axisymmetric counter-rotating cells in which flow moved outward along the end plates and inward at the midheight of the annulus. These cells contribute significantly to the measured torque, and obscured any accurate measurements of the shear or normal stresses.

Before doing the reevaluation of Bagnold's work, our research objective was to examine the effects of the interstitial fluid for flows in which the densities of the two phases were different. In Bagnold's original work, only neutrally buoyant spheres were used. Because of the questions that we have raised regarding Bagnold's measurements, the scope of our work can be expanded because issues associated with neutrally buoyant particles as well as flows of dissimilar densities are of considerable scientific interest and there appears to be no corresponding experimental measurements. The reduced-gravity environment on the KC135 aircraft will enable the measurements of particles of mismatched without having a separation of the two phases.

[1]Division of Engineering and Applied Science, Caltech, Pasadena, CA 91125; phone (626) 395-4231; fax (626) 568-2719; hunt@caltech.edu

After reevaluating Bagnold's work, we redesigned our experimental facility to minimize secondary flow effects. Like Bagnold's facility, we use a concentric cylinder rheometer with a rotating outer wall. The inner cylinder also is able to rotate slightly but will also be restrained by flexible supports; the torque is measured from the deformation of the flexures. The normal force is measured using piezoelectric transducers that record both impacts with the surface and fluid pressure variations resulting from particle collisions. Unlike Bagnold's apparatus, the top and bottom plates of the annulus will not rotate, and the torque measurement will be measured only in the center region of the inner annulus; these changes will minimize the secondary flow effects.

The experiments will cover a range of particle sizes (from d = 1.5 to 4 mm), particle concentrations (up to 55% solids concentration by volume), shear rates (γ = 10-160 sec^{-1}) and solid-to-fluid densities (ρ_p = 1.2 to 8). During one flight of the KC-135 we will change two parameters: the rotational speed and the fluid viscosity (μ). At one time during a flight, we plan to withdraw some of the fluid (water for example) within the annulus while injecting some fluid of a different viscosity (water-glycerin mixture). Hence, the experiments will cover flows where the particle inertia dominates the fluid effects (granular flows) to flows in which the fluid inertia dominates that of the particles (dilute suspension). The range of Stokes numbers ($St=d^2\gamma\rho_p/\mu$) will be from about 5 to 3000.

Currently, the experimental facility has just been completed. We have calibrated the normal impact measurements using carefully controlled single particle impacts with the transducers. The torque measurements have also been calibrated by mounting the inner cylinder in such a way that we could impose a known load on the drum. We use reluctance transducers to measure the motion and deformation of the flexures and calibrate the device with the imposed load. Measurements will also be made of the fluid temperature, acceleration and rotational speed of the outer drum.

The poster will overview the current status of our experiment and the planned experimental program.

REFERENCES

R.A. Bagnold, Experiments on a Gravity-Free Dispersion of Large Solid Spheres in a Newtonian fluid under Shear, ***Proc. R. Soc. London*** **225**, 49-63 (1954).

M.L. Hunt, R. Zenit, C.S. Campbell and C.E. Brennen, Revisiting the 1954 Suspension Experiments by R.A. Bagnold, ***J. Fluid Mechanics***, **452**, 1-24 (2002).

PHASE TRANSITION IN DUSTY PLASMAS:

A MICROPHYSICAL DESCRIPTION*

Glenn Joyce, Gurudas Ganguli, and Martin Lampe

Plasma Physics Division, Naval Research Laboratory, Washington, DC 20375-5346

ABSTRACT

Dust grains immersed in plasma discharges acquire a large negative charge and settle into a dust cloud at the edge of the sheath. In this region, the plasma ions stream toward the electrode at a velocity $\mathbf{u} \sim c_s=(T_e/m_i)^{1/2}$. Experimentally at sufficiently high gas pressure P, the random kinetic energy of the grains is damped by gas friction, and the grains are strongly coupled and self-organize into a crystalline configuration [1-3]. For lower pressures despite the dissipation of grain kinetic energy to gas friction, the dust grains reach a steady-state kinetic temperature T_d which is much larger than the temperature of any other component in the plasma. T_d is so large that the dust acts like a fluid [1-3]. We have used the dynamically shielded dust (DSD) model [4] to simulate these physical processes. We find that the known experimental features are nicely reproduced in the simulations, and that additional features are revealed. In the figure we plot the variation of T_d as P is continuously varied in a DSD code run. A marked difference is evident between the critical pressure P_m for the melting transition as P is decreased, and the critical pressure P_c for the condensation transition as P is increased. For $P_m < P < P_c$, mixed phase states are seen. This hysteresis occurs because the instability which triggers melting is different from the instability that heats the dust in the fluid phase and inhibits freezing.

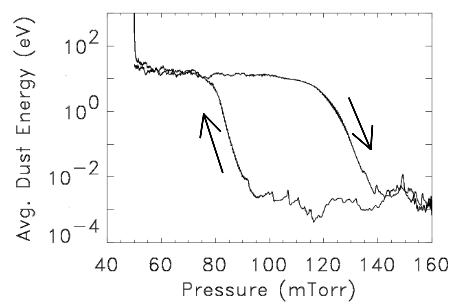

CONDENSATION: At low pressure, the dust is subject to a two-stream instability with the ions. This instability is responsible for the high temperature of the dust at low pressure. For further details we refer the reader to Ref [4].

MELTING: The basic physics underlying the melting transition has been elucidated in a series of papers [2,5,6]. In Refs [2,5] a phenomenological model for the asymmetric interaction between grains is constructed. We are developing a first-principles analytic approach to the melting transition, which embodies the same physics that is present in the DSD code. The inter-grain potential is the dynamically shielded Coulomb interaction, given in k-space by

$$\phi(k) = \sum \frac{Z_i e}{2\pi^2 k^2 D(k, -\mathbf{k}\cdot\mathbf{u} + i\nu_i)}, \qquad (2)$$

where $D(k,\omega)$ is the linear plasma response function defined in Refs [4,7].

Crystal instabilities can be represented at various levels of detail. Experiments and DSD simulations indicate that the mode which initiates the melting process is a shear mode with propagation vector $\mathbf{k}$ parallel to the ion streaming. In the linear stage of this mode, the equation of motion of a grain in the jth layer, due to the forces exerted by the grains directly above and directly below, is

$$m\Delta\ddot{x}_j = C^+(\Delta x_{j+1} - \Delta x_j) + C^-(\Delta x_{j-1} - \Delta x_j) - m\nu_d \Delta\dot{x}_j \tag{3}$$

where

$$C^{\pm} \equiv \left[\frac{\partial^2 Ze\phi(\Delta x, z = \mp d)}{\partial(\Delta x)^2} \right]_{\Delta x = 0}, \tag{4}$$

$\phi(x,z)$ is the Fourier transform of Eq. (2), d is the separation between grain layers, and Δx is the displacement of the grain from its equilibrium position in the x direction (transverse to the propagation direction z). Unlike the situation in ordinary crystals, the force constants $C^{\pm}$ are such that $C^+ \neq C^-$. For a transverse mode in an infinite crystal, $\Delta x_j \sim \exp[i(jkd-\omega t)]$, Eq. (3) leads to a dispersion relation

$$\omega = -\frac{i\nu_d}{2}\left\{1 \mp \sqrt{1 - \frac{4}{m\nu_d{}^2}\left[(C^+ + C^-)(1-\cos kd) - i(C^+ - C^-)\sin kd\right]}\right\}. \tag{5}$$

Eq. (5) is similar to the dispersion relation for phonons in an ordinary crystal, except that here instability occurs because $C^+ \neq C^-$. The instability can be stabilized at high pressure due to the dust collisionality ν_d and/or the ion collisionality ν_i, which appears as damping of the attractive wake force C^- through the dielectric D in Eq. (2). The phonon streaming instability is similar to the two-stream instability that occurs in the fluid-dust phase. However, the stabilization pressure P_m for the phonon instability is lower than the critical pressure P_c for Buneman instability (i.e. for freezing), as indicated by the DSD code results. There is a range of pressures where both the solid and fluid phases of the dust are stable, which allows a mixed-phase system to exist, as observed [2].

REFERENCES

1. Melzer, A., et al, Phys. Rev. E54, R46, 1996; Phys. Rev. E **53**, 2757 (1996); Phys. Lett. A **191**, 301 (1994); Phys. Rev. E54, R46, 1996; Phys. Rev. E **53**, 2757 (1996); Phys. Lett. A **191**, 301 (1994)
2. Thomas, H,. *et al*, Phys. Rev. Lett. **73**, 652 (1994); Nature (London) **379**, 806 (1996); J. Vac. Sci. Technol. A **14**, 501 (1996); Phys. Rev. Lett. **73**, 652 (1994).
3. Chu, J. H. and Lin I, Phys. Rev. Lett. **72**, 4009 (1994).
4. Joyce, G., Lampe, M., and Ganguli, G., Phys. Rev. Lett., 88, 095006-1, 2002
5. Schweigert, V. A., *et al.*, Phys. Rev. E **54**, 4155 (1996); Phys. Rev. Lett. **80**, 5345 (1998).
6. Melandso, F., Phys. Rev. E **55**, 7495 (1997).
7. Lampe, M., Joyce, G., and Ganguli, G., Phys. Scripta T89, 106 (2001); IEEE Trans. Plasma Science **29**, 238 (2001); Proceedings ISSS, 2002 (to appear).

*This work was supported by NASA and ONR.

Glenn Joyce, Code 6790, Naval Research Laboratory, 20375
Phone(202)767-6785. Fax (202)767-0631. joyce@ppd.nrl.navy.mil

Experimental study of turbulence-induced coalescence in aerosols

Paul Duru, Luying Wang, Claude Cohen and Donald L. Koch

School of Chemical Engineering, Cornell University, Ithaca NY 14853, USA.

Abstract

An aerosol consists of a dispersion of liquid particles in a gas. Coalescence occurs when Brownian motion, differential sedimentation or turbulent gas flow drive two drops into contact and the drops form a larger drop. Coalescence modifies the size distribution of an aerosol which in turn affects its main properties. For instance, raindrop coalescence play an important role in cloud dynamics, precipitation and the scavenging of pollutants by precipitation.

The rate of coalescence depends on the forces driving the relative motion of the particles. A good fundamental understanding of the mechanisms of coalescence leading to quantitative predictions of coalescence rates has been achieved for colloidal particles suspended in liquids. This achievement is largely attributable to the ability of researchers to isolate each of the driving forces in turn by judicious use of the density matching of the fluid and particles and adjustment of the fluid viscosity. In contrast, the current understanding of aerosol coalescence is rudimentary. Moreover, in experimental conditions on Earth, one is likely to observe mixed effects of Brownian motion, sedimentation and turbulence on coalescence making a critical test of theory difficult.

We present an experimental ground-based study of aerosol coalescence due to turbulence. It will provide the necessary background to plan a microgravity experiment on aerosol coalescence.

An initially nearly monodisperse aerosol with high particle number density (typically $\sim 10^6$particles/cm^3) is produced using a Condensation Monodisperse Aerosol Generator (TSI 3475). It flows continuously through a plexiglass cell where it experiences a turbulent flow field generated by an oscillating grid (see Figure 1). The initial size distribution is then modified due to turbulence-induced coalescence. Using droplets with an initial mean diameter of 3 μm, we maximize the importance of turbulence on coalescence relative to Brownian motion (important for smaller particles) and sedimentation (important for larger particles).

To be able to compare experimental data on turbulence-induced coagulation with theory, a precise description of the turbulent flow field is necessary. It has been characterized by measuring the velocity fluctuations using a laser Doppler velocimetry technique (a typical result is shown in Figure 2). The turbulent kinetic energy is found to be constant in the central region of the cell (within a distance away from the grid mean position equal to half the stroke of the grid displacement) and then to decay away from the grid. Our results are similar to which one expects, based on previous experiments in liquids. In order to characterize the coalescence, the particle size distribution is measured *in situ* using a Particle Dynamics Analyser. This technique is based on the analysis of the light scattered by the particles as they cross a volume of measurement defined by the intersection of two laser beams. The

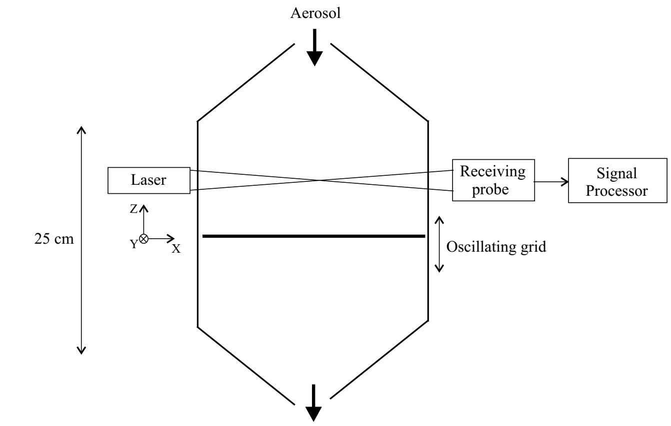

Figure 1: Sketch of the experimental setup.

size distribution being known, the particle number density can be measured using a light attenuation technique.

As already mentioned, the extent to which we can isolate turbulence from the other mechanisms that may lead to coagulation is limited and this forms the motivation for the future microgravity experiments. Under microgravity, we will be able to use substantially larger particles and eliminate Brownian motion without introducing effects of sedimentation. However, this ground-based experiment will demonstrate the validity of our experimental methods to characterize the coalescence.

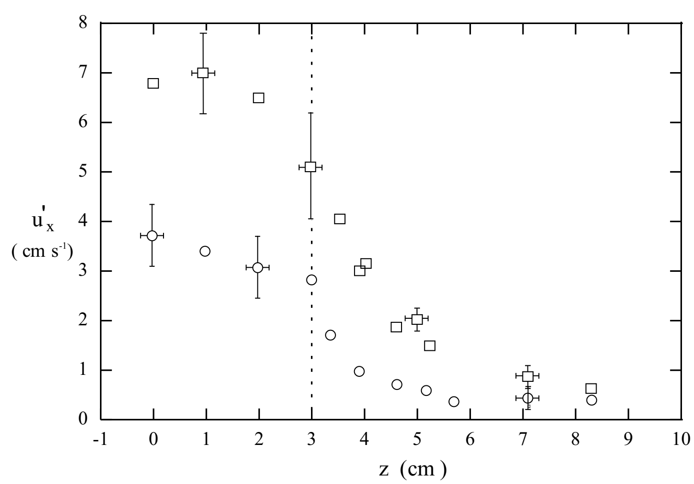

Figure 2: Velocity fluctuation of the x-component of the velocity, u_x', as a function of the distance z to the grid mean position. The grid is oscillating around the position $z = 0$ with a 6 cm stroke, at a frequency $f = 2\,\text{Hz}$ (circle), $f = 4\,\text{Hz}$ (square). At a given z, the value of the velocity fluctuations is obtained by averaging over several positions in the $x\!-\!y$ plane.

NON STEADY STATE GRANULAR SHEAR FLOWS

Wolfgang Losert[1], **Gene Kwon**
Department of Physics, IPST, and IREAP, University of Maryland, College Park, MD 20742

ABSTRACT

We experimentally investigate the shear flow of granular matter in a cylindrical Couette cell. Since granular flows dissipate energy, they must be continuously driven to remain in a flowing state. Previous experiments on steady state shear flows have found that velocity gradients are confined to a thin shear band, and that the shear force is roughly independent of shear rate if the material is allowed to dilate[1,2]. Our experiments in a Couette geometry focus on two related questions about non-steady state flows:

1) How does a granular shear flow start?[3]
2) How does a granular system respond to oscillatory shear?

In particular, we investigate the role of boundary conditions, which we expect to be of particular importance, since granular flows must be continuously driven (in general from a boundary) in order to be sustained. In our Couette cell a shear flow is generated by moving either the inner cylinder or the outer cylinder or both cylinders.

The motion of grains on the top surface is measured directly with fast imaging and particle tracking techniques. Previous studies have indicated that the velocity profile on the top surface is very similar to the velocity profile within the bulk. Measurements of the corresponding shear forces are in progress.

Initial experiments determined the steady state flow profiles under different driving conditions, with either inner, outer or both cylinders moving. In steady state, velocity gradients are confined to a roughly exponential shearband several particle diameters wide. The shear band is always located at the inner cylinder. A probable reason for this observation is the slightly smaller surface area of the inner cylinder compared to the outer cylinder. Since shear forces are transmitted from one cylinder to the other, the smaller surface area of the inner cylinder leads to larger shear stresses. Shear flow confined to regions of high stress can be reproduced in continuum mechanics models which include plastic flow, non-Newtonian fluid models, or locally Newtonian hydrodynamic models that include a strong density dependence of viscosity.

Most of these models are isotropic with respect to the shear direction. However, anisotropies manifest themselves in two distinct flow transients, when rotation of one of the cylinders is started. When the cylinder had been rotated in the same direction before, the thin shear band immediately forms. When the previous motion of the cylinder had been in the opposite direction, particles far from the moving cylinder are initially more mobile. After an extra displacement of up to six particle diameters, a thin shearband forms again in steady state. The extra displacement of particles far from the shear surface does not strongly depend on the shear rate prior or after the stop, solely on the direction of prior shear. This indicates that the static configuration of grains

[1]Additional PI information: wlosert@glue.umd.edu , Fax: 301-405-1678 , phone: 301-405-6759

after a shear flow exhibits anisotropies. The flow transient, at least, can then no longer be modeled with the isotropic form of the models described above.

Finally, we investigate oscillatory shear flow. During small amplitude oscillations the shear flow is confined to a thin shear band. In addition, a gradual compaction and strengthening of the granular material is observed. For sufficiently large oscillation amplitudes, the flow resembles a sequence of shear reversals. In oscillatory flows driven by the outer cylinder, coexistence of shearbands at the outer and inner cylinder can be found.

In summary, we have elucidated important properties of granular shear flows from non-steady state flow measurements: First, shear bands form preferentially near the inner cylinder, even when the outer cylinder is sheared. Transiently a shear band can also form near the outer cylinder during oscillatory driving. These observations should help refine models of granular shear flow.

One challenge in improving models of granular shear flow is the observation that the initial flow transient contains "memory" of the direction of previously applied shear. In order to incorporate this observation into flow models, the nature of the anisotropy requires further study. Currently we are investigating the three dimensional configuration of grains during the start of shear flow using confocal microscopy.

---

[1] W. Losert, L. Bocquet, T.C. Lubensky, and J.P. Gollub, "Particle dynamics in sheared granular matter," *Phys. Rev. Lett* 85, 1428 (2000).

[2] L. Bocquet, W. Losert, T.C. Lubensky, and J.P. Gollub, "Granular Shear dynamics and forces: Experiments and continuum theory," Phys. Rev. E **65**, 011307 (2002).

[3] W. Losert and G. Kwon, "Transient and steady state dynamics of granular shear flows", to appear in Advances in Complex systems (2002).

IMPERMANENCE OF STATIC CHARGES ON GRANULAR MATERIALS: IMPLICATIONS FOR MICROGRAVITY EXPERIMENTS

John Marshall
jmarshall@seti.org; Ph 650-960-4535; Fax 650-961-7099
SETI Institute
2035 Landings Drive, Mountain View, CA 94043

The role of triboelectrostatic charges on granular materials was tested on USML-1 and USML-2, as well as on several KC-135 flights /1/. The goal of these experiments was to determine how static electricity affects the aggregation of particles in natural settings such as volcanic eruptions, dust storms on earth and Mars, and protoplanetary nebulae /2/. Knowledge so gained would also have relevance to industrial processing of a wide variety of granular materials (powdered coal, cement, grain, pharmaceuticals, etc.). The USML flights repeatedly demonstrated the existence of electrostatic polarizing forces that universally created filamentary aggregates from tribocharged (dielectric) grains released into a microgravity chamber. This polarizing force is considered to be an electrostatic dipole created by the random distribution of both positive and negative charges on each grain /3/. A discrete dipole moment on a grain is not to the exclusion of net charge (an imbalance of the charge mixture). In microgravity, the dipoles are able to rotate the grains so that they are always in a mutually attractive orientation with respect to their nearest neighbor grains; the result is the end-to-end stacking of grains that forms chains or filaments (ranging between 2 and 20 grains per chain for grains of about 400 microns diameter). Tribocharging of the grains in the USML experiments was accomplished by a forceful compressed air pulse injection into the experiment chambers, thereby permitting aggregation to occur while the grains were still mobile. After grain motion ceased, aggregation continued only for a few minutes, and then reached a stable inactive equilibrium phase lasting for the remainder of the experiment duration of up to 30 minutes.

These USML data formed the basis for proceeding to the Space Station experiment “Electrostatics of Granular Materials” (EGM), originally slated for a 2004 deployment, but now in stasis, with the exception of ground based studies that continue to hone our understanding of electrostatic phenomena. EGM would attempt to provide unequivocal proof of the dipoles while quantifying their properties. As part of EGM development, laboratory investigations were conducted on the tribocharging of various candidate flight samples. The goal of the tests was to determine the extent of net charging in granular populations as an indicator of the charge levels that would need to be measured on Space Station. It was also important to determine if tribocharging could be achieved with a “conservation of charge” within a given tribocharging apparatus. This conservation idea derives from a modeled concept in which positive charges are created on one surface as a result of transferring electrons to an adjacent surface: charge exchange should theoretically generate an equal number of positive and negative charges so that the system as a whole remains neutral (dipoles would be present, even with net neutrality of the grain population).

The laboratory device used for tribological experiments consisted of a cylindrical glass vessel with an air jet impinging upon particles within the vessel. Particulate material was caused to continually circulate while the impelling air escaped through a diffuser/screen system. Typical circulation/collision speeds of grains were mm/sec to several m/s. Electrostatic charge in the system was determined from a hand-held electrometer (ACL Model 300B) positioned ~ 2 cm from the vessel’s outer wall at 90 degrees orthogonally from the air jet. The electrometer was designed for detecting patch charges on surfaces in clean rooms. The analog readout is calibrated for fixed distances from surfaces, and it is assumed that the meter was reading the electrical field emanating from a surface charge that has a magnitude equal to the reading, presumably with respect to ground. The charge registered near the vessel includes contributions from both vessel walls and grains inside the vessel. If the system had a charge balance --i.e. the grain charging was equal and opposite to that of the vessel, the measured charge would sum to zero. This was not the case --large net charges were observed, but the cause is undetermined. Positive charge could have leaked through the vessel support structure, via leakage to air, or in some cases, via transport on comminution fines vented from the system.

Quartz, glass, and plastic grains have been tested. These are candidate materials for EGM, although for convenience, larger grain sizes than those planned for EGM (~300 micron) were used in the lab tests. All samples being agitated by the air resulted in negative charge readings where the electrometer was located near the base of the vessel, with the grains charging positive in some cases, negative in others (as measured by inserting the electrometer into the vessel). With all materials, and all grain sizes (ranging from several hundred microns to several millimeters), the electrometer registered several thousand volts (negative) in its external position. Glass spheres of 4 mm diameter generated in excess of - 8 kV for example. More important than the actual magnitude of this charging was the fact that the charge very rapidly dissipated as soon as the agitating air jet was turned off (this must have included discharge of the grains). Within seconds or minutes, the charge level would drop an order of magnitude to a few tens or hundreds of volts, particularly for the silicate materials. The appearance of a continuous high charge level during grain agitation and its subsequent almost immediate dissipation is attributed to grains acquiring very high voltage pulses of charge developed at grain contact points, but these charge patches are probably at or above the Gaussian limit locally, and rapidly decay by leakage or corona discharge to air, by discharge to other grains with opposite charge patches, by surface conductivity resulting from the high voltages, and by removal of charges attached to comminution particles carried away in the air stream. Thus, charge patches on one collision spot are degenerating as fast as they are being made by another collision. With so many grains creating tens of thousands of collisions per second, the dynamic equilibrium set up by the system gives the appearance of a stable charge. Thus, the charge ordinarily measured by electrometry on static piles of granular material is probably but a fraction of the charge produced during the causative tribological event.

The implications of these results are twofold. First, it means that electrostatic forces in dynamic granular systems are probably orders of magnitude higher than in static systems. Dust storms on planetary surfaces, volcanic eruption plumes, and mobilized industrial powders will be highly affected by charging and this may be manifest as rapid aggregation /4/ or enhanced Coulombic friction in the granular flow /5/. In the dispersed systems such as eruption clouds, the grain-to-grain interactions will be driven by both net charge and dipole moments on individual grains. In the non-dispersed granular flow systems (as in fluidized beds or grain piles), net charge will again be important, but the dipole coupling will be across grain boundaries rather than discretely contained within a grain itself, and the dipole will be unable to affect grain orientation because of grain-boundary interlocking. Ironically, the more dispersed a system is, the more effective the dipole and monopole effects become (especially in low or zero gravity environments) because grain orientation is facilitated, but at the same time, the dispersion leads to fewer contacts per unit time, thus reducing the magnitude of the charges (recalling the rapidity of charge decay during the interval between tribological contacts).

Secondly, the discovery of charge behavior in relation to tribological action adds a new and very significant enhancement to EGM science. Since charge decay can be very rapid with rates being highly material-dependent, charge cannot be regarded as a constant, and it is obviously a variable warranting investigation. We have added some new procedures to EGM --with very little additional effort, we will be able to shed light on the “non-static” nature of static electricity. It will be especially important to see how these high net charges relate to the dipole, and what their relative decay rates are. The fact that grains were “always attractive” in USML (during the same period when high tribological net charges were being actively developed) suggests that the dipole is commensurably powerful with the monopole. It will also be instructive to ascertain these measurements in a microgravity environment where grains are suspended, and thus unable to lose charge by contact with other grains, or via the vessel walls.

References: (1) Marshall. NASA CP 3272, 717-732 (1994). (2) Marshall & Cuzzi. Proc. LPSC, Houston (2001). (3) Abrahamson & Marshall. J. Electrostatics 55/1, 43-63 (2002). (4) Marshall et al. NASA TM 1998-208697 (1997). (5) Marshall et al. LPSC XXIX, 1135 (1998).

AN INTERFEROMETRIC INVESTIGATION OF MOVING CONTACT LINE DYNAMIC IN SPREADING POLYMER LIQUIDS

Pirouz Kavehpour, Gareth H. McKinley
Hatsopoulos Microfluids Laboratory, Department of Mechanical Engineering
Massachusetts Institute of Technology, Cambridge, MA

Ben Ovryn
Department of Biomedical Engineering, Case Western Reserve University,
Cleveland, OH

ABSTRACT

Studies of dynamic wetting phenomena and contact angle measurements frequently involve either visual or mathematical extrapolations of the macroscopic interfaces due to the difficulties inherent in quantitatively measuring the microscopic fluid physics that arise near the moving contact line. We have developed a phase-shifted laser feedback interferometer (psLFI) that can be used to rapidly and non-invasively measure the interfacial profile in the vicinity of moving contact lines of simple Newtonian and complex fluids [1-2].

The test fluids used in the present study are constant-viscosity silicone oils (Gelest Inc.) which perfectly wet the smooth silicon substrate. The viscosities are varied from $7 \leq \mu \leq 10^4$ cSt in order to explore a wide range of capillary numbers, $Ca = \mu U/\sigma$ (here σ is the surface tension and U is the steady spreading velocity). For wetting systems (in which the liquid spreads spontaneously to give a nominally zero contact angle) a precursor or primary film moves ahead of the main body of liquid [3]. When the disjoining pressures are large and the viscosity small, the precursor films may spread quite rapidly for significant distances ahead of the bulk fluid. A simplifying feature of wetting via a precursor film is that the motion of the bulk liquid is decoupled from the wetting line, hence the liquid may be considered to spread across a pre-wetted surface. The hydrodynamic equations yield a velocity dependence of the apparent contact angle that follows a simple power law for Ca <<1 given by $\theta_a \sim Ca^{1/3}$ (Tanner's law) [4]. Here θ_a is the apparent dynamic contact angle.

A syringe pump delivers a precise volume of liquid onto a clean silicon substrate. During the spreading process, the psLFI system is focused on the substrate in front of the moving wetting line as shown in the Fig. 1 and the spreading film flows past the approximately 1 μm diameter spot focused by the high numerical aperature objective lens. In order to estimate the optical path length (OPL) and interference fringe visibility, the intensity of the laser is monitored in real-time and discrete phase shifts are introduced using an electro-optic modulator (EOM); this process is automated using Labview. From the OPL data we can follow the evolution of the local thickness of the drop, $h(x)$, as a function of time. In Fig. 2 we show an example of the psLFI oresponse close to the wetting line. The left vertical axis shows the drop profile $h(x)$ [in nm] as a function of the lateral position x [in μm]. The right-hand axis shows the interference fringe visibility, m. The polished silicon substrate has a high visibility (m ~0.095) however this drops suddenly about 100 μm *before* the apparent or macroscopic contact line passes the measurement

point. In this offset region a very thin liquid film (~100 nm) can be detected in front of the contact line. The length of this precursor film, L_P, is measured from the position where the visibility drops to the position where the drop thickness starts to increase rapidly. A series of measurements over a wide range of (Newtonian) fluid viscosities and spreading velocities are shown in Fig. 3. The lateral extent of this precursor layer varies inversely with Ca and is in excellent agreement with the theoretical prediction, $L_P = \sqrt{SA/6\pi\sigma^2}\,Ca^{-1}$ where S is the spreading coefficient and A is the Hamaker constant [4]. We are currently using this technique to image the spatio-temporal evolution of the shape of the 'foot' in more complex fluids such as Xanthan gum (a rigid rod polymer), flexible polymer solutions and also highly entangled polymer melts.

BIBLIOGRAPHY:

1. Ovryn, B., et al., *Phase-shifted, real-time laser feedback interferometry.* SPIE, 1996. **2860**: p. 263-275.
2. Ovryn, B. and J.H. Andrews, *Phase-shifted laser feedback interferometry.* Opt. Lett., 1998. **23**(14): p. 1078-1080.
3. Bascom, W.D., R.L. Cottington, and C.R. Singleterry, in *Contact Angle, Wettability and Adhesion*, F.M. Fowkes, Editor. 1964, ACS: Washington, DC. p. 335-379.
4. de Gennes, P.G., *Wetting: Statics and Dynamics.* Rev. Mod. Phys., 1985. **57**: p. 827-863.

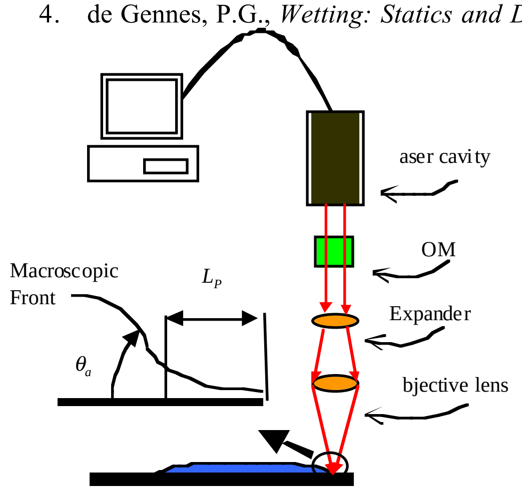

Fig. 1 Schematic of the psLFI instrument setup and (inset) spreading drop in the vicinty of the wetting line.

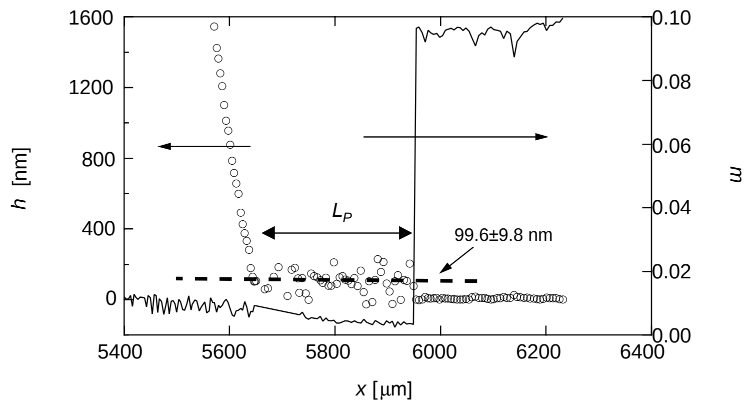

Fig. 2 Evolution in the profile of a silicone oil drop spreads on a silicon substrate. Circles (○) show the local thickness of the drop [in nanometers] and solid line is the visibility of the interference fringes, *m*.

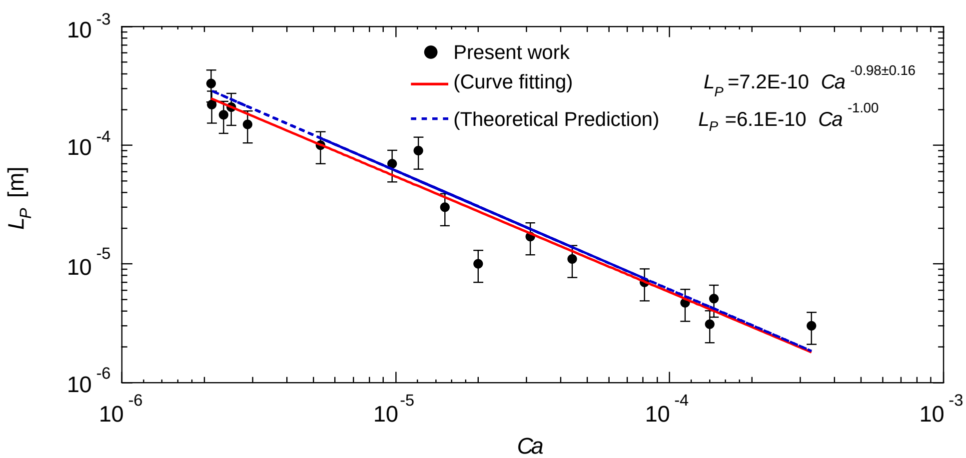

Fig. 3 Length of the precursor film, L_P, as a function of capillary number. Solid line (—) is the regression to the experimental results (●) and the dashed line (---) is the theoretical prediction.

DROPLET FORMATION PROCESSES IN SOLIDS-LADEN LIQUIDS

Roy J. Furbank & Jeffrey F. Morris
Georgia Institute of Technology, Atlanta, GA 30332

ABSTRACT

The formation of droplets is an important phenomenon in many industrial applications as well as an interesting and challenging physical problem. Many of these processes involve the formation of droplets from particle-laden liquids including ink-jet printing technology, fuel combustion, and spray drying operations. This work investigates how the presence of solid particles in a suspending liquid affects the droplet formation process.

Droplet formation from pure liquids has been extensively studied both experimentally and numerically and is fairly well understood. However, little information is available concerning the process for solid-liquid suspensions. Experiments to date have investigated the formation of pendant drops of suspensions of varying particle volume fraction (φ) into both a second immiscible liquid and into ambient air. For each case the thread length achieved at pinch-off and the resulting drop size are measured and the effect of increasing φ observed.

The results of these experiments which illustrate the particle effects most clearly are the qualitative characteristics of the structure developed during the necking and subsequent pinch-off of the drop. For low particle concentration (typically up to $\varphi \approx 0.10$) the structure observed near pinch-off is the asymmetrical "needle-sphere" combination described by Peregrine *et al* (*JFM* **212**, 25 (1990)) for pure fluids. At larger particle fractions the structure observed near pinch-off becomes significantly different and the forming droplet has a less spherical, pear-like shape. This shape is similar to that observed by Shi *et al* (*Science* **265**, 219 (1994)) for increasingly viscous pure fluids and can lead to pinch-off occurring in a more variable manner at a location away from the edge of the forming drop. Simple rheological arguments based on the effective viscosity increase with φ fail to explain these qualitative changes in the drop structure

In addition to studying the case where purely pendant drops are formed at the orifice exit, this work also seeks to understand how particles affect the process after jetting has occurred. Understanding the flow behavior in this regime is critical to any practical application involving the use of particle-laden liquids. With this aim, experiments are in progress to investigate the transition from pendant to jetting droplet formation behavior, focusing on how the presence of solid particles in the liquid affect this transition. Future work will continue these efforts with a focus on expanding these initial experiments towards smaller scales, seeking to determine the generality of the influence of suspended particles.

AVALANCHE DYNAMICS AND STABILITY IN WET GRANULAR MEDIA

Peter Schiffer
Department of Physics and Materials Research Institute, Pennsylvania State University, University Park PA 16802

Pal Tegzes and Tamas Vicsek
Department of Biological Physics, Eötvös Loránd University, 1A Pázmány stny., Budapest, Hungary 1117

ABSTRACT

Avalanches and landslides are among the most dramatic of natural catastrophes, and they also provide an evocative metaphor for a wide range of propagating breakdown phenomena. On the other hand, the existence of avalanches, i.e. the sudden collapse of the system previously frozen into a high energy state, is a fundamental manifestation of the metastable nature of granular materials. Studies of avalanches and surface flows in granular media have largely focused on dry grains. By wetting such media, however, one introduces controllable adhesive forces between the grains which lead to qualitatively new behavior. In our previous work, we identified three fundamental regimes for the repose angle of wet granular materials as a function of the liquid content. The granular regime at very low liquid contents is dominated by the motion of individual grains; in the correlated regime corresponding to intermediate liquid contents, a rough surface is formed by the flow of separated clumps; and the repose angle of very wet samples results from cohesive flow with viscoplastic properties.

Here we report investigations of the avalanche dynamics and flow properties of wet granular materials, employing a rotating drum apparatus (a cylindrical chamber partly filled with a granular medium and rotated around a horizontal axis). At low rotation rates, the medium remains at rest relative to the drum while its surface angle is slowly increased by rotation, up to a critical angle θ_{max} where an avalanche occurs, thus decreasing the surface angle to the repose angle θ_r. The flow becomes continuous at high rotation rates, but the transition between avalanching and continuous flow is hysteretic in rotation rate in dry media. Previous studies of cohesive granular media in a rotating drum have focused on the surface angles of the medium before and after avalanches. In our measurements, we focus instead on characterizing the *dynamics* of cohesive flow. We quantitatively investigate the flow dynamics during avalanches at different liquid contents by analyzing the time evolution of the averaged surface profile obtained from hundreds of avalanche events, and we also measure surface velocities during continuous flow. In particular, we explore the nature of the viscoplastic flow, (observed at the highest liquid contents) in which there are lasting contacts during flow, leading to coherence across the entire sample. This coherence leads to a velocity independent flow depth at high rotation rates and novel robust pattern formation in the granular surface.

REFERENCES: Nature **387**, 765 (1997); Physical Review E **56**, R6271 (1997); Physical Review E **60**, 5823 (1999); cond-mat/0204399.

DRAG FORCE AND PENETRATION IN GRANULAR MEDIA

Peter Schiffer and Yeekin Tsui
Department of Physics and Materials Research Institute, Pennsylvania State University, University Park PA 16802

Istvan Albert and Albert-Laszlo Barabási
Department of Physics, University of Notre Dame, Notre Dame, IN 46556

ABSTRACT

The motion of a solid object being pulled slowly through a granular medium is resisted by jamming of the grains, resulting in a drag force which differs dramatically from viscous drag in a fluid both in its average properties and in having large fluctuations with distinct characteristics. The drag process thus provides an excellent test-bed for the strength of locally jammed states among the grains and the effects of confinement on the jamming.

We have studied the drag force as a function of the velocity, the depth in the medium, the grain size and morphology for a vertical cylinder. The data agree well with theory for spherical media, but show an anomalously strong depth dependence for non-spherical grains. We also study the drag force on discrete objects with circular cross section moving slowly through a spherical granular medium. Variations in the geometry of the dragged object change the drag force only by a small fraction relative to shape effects in fluid drag. The drag force depends quadratically on the object's diameter as expected. We do observe, however, a deviation above the expected linear depth dependence, and the magnitude of the deviation is apparently controlled by geometrical factors.

We also have studied fluctuations in the drag force experienced by a vertical moving through a granular medium. The successive formation and collapse of jammed states give a stick-slip nature to the fluctuations which are periodic at small depths but become "stepped" at large depths, a transition which we interpret as a consequence of the long-range nature of the force chains and the finite size of our experiment. Another important finding is that the mean force and the fluctuations appear to be independent of the properties of the contact surface between the grains and the dragged object. These results imply that the drag force originates in the bulk properties of the granular sample.

Very recent work has focused on the effects of solid barriers within the grains on penetration of a granular medium. We have studied the force required to insert an object vertically into a granular medium, with particular attention to the effect of the bottom boundary. We find that, despite the long range nature of the force chains, the existence of the solid bottom of the granular container only affects the force when the inserted object is within a short range of the bottom, and that the roughness of the bottom surface has a strong effect on the force's depth profile.

REFERENCES: Physical Review Letters **82**, 205 (1999); Physical Review E **60**, 5823 (1999); Physical Review Letters **84** 5122 (2000); Physical Review E **64**, 031307 and **64**, 061303 and **64**, 061303 (2001).

CONSTITUTIVE RELATION IN TRANSITIONAL GRANULAR FLOWS

Hayley H. Shen
Dept. Civil & Env. Eng., Clarkson University, Potsdam, NY 13699-5710

Daniel M. Hanes
Dept. Civil & Coastal Eng., Univ. Florida, Gainesville, FL 32611

James T. Jenkins
Dept. Theoretical & Applied Mech., Cornell Univ., Ithaca, NY 14853

ABSTRACT

The behavior of granular materials spans the whole range from an elastic solid to a non-linear viscous fluid. The constitutive relation depends not only on the material composition, but also on the deformation and the rate of deformation. The key reason for this behavior is that granular materials are not only defined by the properties of the individual grains, but also by the structure of the aggregate. In a very dilute granular flow, the structure of the aggregate is simply defined by a uniform random distribution. As the concentration increases, the internal structure becomes complex. It evolves dynamically with the macroscopic deformation and is an integral part of the constitutive relation. The complexity and importance of the internal structure increase with the concentration. In a gravity field, the weight of a granular material naturally compacts it to produce a concentration gradient. To study the constitutive behavior of granular materials, the presence of gravity is therefore detrimental. Although empirical relations have been obtained for engineering designs to control granular flows on Earth, it is not known how well these Earth-bound relations can be used in another gravity field. Fundamental understanding must be derived to reliably design for granular flows in space exploration.

There are two extremes of granular flows of which significant amount of knowledge is available. One deals with a dense and quasi-static situation where the deformation rate nearly vanishes. The other deals with dilute and rapidly fluctuating grain velocities where particle inertia dominates. In near stationary granular flows the internal normal stress overwhelms the gravity effect. The concentration gradient due to gravity is negligible. In inertia dominant flows the only type of internal structure is the uniform random distribution of grains. As long as the concentration is low, its gradient does not affect this internal structure. However, under most natural conditions, a flowing granular material falls in between these two extremes. It is in this transitional regime that internal structure is sensitive to the concentration variation. This project, funded by the NASA Microgravity Fluid Physics Program, aims to study this transitional regime via physical experiments and computer simulations. A conceptual model has been established as described below.

There are two natural time scales in a granular flow. One is the travel time between two consecutive collisions and the other is the duration of a collision contact. At a very low shear-rate, the shear-induced particle velocity is low. Hence the travel time between collisions is longer than the contact time between colliding particles. Binary collisions prevail. As the shear-rate increases, the traveling time between collisions reduces and the probability of multiple collisions

goes up. These particle groups disperse shortly after and new groups form. When shear-rate is further increased, clusters grow in size due to an increasing chance for free particles to join before groups have the time to disperse. The maximum cluster size may depend on the global concentration and material properties. As the solid concentration approaches zero, the cluster size goes to one particle diameter. The maximum possible cluster size under any condition is the container size, provided that the shear flow is inside a container. The critical shear-rates that dictate the initiation of the multiple contacts, and the size and lifetime of the collision clusters, are functions of the concentration also. A "regime" theory has been proposed in Babic et al. (*J. Fluid Mech.* 219:81-118,1990). This theory suggested that both the solid concentration, C, and the non-dimensional shear-rate, B, are important in determining the regimes of the granular constitutive law, as shown in the figure.

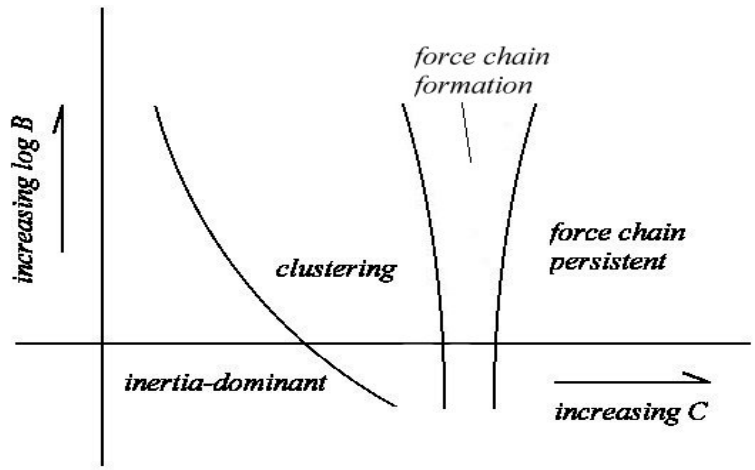

In the coming years, both physical and computer experiments will be conducted. These experiments will determine the stress and strain-rate relation while the microstructure of the granular material dynamically changes. Data obtained from these experiments will be used to link the microstructure of the granular material to the resulting constitutive relations. The above regime theory will be quantified. This poster gives a brief overview of the physical experiment, the computer simulation, and how these two will be integrated.

AGGREGATION AND GELATION OF ANISOMETRIC COLLOIDAL PARTICLES

Ali Mohraz and Michael J. Solomon
Department of Chemical Engineering, University of Michigan Ann Arbor MI 48109-2136.
(mjsolo@umich.edu)

ABSTRACT

The quiescent and flow-induced structure and dynamics of colloidal aggregates and gels of anisometric particles are studied by means of static and dynamic light scattering. Ground-based studies of weak gels are possible due to the submicron size of the boehmite rod suspensions investigated; however, microgravity conditions would be required for more general studies. The properties of colloidal rod suspensions are compared to typical properties of spherical particle gels to understand the role of anisotropic excluded volume on gel structure and dynamics.

The structure and dynamics of colloidal aggregates and gels have long been of scientific and technological interest; however, most research has focused on suspensions of spherical particles. Yet, aggregates and gels of anisometric particles - colloidal rods and platelets - may exhibit structure and dynamics that are quite different from spherical colloids. For example, suspensions of colloidal rods gel at extremely low volume fractions and form birefringent sediments (A.P. Philipse, A.-M. Nechifor and C. Pathmamanoharan, Langmuir **10**, 4451 (1994)). The rheology of solutions and gels of colloidal rods and platelets differs dramatically from that of colloidal spheres (M.J. Solomon and D.V. Boger, J. Rheology **42**, 929 (1998)). Scientifically, studies with anisometric particles offer the opportunity to assess the role of anisotropic excluded volume and particle orientation in aggregates and gels. Technologically, anisometric colloids find use in a wide range of materials such as ceramics, polymer nanocomposites, well-bore drilling fluids and magnetic storage media.

Model colloidal boehmite rods of approximately monodisperse dimension and aspect ratio have been synthesized according to the method of Philipse and coworkers. In aqueous solution, these materials undergo gelation upon the addition of divalent salt. By means of a novel grafting reaction and procedure for solvent refractive index matching, the rods have also been dispersed in mixed organic solvents. In this case, gelation is induced by means of depletion interaction.

We report the effect of particle shape and anisotropic excluded volume on the structure, rheology, and internal dynamics of colloidal gels. The quiescent structure of these gels is characterized over two decades in the scattering vector, q, by combined small and wide-angle light scattering. The effect of particle aspect ratio on the gel microstructure is studied in particular. Light scattering studies conducted as shear deformation is applied to the material quantify how colloidal aggregates are oriented and deformed by flow. The internal dynamics of the gels are quantified by means of photon correlation spectroscopy.

SPLASHING DROPLETS

Randall L. Vander Wal[*], John Patrick Kizito, Gordon M. Berger
National Center for Microgravity Research

J. Iwan D. Alexander
Case Western Reserve University and
National Center for Microgravity Research

Grétar Tryggvason
Worcester Polytechnic Institute

ABSTRACT

Current data on droplet breakup is scarce for the sizes and velocities typical of practical applications such as in spray combustion processes and coating processes. While much more representative of practical applications, the small spatial scales and rapid time-scales prevent detailed measurement of the internal fluid dynamics and liquid property gradients produced by impinging upon surfaces. Realized through the extended spatial and temporal scales afforded by a microgravity environment, an improved understanding of drop breakup dynamics is sought to understand and ultimately control the impingement dynamics of droplets upon surfaces in practical situations.

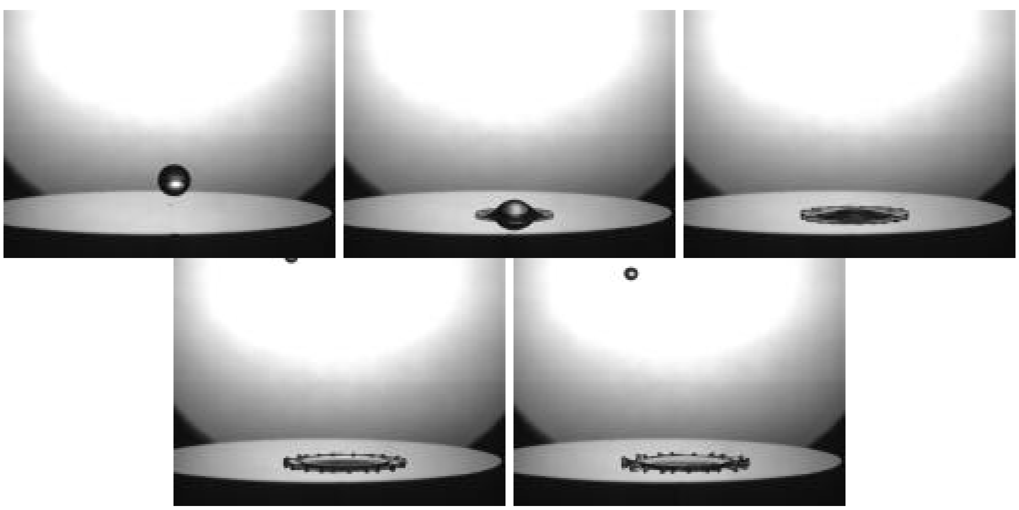

Figure 1: Experimental images of a sequences showing the spreading of a single droplet after impact and ensuing finger instabilities. (We=386, Re=370).

The primary objective of this research will be to mark the onset of different "splashing modes" and to determine their temperature, pressure and angle dependence for impinging droplets representative of practical fluids. In addition, we are modeling the evolution of droplets that do not initially splash but rather undergo a "fingering" evolution observed on the spreading fluid front and the transformation of these fingers into splashed products. An example of our experimental data is presented below. These images are of Isopar V impacting a mirror-polished surface. They were acquired using a high-speed camera at 1000 frames per second. They show the spreading of a single droplet after impact and ensuing finger instabilities.

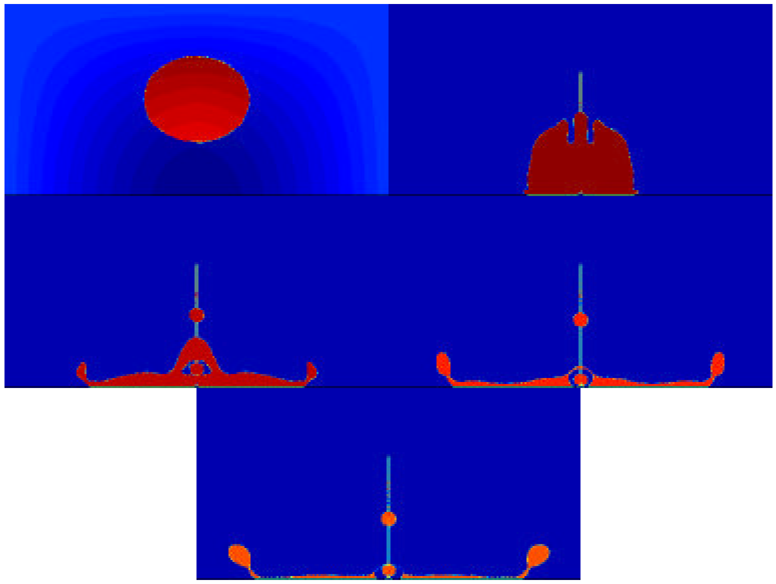

Figure 2: Numerical images sequence showing, axisymmetrically, the spreading of a single droplet after impact (same We, Re).

Normal gravity experimental data such as this will guide low gravity measurements in the 2.2 second drop tower and KC-135 aircraft as available. Presently we are in the process of comparing the experimental data of droplet shape evolution to numerical models, which can also capture the internal fluid dynamics and liquid property gradients such as produced by impingement upon a heated surface.

To-date isothermal numerical data has been modeled using direct numerical simulations of representative splashing droplets. The process involves using fluid front-tracking methods. These numerical methods are based on writing and simultaneously solving a set of basic equations for the whole computational domain using two grids systems to track a single droplet as it interacts with and spreads along a solid wall. The momentum transport equations are solved by a conventional finite volume method on a fixed, structured grid and the interface is tracked explicitly. The fluid-tracking algorithm determines the advections and distribution of the fluid properties such as viscosity and density. The surface tension is implemented as a source term in the momentum equation. At the splashing wall, fluid wall interactions are described by slip boundary conditions. We are in the process of adding contract line hydrodynamics.

The data obtained so far indicates that the present model describes well the droplet wall interactions to a point in time just before splash. We will present a comparison of our experimental data to representative numerical cases. We are also updating the code to take into account multiple tracking of the droplets after splash. As time permits we will present this data also.

*Contact information:

email: Randy.VanderWal@grc.nasa.gov

phone: 216-433-9065

fax: 216-433-3793

Flow around a cylinder immersed in a dense granular flow

D. Chehata, R. Zenit
Instituto de Investigaciones en Materiales,
Universidad Nacional Autónoma de México, Apdo. Postal 70-360,
Ciudad Universitaria, Coyoacán D.F. 04510, México

C. R. Wassgren
School of Mechanical Engineering,
Purdue University, West Lafayette IN 47907-1288, USA

The flow around a fixed cylinder immersed in a uniform granular flow is studied experimentally. Experiments are performed in a tall vertical chute that produces a quasi two-dimensional granular flow. A storage bin at the top of the chute feeds glass particles into the channel while the mean velocity of the flow is controlled by varying the width of a hopper located at the channel exit. Measurements of the drag force acting on a fixed cylinder are made using a strain gauge force measurement system. The flow velocity field is measured through a transparent wall using particle image velocimetry analyses of high speed video recordings of the flow. Experiments are performed for a range of upstream particle velocities, cylinder diameters, and two diameters of glass particles.

For the range of velocities studied, the drag force acting on the cylinder is independent of the mean flow velocity, contrary to what is expected from any ordinary fluid. The drag force scales with the asymptotic static stress state in a tall granular bed. The drag coefficient, defined in terms of a dynamic pressure, scales with the flow Froude number and a length scale parameter that accounts for the effective cylinder size.

Although the drag force on the cylinder does not change with the upstream flow velocity, the flow streamlines do, in fact, change with velocity. A large stagnation zone forms at the leading edge of the cylinder while at the trailing edge an empty wake is observed. The wake size increases with flow velocity.

Collisional granular flow around an immersed cylinder

C.R. Wassgren
School of Mechanical Engineering, Purdue University

R. Zenit
Instituto de Investigaciones en Materiales,
Universidad Nacional Autónoma de México

A. Karion
Carderock Division, Naval Surface Warfare Center

A two-dimensional collisional granular flow past an immersed cylinder is investigated using discrete element computer simulations. The drag force acting on the cylinder, F_d, is proportional to the upstream bulk density, $\rho\nu_\infty$, where ρ is the upstream particle mass density and ν_∞ is the upstream solid fraction, the square of the upstream velocity, U_∞, and the sum of the cylinder diameter, D, and surrounding particle diameter, d. The drag coefficient, defined as $C_d = (2F_d)/(\rho\nu_\infty U_\infty^2(D+d))$ has a strong dependence on the flow Knudsen number and a secondary weak dependence on the Mach number. The drag coefficient decreases slightly with decreasing coefficient of restitution and is relatively insensitive to the inter-particle friction coefficient. Bow shock structures and expansion fans similar to those observed in compressible fluid flows are also observed.

Exposition Session
Topical Area 4:
Multiphase Flow and Phase Change

FUNDAMENTAL STUDIES ON TWO-PHASE GAS-LIQUID FLOWS THROUGH PACKED BEDS IN MICROGRAVITY

Vemuri Balakotaiah
University of Houston

Mark J. McCready
University of Notre Dame

Brian J. Motil
NASA Glenn Research Center

ABSTRACT

In the typical operation of a packed-bed reactor, gas and liquid flow simultaneously through a fixed bed of solid particles. Depending on the application, the particles can be of various shapes and sizes and provide for intimate contact and high rates of transport between the phases needed to sustain chemical or biological reactions. The packing may also serve as either a catalyst or as a support for growing biological material. NASA has flown two of these packed-bed systems in a microgravity environment with limited or no success (Motil et al. [1]). The goal of this research is to develop models (with scale-up capability) needed for the design of the physicochemical equipment to carry out these unit operations in microgravity. New insight will also lead to improvements in normal gravity operations.

Our initial experiment was flown using an existing KC-135 two-phase flow rig with a modified test section. The test section is a clear polycarbonate rectangular column with a depth of 2.54 cm, a width of 5.08 cm, and 60 cm long. The column was randomly packed with spherical glass beads by slowly dropping the beads into the bed. Even though care was taken in handling the column after it was filled with packing, the alternating high and low gravity cycles with each parabola created a slightly tighter packed bed than is typically reported for this type. By the usual method of comparing the weight difference of a completely dry column versus a column filled with water, the void fraction was found to be .345 for both sizes of beads used. Five flush mounted differential pressure transducers are spaced at even intervals with the first location 4 cm from the inlet port and the subsequent pressure transducers spaced at 13 cm intervals along the column. Differential pressure data was acquired at 1000 Hz to adequately observe pulse formation and characteristics. Visual images of the flow were recorded using a high-speed SVHS system at 500 frames per second. Over 250 different test conditions were evaluated along with a companion set of tests in normal gravity. The flow rates, fluid properties and packing properties were selected to provide a range of several orders-of-magnitude for the important dimensionless parameters.

The well known Ergun equation for single phase flow through porous media is written by superposing the pressure drop expression for purely viscous (Blake-Kozeny) and purely inertial losses (Burke-Plummer):

$$\frac{-\Delta P}{Z} = 150\frac{(1-\varepsilon)^2}{\varepsilon^3}\frac{\mu U}{D_p^2} + 1.75\frac{(1-\varepsilon)}{\varepsilon^3}\frac{(\rho U)U}{D_p} \quad \text{where}$$

ε = void fraction, U = fluid superficial velocity, D_P = packing diameter, and Z = column length.

For two-phase flow in the microgravity environment, the measured pressure drop is the true frictional pressure drop since the hydrostatic head is nearly zero. Through dimensional arguments (neglecting gravity and the bed inclination), the non-dimensional form of the pressure drop is:

$$\frac{-\Delta P}{Z}\frac{D_P}{\rho_L U_{LS}^2} = f\left[\varepsilon,\ Re_{GS},\ \frac{1}{Re_{LS}},\ \frac{1}{We_{LS}},\ \frac{\rho_G}{\rho_L},\ \frac{\mu_G}{\mu_L}\right]$$

The pressure drop may be assumed to be a weak function of the last two ratios (density and viscosity) as they are small and do not vary significantly. Rearranging into a dimensionless form and adding an expression for the gas Reynolds number and liquid Weber number, the form of the modified Ergun equation becomes:

$$\frac{-\Delta P}{Z}\frac{D_P}{\rho_L U_{LS}^2} = \frac{150(1-\varepsilon)}{Re_{LS}} + \beta\left(\frac{Re_{GS}}{(1-\varepsilon)}\right)^{a}\left(\frac{(1-\varepsilon)}{Re_{LS}}\right)^{b}\left(\frac{1}{We_{LS}}\right)^{c} + 1.75$$

Determining the parameters by regression, we find that a=1/2, b=1/3, c=2/3 and β =0.8. Recognizing that $\frac{1}{Ca_{LS}} = \frac{Re_{LS}}{(1-\varepsilon)We_{LS}}$, the final form of the modified Ergun equation is:

$$f = \frac{-\Delta P}{Z}\frac{D_P}{\rho_L U_{LS}^2} = \frac{(1-\varepsilon)}{Re_{LS}}\left[150 + 0.8\left(\frac{Re_{GS}}{(1-\varepsilon)}\right)^{\frac{1}{2}}\left(\frac{1}{Ca_{LS}}\right)^{\frac{2}{3}}\right] + 1.75$$

The figure below shows two examples of the experimental data and the corresponding modified Ergun equation. Each plot represents a specific Suratman number indicated in the legend: $\left(Su = \frac{Re_{LS}}{Ca_{LS}(1-\varepsilon)} = \frac{\rho_L D_P \sigma}{\mu_L^2(1-\varepsilon)}\right)$

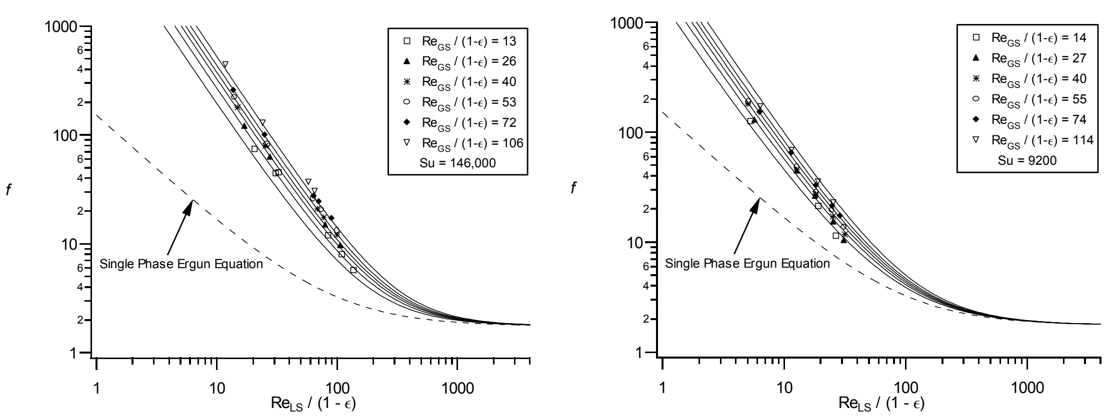

Plot of modified Ergun equation for two Suratman numbers.

[1] Motil, B. J., Balakotaiah, V., Kamotani, Y., "Effects of Gravity on Cocurrent Two-Phase Gas-Liquid Flows Through Packed Columns," AIAA-2001-0767 (2001).

Phase-Field Methods for Structure Evolution in Sheared Multiphase Systems

Vittorio Badalassi*, Hector Ceniceros**, Sanjoy Banerjee*
Department of Chemical Engineering
Department of Mathematics
University of California, Santa Barbara

A homogeneous disordered phase separates into ordered structures when quenched into a broken-symmetry phase. The competition of broken-symmetry phases to select an equilibrium state may be studied in terms of coarse-grained order parameters described by a suitable Landau free-energy function. A network of equilibrium-phase domains develops on quenching and coarsens with time with a topology that may be controlled by shear. We use three-dimensional simulations, in which time-dependent models for conserved–order parameters coupled to Navier-Stokes fluid models are solved, to investigate the evolution of such domains, e.g. spinodal decompositions of polymeric materials under shear. The numerical problems are formidable because of the strong nonlinearities inherent in the coupled model, and these are amongst the first 3D calculations undertaken.

In linear shear fields we find stable nanostrings, also recently seen in experiments. The affinity of the ordered phases to boundaries plays a role in the form of the structures that develop, with stacked plate-like phase distributions emerging under certain conditions. Such methods appear quite promising for design and analysis of multiphase and complex fluid formulations. The behavior of foams in such conditions is of particular interest in microgravity environments.

Computational Techniques for Multiphase Flow and Transport in Microgravity Environments

Ravi Chella, Chemical Engineering, Florida State University, Tallahassee, FL 32310

A mesoscopic approach is taken for modeling flow in multiphase systems, with the system characterized by a coarse-grained conserved order parameter that takes characteristic values in the bulk phases and varies continuously in a narrow interfacial region). This approach (Chella, R. and Vinals, J, "Mixing of a two-phase fluid by cavity flow", Phys. Rev. E 53 , 3832 (1996)) provides significant computational advantages over classical continuum approaches. This formulation has been extended to incorporate interactions with solid boundaries through modification of free energy functionals to include short-range and long range interactions with the walls. This approach has been implemented using a lattice-Boltzmann approach.

Development of Parallel MPI program

To facilitate application of the the lattice-Boltzmann method for immiscible transport to three-dimensional and irregular geometries, a parallel version of the program was developed using MPI (Message Passing Interface) . Both three-dimensional and one-dimensional domain decompositions were tested. Superlinear speedup was observed. This is expected to be due to the large memory requirements for the lattice Boltzmann method in three-dimensions which results in extensive memory paging for all but the smallest systems.

Evolution of microstructure and rheology in complex fluids under externally applied flows

The influence of shear and extensional flows in retarding phase separation and stabilizing certain morphologies was investigated. In particular, the interplay between interfacial tension and viscosity differences between phases are examined. Specific applications are to binary fluids undergoing spinodal decomposition, and the nucleation and growth of droplets. In binary liquid mixtures, the morphology of the phase separating domain varies from interconnected domains (bicontinuous patterns) to droplets, depending on composition and quench depth. Hydrodynamics significantly influences the dynamics of phase separation. For sufficiently strong flows, a non-equilibrium morphology can be stabilized. Results of a simulation of two-dimensional spinodal decomposition under shear is shown. The steady state lamellar morphology developed for three cases corresponding to a Capillary number Ca=0.1, and dimensionless shear-rates of 0.05, 0.075 and 0.1,respectively, are shown below in Fig. 1. Scaling relationships for the structure factor

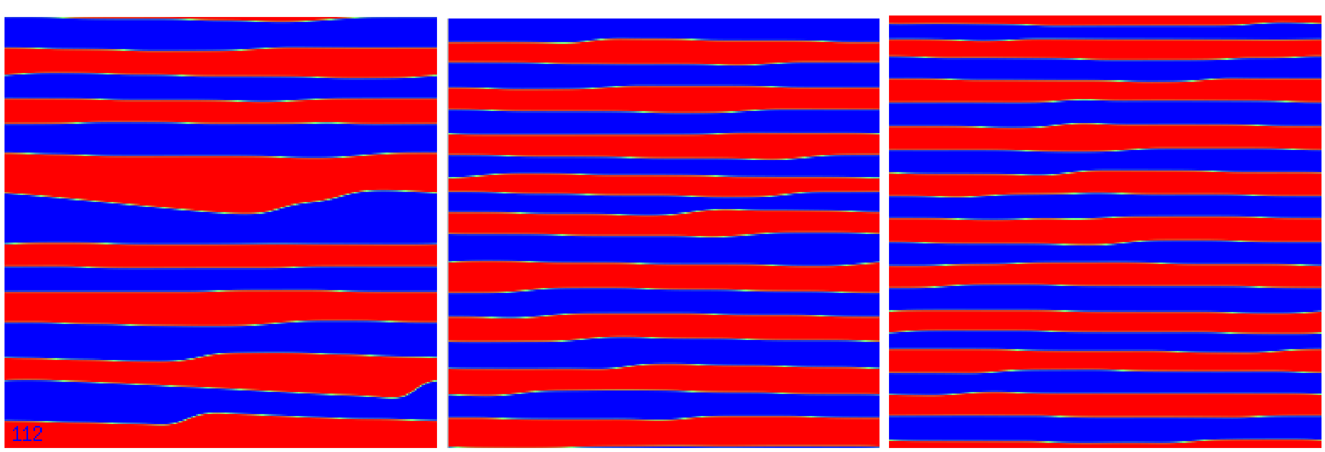

Figure 1: Steady state morphology for shear rates: (a) 0.05, (b)0.075, (c) 0.1

and the growth law of the characteristic domain size length scale were verified for spinodal decomposition in two and three-dimensions for the case of no externally imposed flow. For spinodal decomposition under shear, the system is no longer isotropic, and a useful measure of the morphology of the system is given by:

$$\mathbf{A} = \frac{< \nabla\phi\nabla\phi >}{< |\nabla\phi|^2 >}$$

As the order parameter ϕ varies rapidly in the interfacial region, $\nabla\phi$ is in the direction normal to the interface. Under shear, the off-diagonal components of $\mathbf{A}$ tend to zero at long times because of the alignment of the interfaces along the flow direction. In two-dimensions, for a lamellar structure $A_{xx} \rightarrow 0, A_{yy} \rightarrow constant$, where x is the flow-direction and y the shear direction. For $S \geq 0.05$, a stable lamellar morphology is obtained. In two dimensions, it is relatively easy to directly measure the interfacial length, and the proportionality of $< |\nabla\phi|^2 >$ to the surface to volume ratio is verified. In three-dimensional simulations, it is difficult to directly measure the interfacial area, but $|\nabla\phi|^2$ is readily calculated. The off-diagonal terms of $\mathbf{A}$ tend to zero for long times, and examination of the diagonal terms allow the steady state morphology to be characterized.

Simulations have been carried out both for spinodal decomposition and nucleation and growth under shear. Both cyclic (Lee's) and solid boundary conditions are used. At long times both lamellar and tubular structures are observed depending on the capillary number, shear rate, and the volume fraction of the two phases. Work is underway both theoretically using stability considerations, and computationally to relate the morphology to the shear rate, interfacial tension and viscosity ratio.

The evolution of the scattering pattern in planes parallel to the flow direction were determined and found to be in good qualitative agreement with experimental light scattering measurements on phase separation under shear by Professor Beysen's group, reported in the literature. Contributions of the domains to the excess viscosity $\delta\eta$ and the normal stresses W_1 and W_2 in the weak-shear regime [Onuki, A, Phys. Rev. A, 35, 5149 (1987)]: were calculated for different fluid properties and processing conditions.

Spinodal Decomposition in Confined Geometries

In phase separation in confined geometries, bicontinuous, capsule, or plug configurations have been experimentally observed depending depending on the relative strength of the interfacial to wetting forces. The influence of solid surfaces on the dynamics of phase separation in confined geometries in three-dimensions was investigated. The influence of both long range and short range surface forces are of interest. Results of a simulation that show the transition from from plug to continuous configurations with increasing magnitude of surface forces are shown in Fig. . In larger channels an intermediate capsule regime is also observed.

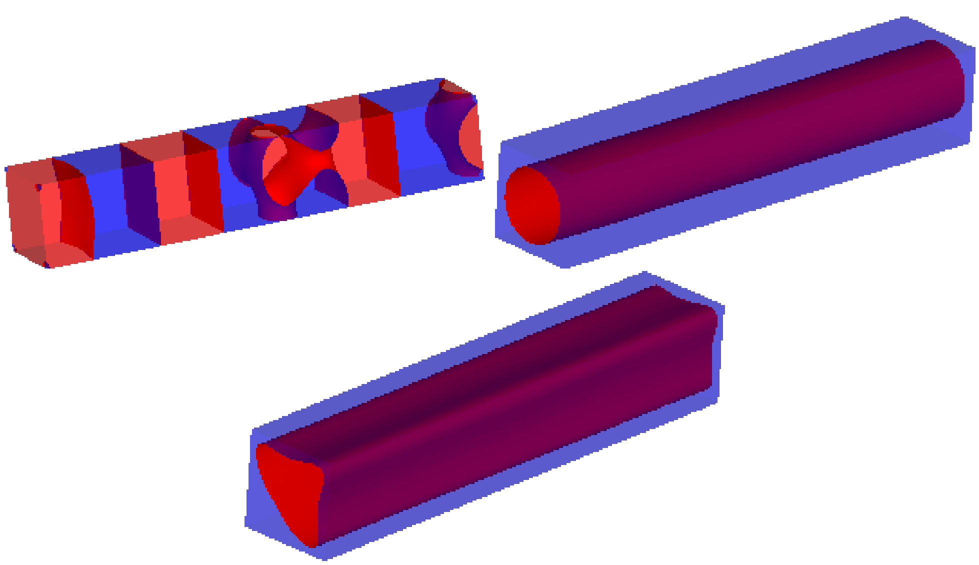

Figure 2

EXPERIMENTS ON HYDRODYNAMIC AND THERMAL BEHAVIORS OF THIN LIQUID FILMS FLOWING OVER A ROTATING DISK INCLUDING NUCLEATE BOILING

Basar Ozar, Baki M. Cetegen and Amir Faghri *
Mechanical Engineering Department
University of Connecticut, Storrs, CT 06269-3139

ABSTRACT

Experiments on characterization of thin liquid films over stationary and rotating disks are described in this study. The thin liquid film is created by controlled liquid impingement by introducing deionized water from a flow collar at the center of an aluminum disk at a known initial film thickness with uniform radial velocity. Experiments were performed for a range of Reynolds numbers based on the liquid inlet gap height and velocity and (flow rates) between 238 (3.0 lpm) and 1188 (15.0 lpm). The angular speed of the disk was varied from 0 rpm to 300 rpm. Radial film thickness distribution was measured using a non-intrusive laser light reflection technique that enabled the measurement of the instantaneous film thickness over a finite segment of the disk. When the disk was stationary, a circular hydraulic jump was present. The liquid film thickness in the subcritical region (downstream of the hydraulic jump) was an order of magnitude greater than that in the supercritical region (upstream of the hydraulic jump) which was of the order of 0.3 mm. As the Reynolds number increased, the hydraulic jump migrated toward the edge of the disk. In case of rotation, the liquid film thickness exhibited a maximum on the disk surface. The liquid film inertia and friction influenced the inner region where the film thickness progressively increased. The outer region where the film thickness decreased was primarily affected by the centrifugal forces. A flow visualization study of the thin film was also performed to determine the characteristics of the waves on the free surface. At high rotational speeds, radial waves were observed on the liquid film. It was also found that the tangent of the waves present on the liquid surface was a function of the ratio of local radial velocity and local azimuthal velocity. Radial temperature distribution was measured using an amplified thermocouple/slip ring arrangement. Local Nusselt number was seen to increase with flow rate and angular velocity. The inertia forces rather than rotation was found to have more significance on the Nusselt number at the inner parts of the disk. Semi-empirical correlations were presented in this study for the local and average Nusselt numbers. For nucleate boiling experiments, temperature profile over the disk was measured using the same amplified thermocouple/slip ring arrangement. Laser light reflection technique was utilized to measure the bubble size, its growth and motion. The bubbles were found to grow to diameters that were larger than the film thickness. The dynamics of bubble motion was characterized as a function of rotational speed of the disk, liquid flowrate over the disk as well as the overheat level.

* Principal Investigator. Phone: (860) 486-2221, Fax: (860) 486-0318,
E-mail: faghri@engr.uconn.edu

MELTING PROCESSES FOR UNFIXED PHASE CHANGE MATERIAL IN THE PRESENCE OF ELECTROMAGNETIC FIELD – SIMULATION OF LOW GRAVITY ENVIRONMENT –

Eduardo Gonçalves and **Mohammad Faghri**
Department of Mechanical Engineering
University of Rhode Island, Kingston, Rhode Island, USA

Yutaka Asako
Department of Mechanical Engineering
Tokyo Metropolitan University, Tokyo, Japan

Majid Charmchi
Department of Mechanical Engineering
University of Massachusetts, Lowell, Massachusetts, USA

ABSTRACT

Electromagnetic simulation of low-gravity environment has been numerically investigated to study the transport phenomena associated with melting of an electrically conducting Phase Change Material (PCM) inside a rectangular enclosure. Electromagnetic fields are configured in such a way that the resulting Lorentz force can be used to damp and/or counteract the natural convection as well as the flow induced by sedimentation and/or floatation, and thereby simulating the low gravity environment of outer space. Computational experiments are conducted for unfixed (top-wall heated) gallium as shown in Fig. 1. The governing equations are discretized using a control-volume-based finite difference scheme. Numerical solutions are obtained for true low-gravity environment as well as for the simulated-low-gravity. The result shows that when the Lorentz force is caused by the presence of magnetic field alone, the low-gravity condition is simulated by the damping effect, which is shown to have a profound effect on the flow field (see Fig. 2(c)). On the other hand, it is shown that under electromagnetic field simulation, where the Lorentz force is caused by the transverse electric and magnetic fields, it is possible to minimize the flow field distortion caused by the high magnetic field and therefore achieving a much better simulation of low-gravity. See Figs. 2(b) and 3.

Fig. 3 illustrate the effects of actual and simulated low-gravity on the major melting characteristics such as the Solid velocity, Melt thickness and Melt rate. As seen here, low-gravity simulated by the electromagnetic field (or electric low-gravity), show good agreement with those of actual low gravity whereas the magnetically simulated cases, show some discrepancies. Among these discrepancies are the fact that the melt rate under some ranges magnetic low-gravity (i.e., $g_B \geq g_0 10^{-3}$) are higher than those of electric low-gravity, See Fig. 3 (c). This suggests that these higher melt rate cannot be attributed to the effects of Joule heating, which would otherwise favor the electric field simulation, therefore the damping effect must be the cause. Also, the "no transient regions" on the solid velocities, suggests that the solid velocity under magnetic low-gravity respond directly to the magnetic forces, which respond much faster than the momentum diffusion associated with the melting evolution.

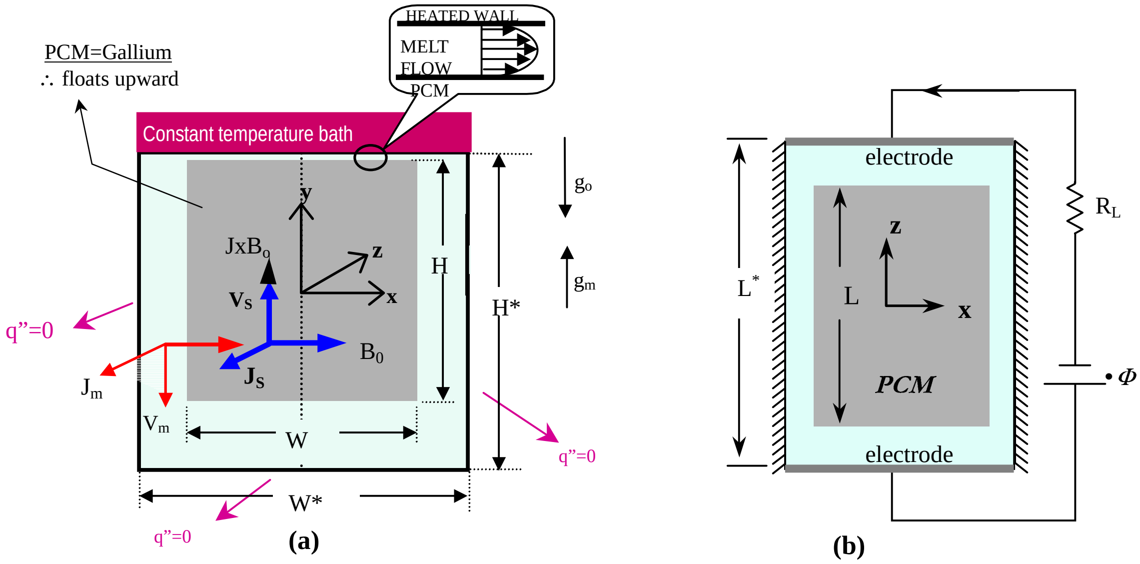

Figure 1: schematic setup of the problem:. (a) flow Configuration and (b) external circuit

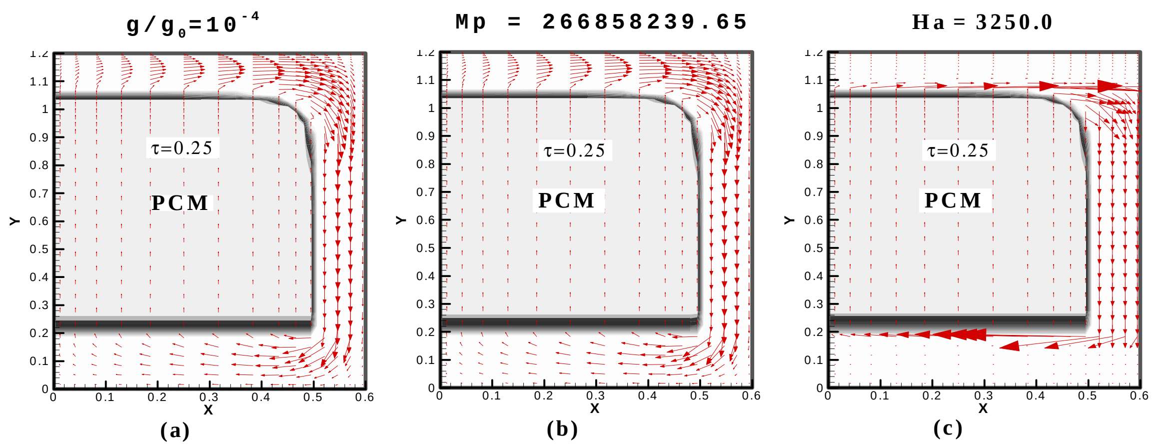

Figure 2: Effects of actual and simulated low-gravity on the melt flow structure; (a) actual low-g, (b) low-g simulation by electromagnetic field and (c) low-g simulation by magnetic field

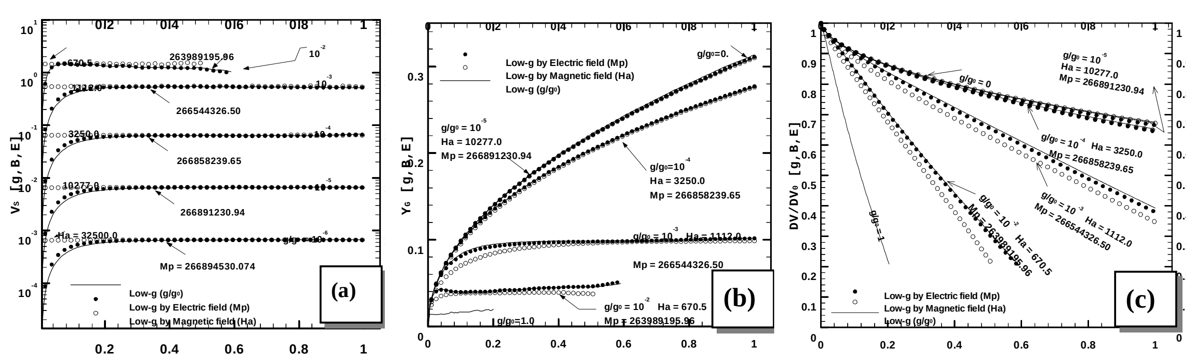

Figure 3: Effects of actual and simulated low-gravity on; (a) Solid velocity, (b) Melt thickness (c) Melt rate
Solid line = actual low-g ⇔ solid circles = electric low-g ⇔ hollow circles = magnetic low-g

INSTABILITIES AND THE DEVELOPMENT OF DENSITY WAVES IN GAS-PARTICLE AND GRANULAR FLOWS

Benjamin J. Glasser, Elizabeth D. Liss, Stephen L. Conway and Jayati Johri
Department of Chemical and Biochemical Engineering
Rutgers University
Piscataway, New Jersey 08854
Email: bglasser@sol.rutgers.edu, Tel: 732-445-4243, Fax: 732-445-2581

ABSTRACT

The dynamics of gas-particle and granular flows impact numerous technologies related to the local utilization of Lunar and Martian soils and the Martian atmosphere. On earth, such flows occur in a large number of industries including the chemical, pharmaceutical, materials, mining and food industries.

DENSITY WAVES IN GRAVITY-DRIVEN GRANULAR FLOW

A particle dynamic computer simulation is used to examine rapid granular flow in a vertical channel. Flow in the channel leads to an inhomogeneous distribution of the particles and two distinct types of density waves are identified: an S-shaped wave and a clump. The density waves are further characterized by quantifying their temporal evolution using Fourier methods and examining local and global flow properties of the system, including velocities, mass fluxes, granular temperatures and stresses. A parametric study is used to characterize the effect of the system parameters on the density waves. In particular we are able to show that the dynamics of large systems are often qualitatively and quantitatively different from those of small systems. Finally, the types of density waves and dominant Fourier modes observed in our work are compared to those that are predicted using a linear stability analysis of equations of motion for rapid granular flow.

CONNECTIONS BETWEEN DENSITY WAVES IN GAS-PARTICLE FLOWS AND COMPRESSIBLE FLOWS

It is shown that under certain simplifying assumptions, model equations of motion and continuity for the particles in a fluidized bed can be related to those of a compressible fluid acted upon by a density dependent force. A linear stability analysis shows that the base state of the compressible flow equations can lose stability in the form of plane density waves. The plane waves emerge through a Hopf bifurcation and propagate through the bed as traveling waves. Through a bifurcation analysis coupled with parameter continuation we compute the solution structure of the fully-developed plane waves. It is found that as the amplitudes of the plane waves increase, they lose stability in the lateral direction. A comparison of these results with previous work on gas-fluidized beds shows that the salient features of the instability of a gas-fluidized bed are captured by the basic physics of compressible flows.

Bubble formation and detachment in reduced gravity under the influence of electric fields

Cila Herman, Estelle Iacona and Shinan Chang
Department of Mechanical Engineering, The Johns Hopkins University, 3400 N. Charles Street, Baltimore, MD 21218, USA

Objectives

The objective of the study is to investigate the behavior of individual air bubbles injected through an orifice into an electrically insulating liquid under the influence of a static electric field (Figure 1a). Both uniform and nonuniform electric field configurations were considered. Bubble formation and detachment were recorded and visualized in reduced gravity (corresponding to gravity levels on Mars, on the Moon as well as microgravity) using a high-speed video camera. Bubble volume, dimensions and contact angle at detachment were measured. In addition to the experimental studies, a simple model, predicting bubble characteristics at detachment was developed. The model, based on thermodynamic considerations, accounts for the level of gravity as well as the magnitude of the uniform electric field. Measured data and model predictions show good agreement and indicate that the level of gravity and the electric field magnitude significantly affect bubble shape, volume and dimensions.

Experimental setup

The experimental setup designed for this study is arranged in three racks. The experimental rack carries the test cell and the measurement and actuation equipment. The personal computer rack carries the

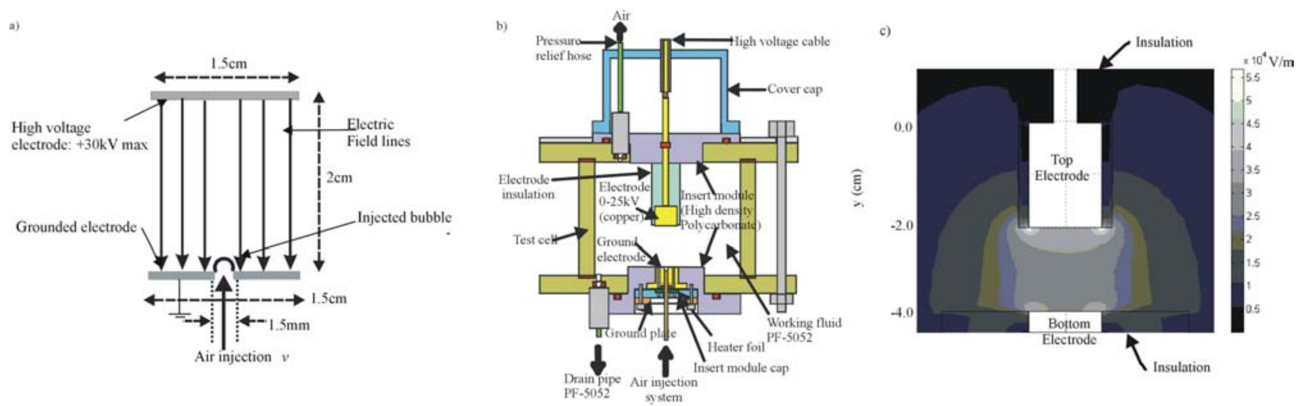

Fig. 1. a) Schematic of the investigated physical situation b) test cell and c) magnitude of the electric field in the test cell for potential difference between the electrodes determined numerically.

computer, monitor, data acquisition and control hardware and power backup units. The camera rack with the high-speed video recorder is connected to the camera head on the experimental rack through the umbilical. A triaxial accelerometer measures the components of the acceleration vector. The NEC 500 high-speed video recorder (provided by NASA GRC) allows visualization of the bubble formation process. The test cell is a rectangular vessel (Figure 1b). Its four walls are manufactured of 12.5mm thick, clear Polycarbonate to allow visualization experiments. The volume of the test cell is 9cmx9cmx10cm. A static electric field E (0-15.5kV/cm) is formed between the bottom electrode and a parallel top electrode, spaced 20mm apart. The bottom electrode is a 15mm diameter, electrically grounded copper cylinder. Air is injected into the test cell (at constant flow rate through a 1.5mm diameter orifice in the bottom electrode) with a syringe, driven by a linear translation stage. The working fluid, PF5052, is chemically inert and electrically insulating. Its relative permittivity is 1.73. In order to better understand the structure of the electric field in the test cell, the electric field distribution was computed assuming a 2D configuration, using the commercial finite element code, FEMLAB 2.0 (Figure 1c).

Results

The reduced gravity environment was realized during parabolic flights in NASA's KC-135 aircraft. A period of about 20s of low gravity was available per parabola. Experiments were carried out in bolted-down and free-floating configurations. Bubbles shown in this section represent typical behavior of injected bubbles at detachment for a particular set of experimental conditions. When the detachment of the bubble occurred after a regular and periodic formation behavior, key bubble dimensions (volume V_{dm}, major axis a_m, minor axis b_m, aspect ratio a_m / b_m and contact angle ϕ_m) were measured in the selected image sequences. Shapes of injected air bubbles recorded at the moment of detachment and their key dimensions for electric field magnitudes of $E = 0,\ 2.5,\ 5,\ 7.5$ and 10kV/cm are presented in Figure 2.

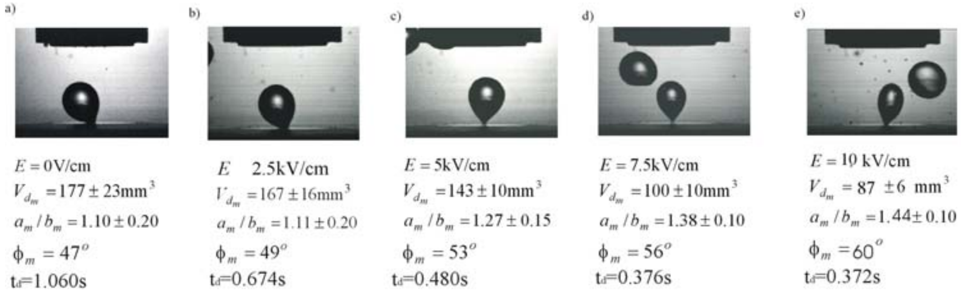

Fig 2. Experimentally visualized bubble shapes at detachment in microgravity for a) $E = 0$V/cm **, b)** 2.5kV/cm **, c)** 5kV/cm **, d)** 7.5kV/cm **and e)** 10kV/cm **.**

Without the electric field, the bubble in Fig. 2a is almost spherical (aspect ratio of 1.1) and slightly tilted due to small, residual, lateral acceleration components. Based on Figs. 2c-e it can be concluded that the bubble is increasingly elongated in the direction parallel to the applied electric field and the bubble axis is vertical. This behavior indicates that a uniform electric field affects bubble detachment and defines the preferential direction of the bubble axis. As a result of shape changes, the aspect ratio and the contact angle increase by 27% and 32%, respectively, when increasing the electric field magnitude from 0 to 10kV/cm. Under the same conditions, the volume at detachment is also affected by the presence of the electric field and it decreases by 51%. The period of bubble formation t_d (the time between bubble apparition and its detachment) decreases 50%. The influence of gravity level on bubble shape at detachment is illustrated in Figure 3. As expected, in the investigated range of gravity levels and electric field magnitudes, the influence of gravity level is more pronounced than that of the electric field.

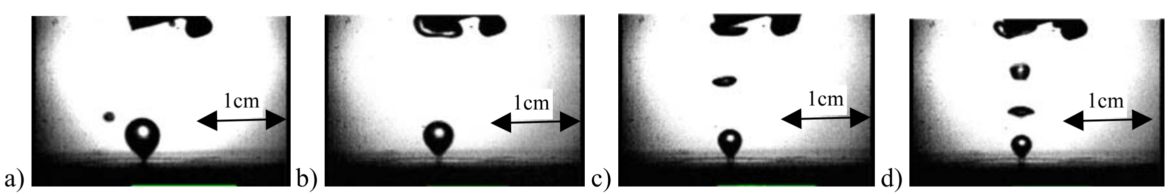

Fig 3. Bubble at detachment for U=10kV and different gravity levels
a) A_Z =-0.006 g V_d =32.483mm^3, b) A_Z =0.085 g V_d =18.851mm^3, c) A_Z =0.134 g V_d =10.964mm^3 and d) A_Z =0.374 g V_d =6.648mm^3

Acknowledgments

The research reported in this paper was supported by NASA research grant NAG3-1815. Support for Estelle Iacona was provided by the ESA postdoctoral fellowship. Support for Shinan Chang is provided by China Scholarship Council. The experiments in the KC-135 aircraft were carried out by Cila Herman, Gorkem Suner, Steven Marra and Ed Scheinerman. The support by the KC-135 crew and by NASA Glenn Research Center was invaluable for the successful completion of the experiments.

Stability and Heat Transfer Characteristics of Condensing Films

J.C. Hermanson,* P.C. Pedersen,† J.S. Allen,‡ M.A. Shear,†
Z.Q. Chen,* A.N. Alexandrou,° and W.W. Durgin*

*Mechanical Engineering Department, Worcester Polytechnic Institute, Worcester, MA 01609; †Electrical and Computer Engineering Department, Worcester Polytechnic Institute, Worcester, MA 01609; ‡National Center for Microgravity Research, Cleveland, OH 44135; °Department of Mechanical and Manufacturing Engineering, University of Cyprus, 1678 Nicosia, Cyprus; Corresponding author: jherm@wpi.edu

The overall objective of this research is to investigate the fundamental physics of film condensation in reduced gravity. The condensation of vapor on a cool surface is important in many engineering problems,[1,2] including spacecraft thermal control and also the behavior of condensate films that may form on the interior surfaces of spacecraft.

To examine the effects of body force on condensing films, two different geometries have been tested in the laboratory: 1) a stabilizing gravitational body force (+1g, or condensing surface facing "upwards"), and 2) de-stabilizing gravitational body force (-1g, or "downwards"). For each geometry, different fluid configurations are employed to help isolate the fluid mechanical and thermal mechanisms operative in condensing films. The fluid configurations are a) a condensing film, and b) a non-condensing film with film growth by mass addition by through the plate surface.

Condensation experiments are conducted in a test cell containing a cooled copper or brass plate with an exposed diameter of 12.7 cm. The metal surface is polished to allow for double-pass shadowgraph imaging, and the test surface is instrumented with imbedded heat transfer gauges and thermocouples. Representative shadowgraph images of a condensing, unstable (-1g) n-pentane film are shown in Fig. 1a-b. The interfacial disturbances associated with the de-stabilizing body force leading to droplet formation and break-off can be clearly seen in Fig. 1b. The heat transfer coefficient associated with the condensing film is shown in Fig. 2. The heat transfer coefficient is seen to initially decrease, consistent with the increased thermal resistance due to layer growth. For sufficiently long time, a steady value of heat transfer is observed, accompanied by continuous droplet formation and break-off.[1,2]

The non-condensing cell consists of a stack of thin stainless steel disks 10 cm in diameter mounted in a brass enclosure. The disks are perforated with a regular pattern of 361 holes each 0.25 mm in diameter. Non-condensing experiments in -1g have employed 50 cSt and 125 cSt silicone oil pumped through the perforated disks at a specified rate by a syringe micropump. The time to droplet break-off and the disturbance wavelengths appear to decrease with increasing pumping rate.

The ability to reliably perform multi-point, ultrasonic measurements of the film thickness has been demonstrated. A linear array of eight transducers of 6 mm diameter (with a beam footprint of comparable size) are pulsed with a square-wave signal at a frequency of 5 MHz and a pulse duration of approximately 0.3 μs. For thin films (60 μm to 2-3 mm in thickness) the layer thickness is determined by frequency analysis, where the received ultrasound pulse is Fourier transformed and the spacing between the peaks in the frequency spectrum is analyzed.[3] For thicker layers (up to at least 1 cm in thickness), time-domain analysis is performed of the received ultrasound pulses to generate directly the layer thickness.

A time-trace of the film thickness at a point using a single transducer in the linear array is shown in Fig. 3 for the case of an unstable (-1g) n-pentane film. The oscillations in film thickness are evidently due to the passage and/or shedding of droplets from the cooled plate surface. The entire transducer array was used to measure the changes in film thickness resulting from the passage of gravity waves generated either by an oscillating wall or the impact of a single droplet on the free surface of a film. The enclosure in both cases was 14 cm square and the transducer spacing was 12 mm. Best results were obtained using as test fluid a mixture of 50% glycerol and 50% water with a fluid layer thickness of 3-5 mm. In both cases the measured wavelengths and wave propagation speeds using the ultrasound technique compared reasonably well with those observed by optical imaging.

The authors acknowledge the assistance of Ms. L.A. Deluca and Ms. K.A. Hufnagle. This research is supported by NASA under Cooperative Agreement NAG3-2395.

References

[1]Gerstmann, J. and Griffith, P., "Laminar film Condensation on the Underside of Horizontal and Inclined Surfaces," *Int. J. Heat Mass Transfer*, Vol. 10, 567-580, 1967.

[2]Yanadori, M., Hijikata, K., Mori, Y. and Uchida, M., "Fundamental study of laminar film condensation heat transfer on a downward horizontal surface," *Int. J. Heat Mass Transfer* Vol. 28, No. 10, 1937-1944, 1985.

[3]Pedersen, P.C., Cakareski, Z., and Hermanson, J.C., "Ultrasonic Monitoring of Film Condensation," *Ultrasonics* **38**, 486-490, 2000.

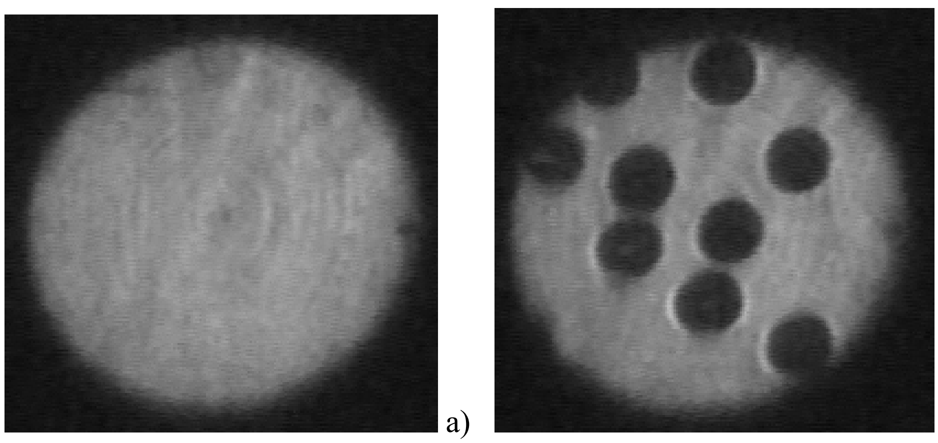

a) b)

Fig. 1a-b Condensing n-pentane film in unstable (-1g) configuration. a) 30 s after start of condensation, T_{wall} = 13.9 C, T_{sat} = 18.1 C; b) 40 s after start of condensation, T_{wall} = 13.9 C, T_{sat} = 21.3 C.

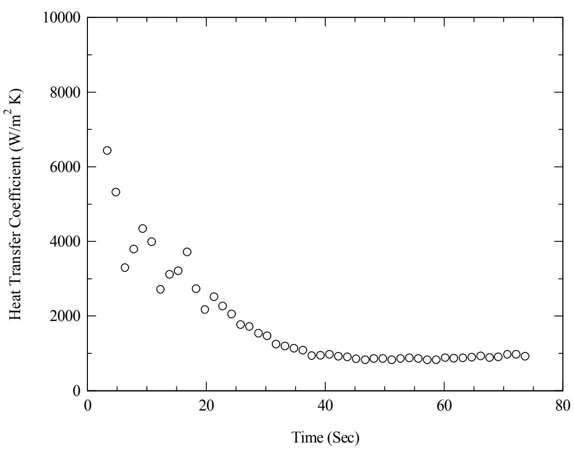

Fig. 2 Time evolution of heat transfer coefficient for unstable (-1g), condensing n-pentane film.

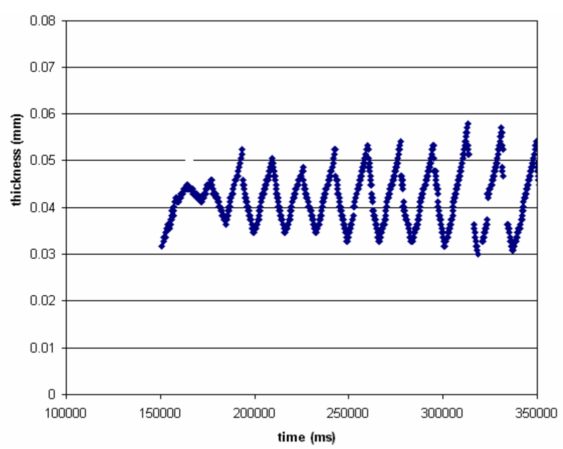

Fig. 3 Ultrasound point measurements of film thickness for unstable (-1g) condensing n-pentane film.

TWO-PHASE FLOW IN MICROCHANNELS WITH NON-CIRCULAR CROSS SECTION

Chris A. Eckett and Hal J. Strumpf
Honeywell International

ABSTRACT

Two-phase flow in microchannels is of practical importance in several microgravity space technology applications. These include evaporative and condensing heat exchangers for thermal management systems and vapor cycle systems, phase separators, and bioreactors. The flow passages in these devices typically have a rectangular cross-section or some other non-circular cross-section; may include complex flow paths with branches, merges and bends; and may involve channel walls of different wettability. However, previous experimental and analytical investigations of two-phase flow in reduced gravity have focussed on straight, circular tubes. This study is an effort to determine two-phase flow behavior, both with and without heat transfer, in microchannel configurations other than straight, circular tubes. The goals are to investigate the geometrical effects on flow pattern, pressure drop and liquid holdup, as well as to determine the relative importance of capillary, surface tension, inertial, and gravitational forces in such geometries.

An evaporative heat exchanger for microgravity thermal management systems has been selected as the target technology in this investigation. Although such a heat exchanger has never been developed at Honeywell, a preliminary sizing has been performed based on knowledge of such devices in normal gravity environments. Fin shapes considered include plain rectangular, offset rectangular, and wavy fin configurations. Each of these fin passages represents a microchannel of non-circular cross section. The pans at the inlet and outlet of the heat exchanger are flow branches and merges, with up to 90-deg bends. R-134a has been used as the refrigerant fluid, although ammonia may well be used in the eventual application.

The experimental portion of the program consists of two phases:

1. Ground laboratory testing of various microchannels in normal gravity
2. KC-135 reduced gravity testing of selected channels

The first phase of the program is in progress. Ground testing is being conducted in the Morrin-Martineli-Gier Memorial Heat Transfer Laboratory at UCLA. This experiment is an investigation of two-phase flow in small rectangular channels, without heat transfer. For simplicity, nitrogen and water are used as the working fluids. The experimental setup consists of a gas-pushed liquid feeding system, a nitrogen feeding system, the test section, a differential pressure drop measurement, still frame and video flow visualization via CCD camera, a nitrogen flow meter, and a liquid exit collection with precision scale for liquid flow rate measurement. The setup has been completed and preliminary experiments have been conducted to verify the measurements and visualization. Initial experiments have been performed on a set of three channels, each with a rectangular cross section of 0.04 in. width and 0.02 in. height. The first channel is straight, the second has a 45-deg corner, and the third has a 90-deg corner. A second

set of three test sections to be investigated involves straight rectangular channels of various cross-sectional dimensions. A later set will involve channels of different sizes and geometries, to be determined on the basis of the results from the first two sets.

The ground experiments are intended to model the flow in a single fin passage of a plain fin heat exchanger. In the absence of phase change, the relative mass flow rates of the gas and liquid are chosen to model various different refrigerant vapor qualities between 0 and 1 in the real application. A scaling analysis has been performed to match the liquid and gas superficial Reynolds numbers in the nitrogen-water experiments with those in the proposed R-134a evaporative heat exchanger. Typical Reynolds numbers are on the order of 10^2 for the liquid and 10^3 for the gas. The ground experiment test section sizes have been chosen to cover a range of Bond numbers and Suratman numbers representative of the proposed evaporative heat exchanger at normal gravity and at KC-135 reduced gravity.

One feature of the proposed evaporative heat exchanger in reduced gravity is that the Bond number is very low, on the order of 10^{-2} (for the KC-135) to 10^{-4} (for space-based applications), while the Suratman number is quite high, greater than 10^5. Thus, the two-phase flow is expected to be gravity independent, and surface tension forces are expected to dominate viscous forces. Such a combination of Bond number and Suratman number cannot be obtained in a 1-g experiment within the realm of practical working fluids. This is the justification for flight experiments.

The second phase of the program involves future experiments performed on the NASA KC-135 aircraft. The working fluid will be R-134a. Test section sizes and shapes will be selected on the basis of the findings from the ground experiment. Initial flights are expected to be adiabatic experiments with fixed qualities. A second set of flights is expected to incorporate a heating element and investigate the effect of phase change on the two-phase flow.

Principal Investigator:
Dr. Hal J. Strumpf
Chief Engineer, Heat Transfer
Airframe Systems
Honeywell International
2525 W. 190th St.
M/S 36-1-93010
Torrance, CA 90504
hal.strumpf@honeywell.com
Phone: (310) 512-3359
FAX: (310) 512-3432

GAS EVOLUTION IN ROTATING ELECTROCHEMICAL SYSTEMS UNDER MICROGRAVITY CONDITION

Yasuhiro Kamotani and Thaveesak Boonpongmane
Department of Mechanical and Aerospace Engineering
Case Western Reserve University
Cleveland, Ohio 44106

ABSTRACT

The effect of gas evolution on mass and heat transfer in rotating electrochemical cells is being investigated experimentally, both in 1-g and in reduced gravity. This work is motivated by the need of efficient electrochemical cells in microgravity. In microgravity, gas bubbles that are generated in an electrochemical cell must be removed from the electrode surface. In the present work, we investigate a means to enhance heat and mass transfer and, at the same time, to remove gas bubbles effectively for electrochemical systems.

Currently, we are investigating the effect of gas evolution on heat transfer. A cylindrical enclosure is rotated around its axis on a rotating table. The container diameter is 0.15 m and the depth is 0.05 m. The top wall is heated and the bottom wall is cooled. The container is filled with water. Without gas evolution, the flow in the cell is driven mainly by the centrifugal buoyancy, which generates radially outward flow along the bottom wall and inward flow along the top wall. In the present experiment, the Ekman number (Ek) is very small ($1 \times 10^{-5} < Ek < 4 \times 10^{-5}$). Consequently, the radial flow is confined to relatively thin Ekman layers along the top and bottom walls. The fluid is mainly in solid-body rotation with the enclosure, but the radial flow induces additional azimuthal flow through the Coriolis force. As a result, the azimuthal flow is slower (faster) than the container rotation near the cold (hot) wall. In the present heat transfer experiment, we are in the so-called Ekman suction regime, where the centrifugal buoyancy is mainly balanced by the Coriolis force, so that the radial flow is very much suppressed. The main quantity of interest in the present experiment is the overall heat transfer rate from the hot to cold walls, non-dimensionalized as the average Nusselt number (Nu). The experimentally measured Nusselt is about 2, which agrees well with the numerical simulation that is being conducted to supplement the experiment. Since the radial flow is suppressed by the Coriolis force, in some tests we place partitions in the container to retard the azimuthal flow and to increase the heat transfer rate. It is shown that Nu more than doubles when the partitions are used.

In the heat transfer experiment we generate bubbles by water electrolysis. Both oxygen (at the anode) and hydrogen (at the cathode) are generated. The bubbles move toward the container axis. A cylindrical post is placed along the container axis with a special filter so that only the bubbles are removed through the center post. The bubble behaviors are observed by a CCD camera. The camera is either stationary or rotates with the container. Along the cold (hot) wall, the liquid flow is opposed (aided) by the bubble flow. In normal gravity, the bubbles tend to move nearly upward near the bottom wall after they are generated, while they move along the top wall forming a so-called bubble layer. Thus, there exist three boundary layers, thermal, Ekman

and bubble layers along the top wall. The top wall situation somewhat resembles that in microgravity. The bubbles could affect the centrifugal buoyancy and Coriolis forces significantly. The present experiment covers from the thermal buoyancy dominant situation to the bubble buoyancy dominant situation. The amount of bubble generation is controlled by the electrical potential applied to the cell. The flow fields and heat transfer data taken under various conditions are presented.

We have also conducted normal gravity experiments on the gas evolution effect on mass transfer in a rotating electrochemical cell. In this experiment, we are in the so-called centrifugal buoyancy regime so that the Coriolis force has relatively weak influence on the mass transfer. It is found that in normal gravity the cell current is basically controlled by the kinetic reaction at the electrode. Thus the current is independent of the rotation speed unless the rotation speed is very high.

A test apparatus for parabolic flight tests is being designed. The basic concept is similar to the ground-based work. Since the time for each test is limited during parabolic flights, we just focus on the bubble behavior in a rotating system without heat transfer, in particular we are interested in the bubble layer characteristics in reduced gravity. We have already conducted preliminary student experiments during parabolic flights on the bubble behavior. Some results from the tests are presented.

ADSORPTION EQUILIBRIUM FOR SEPARATION OF CARBON MONOXIDE AND CARBON DIOXIDE FOR MARS ISRU

Krista S. Walton and M. Douglas LeVan
Department of Chemical Engineering, Vanderbilt University
VU Station B 351604, Nashville, TN 37235
krista.s.walton@vanderbilt.edu m.douglas.levan@vanderbilt.edu
Ph: (615) 322-2441 Fax: (615) 343-7951

ABSTRACT

The overall goal of this part of our research is to determine experimentally the adsorption equilibrium data that will enable efficient design of a separation process to remove carbon dioxide from a CO/CO_2 mixture. An effective separation process will depend on the adsorbent capacity for both the strongly and weakly adsorbed components at the desired operating temperature and pressure ranges, as well as regeneration requirements.

Pure component and binary adsorption isotherms are used to determine the most CO_2-selective adsorbent. A quick uptake of pure CO_2 on a given adsorbent at low pressures compared to the uptake of pure CO on the same adsorbent indicates that CO_2 molecules have a much stronger interaction with the adsorbent surface than CO. This is a necessary property for successful separation by adsorption. Adsorption isotherms are widely available in the literature for many pure components on various adsorbents. Pure component isotherms can be found in various publications and data handbooks for CO and CO_2 on activated carbon and many zeolites [1]. However, the pressure range seldom extends beyond 300 kPa, and the temperature is usually limited as well. Binary adsorption data are much less abundant and are more difficult to measure experimentally [2]. There are models that can predict binary adsorption from the pure component isotherms, but such models rarely provide the desired accuracy. Hence it is necessary to determine both pure component and binary adsorption isotherms to accurately design the separation system [3].

A gravimetric apparatus was used to measure pure adsorption isotherms. This is a desirable method for adsorbent screening due to its ability to provide quick measurements with acceptable accuracy. A sample pan is suspended from a highly sensitive microbalance and is enclosed by a glass tube that is equipped with a water jacket for isothermal experiments. The glassware also contains a coil of nichrome wire that is located around the sample pan and is used to regenerate the adsorbent. During regeneration helium is used to purge impurities from the system as it flows in from the bottom of the glassware and is vacuumed out the top. After regeneration, the system is placed under vacuum, and a data acquisition program is used to record the weight change of the adsorbent with time as the adsorbate is introduced into the system. Equilibrium is reached when the weight of the adsorbent remains constant. The balance can detect weight changes of 10^{-6} grams. CO_2 adsorption isotherms were measured on many adsorbents including

activated carbon and various zeolites. CO adsorption isotherms were measured for the adsorbents with the highest capacity for CO_2. These data are shown in Figure 1.

A volumetric apparatus has been constructed inside an environmental chamber to allow measurement of high-pressure pure component data and binary adsorption data at various temperatures. This apparatus consists of a closed loop containing a circulation pump and a fixed bed packed with adsorbent. The loop is equipped with a pressure transducer to monitor system pressure. A sample cylinder with a pressure transducer is connected to the loop to inject known amounts of gas. After injection, the pump is used to circulate the gas through the fixed bed. An injector and switching valve are used to take 100 μL samples from the loop and inject them into a gas chromatograph. A thermal conductivity detector is used to analyze the composition of the gas after adsorption equilibrium has been reached. Initial moles injected into the loop and final moles remaining in the gas phase at equilibrium are used to calculate the loadings from a material balance. This apparatus has been used to measure adsorption isotherms for pure CO_2 on NaY at 25, 75 and 125°C. These are shown in Figure 2. Mixture data have also been measured to determine the best adsorbent for our application.

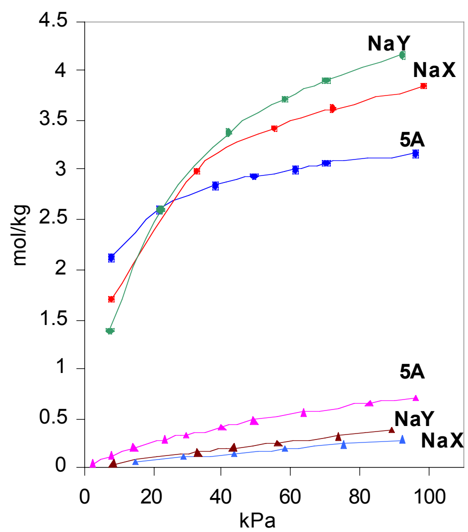

Figure 1. Adsorption equilibria of CO_2 (top three curves) and CO at 25°C.

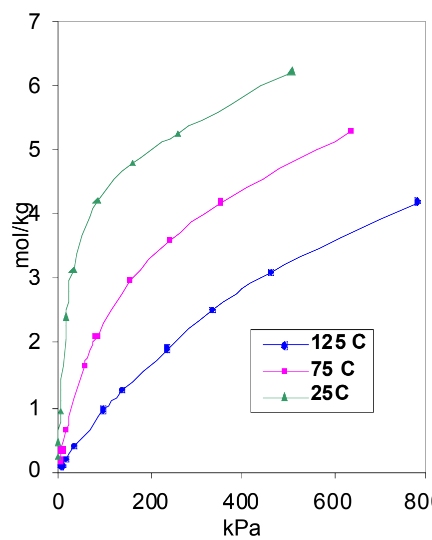

Figure 2. Adsorption equilibria of CO_2 on NaY zeolite using volumetric method.

References:

1. Valenzuela, D. P.; A. L. Myers. *Adsorption Equilibrium Data Handbook.* Prentice-Hall, Inc., Englewood Cliffs, NJ (1989).
2. Vansant, E. F.; G. Peters, I. Michelena. *J. Chem. Res.-S.,* **3**, 90-91 (1978).
3. Talu, O. *Adv. Colloid. Interfac. Sci.*, **76-77**, 227, (1998).

ON THE MOTION OF AN ANNULAR FILM IN MICROGRAVITY GAS-LIQUID FLOW

John B. McQuillen
Microgravity Fluid Physics Branch
NASA Glenn Research Center
21000 Brookpark Road,
Cleveland, OH 44135
PH (216)433-2876
FAX (216)433-8050
j.mcquillen@grc.nasa.gov

ABSTRACT

Three flow regimes have been identified for gas-liquid flow in a microgravity environment: Bubble, Slug, and Annular. For the slug and annular flow regimes, the behavior observed in vertical upflow in normal gravity is similar to microgravity flow with a thin, symmetrical annular film wetting the tube wall. However, the motion and behavior of this film is significantly different between the normal and low gravity cases. Specifically, the liquid film will slow and come to a stop during low frequency wave motion or slugging. In normal gravity vertical upflow, the film has been observed to slow, stop, and actually reverse direction until it meets the next slug or wave.

Using the unit slug approach, as seen in Figure 1, a quick estimate for the film thickness can be derived by the following relationship:

$$\alpha = 1 - \left(\frac{2h}{D}\right)^2$$

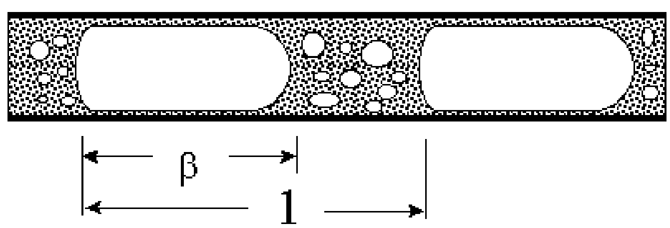

Figure 1: Unit Slug Concept

Combined with the following from the drift flux model:

$$\alpha = \frac{\frac{\rho_L}{\rho_G}\frac{x}{1-x}}{C_0\left(1+\frac{\rho_L}{\rho_G}\frac{x}{1-x}\right)}$$

Rearranging yields the film thickness, however, this estimate assumes that the vapor and liquid phases are either distributed in an annular flow with very thin liquid slugs separating annular pockets or with significant gas entrainment in the liquid slugs.

A minimum film thickness can be attained by assuming that most of the gas is contained in the Taylor bubble. Therefore, if one slug unit consists of both a liquid slug and a Taylor bubble and assuming that the void fraction is zero in the slug, a mass balance performed on the Taylor bubble portion of the slug unit will obtain the following:

$$\alpha_B V + (1-\alpha_B)U_{LB} = j_L + j_G$$

By rearrangment, the void fraction in the Taylor bubbles is given by:

$$\alpha_B = 1 - \frac{V-(j_G + j_L)}{V - U_{LB}}$$

where V is the velocity of the Taylor bubble and U_{LB} is the velocity of the liquid film. Within the Taylor bubble, the film thickness decreases from the nose to the tail. Far from the nose, it reaches its fully developed thickness. This thickness may be found directly by noting that there is no driving force acting on the film except for the interfacial shear stress. By disregarding this effect, the film does not experience a driving force and its velocity must be zero with respect to the standing frame (U_{LB}=0). This has been experimentally confirmed by watching small bubbles that are entrained in the thin liquid film around the Taylor bubble and gives the minimum film thickness in these bubbles:

$$h_{min} = \frac{D}{4}\frac{V-(j_G + j_L)}{V}$$

If $V \approx C_0(U_{LS} + U_{GS})$, then

$$h_{\min} = \frac{C_0 - 1}{C_0}\frac{D}{4}$$

For values of C_0=1.2, the minimum film thickness is approximately 0.8 mm, which is significantly smaller than the values found using the drift flux model.

Data obtained for air-water, air-water and glycerine mixture (50 w/o and viscosity @), and an air-water and surfactant mixture (Zonyl FSP™, 1 w/o and surface tension of 20 dynes/cm) was obtained at in a 1.27 cm ID tube at low gravity[1]. 16 mm movie film data was obtained at 400 frames per second. Bubbles located within the thin liquid annular film were tracked for their position as a function of time and analyzed as a measure of the liquid axial velocity relative to the passage of slugs or annular roll waves. It was found that there was always a slowing of the thin liquid film or substrate until the next slug or roll wave accelerated the film again.

Liquid film thickness data was obtained at 1000 Hz from thin wire conductivity probes. Their accuracy was about 0.02 mm. A histogram analysis was used to obtain a truncated film thickness, by excluding values greater than 1.5 mm film thickness, the mode, and a minimum film thickness. These are compared with an average value that includes wave heights or slugs. In several cases, for both when the liquid film motion stopped or even just significantly slowed, it was found that, for obvious reasons, that the truncated averaged film thickness was less than the average film thickness, the mode value was less than both of the averages and that the "minimum" experimental film thickness was typically less than half of the both averages.

---

[1] Bousman, W. S., "Studies of Two-Phase Gas-Liquid Flow in Microgravity," *NASA Contractor Report 195434*, 1995.

MIXING OF CONCENTRATED OIL-IN-WATER EMULSIONS MEASURED BY NUCLEAR MAGNETIC RESONANCE IMAGING (NMRI)

M.A. d'Avila, N.C. Shapley, J.H. Walton*, S.R. Dungan, R.J. Phillips and R.L. Powell
Department of Chemical Engineering and Materials Science,
University of California, Davis
*** NMR Facility, University of California, Davis**

In most emulsions, a density difference between the dispersed and the continuous phases leads to separation of the components by gravity, known as "creaming." Typically, a uniform emulsion is desirable, and hence it is important to examine the kinetics and mechanism of emulsion mixing required to achieve this uniform state. In addition, previous mixing research has focused on the impact of known flow fields on the microstructure of the system, where the microstructures do not modify the flow field in the process. In contrast, in the case of concentrated emulsions, it is shown here that the evolution of the nonuniform droplet concentration profile has a major impact on the observed flow field.

Mixing of concentrated oil-in-water emulsions in a horizontal, concentric-cylinder geometry was studied using nuclear magnetic resonance imaging (NMRI). The NMRI technique provides droplet concentration and velocity profiles noninvasively and *in situ* within a flowing, concentrated emulsion of isooctane and water stabilized with nonionic surfactant. An initial nonuniform concentration profile is established by creaming of a homogeneous emulsion. We then measure the time-dependent effect of slow shear flow on the concentration and velocity profiles. Time-of-flight and chemical shift imaging methods were used to measure velocity profiles and concentration maps during the mixing process, respectively.

The results obtained show detailed information about the mixing process in concentrated emulsions. It was found that the thickness of the cream layer remains constant during mixing while the concentration in that layer decays exponentially as a function of time. It was also observed that while mixing occurs, most of the emulsion is quiescent, the only detectable motion being in a thin moving layer close to the rotating outer cylinder wall. A simple model is introduced that is able to give a reasonable explanation of these experimental observations. These results indicate that the mixing mechanism and kinetics in concentrated emulsions are significantly different from those in single-phase liquids.

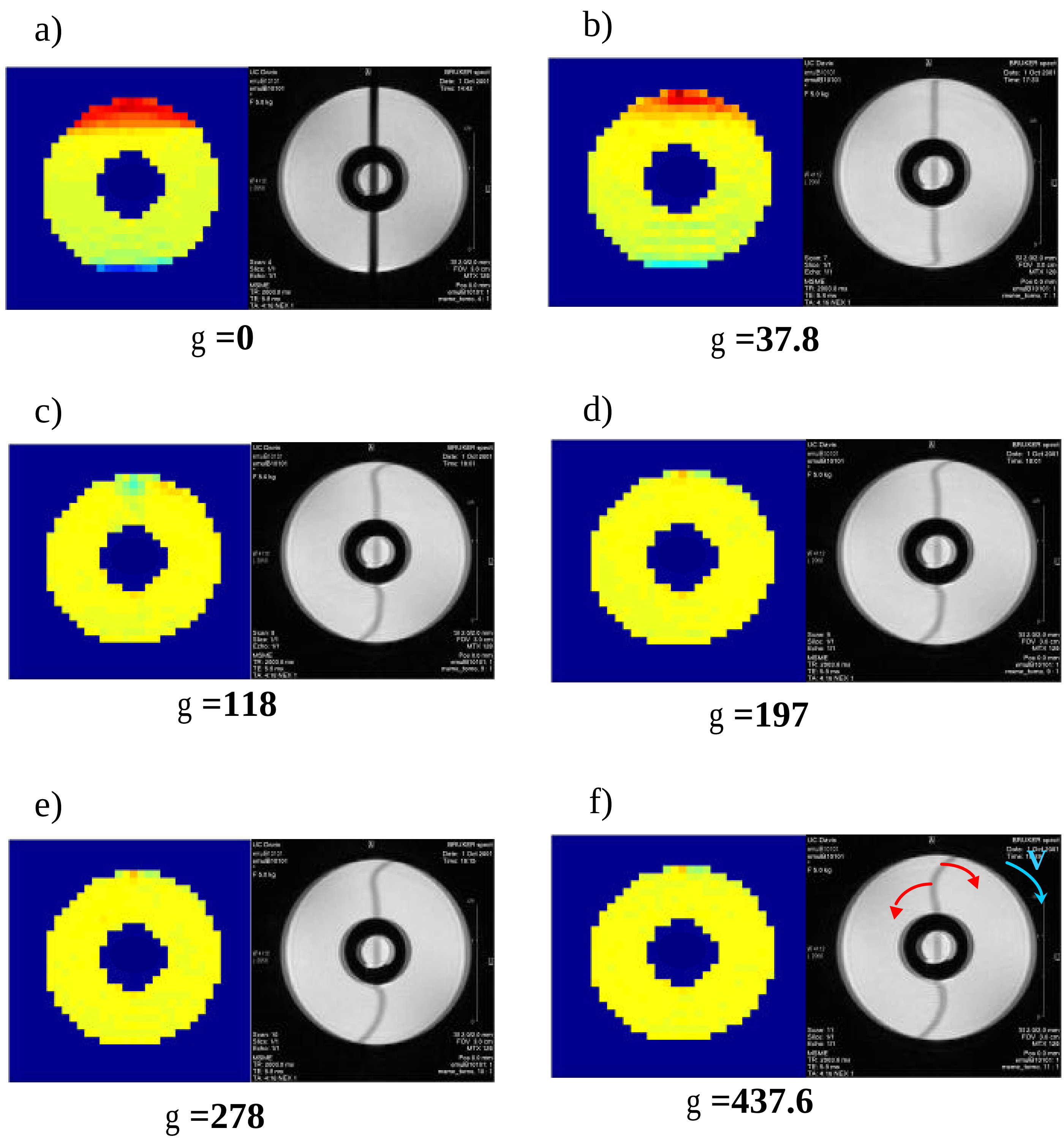

Side by side oil concentration maps and time-of-flight images for an emulsion with f = 0.5 and V = 0.05 cm/s, after 3 hours of creaming. The series of images shows the progression of mixing as the strain increases from a) g =0, b) g =37.8 , c) g =118, d) g =197, e) g =278, to f) g =437.6.

A NUMERICAL METHOD FOR GAS-LIQUID FLOWS

Y. Hao and A. Prosperetti
Department of Mechanical Engineering, The Johns Hopkins University
Baltimore MD 21218

The numerical simulation of two-phase flow processes with heat transfer and phase change requires an accurate representation of the flow and temperature fields near gas-liquid (or vapor-liquid) interfaces. This circumstance renders rather problematic the use of several existing methods in which the interface is smeared over a few cells. The present method avoids this shortcoming by maintaining the interface sharp by means of a suitably modified front-tracking approach. In addition, the compressibility of the gas or vapor field can be accounted for, and realistic density ratios can be used. For the time being, the method has been developed and tested for three-dimensional adiabatic calculations. It has been found to perform very well, and its extension to the energy equation is planned for the near future.

The salient aspects of the method are the following:

1. We use a fixed Cartesian three-dimensional grid over which the interface moves. We follow the approach of Tryggvason and co-workers (see e.g. Ref. [1]) in discretizing the free surface by means of triangular finite elements the vertices of which are Lagrangian points. These points are advected normally to the interface with a velocity calculated from

$$\mathbf{v}(\mathbf{x},t) = \int d^3y \; \delta(\mathbf{x}-\mathbf{y})\,\mathbf{u}(\mathbf{y},t) \tag{1}$$

where $\mathbf{u}$ is the liquid velocity. The delta distribution $\delta(\mathbf{x}-\mathbf{y})$ is approximated by a standard regularized form.

Again as in Tryggvason's work, the liquid region is distinguished from the gas region by solving a Poisson equation for the indicator function I which equals +1 in the liquid and -1 in the gas:

$$\nabla^2 I = \boldsymbol{\nabla}\cdot\left(2\int_S dS_y\;\hat{\mathbf{n}}\;\delta(\mathbf{x}-\mathbf{y})\right), \tag{2}$$

in which again the delta distribution is regularized. The solution of this equation gives a smooth approximation to I, but the interface can be maintained sharp by focusing on the line where the function changes sign.

2. In order to be able to use standard differentiation formulae near the interface, the liquid velocity field is extrapolated into the gas region by extending to three dimensions an idea of Popinet & Zaleski [2]. Specifically, the velocity field near an interface point $\mathbf{y}$ is approximated by a linear distribution, $\mathbf{u}(\mathbf{x},t) \simeq \mathbf{u}_0 + \mathsf{T}\cdot(\mathbf{x}-\mathbf{y})$, and the quantities $\mathbf{u}_0$, T are found by a least squares fit incorporating the condition of vanishing tangential stress by means of of a Lagrange multiplier.

3. The liquid flow field is calculated by means of a first-order projection method. In order to facilitate the solution of the Poisson equation for the pressure, the liquid pressure is extended into the gas region by using an idea similar to the one used in the Ghost Fluid method [3]: a fictitious pressure is defined in the gas nodes by using the actual gas pressure and the jump in the normal stresses caused by surface tension.

The figures demonstrate the performance of the method in a few cases. In particular the last example shows the "swimming" of a bubble in microgravity under the action of a modulated liquid velocity including the natural frequency of the $n = 2$ and $n = 3$ shape modes.

References

1. G. Tryggvason, B. Bunner, A. Esmaeeli, D. Juric, N. Al-Rawahi, W. Tauber, J. Han, S. Nas, and Y.-J. Jan. *J. Comput. Phys.*, **169**, 708, (2001).
2. S. Popinet and S. Zaleski. in press, *J. Fluid Mech.*, (2002).
3. X.-D. Liu, R. Fedkiw and M. Kang. *J. Comput. Phys.*, **160**, 151, (2000).

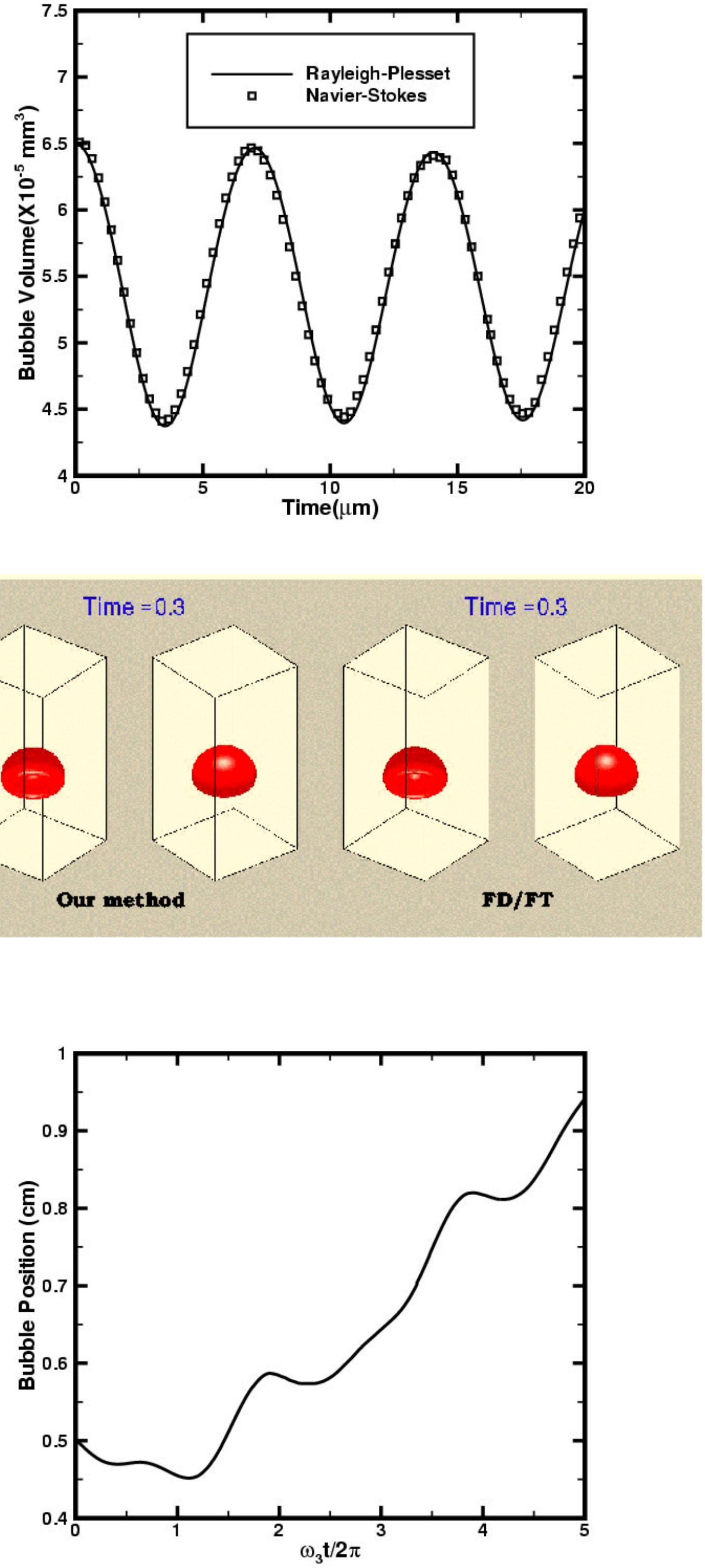

Figure 1: TOP: Comparison of the present results (squares) with the numerical solution of the Rayleigh-Plesset equation for a spherical gas bubble with an equilibrium radius of 23.75 μm released at time 0 from a radius of 25 μm.
MIDDLE: Comparison of the present results with those of the front-tracking code of Tryggvason et al. for a bubble rising under buoyancy; The Eötvös number is 3.57 and the Morton number 3×10^{-7}.
BOTTOM: Position of the center of a bubble in a square tube with a modulated liquid velocity and zero gravity; the modulation includes the natural frequency of the $n = 2$ and $n = 3$ shape modes and causes the bubble to "swim".

STUDY OF CO-CURRENT AND COUNTER-CURRENT GAS-LIQUID TWO-PHASE FLOW THROUGH PACKED BED IN MICROGRAVITY

Shripad T. Revankar
School of Nuclear Engineering, Purdue University, West Lafayette, IN 47907

ABSTRACT

The main goal of the project is to obtain new experimental data and development of models on the co-current and counter-current gas-liquid two-phase flow through a packed bed in microgravity and characterize the flow regime transition, pressure drop, void and interfacial area distribution, and liquid hold up. Experimental data will be obtained for earth gravity and microgravity conditions. Models will be developed for the prediction of flow regime transition, void fraction distribution and interfacial area concentration, which are key parameters to characterize the packed bed performance. Thus the specific objectives of the proposed research are to: (1) Develop experiments for the study of the gas liquid two-phase flow through the packed bed with three different flow combinations: co-current down flow, co-current upflow and counter current flow. (2) Develop pore scale and bed scale two-phase instrumentation for measurement of flow regime transition, void distribution and gas-liquid interfacial area concentration in the packed bed. (3) Obtain database on flow regime transition, pressure drop, void distribution, interfacial area concentration and liquid hold up as a function of bed characteristics such as bed particle size, porosity, and liquid properties such as viscosity and surface tension. (4) Develop mathematical model for flow regime transition, void fraction distribution and interfacial area concentration for co-current gas-liquid flow through the porous bed in gravity and micro gravity conditions.(4) Develop mathematical model for the flooding phenomena in counter-current gas-liquid flow through the porous bed in gravity and micro gravity conditions.

The present proposal addresses the most important topic of HEDS-specific microgravity fluid physics research identified by NASA 's one of the strategic enterprises, OBPR Enterprise. The proposed project is well defined and makes efficient use of the ground-based parabolic flight research aircraft facility. The project spans for four years. The first two years are devoted to ground based flight definition experimental and modeling program. During the next two years microgravity flight tests are carried out using the ground-based parabolic flight research aircraft.

The experimental program consists of a design of a packed bed loop using a scaling analysis, performing experiments for various parameters: bed diameter, packing size, liquid surface tension, and liquid viscosity. Figure 1 shows the schematic of the test loop. A packed bed sections of 15 cm diameter and 10 cm diameter are designed with sphere packing particles of diameter, 6 mm and 3 mm. The fluid combination used are : 1)water, air, (2) alcohol-water mixture (50%, 80% methanol) and air, and (3) glycerol-water mixture and air (50%, and 64% glycerol weight percent). The loop is instrumented to provide detailed measurement at pore and bed level parameters.

The data analysis involves: (1) generating maps of global mode of operation such as flow regime maps and pressure drop characteristics, (2) identification of the active and passive pores, (3) identification of void fraction in pores, (4) local void and interfacial area distribution, and (5) bed liquid holdup.

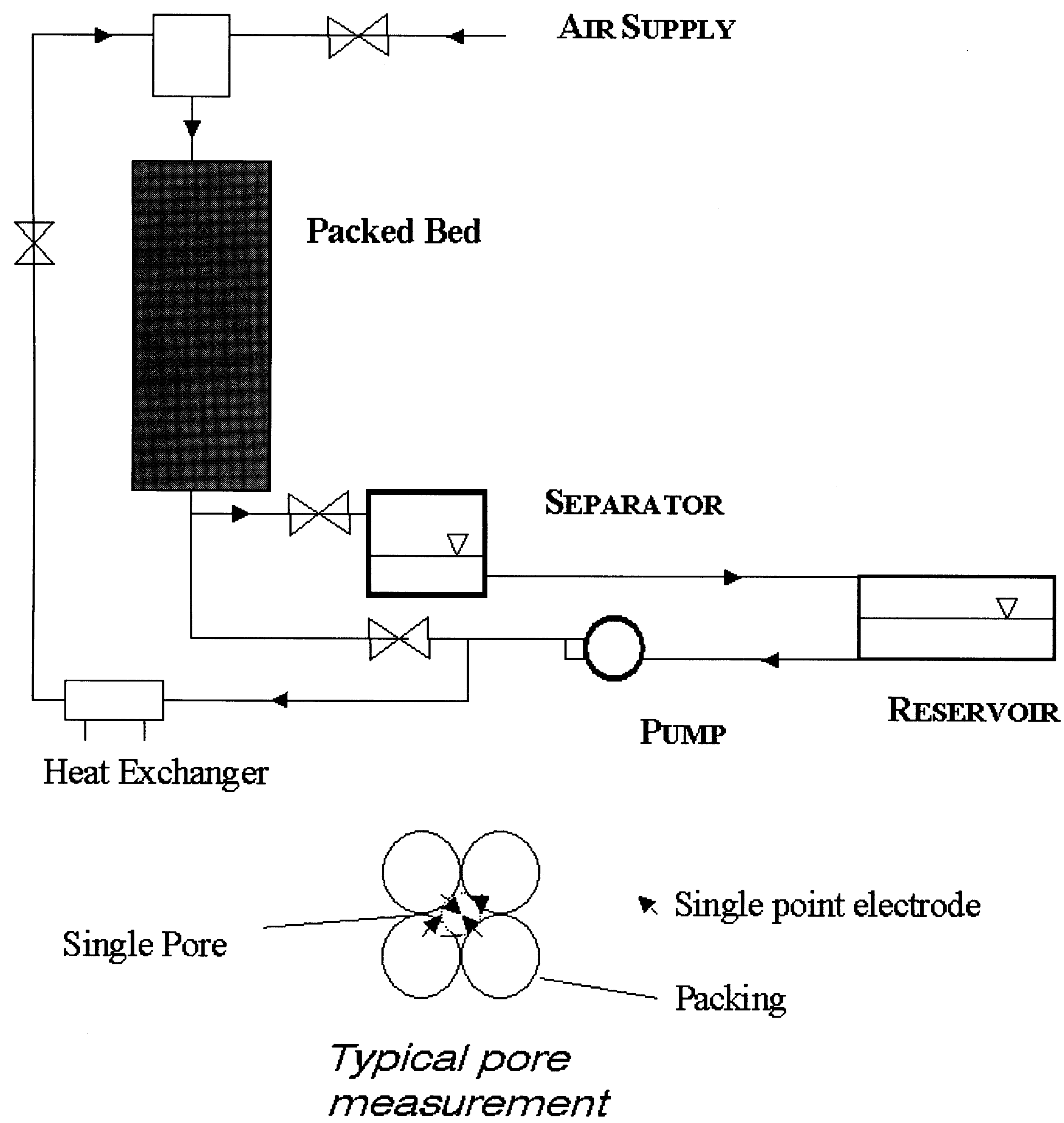

Figure 1. Schematic of the packed bed test loop.

AUGMENTATION OF PERFORMANCE OF A MONOGROOVE HEAT PIPE WITH ELECTROHYDRODYNAMIC CONDUCTION PUMPING

S.I. Jeong
Department of Mechanical Engineering, Texas A&M University
College Station , Texas 77843

J. Seyed-Yagoobi
Department of Mechanical, Materials, and Aerospace Engineering
Illinois Institute of Technology
Chicago, Illinois 60616

The electrohydrodynamic (EHD) phenomena involve the interaction of electric fields and flow fields in a dielectric fluid medium. There are three types of EHD pumps; induction, ion-drag, and conduction. EHD conduction pump is a new concept which has been explored only recently. Net pumping is achieved by properly utilizing the heterocharge layers present in the vicinity of the electrodes.

Several innovative electrode designs have been investigated. This paper presents an electrode design that generates pressure heads on the order of 600 Pa per one electrode pair at 20 kV with less than 0.08 W of electric power. The working fluid is the Refrigerant R-123. An EHD conduction pump consisting of six pairs of electrodes is installed in the liquid line of a mono-grove heat pipe.

The heat transport capacity of the heat pipe is measured in the absence and presence of the EHD conduction pump. Significant enhancements in the heat transport capacity of the heat pipe is achieved with the EHD conduction pump operating. Furthermore, the EHD conduction pump provides immediate recovery from the dry-out condition.

The EHD conduction pump has many advantages, especially in the micro-gravity environment. It is simple in design, non-mechanical, and lightweight. It provides a rapid control of heat transfer in single-phase and two-phase flows. The electric power consumption is minimal with the very low acoustic noise level.

MICROGRAVITY BOILING ENHANCEMENT USING VIBRATION-BASED FLUIDIC TECHNOLOGIES

Marc K. Smith, Ari Glezer, and Samuel N. Heffington
The George W. Woodruff School of Mechanical Engineering,
Georgia Institute of Technology, Atlanta, GA 30332-0405

ABSTRACT

Thermal management is an important subsystem in many devices and technologies used in a microgravity environment. The increased power requirements of new Space technologies and missions mean that the capacity and efficiency of thermal management systems must be improved. The current work addresses this need through the investigation and development of a direct liquid immersion heat transfer cell for microgravity applications. The device is based on boiling heat transfer enhanced by two fluidic technologies developed at Georgia Tech.

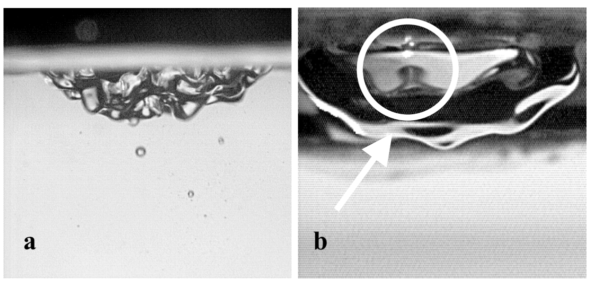

Figure 1. (a) Violent oscillations of a 5 mm air bubble in water driven at 440 Hz. (b) Possible interfacial collapse occurring inside the same gas bubble (white circle and arrow).

The first of these fluidic technologies, called vibration-induced bubble ejection, is shown in Fig. 1. Here, an air bubble in water is held against a vibrating diaphragm by buoyancy. The vibrations at 440 Hz induce violent oscillations of the air/water interface that can result in small bubbles being ejected from the larger air bubble (Fig. 1a) and, simultaneously, the collapse of the air/water interface against the solid surface (Fig. 1b). Both effects would be useful during a heat transfer process. Bubble ejection would force vapor bubbles back into the cooler liquid so that they can condense. Interfacial collapse would tend to keep the hot surface wet thereby increasing liquid evaporation and heat transfer to the bulk liquid.

Figure 2 shows the effect of vibrating the solid surface at 7.6 kHz. Here, small-scale capillary waves appear on the surface of the bubble near the attachment point on the solid surface (the grainy region). The vibration produces a net force on the bubble that pushes it away from the solid surface. As a result, the bubble detaches from the solid and is propelled into the bulk liquid. This force works against buoyancy and so it would be even more effective in a microgravity environment. The benefit of the force in a boiling process would be to push vapor bubbles off the

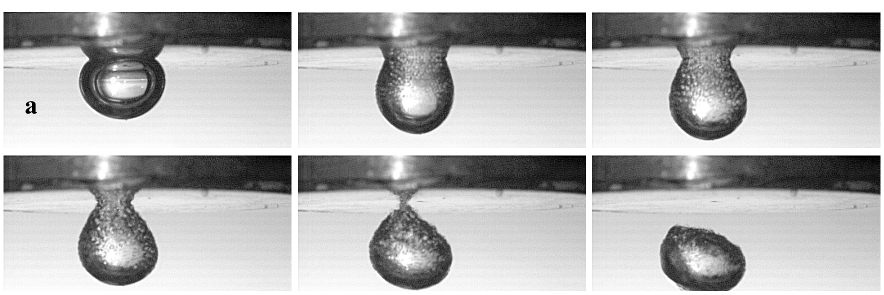

Figure 2. An air bubble in water (5 mm diameter) resting against the underside of a submerged vibrating diaphragm. The upper left image (a) is with no vibration. When the diaphragm vibrates at 7.6 kHz, the image sequence shows the air bubble being pushed away from the surface against the force of buoyancy.

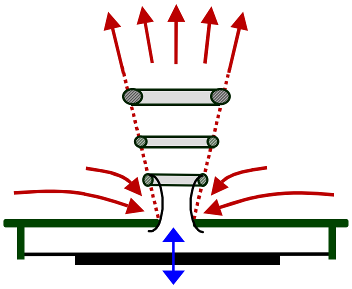

Figure 3. A vibrating diaphragm alternately entrains and expels fluid from a cavity resulting in a synthetic jet.

solid surface, thus helping to keep the solid surface wet and increasing the heat transfer.

The second fluidic technology to be employed in this work is a synthetic jet, shown schematically in Fig. 3. The jet is produced using a small, sealed cavity with a sharp-edged orifice on one side and a vibrating diaphragm on the opposite side. The jet is formed when fluid is alternately sucked into and then expelled from the cavity by the motion of the diaphragm. This alternating motion means that there is no net mass addition to the system. Thus, there is no need for input piping or complex fluidic packaging.

The efficiency of boiling heat transfer is hindered in microgravity because there is no inherent mechanism to remove vapor bubbles from the heated surface (this is the role of buoyancy on Earth). To circumvent this problem, the fluidic technologies described above will be used to develop a nucleate boiling heat transfer cell for efficient, high-flux cooling in microgravity. The cell will be composed of a liquid-filled cavity with one surface attached to the surface to be cooled and with another surface attached to an array of heat transfer fins or some other device that serves to reject the heat to an outside environment. An array of vibration actuators will be designed and fabricated on the hot surface. These actuators will aid nucleate boiling in the cell by vibration-induced bubble ejection from larger vapor bubbles (Fig. 1a), vibration-induced collapse of vapor bubbles against the heated surface (Fig. 1b), and the direct removal of vapor bubbles from contact with the heated surface (Fig. 2). Synthetic jets placed inside the cell (Fig. 3) will produce a flow that will transport vapor bubbles away from the heated surface into the cooler bulk liquid. Since the synthetic jets operate on time scales that are much shorter than the characteristic thermal time scale of the flow, they will also substantially enhance small-scale mixing within the liquid, thus enhancing the condensation of vapor bubbles back into the liquid and the heat transfer out of the cell.

The primary objectives of this research are as follows.

1. Develop, design, and construct a nucleate boiling heat transfer cell based on the vibration-induced bubble ejection and synthetic-jet technologies.
2. Examine the formation, spreading, and detachment of vapor bubbles from a heated surface during boiling in microgravity.
3. Determine the influence of vibration of the heated surface on the spreading, merging, and detachment of vapor bubbles from the surface.
4. Determine the vibration conditions that maximize the interfacial motion of a vapor bubble and that ensure its collapse against the heated surface.
5. Determine the conditions for the effective use of forced convection induced by synthetic jets to remove vapor bubbles from the heated surface.

Both experimental and numerical work will be done during this investigation. If these technologies behave as expected, the simplicity and scalability of the resulting heat transfer cell would make it a very attractive method for thermal management in microgravity. In addition, the technology may also be transferable to Earth-based, boiling applications and provide improved performance over normal pool-boiling technologies.

Using Surfactants to Control Bubble Growth and Coalescence

K. Stebe
Johns Hopkins University

The effects of surfactant adsorption on bubble formation at an orifice are studied numerically at finite Reynolds number. Establishing the hydrodynamics and mass transfer during bubble growth and detachment will improve insight into the nucleate boiling process and aid in developing paradigms for enhancement of the heat transfer coefficient during nucleate boiling. The volume-of-fluid method is employed to solve the two-dimensional axisymmetric Navier-Stokes equations. The interface is tracked using marker points that accurately represent the surface tension forces at the interface. The evolution and detachment of the bubble is examined as a function of the capillary and Bond numbers. At low surface tension, strong deformations of the interface are observed leading to bubbles that assume a mushroom shape. Surfactants change the surface tension according to a non-linear equation of state that takes into account maximum packing at the interface. A variety of behaviors are predicted, depending upon the ratio of the convection rate to the prevailing mass transfer rates. In particular, if these rates are comparable, regions of local surfactant accumulation develop where the surfactant concentration approaches its upper bound, causing the local surface tension to reduce strongly and rendering the interface highly deformable.

SUPERCRITICAL AND TRANSCRITICAL SHEAR FLOWS IN MICROGRAVITY: EXPERIMENTS AND DIRECT NUMERICAL SIMULATIONS

Doug Talley
Air Force Research Laboratory, AFRL/PRSA, 10 E. Saturn Blvd., Edwards AFB, CA 93524

Josette Bellan
Jet Propulsion Laboratory, 4800 Oak Grove Drive, MS 125-09, Pasadena, CA 91109-8099

Bruce Chehroudi
ERC, Inc., 10 E. Saturn Blvd., Edwards AFB, CA 93524

ABSTRACT

The objective of this research, which began in April 2002, is to develop and experimentally validate a near-critical transcritical and supercritical fluid shear flow model independent of turbulence. We define a supercritical shear flow to be one in which all of the fluid particles remain above their critical temperature and pressure. We define a transcritical shear flow to be one in which at least some of the fluid particles undergo a transition between a subcritical and a supercritical temperature, between a subcritical and a supercritical pressure, or both. The reason it is necessary to validate the fluid model independent of turbulence is that turbulence introduces a large number of additional mechanisms the understanding of which is embryonic at best for near-critical transcritical and supercritical flows. Validating the fluid model without turbulence uncertainties therefore requires laminar flows. However, laminar flows that are not influenced by gravity are difficult to produce in normal gravity due to the large density gradients involved. Therefore, microgravity experiments are necessary.

The co-investigators have considerable experience modeling supercritical mixing and shear layers (JPL), and considerable experience in performing transcritical and supercritical droplet and jet experiments in normal gravity (AFRL/ERC). This experience will be applied to perform a microgravity experiment where the results can be directly compared with direct

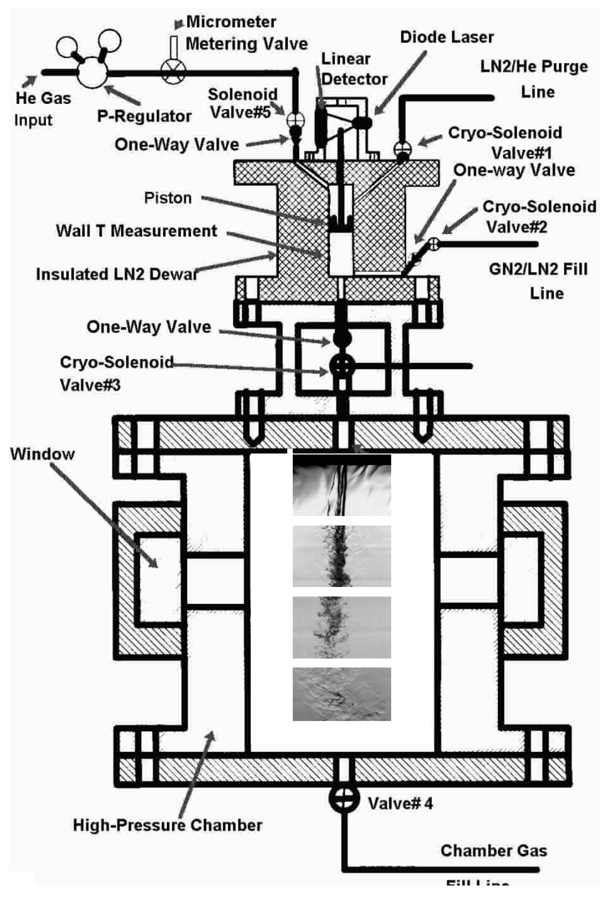

Figure 1. Preliminary Schematic of a Drop Tower Experiment; supercritical jet at 1g..

numerical simulations. An entry into the related publications of the co-investigators can be found in refs. [1-3].

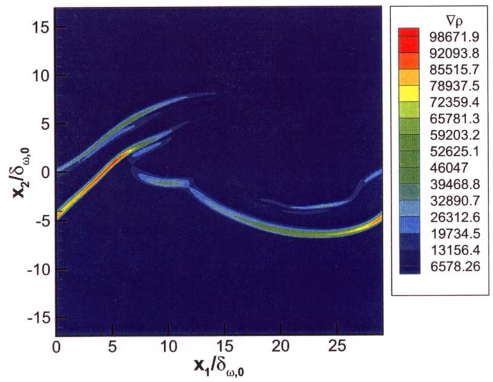

Figure 2. Density gradient magnitude computations in a laminar heptane/nitogen shear layer.

Experimental Approach

Liquid nitrogen (LN_2) initially below the critical temperature will be injected into room temperature gaseous nitrogen (GN_2) and GN_2/He mixtures at various subcritical to supercritical pressures. AFRL/ERC has considerable previous experience with these mixtures under normal gravity, and the substances are inherently safe. A conceptual design of the drop tower rig is illustrated in Fig. 1. Two separate chambers, one for LN_2, and the other for the ambient fluid, are connected through a one-way valve and a cryo-solenoid valve. The LN_2 chamber is an insulated dewar with several inlet and outlet passages as shown. Injection is achieved through pressurized He gas exerted on the upper side of a small piston inside the chamber. Injection initiation is controlled by the Cryo-solenoid-valve #3. The high pressure chamber will be designed to have optical access for flow visualization. The entire setup will be designed to withstand the total stresses caused by internal pressure and decelerating inertia forces. The volumes of the chambers are selected based on the test periods of less than 2.2 seconds and the range of flow rates desired to produce a range of Reynolds numbers, with minimal pressure rise during a test. Several ways to measure the instantaneous flow rates have been discussed, including the method shown in Fig. 1, where piston motion is detected by a diode laser and linear array optical array arrangement. The experimental procedure will be to complete chill down and establish the flow before the drop. Estimates confirm that there should be ample time for the flow to relax from 1 g to μg before the end of the drop.

Theoretical Approach

The theoretical approach includes real-gas equations of state, conservation equations that account for Soret and Dufour effects, and accurate transport properties. This model has already been validated with suspended-drop microgravity data. Preliminary simulations of a forced, laminar heptane/nitrogen mixing layer yielded encouraging results when compared to experimental observations of supercritical jets. An example of the simulation results is depicted in Fig. 2 showing the magnitude of the density gradient, which is pertinent to optical measurements: the finger-like features detected in the simulations qualitatively replicate some features observed experimentally [3]. Further studies will focus on using the same fluids in simulations and experiments, and performing simulations and observations at same conditions.

1. Harstad, K. and Bellan, J., Int. J. of Multiphase Flow, 26(10), 1675-1706, 2000.
2. Chehroudi, B., and Talley, D.G., 40th AIAA Aerospace Sciences Meeting and Exhibit, paper AIAA 2002-0342, Reno, NV, 14-17 January, 2002.
3. Chehroudi, B., Coy, E., and Talley, D.G., Physics of Fluids, 14(2), 850-861, 2002.

THE SCALES SEPARATION PHENOMENON IN HIGH HEAT FLUX POOL BOILING

T.G Theofanous, G.J. Li, J.P. Tu and T.N. Dinh
Center for Risk Studies and Safety
University of California, Santa Barbara
6740 Cortona Drive, Goleta CA 93117
Phone/Fax: (805) 893-4900/4927, theo@crss.ucsb.edu

This is the first progress report on a recently-initiated research project aiming to a basic understanding of Boiling Crisis in forced convection boiling. The work is a continuation and extension of a project that addressed coolability limits in pool boiling carried out over the previous funding cycle. A key result of this previous work was the identification of a scales separation phenomenon, that effectively "isolates" the microhydrodnamics on the heater surface from the chaotic two-phase flow motions away from it. This separation is effected by a persistent very high void fraction region (like a vapor "blanket"), and it is of immense significance in allowing to focus the physics of a long-standing apparently intractable problem (Theofanous et al., 2002a,b).

We expect that such a separation of scales would be present also in convective boiling, especially in the low flow rates regimes that are of interest in space applications, so the subject is pursued as a key component of the present effort as well. In this report we describe our efforts towards a more precise and detailed characterization as needed to elucidate the key mechanisms for both pool and convective boiling geometries.

The region of interest extends from outside the microlayer, undulating on the heater surface (10s of microns), up to a few millimeters away from it. This requires high spatial resolution in the vertical dimension over the whole horizontal macroscopic dimension needed to reveal the pattern (the whole 2.5 cm x 4 cm surface area of the heater), and obviously the measurement must be non-intrusive. Our previous work demonstrated the value and potential of the X-ray radiography technique for this purpose (Theofanous et al., 2002a,b). The point of departure here is consideration of scattered X-rays, associated improvements to our test section and radiography imaging techniques including positioning, collimating, and film/intensifier choice and development. Further, the work included extensive calibrations, especially using "ghosts" of known and similar (but static) material configurations. Of special importance was the replacement of the glass wall of our test section by pieces made of KAPTON material.

Sample results are shown in Figure 1. The radiographs depict projections over the narrow dimension of the test section (2.6 mm) and the gray scales show local (in 2D, heights—width) void fraction distributions and their variation with heat flux. Ensemble averages can be constructed from such images taken repeatedly. The line diagram shows the results of horizontal averaging of these radiographs --- that is, area averages over horizontal planes as function of their distance from the heater. The high void fraction region is seen to be well established at heat flux levels over ~700 kW/m^2. Closer examination can reveal further details on the internal structures of this important region.

References

1. T.G. Theofanous, T.N. Dinh, J.P. Tu, and A.T. Dinh, The boiling crisis phenomenon. Part I: Nucleation and nucleate boiling heat transfer. *Experimental Thermal Fluid Science* (2002a).
2. T.G. Theofanous, T.N. Dinh, J.P. Tu, and A.T. Dinh, The boiling crisis phenomenon. Part II: Dryout dynamics and burnout. *Experimental Thermal Fluid Science* (2002b).

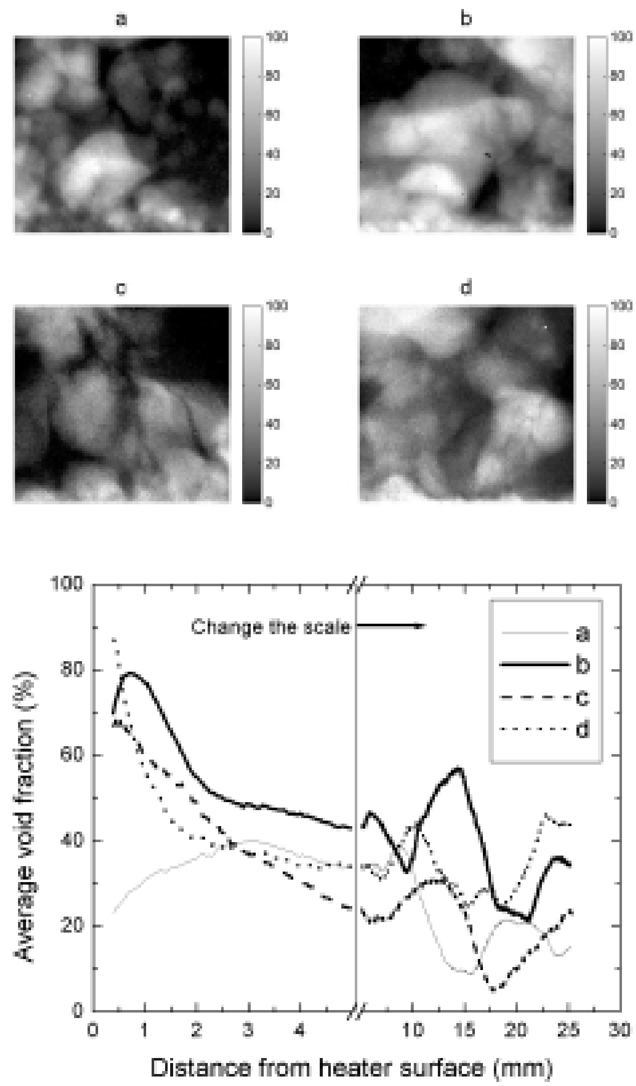

Figure 1. Void fraction distributions in pool boiling as measured by X-ray radiography. (a) 225 kW/m^2, (b) 690 kW/m^2; (c) 1214 kW/m^2; (d) 1656 kW/m^2 (prior to burnout). The bottom figure shows cross-sectional average void fractions.

NUCLEATION ON NANOSCOPICALLY SMOOTH SURFACES

T.G. Theofanous, J.P. Tu, and T.N. Dinh
Center for Risk Studies and Safety
University of California, Santa Barbara
6740 Cortona Drive, Goleta CA 93117
Phone/Fax: (805) 893-4900/4927, theo@crss.ucsb.edu

This is the first progress report on a recently-initiated research project aiming to a basic understanding and prediction of the Boiling Crisis phenomenon in convective boiling. The work is a continuation and extension of a project that addressed coolability limits in pool boiling and was carried out over the previous funding cycle. A key ingredient of our approach is the use of high speed, high resolution infrared imaging in conjunction with nanofilm (in thickness) heaters of macroscopic dimensions to detect the evolution of thermal patterns at the solid-fluid interface. In particular the configuration allows the detection of bubble nucleation events, and it has permitted the first direct determination of bubble nucleation densities in high heat flux boiling (Theofanous et al, 2002a).

This work established a strong connection of the surface nucleation characteristics and it's resistance to burnout (Theofanous et al 2000b), so nucleation is pursued as a key component of the present effort on convective boiling as well. The point of departure is a further finding of this work that nucleation on nanoscopically smooth (±4 nm rms roughness) surfaces is not consistent with the apparently (and firmly) established preexisting cavity nucleation theory (PEN) as propounded by Zeldovich (1943), Dean (1944),and Bankoff (1958), and elaborated more recently by Wang and Dhir (1993). More specifically our work points to surface nanomorphology and chemistry at the origin of heterogeneous nucleation, thus leading us to question whether there is any role left to "roughness" (as conceived in PEN), even for rough, engineering surfaces. Thus, in this nucleation-focus portion of our project, the domain of interest includes all kinds of surfaces, rough and "dirty" ones as found in traditional engineering equipment, as well as ultrasmooth and "clean" ones as found in new micro scale technologies such as cooling of microelectronic equipment, and operation of micro fluidic devices.

In this report we present the results of our first steps in addressing the potential role of ``roughness''. The idea is that this role can be isolated by using nanofilms on preroughened glass substrates. Using precision sandblasting we can create micron-scale roughnesses that resemble those of common engineering surfaces. On the other hand, using metal vapor deposition techniques, we can build films (on these substrates) with chemistries and nanomorphologies precisely similar to those found on our smooth nanofilms of our previous work. All other aspects of the experimental apparatus and diagnostics are also the same. Experiments are conducted either on a pulse-heating mode, where a significant change in heat flux is instantaneously imposed, or in a steady-state mode, where heating is changed by small increments (or decrements).

Sample results are shown on Figures 1 and 2. The gray scales are in degree cemtigrade.

References

1. Bankoff, S.G., Entrapment of gas in the spreading of liquid over a rough surface, AIChE J., 4 (1958) 24-26.
2. Dean, R.B., The formation of bubbles. J.Appl.Phys. 15 (1944) 446-51
3. Theofanous, T.G. , T.N. Dinh, J.P. Tu, and A.T. Dinh, The boiling crisis phenomenon. Part I: Nucleation and nucleate boiling heat transfer. *Experimental Thermal Fluid Science* (2002a).
4. Theofanous, T.G. , T.N. Dinh, J.P. Tu, and A.T. Dinh, The boiling crisis phenomenon. Part II: Dryout dynamics and burnout. *Experimental Thermal Fluid Science* (2002b).
5. Wang, C.H.; Dhir, V.K. On the gas entrapment and nucleation site density during pool boiling of saturated water. ASME Journal of Heat Transfer, vol.115, (3) (1993) 670-9.
6. Zeldovich, Ya.B., On the theory of new phase formation: cavities. Acta Physico. Chim. URSS 18 (1943) 1

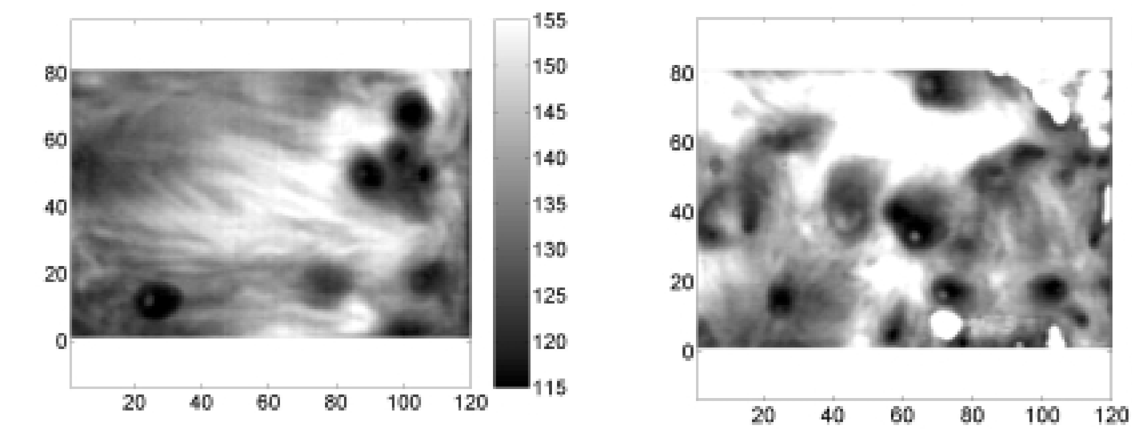

(i) (ii)

Figure 1. IR thermal pattern prior (i) and after (ii) power surge.

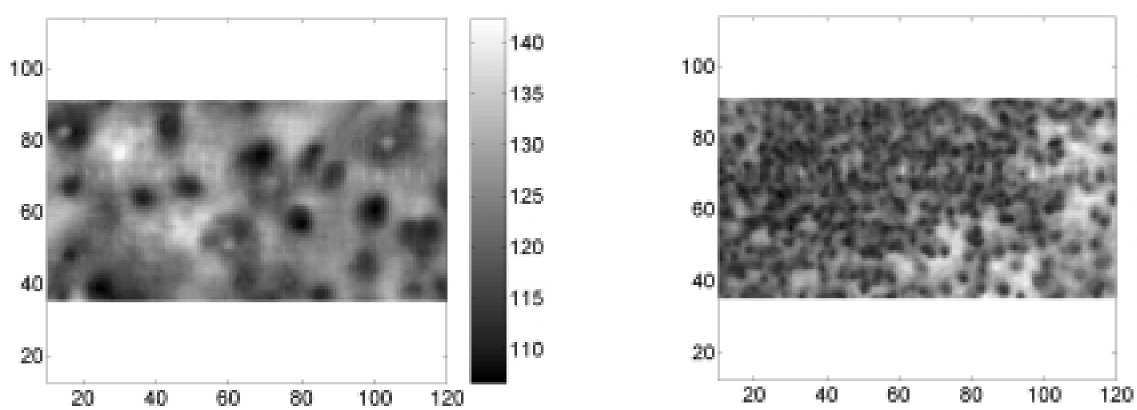

(a) (b)

Figure 2. Infrared thermal imaging of nucleation patterns on,
(a) fresh smooth heater, (b) aged smooth heater at 600 kW/m^2.

ELECTROSTATIC EFFECTS ON DROPLET SUSPENSIONS

Gretar Tryggvason, Arturo Fernandez, and Asghar Esmaeeli
Mechanical Engineering Department
100 Institute Road
Worcester Polytechnic Institute
Worcester, MA 01609-2280
gretar@wpi.edu, Tel.: 508 831-5759, FAX: 508 831-5680

ABSTRACT
Direct numerical simulations are used to examine the effect of electric fields on the behavior of a suspensions of drops in channels. The effect of the electric field is modeled using the "leaky dielectric" model, coupled with the full Navier-Stokes equations. The governing equations are solved using a front-tracking/finite volume technique. The method has been validated by detailed comparison with previous results for the axisymmetric interactions of two drops in Stokes flow.

An extensive set of two-dimensional simulations has allowed us to explore the effect of the conductivity and permittivity ratios in some detail. The interaction of two drops is controlled by two effects. The drops are driven together due to the charge distribution on the surface. Since the net charge of the drops is zero, the drops see each other as dipoles. This dielectrophoretic motion always leads to drops attraction. The second effect is fluid motion driven by tangential stresses at the fluid interface. The fluid motion depends on the relative magnitude of the permittivity and conductivity ratios. When the permittivity ratio is higher than the conductivity ratio, the tangential forces induce flow from the poles of the drops to the equator. If the center of two such drops lies on a line parallel to the electric field, the flow drains from the region between the drops and they attract each other. When the ratios are equal, no tangential motion is induced and the drops attract each other by dielectrophoretic motion. When an electric field is applied to many drops suspended in a channel flow, drops first attract each other pair-wise and some drops move to the wall. If the forces are strong (compared to the fluid shear) the drops can form columns or fibers, spanning the channel and blocking the two-dimensional flow. Electronic "fibration" of suspensions has been observed in a number of systems, including dispersion of milk droplets and red blood cells. If the attractive forces are weak compared to the shear, the columns are immediately broken up. For drops with the permittivity ratio lower than the conductivity ratio, the tangential forces induce flow in the opposite direction (from the equator to the poles of the drops) and if the induced fluid motion is sufficiently strong, the drops repel each other. In two-dimensions, this results in interactions between the drops that are similar to the previous case, except that the attractions take place perpendicular to the electric field. The drops therefore tend to form rows aligned with the flow, or "slugs" where many drops clump together. When the conductivity ratio is much higher than the permittivity ratio, the drops become prolate, expel each other and are spread more uniformly across the channel. Figure 1 shows two frames from one simulation of 36 drops in a channel. The parameters used result in oblate drops and two drops whose centers are on a line parallel to the electric field attract each

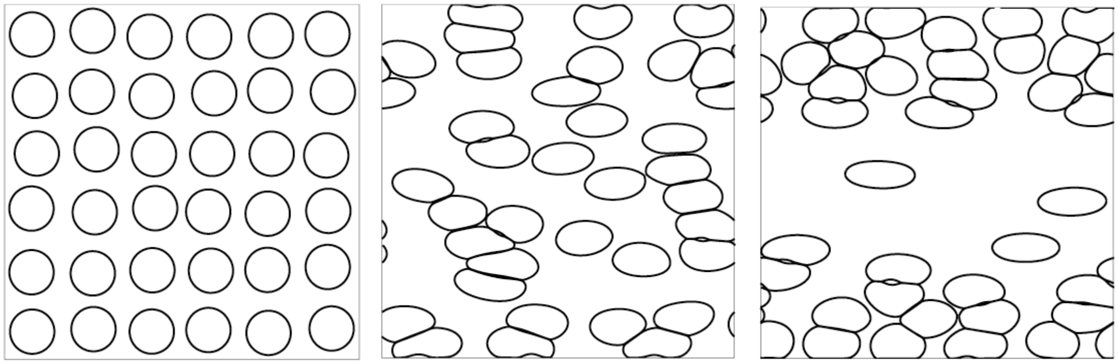

Figure 1. Three frames from a simulation of two-dimensional drops in a channel

other. After the electric field is turned on, the pairwise interactions of drops initially leads to the formation of drop pairs and columns of drops parallel to the field. The drops are also attracted to the walls by the same mechanism that drops are attracted to each other and eventually all the drops migrate to the walls. In this case the drops are not allowed to coalesce, but in reality we would expect the drops to form fluid layers next to the walls.

While the two-dimensional simulations have allowed us to conduct a large number of simulations relatively inexpensively, and explore a large range of conductivity and permittivity ratios, it is clear that fully three-dimensional systems are needed for quantitative predictions. We have developed a fully parallel code to examine three-dimensional systems. Preliminary simulations for oblate drops show that the results are similar to the two-dimensional ones, except that the rate of accumulation at the walls is slower. Large scale computations with many drops, as well as simulations of a wider range of parameters are in progress. Figure 2 show one frame from a simulation of a three-dimensional system. The drops and the electric field is shown after the drops have been deformed by the electric field moved, but before any significant pairwise interaction has taken place.

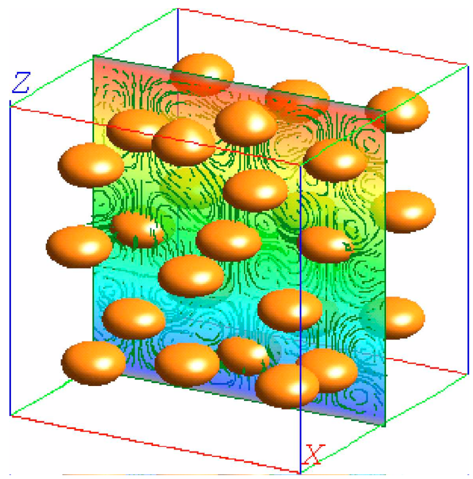

Figure 2. One frame from a three-dimensional simulation.

Our examination of the effect of electric fields on suspensions is still in its early stage and several aspects of the flow remains poorly understood. We have only done a limited number of simulations to examine the effect of the flow, for example. For flows where the drops tend to form fibers across the channel, strong flow (or weaker electric field) breaks up the columns. In some cases this promotes drop accumulation at the walls, but in other case the result is a statistically steady state where drop pairs and short drop chains continuously form and break up.

Characteristics of pool boiling on graphite-copper composite surfaces

Nengli Zhang
Ohio Aerospace Institute, Cleveland, OH 44142
David F. Chao
NASA Glenn Research Center, Cleveland, OH 44135
Wen-Jei Yang
ME Department, The University of Michigan, Ann Arbor, MI 44109

ABSTRACT

Nucleate pool boilng performance of different liquids on graphite-copper composite (Gr-Cu) surfaces has been experimentally studied and modeled. Both highly wetting fluids, such as freon-113 and pentane, and a moderately wetting fluid (water) were tested on the Gr-Cu surfaces with different graphite-fiber volume fractions to reveal the enhancement effects of the composite surfaces on the nucleate pool boiling. Results of the experiments show that the graphite-fiber volume fraction has an optimum value. The Gr-Cu composite surface with 25 percent graphite-fiber volume (ϕ=0.25) has a maximum enhancement effect on the nucleate boiling heat transfer comparing to the pure copper surface. For the highly wetting fluid, the nucleate boiling heat transfer is generally enhanced on the Gr- Cu composite surfaces by 3 to 6 times, as shown in Fig.1. In the low heat flux region, the enhancement is over 6 times, but in the high heat flux region, the enhancement is reduced to about 40%. For the moderately wetting fluid (water), stronger enhancement of nucleate boiling heat transfer is achieved on the composite surface. Figure 2 depicts the experimental results in which one observes the nucleate boiling heat transfer enhancement of 5 to 10 times in the low heat flux region and an enhancement of 3 to 5 times in the high heat flux region.

Photographs of bubble departure during the initial stage of nucleate boiling indicate that the bubbles detached from the composite surface are much smaller in diameter than those detached from the pure copper surface. Typical photographs are presented in Fig. 3. It is seen in Fig.3(a) that the bubbles departed from the composite surface have diameters of only O(0.1) mm, while those departed from the pure copper surface have diameters of O(1) mm, as seen in Fig. 3 (b). It is also found that the bubbles depart from the composite surface at a much higher frequency, thus forming vapor columns, as seen in Fig.3 (a). These two phenomena combined with high thermal conductivity of the graphite fiber are considered the mechanisms for such a significant augmentation in nucleate boiling heat transfer on the composite surfaces.

A physical model is developed to describe the phenomenon of bubble departure from the composite surface: The preferred site of bubble nucleation is the fiber tip because of higher tip temperature than the surrounding copper base and poor wettability of the graphite tip compared with that of the base material (copper). The high evaporation rate near the contact line produces the vapor cutback due to the vapor recoil pushing the three-phase line outwards from the fiber tip, and so a neck of the bubble is formed near the bubble bottom. Evaporation and surface tension accelerate the necking process and finally result in the bubble departure while a new small bubble is formed at the tip when the surface tension pushes the three-phase line back to the tip. The process is

schematically shown in Fig. 4. The proposed model is based on and confirmed by experimental results.

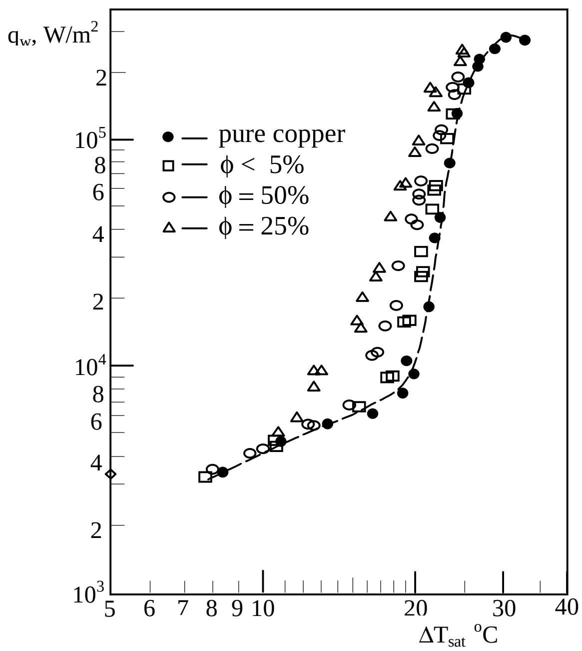

Fig. 1 Experimental data comparison between the Gr-Cu composite surfaces (ϕ < 5%, ϕ=25% and ϕ=25% fiber volume) and the pure copper surface using freon-113.

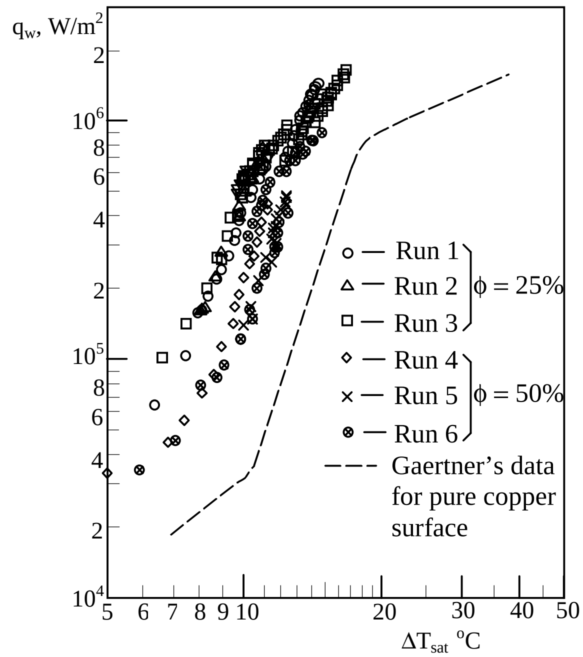

Fig. 2 Experimental data comparison between the Gr-Cu composite surface (25% and 50% fiber volume) and the pure copper surface using water.

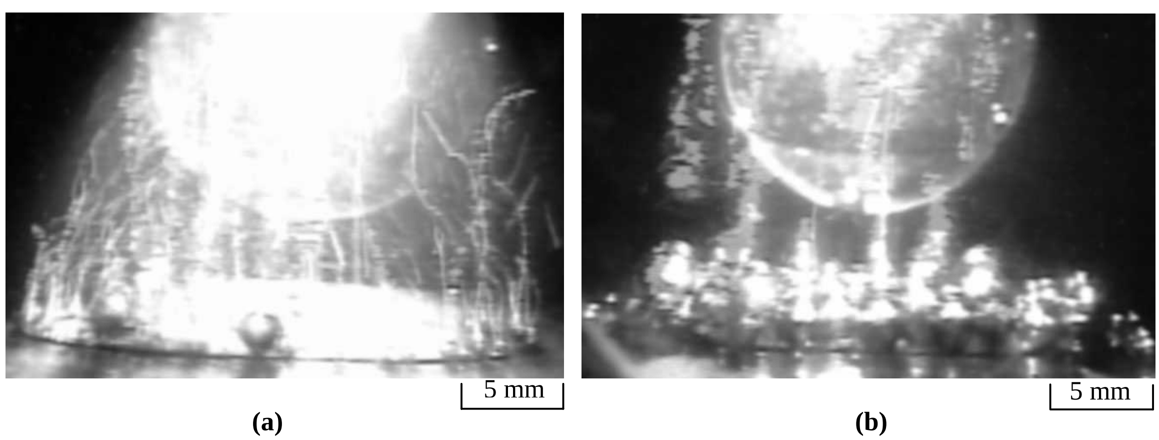

Fig. 3 Photos of water bubble departure during the initial stage of nucleate boiling: (a) on Gr-Cu composite surface (ϕ=0.25); (b) on pure copper surface.

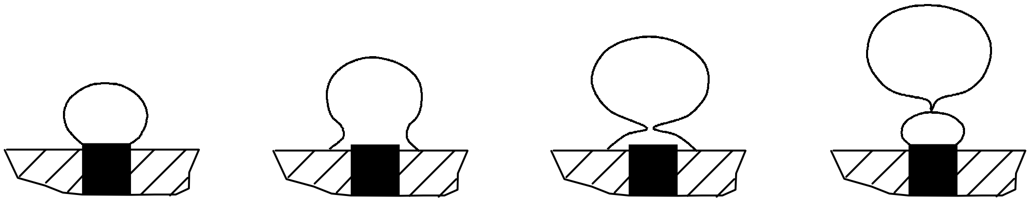

Fig. 4 Bubble necking and departure process.

Exposition Session
Topical Area 5:
Biological Fluid Physics

BLOOD CELL MIGRATION IN PRESSURE-DRIVEN AND ELECTROKINETIC FLOWS

Hsueh-Chia Chang and Paul Takhistov
Department of Chemical Engineering, University of Notre Dame

ABSTRACT

We report our preliminary results on the transverse migration of red blood cells and other particles when they are driven electrokinetically and by pressure-driven flows in micro-channels. The overall objective is to explain the Fahraeus-Lindqvist effect in blood circulation dynamics- blood cells tend to migrate and aggregate at the blood vessel axis and reduce the overall viscous dissipation in the process. At the same hematocrit (blood cell concentration) , blood cell flux at smaller capillaries is higher than in the large ones because of this effect. To avoid blood cell accumulation and depletion, the physiological dynamics maintain the hematocrit for small vessels at a level significantly lower than that in larger ones. However, the migration disappears for capillary radii beyond 250 microns. Hence, hematocrit is uniform within large blood vessels above this cutoff radius. This curious micro-circulation phenomenon has not been satisfactorily explained and is the focus of our research. Once the transverse migration mechanisms for blood cells and other micro-particles are understood, we also intend to exploit the principles to design electrophoretic and flow separation methods for micro-particles, including blood cells.

We drive mouse blood and human blood suspensions in a mm-size capillary and a Hele-Shaw slot with a mm-size gap. They are driven by both a pressure-driven flow applied by a syringe and an electrokinetic flow due to a longitudinal electric field of about 50 V/cm. Significant lateral migration and aggregation are only observed in the former for both concentrated and dilute suspensions. For dilute blood suspensions, the bi-convex doughnut-shaped blood cells form a single file with their axis roughly aligned in the direction of flow. Some precession about this axis is observed in a Hele-Shaw slot. In electrokinetic flow, there is a very thin depleted marginal layer of less than a micron but otherwise no blood cell segregation/migration is observed. Since the electro-osmotic flow field is shear-free away from the Debye layer, we conclude that lateral migration is only possible in the presence of bulk shear.

However, migration is not observed in pressure-driven flow experiments with ion-exchange granules of dimensions similar to blood cells. A preliminary scaling analysis suggests that the migration is only possible with bulk shear, particle deformation and non-spherical geometry. Inertia is ruled out due to the miniscule particle Reynolds number. Without deformation, an ellipsoid is shown to rotate in the vorticity direction but the net lateral hydrodynamic force is zero.

The migration scenario is quite different, however, if an electric field is applied and if the particles are charged. The Maxwell stress can also impart a torque on an asymmetric particle. However, the direction of this torque exerted by the electrokinetic stress depends on the inclination of the ellipsoid whereas that from the bulk hydrodynamic shear depends on the

vorticity of the bulk velocity field. This vorticity changes sign across the capillary axis. Consequently, if electrophoretic motion and hydrodynamic shear are both present, the two torques can balance at a particular equilibrium inclination angle that is not parallel to the flow direction. This angle is also different for different hydrodynamic vorticities. We hence predict a preferred inclination angle for a rigid ellipsoid that is driven electro-phoretically in a pressure-driven flow field. This non-zero angle also implies a net migration even for rigid particles. Preliminary experimental evidence of this new migration mechanism will also be reported. Since blood cells possess significant surface charge, their electrophoretic motion in the presence of a shear flow is quite different from that of a pure pressure-driven flow.

We have also investigated the transport of blood cells by AC dielectrophoresis at hundreds of kilo Hz. A sub-millimeter electrode configuration is designed to produce a non-uniform AC electric field. The blood cells are observed to polarize in the AC field and aggregate along the field lines. They then migrate slowly across the field lines towards regions of low electric fields, as is the case in classical dielectrophoresis. Like all nonlinear electrokinetic phenomena, the dipole formation and the migration are both frequency and particle size dependent. We have exploited these properties to separate large fish blood cells from smaller mouse cells. However, unlike the classical dielectrophoresis, the polarization that occurs in the plasma electrolyte around the blood cell is quite different from that of a dielectric liquid. The high frequency required is expected to be due to the small migration/diffusive time of ions across the blood cell Debye layer. A parallel theory is being pursued to explain this nonlinear AC electrokinetic phenomenon of blood cells. The theory captures the migration of ions within the Debye layer that causes the polarization responsible for aggregation and drift out of the field lines. It extends the classical theories for dielectrophoresis from dielectric liquids to electrolytes.

Total Internal Reflection Tomography (TIRT) for Three-Dimensional Sub-Wavelength Imaging

David G. Fischer
P. Scott Carney

We will present a novel new form of near-field microscopy known as total internal reflection tomography (TIRT), which allows for true three-dimensional sub-wavelength imaging. It is based on recent theoretical advances regarding the fundamental interaction of light with sub-wavelength structures, as well as stable algorithms for the near-field inverse problem. We will discuss its theoretical underpinnings, as well describe current efforts at the NASA Glenn Research Center to implement a TIRT system for biofluid research.

A CRITERION FOR THE DEVELOPMENT OF BIOCONVECTION INSTABILITY IN A SUSPENSION OF GYROTACTIC MOTILE MICROORGANISMS IN A FLUID SATURATED POROUS MEDIUM

A.V. Kuznetsov
Dept. of Mechanical & Aerospace Engineering, North Carolina State University, Raleigh, NC 27695-7910. E-mail: avkuznet@eos.ncsu.edu

A.A. Avramenko
Institute of Engineering Thermophysics, National Academy of Sciences, Kiev, Ukraine

ABSTRACT

In recent years, there has been increased interest in investigating spontaneous pattern formation in suspensions of motile microorganisms. This phenomenon is called bioconvection. Different from solid particles in traditional multiphase flow systems, motile cells are self-propelled. These microorganisms propel themselves by rotating flagella which are driven by reversible molecular motors that are embedded in the cell wall. They tend to swim in a particular direction in response to certain stimuli such as gravity (gravitaxis), light (phototaxis), or chemical gradients (chemotaxis).

This investigation deals with bioconvection in a suspension of gyrotactic motile microorganisms. Gyrotaxes is a behavior typical for algal suspensions. The direction of swimming of gyrotactic microorganisms is determined by the balance of two torques. The first one is the viscous torque that acts on a body placed in a shear flow. The second torque is generated by gravity because the center of mass of a typical microorganism is displaced from its center of buoyancy. The microorganisms considered in this paper are heavier than water and gyrotactic behavior results in their swimming towards the regions of most rapid downflow. Because of that, the regions of downflow become denser than the regions of upflow. Buoyancy increases the upward velocity in the regions of upflow and downward velocity in the regions of downflow, thus enhancing the velocity fluctuations. The formation of almost regular patterns and gyrotactic plumes in algal suspensions has been documented in numerous experimental papers. This instability is similar to the Rayleigh-Benard convection instability but its development does not require the vertical temperature gradient.

Despite the large number of publications on bioconvection in suspensions of gyrotactic microorganisms, very little has been done to address this type of bioconvection in a fluid saturated porous medium. This phenomenon is important because it may occur in nature (bioconvection in a layer of sand at the floor of a body of water that contains gyrotactic microorganisms) and may also have numerous applications. Upswimming of algal cells can be utilized to concentrate the cells, purify cultures, and separate vigorously swimming subpopulations. For these applications, bioconvection is undesirable, because it would prevent up-swimming cells from concentrating near the surface of the culture. To suppress bioconvection, a porous medium (for example, a surgical cotton wool) can be utilized, which must be sufficiently permeable to allow cells to swim through it but also sufficiently tight to damp out

bioconvection. For practical purposes, it is desirable to have the permeability of the porous medium as high as possible. This would insure that the cells can swim through it without cutting their tails off and this will also maximize the flux of the cells in the upward direction. Numerical results suggest that there is a critical value of the permeability of a porous medium. If permeability is smaller than this critical value, bioconvection does not occur and microorganisms simply swim in the upward direction; if it is larger than the critical value, bioconvection instability develops. The purpose of this research is to obtain the exact expression for the critical permeability based on a full three-dimensional stability analysis.

As a result of this investigation, it is established that an infinite uniform dilute suspension of gyrotactic microorganisms in a fluid saturated porous medium is stable if the permeability of the porous medium is sufficiently small. A critical value of the permeability exists and if a porous medium has larger permeability than this critical value, the suspension is unstable. By performing a liner stability analysis, an analytical expression for the critical permeability of a porous medium is obtained. It is established that increasing the cell diffusivity and fluid viscosity increases critical permeability, while increasing the number density of the cells in the basic state, volume of the cell, density difference, gravitational acceleration, and the average swimming velocity of the cells decreases the critical permeability. This critical permeability value is also presented in terms of a critical Darcy number, which depends only on the cell eccentricity, as

$$\left(Da_{1/\gamma}\right)_{crit} = \begin{cases} 1/\left(1-\alpha_0\right) & \text{for } 0 \le \alpha_0 \le 1/3 \\ 8\alpha_0/\left(1+\alpha_0\right)^2 & \text{for } 1/3 \le \alpha_0 \le 1 \end{cases} \tag{1}$$

where α_0 is the cell eccentricity.

STUDY OF FLUID FLOW CONTROL IN PROTEIN CRYSTALLIZATION USING STRONG MAGNETIC FIELDS

Narayanan Ramachandran[1]
Universities Space Research Association, SD 46, NASA MSFC, Huntsville, AL

Fred Leslie and **Ewa Ciszak**
SD 46, NASA MSFC, Huntsville, AL

ABSTRACT
An important component in biotechnology, particularly in the area of protein engineering and rational drug design is the knowledge of the precise three-dimensional molecular structure of proteins. The quality of structural information obtained from X-ray diffraction methods is directly dependent on the degree of perfection of the protein crystals. As a consequence, the growth of high quality macromolecular crystals for diffraction analyses has been the central focus for biochemists, biologists, and bioengineers.

Macromolecular crystals are obtained from solutions that contain the crystallizing species in equilibrium with higher aggregates, ions, precipitants, other possible phases of the protein, foreign particles, the walls of the container, and a likely host of other impurities. By changing transport modes in general, i.e., reduction of convection and sedimentation, as is achieved in “microgravity”, researchers have been able to dramatically affect the movement and distribution of macromolecules in the fluid, and thus their transport, formation of crystal nuclei, and adsorption to the crystal surface. While a limited number of high quality crystals from space flights have been obtained, as the recent National Research Council (NRC) review of the NASA microgravity crystallization program pointed out, the scientific approach and research in crystallization of proteins has been mainly empirical yielding inconclusive results [1].

We postulate that we can reduce convection in ground-based experiments and we can understand the different aspects of convection control through the use of strong magnetic fields and field gradients. Whether this limited convection in a magnetic field will provide the environment for the growth of high quality crystals is still a matter of conjecture that our research will address. The approach exploits the variation of fluid magnetic susceptibility with concentration for this purpose and the convective damping is realized by appropriately positioning the crystal growth cell so that the magnetic susceptibility force counteracts terrestrial gravity.

The general objective is to test the hypothesis of convective control using a strong magnetic field and magnetic field gradient and to understand the nature of the various forces that come into play. Specifically we aim to delineate causative factors and to quantify them through experiments, analysis and numerical modeling. Once the basic understanding is obtained, the study will focus on testing the hypothesis on proteins of pyruvate dehydrogenase complex (PDC),

[1] E-mail address: narayanan.ramachandran@msfc.nasa.gov

proteins E1 and E3. Obtaining high crystal quality of these proteins is of great importance to structural biologists since their structures need to be determined.

Specific goals for the investigation are:

1. To develop an understanding of convection control in diamagnetic fluids with concentration gradients through experimentation and numerical modeling. Specifically solutal buoyancy driven convection due to crystal growth will be considered.
2. To develop predictive measures for successful crystallization in a magnetic field using analyses and numerical modeling for use in future protein crystal growth experiments. This will establish criteria that can be used to estimate the efficacy of magnetic field flow damping on crystallization of candidate proteins.
3. To demonstrate the understanding of convection damping by high magnetic fields to a class of proteins that is of interest and whose structure is as yet not determined.
4. To compare quantitatively, the quality of the grown crystals with and without a magnetic field. X-ray diffraction techniques will be used for the comparative studies.

In a preliminary set of experiments, we studied crystal dissolution effects in a 5 Tesla magnet available at NASA Marshall Space Flight Center (MSFC). Using a Schlieren setup, a 1mm crystal of Alum (Aluminum-Potassium Sulfate) was introduced in a 75% saturated solution and the resulting dissolution plume was observed. The experiment was conducted both in the presence and absence of a magnetic field gradient. The magnet produces a gradient field of ~ 1 $Tesla^2/cm$. Image analysis of the recorded images indicated an enhanced plume velocity that was of the order of the measurement limit. For this experiment, both the gradient and gravity fields are in the same direction resulting in an enhanced effective gravity that tends to accelerate the observed plume velocity. While the results are not conclusive, pending further tests, it clearly points out the inadequacy of the MSFC magnet for conducting protein crystallization experiments and the need for a stronger magnet. In space-based experiments, however, where the gravitational effects are small, only a weak magnetic field will be required to control or mitigate the effects of convective contamination.

The typical magnetic field – field gradient product required to balance thermal buoyancy for a diamagnetic fluid is given as $B\partial B/\partial z \sim 12.5$ $Tesla^2/cm$, where B is the magnetic induction and z is the vertical coordinate. The field gradient product required for countering solutal buoyancy is $B\partial B/\partial z \sim 14$ $Tesla^2/cm$. These fields are realizable in large magnets. We plan to do the first series of experiments to test the flow control hypothesis at the National High Magnet Field Laboratory in Tallahassee, Florida, in Aug. 2002.

1. National Research Council, Space Studies Board, Commission on Physical Sciences, Mathematics and Applications, in Future Biotechnology Research on the International Space Station, national Academy Press, Washington, DC., 2000, 10-16.

SIMULATIONS OF DROP BREAKUP AND DNA DYNAMICS IN FLOW THROUGH ARRAYS OF OBSTACLES

Eric S.G. Shaqfeh
Departments of Chemical and Mechanical Engineering

Prateek Patel, Victor Beck
Department of Chemical Engineering

Stanford University
Stanford, CA 94305-5025

ABSTRACT
The flow through arrays of fixed obstacle beds provides important new methods for creating microstructural dynamics of drops and flexible macromolecules. In the latter instance, new separation techniques for DNA have been suggested based on the mobility change that comes from interactions with obstacles during flow (either electrophoretically driven or hydrodynamically driven motion). Interestingly, the dynamics is so diverse in terms of variation with obstacle concentration, strength of flow driving force, and molecular length, that large-scale simulation can play a very important role in determining where interesting flow parameter regimes are located. In this poster, we will present large-scale simulations of drops and DNA moving through fiber obstacle arrays. We will discuss the breakup mechanisms that are engendered in the former and compare our results to ongoing experiments. In the latter instance we will discuss the efficiency of separation in these arrays and isolate parameter regimes where separation is most efficient.

Two-Photon Fluorescence Correlation Spectroscopy

Gregory A. Zimmerli
David G. Fischer

We will describe a two-photon microscope currently under development at the NASA Glenn Research Center. It is composed of a Coherent Mira 900 tunable, pulsed Titanium:Sapphire laser system, an Olympus Fluoview 300 confocal scanning head, and a Leica DM IRE inverted microscope. It will be used in conjunction with a technique known as fluorescence correlation spectroscopy (FCS) to study intracellular protein dynamics. We will briefly explain the advantages of the two-photon system over a conventional confocal microscope, and provide some preliminary experimental results.

Exposition Session
Topical Area 6:
Dynamics and Instabilities

Effect of Gravity on the Near Field Flow Structure of Helium Jet in Air

Ajay K Agrawal[1] and Ramkumar Parthasarathy
School of Aerospace and Mechanical Engineering, University of Oklahoma

DeVon Griffin
Microgravity Science Division, NASA Glenn Research Center

ABSTRACT

Experiments have shown that a low-density jet injected into a high-density surrounding medium undergoes periodic oscillations in the near field. Although the flow oscillations in these jets at Richardson numbers about unity are attributed to the buoyancy, the direct physical evidence has not been acquired in the experiments. If the instability were indeed caused by buoyancy, the near-field flow structure would undergo drastic changes upon removal of gravity in the microgravity environment. The present study was conducted to investigate this effect by simulating microgravity environment in the 2.2-second drop tower at the NASA Glenn Research Center. The non-intrusive, rainbow schlieren deflectometry technique was used for quantitative measurements of helium concentrations in buoyant and non-buoyant jets.

Results in a steady jet show that the radial growth of the jet shear layer in Earth gravity is hindered by the buoyant acceleration. The jet in microgravity was 30 to 70 percent wider than that in Earth gravity. The microgravity jet showed typical growth of a constant density jet shear layer. In case of a self-excited helium jet in Earth gravity, the flow oscillations continued as the jet flow adjusted to microgravity conditions in the drop tower. The flow oscillations were however not present at the end of the drop when steady microgravity conditions were reached. The oscillations in Earth gravity were confirmed by a dominant frequency of 12.2 Hz at several jet locations as shown by the power spectra in Fig. 1. In microgravity, a similar analysis was performed using 1.1s of data taken at the beginning and towards the end of the drop to distinguish initial transients from steady conditions in microgravity. The results in Fig. 2 show that no flow oscillations were detected at the end of the drop, thereby, providing direct physical evidence that the flow oscillations in the jet were buoyancy induced. Figure 3 depicts temporal evolution of the jet flow at various axial planes using data from a sequence of schlieren images obtained at 1000Hz. Results clearly demonstrate that buoyancy plays a key role on the near field flow structure of low density jets.

In order to investigate the influence of gravity on the near-injector development of the flow, a linear temporal stability analysis and a spatio-temporal stability analysis of a low-density round jet injected into a high-density ambient gas were performed. The flow was assumed to be isothermal and locally parallel; viscous and diffusive effects were ignored. The variables were represented as the sum of the mean value and a normal-mode small disturbance. An ordinary differential equation governing the amplitude of the pressure disturbance was derived. The velocity and density profiles in the shear layer, and the Froude number (signifying the effects of gravity) were the three important parameters in this equation. Together with the boundary conditions, an eigenvalue problem was formulated. The eigenvalue problem was solved for various values of Froude number; the temporal growth rates and the phase velocity of the disturbances were obtained. It was found that the presence of variable density within the shear

[1] 865 Asp Avenue, Room 212, Norman, OK 73019
Email: aagrawal@ou.edu; Phone: (405) 325-1754, fax: (405) 325-1088

layer resulted in an increase in the temporal amplification rate of the disturbances and an increase in the range of unstable frequencies, accompanied by a reduction in the phase velocities of the disturbances. Also, the temporal growth rates of the disturbances were increased as the Froude number was reduced (i.e. gravitational effects increased), indicating the destabilizing role played by gravity. The spatio-temporal stability analysis was performed to determine the nature of the absolute instability of the jet. The roles of the density ratio, Froude number, Schmidt number, and the lateral shift between the density and velocity profiles on the absolute instability of the jet were determined. The results show that the combination of these variables determines how absolutely unstable the jet will be.

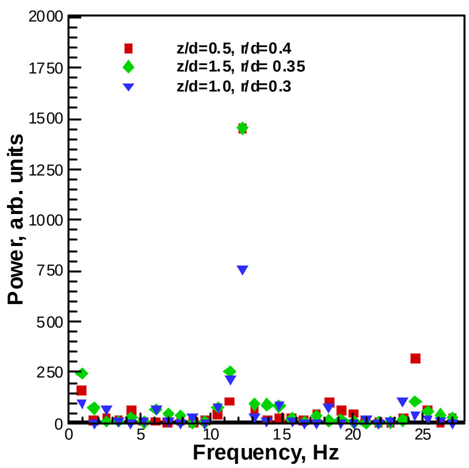

Figure 1. Frequency Power Spectra of an Oscillating Jet in Earth Gravity.

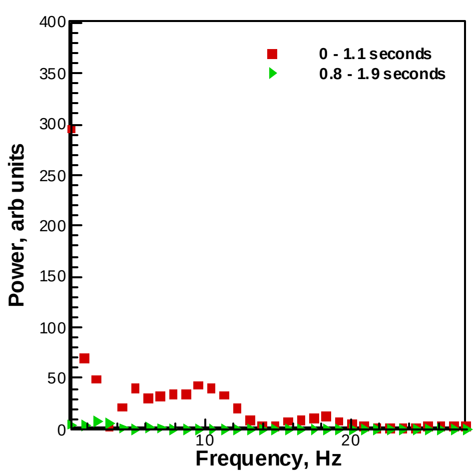

Figure 2. Frequency Power Spectra for two Microgravity Periods at z/d=1.0, r/d=0.6.

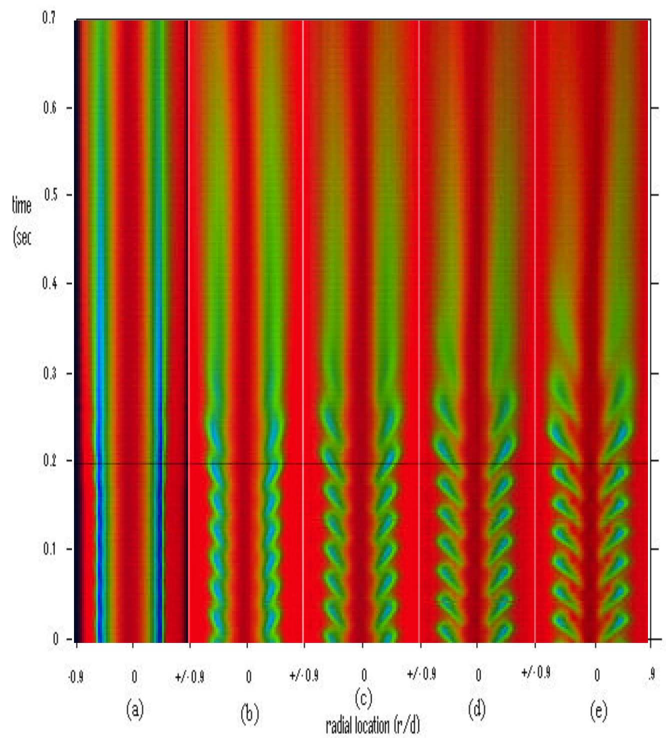

Figure 3. Temporal Evolution of Helium Jet in Microgravity for z/d=0.0, 0.5, 1.0, 1.5, and 2.5 (from left to right). The package is released at time t = 0.2s, as indicated by thin black line.

THERMAL IMAGING OF CONVECTING OPAQUE FLUIDS USING ULTRASOUND

Hongzhou Xu, Sean Fife, and C. David Andereck*

Department of Physics, The Ohio State University
174 W. 18th Ave., Columbus, OH 43210
*andereck.1@osu.edu, phone: (614) 292-2360, FAX: (614) 292-7557

ABSTRACT

An ultrasound technique has been developed to non-intrusively image temperature fields in small-scale systems of opaque fluids undergoing convection. Fluids such as molten metals, semiconductors, and polymers are central to many industrial processes, and are often found in situations where natural convection occurs, or where thermal gradients are otherwise important. However, typical thermal and velocimetric diagnostic techniques rely upon transparency of the fluid and container, or require the addition of seed particles, or require mounting probes inside the fluid, all of which either fail altogether in opaque fluids, or necessitate significant invasion of the flow and/or modification of the walls of the container to allow access to the fluid. The idea behind our work is to use the temperature dependence of sound velocity, and the ease of propagation of ultrasound through fluids and solids, to probe the thermal fields of convecting opaque fluids non-intrusively and without the use of seed particles. The technique involves the timing of the return echoes from ultrasound pulses, a variation on an approach used previously in large-scale systems.[1,2]

We initially validated our method by comparing ultrasound measurements with simultaneous visualization using thermochromic liquid crystals suspended in glycerol in a transparent convection cell. As a next step we assembled a linear array of Panametrics M110 ultrasound transducers and calibrated it using the experimentally determined temperature variation of sound speed in mercury. We then used this array to measure temperature profiles in a narrow (2 cm) and shallow (1.3 cm) stainless steel Rayleigh-Bénard convection cell filled with mercury. Figure 1 shows typical data. In this case the array of transducers was aligned with the long dimension of the chamber, and located at mid-height. The data output yields a temperature profile along the chamber, perpendicular to the imposed temperature gradient. The profile clearly reveals the formation of cells driven by natural convection as the temperature difference between the bottom and top plates was slowly increased from 0 to 1.0 ºC, the final temperature corresponding to a Rayleigh number (Ra) of 7550.

Figure 2 is a 2D image of the thermal field in convecting mercury for an imposed vertical temperature difference of 5.8 ºC (Ra = 43790). This image was obtained by translating one Panametrics V129, under computer control, from location to location across the outside of the chamber. The flow consists of four convection rolls. The warmer, rising plumes are in the middle and at either end, while the cooler, falling plumes are in between.

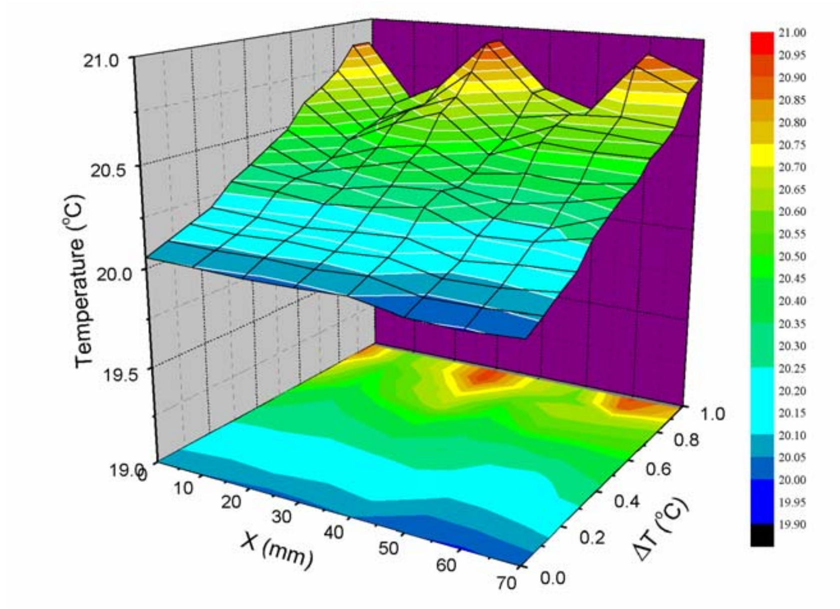

Fig. 1. Temperature profile evolution of Rayleigh-Bénard convection in mercury.

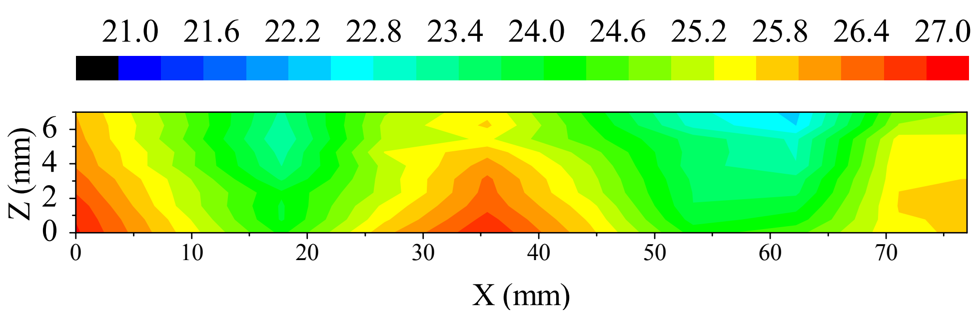

Fig. 2. 2D thermal image of convection in mercury.

Details of our technique, including its limitations and future prospects, will be presented.

This work was supported by NASA Microgravity Fluid Physics Program grant NAG 3-2138.

REFERENCES

[1] Green, S. F., An Acoustic Technique for Rapid Temperature Distribution Measurement, *J. Acoust. Soc. Am.* 77, 759-763 (1985).

[2] Bramanti, M., Salerno, E. A., Tonazzini, A., Pasini, S. and Gray, A., An Acoustic Pyrometer System for Tomographic Thermal Imaging in Power Plant Boilers, *IEEE Trans. Instr. Meas.* 45, 159-167 (1996).

TRANSIENT MIXING DRIVEN BY BUOYANCY FLOWS

W.M.B. Duval
NASA Glenn Research Center, Cleveland, Ohio 44135
Email:Walter.M.Duval@grc.nasa.gov, tel 216-433-5023, fax 216-433-5033
C. Batur[+], H. Zhong
University of Akron, Dept. of Mech. Eng., Akron, Ohio 44325

Mixing driven by buoyancy-induced flows is of particular interest to microgravity processes, as the body force that governs the intensity of flow fields can be directly controlled. We consider a model experimental system to explore the dynamics of mixing which employs two miscible liquids inside a cavity separated initially by a divider. The two liquids are oriented vertically inside a rectangular cavity with constant width and height, and varying depths to approach a cubical configuration. The two miscible liquids can be sufficiently diluted and died, for example water and deuterium oxide, such that a distinct interface exists across the divider. The transient mixing characteristic of the two fluids is addressed by following the Lagrangian history of the interface for various aspect ratios in the z-plane (depth variation) as well as a range of pulling velocities of the divider.

The mixing characteristic of the two fluids is quantified from measurement of the length stretch of the interface using image processing techniques. Scaling analysis shows that the length stretch depends on four governing parameters, namely the Grashof number (Gr), Schmidt number (Sc), aspect ratio (Ar), and Reynolds number (Re). We fix the Grashof number as well as the Schmidt number. Thus our problem reduces to a co-dimension two bifurcation in parametric space for Ar and Re.

Our experimental results show that for Gr on the order of 10^6 and a nominal cavity aspect ratio Ar=0.2, the net effect of removal of the divider and the overwhelming buoyancy force causes an overturning motion which stretches and fold the interface to produce an internal breakwave. The structure of the breakwave is similar to the ubiquitous Rayleigh-Taylor instability morphology. The breakwave is dissipated either through internal or wall collision depending on the impulsive velocity of the divider as prescribed by the Reynolds number. The decay of the collision event occurs through sloshing oscillations over a short time scale. The two fluids then become stably stratified with a diffusive band at the interface indicating mass transport.

The local bifurcation of the internal breakwave is investigated as a function of aspect ratio. Results show that for narrow cavities on the order of 2mm (Ar=0.04), folding does not occur the interface only stretches. As the cavity size increases folding occurs through a supercritical bifurcation. Insight into the mechanism of folding is obtained from measurement of the flow field using Particle Imaging Velocimetry. These results show that in the neighborhood of the folding event, there exists hyperbolic points in the flow caused by multiple vortex interactions. The global stretch of the interface as a function of time is nearly Gaussian; calculations of finite-time Lyapunov exponents as well as construction of horseshoe maps indicate the likelihood of a chaotic transient.

Geophysical flows in spherical geometry from electric fields and near-critical fluids

John Hegseth, Arun Roy, and Ana Oprisan
Department of Physics, University of New Orleans
New Orleans, LA 70148 USA
Telephone: 504-280-6706, FAX: 504-280-6048, E-mail: jhegseth@uno.edu

ABSTRACT

The use of near-critical fluids allows important parameters (e.g., compressibility of supercritical fluids, density of gas and liquid phases, surface tension) to be easily varied by using small changes in temperature. These highly variable properties of near-critical fluids makes it possible to study interesting phenomena when external forces are applied to the fluid. In particular, I plan to study geophysical flows in a spherical capacitor. The spherical capacitor will exert a central polar (di-electrophoretic) force on a supercritical fluid. This creates a central body force on the hyper-compressible fluid with a resultant radial density gradient. Large-scale geophysical flows, analogous to a planetary liquid core, a planetary ocean or atmosphere, etc., could be studied when a Coriolis force is also applied in a rotating frame of reference. In this presentation, I will show experimental results in support of this goal.

In spherical geometry, such as concentric spheres with dielectric fluid between them (a spherical capacitor), an electric field gradient produces a central body force that is similar to the gravitational field of a planet. By using an AC electric field this force is retained and the extraneous effects of free charges are eliminated. Variations in the dielectric constant produce a buoyancy force in the presence of this polarization force, just as variations in mass density produce a buoyancy force in the presence of gravity. We have found, with a sufficiently small capacitor, that this dielectric buoyancy is effective to produce instability near the center electrode in incompressible fluids, on Earth. I will present results of our experiments in this small spherical capacitor that systematically studies this instability when the center sphere is heated. Specifically, we have found upward traveling toroidal or spiral rolls that form along the inner sphere when ΔT (the temperature difference between the spheres) and ΔV (the voltage difference between the spheres) are sufficiently high. These rolls start near the center sphere's equator and travel vertically upward. The onset of this instability depends on both ΔT and ΔV, and these two quantities appear to be related, within the parameter range accessible to our experimental system, by a power law. Measurements of the heat transfer show that these traveling rolls also significantly increase the heat transfer at onset.

In a *compressible* dielectric (near-critical) fluid, the central polarization force present in a spherical capacitor will lead to a density gradient in a manner similar to a compressible fluid in a gravitational field. I have performed experiments on parabolic flights using NASA's KC135A aircraft in a spherical capacitor filled with near-critical fluid. Our attempts to induce a spherical density gradient showed that the 20 seconds of low gravity was insufficient time. The horizontal density gradient from normal gravity never disappears. We did see, however, appreciable density changes in the capacitor in a fluid near the critical point when the field was applied. Our current effort is directed at placing this system in a rotating frame of reference in preparation for a space experiment including: shadowgraph visualization optics appropriate for a rotating frame, precision temperature control using thermoelectric heat pumps, control and data acquisition in a rotating frame.

Because near-critical fluids are full of novelty when they are driven far-from-equilibrium, it is important to understand near-critical fluid convection so that we can have a reasonable understanding of how such a fluid will respond in the rotating spherical capacitor (RoSCA). To this end we are studying a compressible near-critical fluid in a Rayleigh-Bénard cell (flat fluid layer heated from below). One such novelty that we have discovered is a Rayleigh-Taylor instability, when the top plate is held below the critical temperature in the two-phase regime. A hexagonal droplet pattern forms on the wetted top plate when the bottom is heated. Because the liquid-gas density difference and surface tension become zero as the critical temperature is approached, this is an ideal system to see the effect of thermal fluctuations on pattern formation. By controlling the ambient temperature, the size and periodicity of the droplet pattern is also controlled. As the surface tension gets very small near the critical point the droplets also become very small and randomly positioned (as opposed to the hexagonal pattern). The thin wetting layer is stabilized by the Van der Waal's force from top sapphire plate and the small liquid-gas density difference. On approaching the critical temperature, these droplets decrease in size as the density fluctuations increase in size. Near the critical point, when the forming droplets and the density fluctuations are of the same order of size, we have observed droplets forming in the presence of thermal fluctuations. It appears that the droplets begin to form a pattern that is highly perturbed by fluctuations.

Another novel effect in near critical fluids, that is important for the RoSCA, is the effect of an electric field on the critical temperature. Different theories predict upward or downward shifts in the critical temperature when an electric field is applied. Some experiments have reported a downward shift in the critical temperature for polymers and binary mixtures. These previous experiments have also been criticized for not controlling heating effects and ignoring pressure/density from an external mass reservoir. We have performed an experiment that has avoided these difficulties and I believe resolved this controversy. Using a spherical capacitor of similar dimensions of the RoSCA with near critical fluid between the inner and outer sphere, we have applied an AC field that avoids joule heating. These experiments are performed in a ground-based environment so that a gravitationally induced density gradient assures a small layer of critical fluid somewhere in the capacitor that the light must pass through. In this cell I have found an upward shift in the critical temperature that depends on the electric field, as predicted separately by Landau and Onuki. This shift is repeatable and is found by measuring the average turbidity through the vertical density gradient (monochromatic beam axis is vertical) while slowly ramping the temperature downward through the critical temperature. By measuring the light intensity of a beam that travels through the fluid and varying the ramping rate and voltage, we found a repeatable upward shift of the critical temperature as a function of the applied electric field.

SONOLUMINESCENCE IN SPACE: THE CRITICAL ROLE OF BUOYANCY IN STABILITY AND EMISSION MECHANISMS

Charles R. Thomas (crt@bu.edu) ,R. Glynn Holt (rgholt@bu.edu) and Ronald A. Roy (ronroy@bu.edu), Boston University, Dept. of Aerospace and Mechanical Engineering, 110 Cummington St, Boston, MA 02215

INTRODUCTION AND MOTIVATION

Sonoluminescence is the term used to describe the emission of light from a violently collapsing bubble. Sonoluminescence ("light from sound") is the result of extremely nonlinear pulsations of gas/vapor bubbles in liquids when subject to sufficiently high amplitude acoustic pressures. In a single collapse, a bubble's volume can be compressed more than a thousand-fold in the span of less than a microsecond. Even the simplest consideration of the thermodynamics yields pressures on the order of 10,000 ATM. and temperatures of at least 10,000K. On the face of things, it is not surprising that light should be emitted from such an extreme process. Since 1990 (the year that Gaitan discovered light from a single bubble) there has been a tremendous amount of experimental and theoretical research in stable, single-bubble sonoluminescence (SBSL), yet there remain at least four unexplained phenomena associated with SBSL in 1g:

- *the light emission mechanism itself,*
- *the existence of anisotropies in the emitted light,*
- *the disappearance of the bubble at some critical acoustic pressure, and*
- *the appearance of quasiperiodic and chaotic oscillations in the flash timing.*

Gravity, in the context of the buoyant force, is implicated in all four of these.

We are developing KC-135 experiments probing the effect of gravity on single bubble sonoluminescence. By determining the stability boundaries experimentally in microgravity, and measuring not only light emission but mechanical bubble response, we will be able to directly test the predictions of existing theories. By exploiting the microgravity environment we will gain new knowledge impossible to obtain in earth-based labs that will enable explanations for the above problems. We will also be in a position to make new discoveries about light-emitting bubbles.

OBJECTIVES

The objectives of the investigation are:

(1) To develop an experimental apparatus to fly on the KC-135 that will monitor cabin pressure, water temperature, bubble position and size, acceleration, emitted light intensity, and acoustic pressure.

(2) To model the hydrodynamic effects of acceleration on bubble dynamics and SBSL in realistic acoustic resonators. The primary Bjerknes force, buoyancy, ambient pressure, drag, mass diffusion, shape stability and (empirically) light emission will be accounted for in the model.

(3) To measure (as a function of acceleration during parabolic flight) a bubble's position, equilibrium radius, maximum radius, oscillatory radius, and spatially and temporally resolved light emission. This will be done for a range of dissolved gas concentrations in order to compare with predictions of our hydrodynamic model.

(4) To measure (as a function of acceleration during parabolic flight) the precise values of acoustic pressure and equilibrium radius that leads to the extinction of a light-emitting bubble, a phenomenon which occurs at a well defined critical acoustic pressure in 1g experiments. This will test theories that postulate either a nonlinear levitation instability, or a Rayleigh-Taylor instability mechanism for the bubble disappearance.

RESULTS

We have completed 3 KC-135 flight campaigns. We attempted to test the prediction of our model [1] that hydrodynamics alone dictate a 5 – 35 % change in SBSL intensity, (depending approximately linearly on the dissolved gas concentration) for the 10^{-4}g to 1.8g swing typical of a K-135 parabolic maneuver. The driving mechanism for this effect is the small change in head pressure experienced by the bubble when the acceleration changes. Figure 1 shows the measured bubble dynamics during a single parabola. The main result [2] is that for nearly 0g, the bubble grows and emits more light, while at 2g the bubble shrinks and emits less light. The results are in rough agreement with our model.

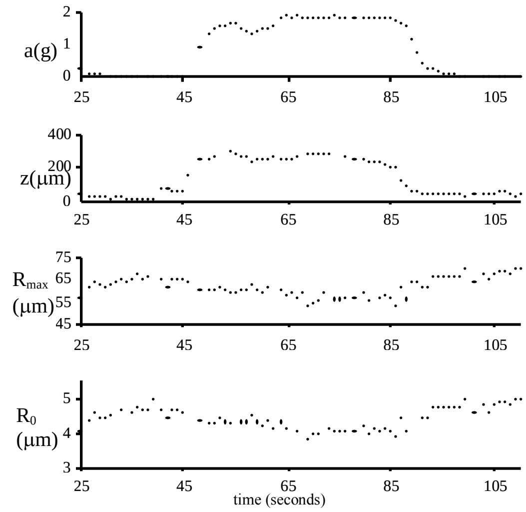

Figure 1. Measured (R_0 inferred) bubble dynamics during KC-135 parabolic maneuver.

We have completely overhauled the data acquisition system to make better use of available computer resources. We have installed a joystick-controlled three axis positioning system, using this system we can better position the cell and track its motion. We have completely replaced the light intensity detection system, including fabrication of a NIM-BIN style gated peak detector. Finally we have divided the apparatus into two equipment racks to facilitate transporting the experiment.

MICROGRAVITY RELEVANCE

SBSL bubbles experience a time-varying buoyancy (quantified by the oscillatory volume ratio V_{max}/V_0, see Fig. 2) which reaches maximal excursions precisely where sonoluminescence is observed. This results in a strong nonlinear coupling between volume and translatory motions. Removing the acceleration of gravity from the system will eliminate buoyancy-driven translatory oscillations of the bubble. This would be a decisive test of light emission mechanisms, and will also shed light on the chemical reaction theory of mass flux for volume stability as well as the resonance-controlled shape oscillation instability. Thus, a microgravity environment will change the geography of the parameter space, and the only hope for a clear understanding of the SBSL phenomenon is to perform experiments which locate light emission within the context of the instability boundaries that exist in the parameter space.

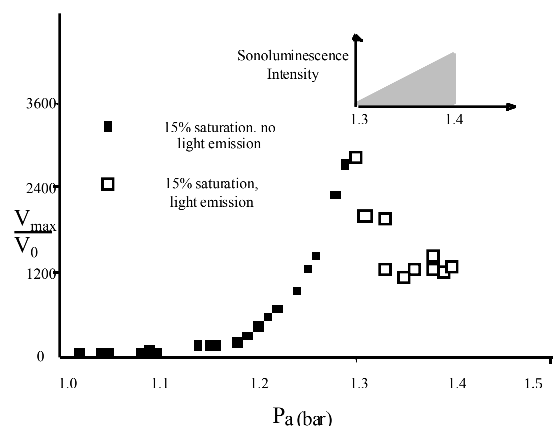

Figure 2. The measured (1g) ratio of V_{max} / V_0 during 1 acoustic cycle as a function of acoustic

REFERENCES

[1] Holt, RG, RA Roy and SC Wyatt, J. Acoust. Soc. Am. 105, No. 2, Pt. 2, p. 960. (Joint EAA/ASA/DAGA meeting, Berlin, 1999)

[2] Thomas, CR, SC Wyatt, RA Roy, R. Glynn Holt, J. Acoust. Soc. Am. 108, No. 5, Pt. 2, p. 2493. (ASA Meeting, Newport Beach, California)

THEORY OF MICRO- AND MACRO- ENCAPSULATION

S.P. Lin and J.N. Chen
Department of Mechanical and Aeronautical Engineering,
Clarkson University, Potsdam, NY 13676-5725
Tel: 315-2686584 Fax: 315-2686438
Email: gw02@clarkson.edu

THEORY OF MACRO- AND MICRO- ENCAPSULATION

Macro-capsules are defined to be the capsules whose radii are larger than 100 μm. Micro capsules have radii between 100 μm and 10 μm. Continuum theory is valid for the investigation of macro-capsule and micro-capsules formation is expected to be valid up to the lower range of micro-encapsulation.

Consider the flow in an annular liquid jet of a constant thickness h, a constant inner radius R_i, and a constant outer radius R_0. The jet with density ρ and viscosity μ emanates from an annular nozzle which is coaxial with a circular cylinder of radius R_w. The fluid inside the annular jet has density ρ_i and μ_i. The jet is surrounded by another fluid of density ρ_0 and viscosity μ_0. All three fluids are Newtonian. The governing equations are the Navier-Stokes equations. The corresponding boundary conditions are the dynamic and kinematic boundary conditions at each fluid-fluid interface. And the no-slip conditions at the pipe wall. An exact solution for a steady basic flow which satisfies the governing differential system has been obtained [15]. The relevant flow parameters are: Weber number of the inner interface $We_i = \rho_i U^2 h / S_i$, Weber number of the inner interface $We_0 = \rho_0 U^2 h / S_0$, Reynolds number $\rho U^2 h / \mu$, Froude number $Fr = U^2 / gh$, viscosity ratios $N_i = \mu_i / \mu$, $N_0 = \mu_0 / \mu$, density ratios $Q_i = \rho_i / \rho$, $Q_0 = \rho_0 / \rho$, and radius ratios $r_i = R_i / h$, $r_0 = R_0 / h$, where S_i and S_0 are respectively the surface tension of the inner and the outer interface and U is the liquid jet velocity at $R = (R_i + R_0)/2$, R being the radial distance measured from the axis of the annular. The curve for $Fr^{-1} = 0$ in this figure corresponds to 0-g condition. The other curves correspond to the case of finite gravity.

The onset of instability of this basic flow with respect to temporal and spatial-temporal disturbances has been analyzed by use of a spectra collocation method. Extension of the well tested analytical and numerical method to the present problems is straightforward, but results in a relatively larger system for numerical computation which required a high precision. Extraction of information from the numerical results also becomes more laborious because of the larger number of flow parameters involved. The results we have obtained show that [1] there are two independent interfacial modes of convective instability. Two independent modes of instability were also found in the earlier work for a two dimensional plan liquid sheet as well as an annular jet in an invisid gas, i.e., sinuous and varicose modes [16, 17, 18]. Two interfaces move in phase in the sinuous mode but they move 180^o out of phase in the varicose mode. However unlike the plan sheet, there is no surface of symmetry within the annulus, and consequently a completely in-phase or out-of-phase interfacial motion does not exit. Nevertheless the two independent modes of the interfacial motion are actually almost in phase or out of phase. They are call here para-sinuous and para-varicose modes. The emergence of either one of these modes or both of them depends on the initial condition at the nozzle exit. This fact has an important practical implication in encapsulation applications. The onset of para-varicose mode needs to be suppressed, since it leads to breakup at the thinnest of the annulus and leaves part of the core material unencapsulated as depicted in Fig. 1. On the other hand the onset of para-sinuous mode should be promoted, since it leads to a uniform shell thickness as is also depicted in the same figure. This fact has not been made aware of in the know literature. Fig. 1 also shows the spatial exponential amplification rate k_i as functions of the wave length $\lambda = 2\pi hh/k_r$, k_r being the wave number, for two values of Fr and the rest of parameters specified in the caption. Note that the amplification curves for the two modes for the case of finite g corresponding to $Fr^{-1} = 10000$ intersect at point e. Below the wave number corresponding to point e the para-sinuous mode dominates. Above this wave number the para-varicose mode dominates. Hence if one attempts to produce macro capsules by introducing an external forcing with frequency corresponding to k_r for which the sinuous mode is unstable one will not be able to completely encapsulate the core material, because the para-varicose mode is also present. The same figure also shows that when the finite gravity is reduced to zero, the amplification curves (solid line) for the two modes cease to intersect and the para-varicose mode is absent between the two cutoff wave number f *and* f'. The para-sinuous and para-varicose modes are stable respectively if the wave numbers are larger than that at point f and f' in Fig. 1. Thus in the wave number range between f and f', one may impart a monocramatic external forcing of a frequency corresponding to the selected wave number, and excite a sinuous wave to initiate production of a capsule of desired radius.

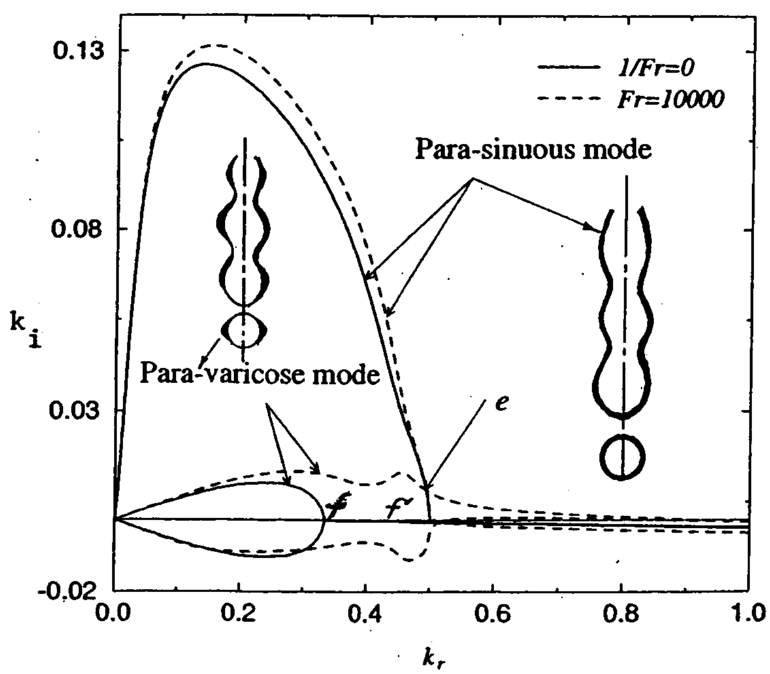

Figure 1. The effects of Froude number on the disturbance growth rate for both modes. Re=1000, We_i=We_o=20.0, Q_i=Q_o=0.0013, N_i=N_o=0.0018, r_i=r_w=13.

Enhancing the Thermocapillary Migration of Bubbles Retarded by the Adsorption of Surfactant Impurities By Using Remobilizing Surfactants

Charles Maldarelli
Levich Institute
Department of Chemical Engineering
City College of New York
Charles@chemail.engr.ccny.cuny.edu
(212)6508160

R. Balasubramanian
National Center for Microgravity Research
NASA Glenn Research Center

Abstract

Thermocapillary migration is a method for moving bubbles in space in the absence of buoyancy. A temperature gradient is applied to the continuous phase in which a bubble is situated, and the applied gradient impressed on the bubble surface causes one pole of the drop to be cooler than the opposite pole. As the surface tension is a decreasing function of temperature, the cooler pole pulls at the warmer pole, creating a flow which propels the bubble in the direction of the warmer fluid. A major impediment to the practical use of thermocapillarity to direct the movement of bubbles in space is the fact that surfactant impurities which are unavoidably present in the continuous phase can significantly reduce the migration velocity. A surfactant impurity adsorbed onto the bubble interface is swept to the trailing end of the bubble. When bulk concentrations are low (which is the case with an impurity), diffusion of surfactant to the front end is slow relative to convection, and surfactant collects at the back end of the bubble. Collection at the back lowers the surface tension relative to the front end setting up a reverse tension gradient. (This can also be the case if kinetic desorption of surfactant at the back end of the bubble is much slower than convection.) For buoyancy driven bubble motions in the absence of a thermocapillarity, the tension gradient opposes the surface flow, and reduces the surface and terminal velocities (the interface becomes more solid-like and bubbles translate as solid particles). When thermocapillary forces are present, the reverse tension gradient set up by the surfactant accumulation reduces the temperature induced tension gradient, and can decrease to near zero the bubble's thermocapillary velocity.

The objective of our research is to develop a method for enhancing the thermocapillary migration of bubbles which have been retarded by the adsorption onto the bubble surface of a surfactant impurity. Our remobilization theory proposes to use surfactant molecules which kinetically rapidly exchange between the bulk and the surface and are at high bulk concentrations. Because the remobilizing surfactant is present at much higher concentrations than the impurity, it adsorbs to the bubble surface much faster than the impurity when the bubble is formed, and thereby prevents the impurity from adsorbing onto the surface. In addition the rapid kinetic exchange and high bulk concentration maintain a saturated surface with a uniform surface concentrations. This prevents retarding surface tension gradients and keeps the thermocapillary velocity high.

In this report, we detail experimental observations of remobilization for the buoyancy driven motion of air bubbles in a glycerol/water mixture.. Two polyethylene oxide surfactants were studied, $C_{12}E_6$ ($CH_3(CH_2)_{11}(OCH_2CH_2)_6OH$) and $C_{10}E_8$ ($CH_3(CH_2)_9(OCH_2CH_2)_8OH$). Measurements of the kinetic exchange for these surfactants show that the one with the longer hydrophobe chain $C_{12}E_6$ has a lower rate of kinetic exchange. In addition, this surfactant is much less soluble in the glycerol/water mixture because of the shorter ethoxylate chain. As a result, we found that $C_{12}E_6$ had no ability to remobilize rising bubbles because of the limited kinetic exchange and reduced solubility (Fig. 1). However, $C_{10}E_8$, with its higher solubility and more rapid exchange was found to dramatically remobilize rising bubbles (Fig. 2).

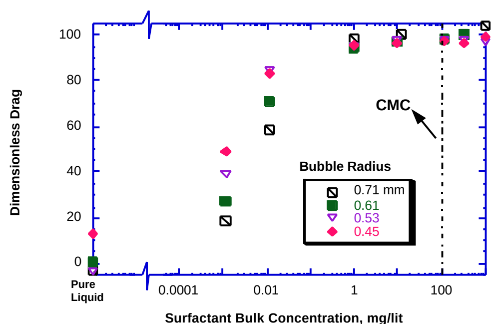

Figure 1: Effect of Addition of $C_{12}E_6$ on the Drag of a Bubble Rising in a 7:3 Glycerol/Water Mixture.

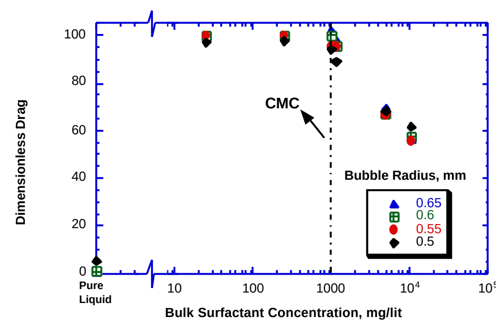

Figure 2: Effect of Addition of $C_{10}E_8$ on the Drag of a Bubble Rising in a 7:3 Glycerol/Water Mixture.

We also report results on describing theoretically the remobilization observed in our ground based buoyancy driven experiments. We construct a model in which a bubble rises steadily by buoyancy in a continuous (Newtonian) viscous fluid containing surfactant with a uniform far field bulk concentration. We account for the effects of inertia as well as viscosity in the flow in the continuous phase caused by the bubble motion (order one Reynolds number), and we assume that the bubble shape remains spherical (viscous and inertial pressure forces are smaller than capillary forces, i.e. small Weber and capillary numbers). The surfactant tension gradients which retard the surface velocity are incorporated by equating the viscous shear stress at the bubble surface to the surface tension gradient created by the surfactant surface concentration distribution. This distribution is calculated by solving the mass transfer equations including convection and diffusion in the bulk, and finite kinetic exchange between the bulk and the surface. Convective effects dominate diffusive mass transfer in the bulk of the liquid (high Peclet numbers) except in a thin boundary layer near the surface. A finite volume method is used to numerically solve the hydrodynamic and mass transfer equations on a staggered grid which accounts specifically for the thin boundary layer. We present the results of the nondimensional drag as a function of the bulk concentration of surfactant for different rates of kinetic exchange, and we compare our theoretical calculations to the experimental measurements of velocity for both the non-remobilizing and remobilizing surfactants, and found excellent agreement.

RIVULET DYNAMICS WITH VARIABLE GRAVITY AND WIND SHEAR

S. Wang, G. McAlister, J.S. Marshall, R. Ettema
IIHR – Hydroscience and Engineering, University of Iowa, Iowa City, IA 52242
jeffrey-marshall@uiowa.edu, FAX (319) 335-5669, phone (319) 335-5817

ABSTRACT

A combined computational and experimental study is conducted of the development of rivulets from a liquid sheet driven by wind shear in different gravitational states. The study concentrates on the effect of the normal component of gravity on rivulet formation and evolution. Understanding of rivulet development in the presence of wind shear is important for a number of coating processes, for modeling development of ice rivulets on aircraft wings and of water motion on vehicle windshields, and for modeling the breakup of annular flow in a tube into a rivulet flow regime. The current study is at the midway point of a four-year project.

The experimental part of the project has focused on the dynamics of gravity- and wind-driven rivulets. The experimental setup comprises a small "rivulet windtunnel", which consists of a flat plate into which a liquid is injected at an upstream location, and through which air flow passes. The entire setup is mounted on a mobile cart that can be tilted to angles varying from 0^o to 90^o. Preliminary experiments revealed significant differences in rivulet dynamics for gravity-driven and shear-driven cases. Gravity-driven rivulets initially formed as a lobe extending from the liquid source, which flowed for a short distance straight down the base surface and then eventually adopted a meandering form. Shear-driven rivulets start out in a similar manner to gravity-driven rivulets, but instead of extending as a long liquid finger the shear-driven rivulets exhibit an interesting phenomenon that we refer to as "blobbing". Blobbing (illustrated in Fig. 1) is a cyclical process whereby the rivulet progresses by formation of blobs, which enlarge and oscillate in the air flow. After some time a lobe in the blob's downstream side develops and the liquid extends downstream, thus draining the blob. The process then repeats at a downstream location.

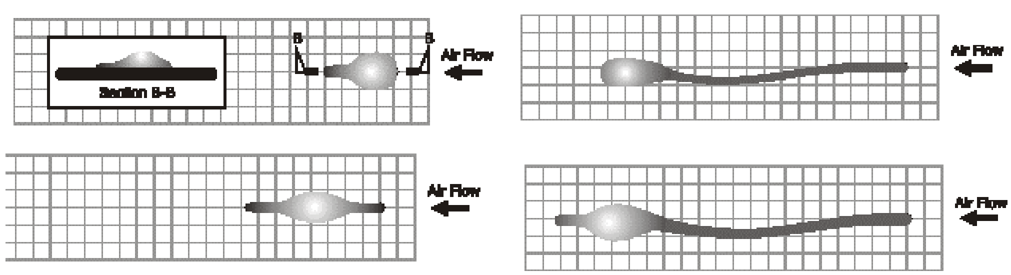

Fig. 1. Blob formation on a shear-driven rivulet.

The computational part of the project uses lubrication theory with a precurser film to remove the contact line singularity and constant surface shear stress. The effect of contact angle is modeled using a disjoining pressure approach. Two-dimensional equilibrium solutions for a shear-driven liquid film front are obtained which show that the ridge of liquid just downstream of the front has layer thickness which decreases with increase in the normal body force to the substrate. A linear stability analysis of the equilibrium liquid front indicates that the decrease in thickness of the front ridge leads to suppression of the fingering instability, and with sufficient normal body force may even eliminate the fingering instability. These results confirm and extend the analysis of Bertozzi and Brenner (*Phys. Fluids* **9**(3), 530-539, 1997) for flow down an inclined plate at different inclination angles. Nonlinear computations are performed using an ADI method which confirm the results cited above. The nonlinear computations (shown in Fig. 2) indicate that rivulet develop in the presence of normal body force proceeds in much the same manner as without body force, only more slowly. We are currently using the numerical computation method to investigate the effect of surface contamination on rivulet formation. In these computations, surface contamination is modeled by driving the liquid front over an array of either droplets or spots of different contact angle. This part of the study is examining the amplification that occurs as a small upstream perturbation passes through the liquid front, and the effect of this amplification on rivulet development for different normal gravity states. Our future computational work will couple a laminar wind flow calculation to the liquid film calculation in order to account for variable shear and pressure on the liquid surface. The wind flow computation will employ a finite-volume approach with moveable mesh, where the bottom boundary condition is set by the liquid layer thickness and velocity.

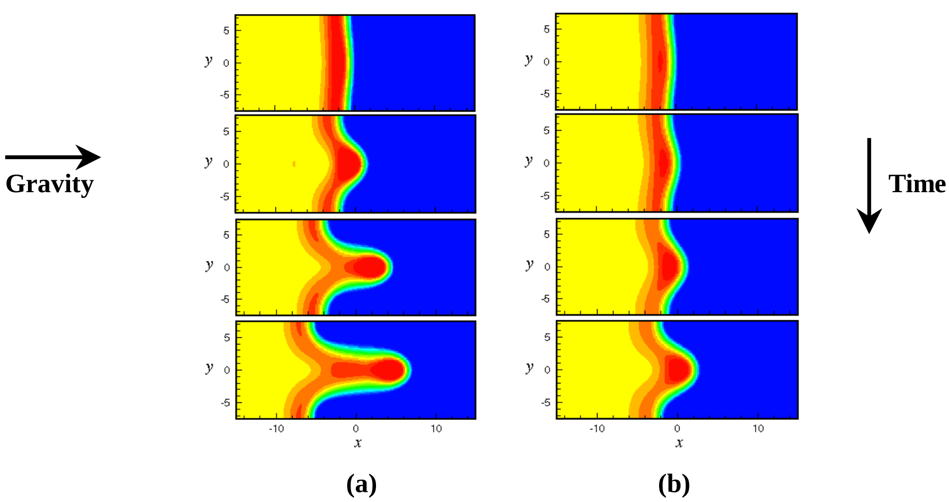

Fig. 2. Contours of liquid layer thickness as the fingering instability leads to rivulet formation, both (a) with no normal body force and (b) with normal body force parameter $P_2 = 0.5$.

ACOUSTIC EXPERIMENT TO MEASURE THE BULK VISCOSITY OF NEAR-CRITICAL XENON IN MICROGRAVITY

K.A. Gillis, I. Shinder, and M.R. Moldover
National Institute of Standards and Technology, Gaithersburg, MD 20899

G.A. Zimmerli
National Center for Microgravity Research, Cleveland, OH 44135

ABSTRACT

We plan a rigorous test of the theory of dynamic scaling by accurately measuring the bulk viscosity of xenon in microgravity 50 times closer to the critical temperature T_c than previous experiments. The bulk viscosity z (or “second viscosity” or “dilational viscosity”) will be determined by measuring the attenuation length of sound a_l and also measuring the frequency-dependence of the speed of sound. For these measurements, we developed a unique Helmholtz resonator and specialized electro-acoustic transducers. We describe the resonator, the transducers, their performance on Earth, and their expected performance in microgravity.

Any fluid very near its liquid-vapor critical point contains highly-correlated density fluctuations characterized by a long relaxation time t. When wt 1 [where $w = 2$ /(period of sound wave)] the attenuation of the sound greatly exceeds the attenuation calculated from the shear viscosity and thermal conductivity. The excess sound attenuation is associated with dilatational motion of the fluid and is accounted for by the bulk viscosity. The excess attenuation encountered in monatomic, near-critical, xenon somewhat resembles the excess attenuation encountered in polyatomic molecules that have a long relaxation time characterizing energy exchange between translational and internal degrees of freedom

According to the theory of dynamical scaling, both the attenuation length a_l and the sound-speed dispersion become universal functions of wt as the reduced temperature $t \rightarrow 0$. [Here $t \equiv (T - T_c)/T_c$.] The best prior tests of the theory were conducted in near-critical xenon and helium [1,2] at frequencies of 0.5 MHz and higher. These tests encountered the condition $wt = 1$ at $t \approx 10^{-3}$. The experimenters introduced empirical parameters to describe how their $a_l(wt)$ data might cross over from the experimentally accessible region to the expected asymptotic region at smaller values of t. Even with such parameters, the data disagreed with theory, within combined uncertainties. Because we are using lower frequencies (130 Hz to 1300 Hz) and because we will use microgravity to evade the stratification of near-critical xenon in the Earth’s gravity, we expect to encounter $wt < 1$ at $t \geq 2 \times 10^{-5}$, 50 times closer to T_c.

For these measurements, we designed the acoustic resonator shown in Figs. 1a and 1b. It is composed of two chambers connected by a small tube. The chambers are cylindrical with perpendicular axes. The chambers have nearly equal volumes (~10 cm^3), but very different aspect ratios. One is 48 mm long with a 16 mm ID; the other is 22.2 mm long with a 23.5 mm ID. The connecting tube is 15 mm long with a 4 mm ID. This resonator has two low-frequency acoustic modes that are well separated from each other and all other modes. The lowest-frequency mode is a Helmholtz mode in which the gas oscillates between the chambers through the small tube. In the next mode, the gas oscillates along the length of the longer chamber. For these two modes in microgravity, Figure 2 shows the expected contributions to the acoustic losses Q^{1} from the bulk viscosity, the shear viscosity, and the thermal conductivity. On Earth, the stratification of the xenon's density from the top to the bottom of the resonator will prevent accurate measurements of the bulk viscosity closer than 150mK to the critical point ($t < 5 \times 10^{-4}$).

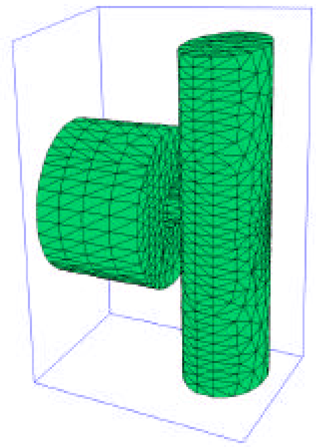

(a) Fig. 1 (b)

Two types of transducers have been developed to both excite and detect sound. The first type uses piezo-ceramic disks epoxied to the outside of a 2.5mm thick diaphragm at each end of the chambers. Flexure of the diaphragms couples to the radial displacement of the ceramics and, therefore, to the voltages that are applied or detected at the electrodes. The advantages of this technique are (1) electrical feedthroughs are not necessary, (2) no foreign materials come in contact with the xenon, and (3) coupling to the xenon is independent of temperature.

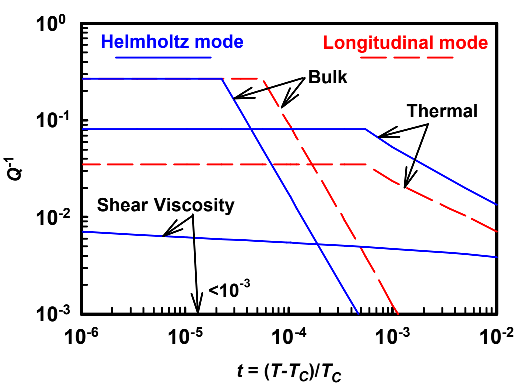

Fig. 2

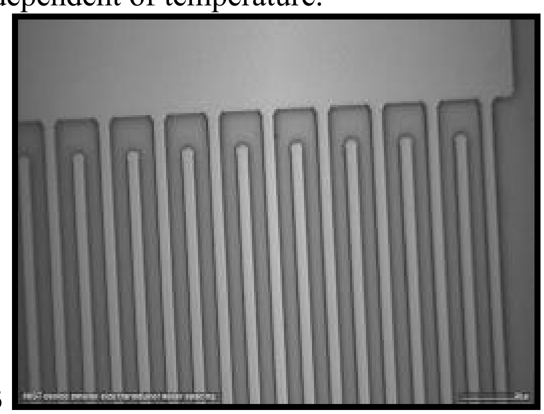

Fig. 3

The second type of transducer is immersed in the xenon. It consists of closely-spaced (< 10 m), interdigitated electrodes deposited on a quartz substrate. (The electrodes are the lighter areas in Fig. 3.) For detecting sound, the electrodes are biased with a DC voltage. An impinging acoustic wave changes the density of the xenon near the electrodes. The resulting change in capacitance generates an AC signal. To generate sound, an AC voltage V at frequency f is applied to the interdigitated electrodes. The resulting electric field creates a pressure (proportional to V^2) that pulls the xenon towards the electrodes at frequency $2f$. This phenomenon is called electrostriction. The advantages of the interdigitated transducers are (1) the frequency response is straight forward to model, (2) low dissipation, (3) no cross talk between drive and detection circuits, and (4) the sensitivity increases with the isothermal compressibility as $t \to 0$.

[1] Garland, C. W., and R. D. William, 1974, Phys. Rev. **A10**, 1328.
[2] Doiron, T., Gestrich, D., and H. Meyer, 1980, Phys. Rev. **B22**, 3202.

SUBMERGED GAS INJECTION FROM A TUBE IN MICROGRAVITY

J. Carrera, R. N. Parthasarathy, S. R. Gollahalli
School of Aerospace and Mechanical Engineering
The University of Oklahoma
212 Felgar Hall, 865 Asp Avenue
Norman, OK 73019
E-mail: rparthasarathy@ou.edu
Tel: 405-325-1735
Fax: 405-325-1088

ABSTRACT

The effects of buoyancy on the flow regimes, the bubble characteristics, and the bubble detachment mechanisms of submerged gas injection from a free-standing capillary tube were studied. The effects of liquid coflow, reduced surface tension, and increased viscosity were also analyzed. The microgravity experiments were carried out in the 2.2 Second Drop Tower at the NASA Glenn Research Center. The two-phase flow rig (97cm x 41cm x 84 cm) was totally autonomous from the instant of release in the drop tower; photographs of the bubbles were captured by a high-speed camera and stored on the onboard computer. A Lexan rectangular test section with the dimensions: 5cm x 5cm and 41cm in height was used. The injection was vertically upwards from a free-standing tube of 0.51mm in diameter and 150mm in length. The dimensions of the test section ensured that the confinement effects on the bubble formation were minimized for low gas flow rates.

The liquid velocity could be varied from 2 cm/s to 4 cm/s by means of a compressed air system. For all gas and liquid throughputs tested, a pre-flowing procedure of the two phases was followed for an interval of ten seconds before every drop to bring the system to steady state conditions. To reduce the surface tension, a non-ionic surfactant (ChemSurf 90) was added to the deionized water. For the increased liquid viscosity experiments, a mixture of deionized water and glycerin was used. Video images were recorded with a high-speed camera (Kodak EktaPro RO Imager) at a rate of 500 frames/second using backlighting against a reflective white surface. The camera began to record 200ms after the drop was initiated to avoid the transient environment from normal gravity to microgravity conditions. All images were analyzed with a computer image-processing unit.

For the experiments of gas injection into a quiescent liquid, bubble detachment was observed for all the Weber numbers tested (0.28 to 31.12). Also, the bubbles were effectively displaced from the near-injector region. Experiments with liquid coflow (2 cm/s and 4 cm/s), and low gas flow rates indicated faster and more controllable bubble detachment than those injected into a quiescent liquid. For high gas flow rates (We > 10) with the liquid coflow, the bubble sizes were more uniform when compared to injection in a quiescent liquid. Similarly, reduced surface tension (4.2mN/m) decreased detachment times, resulting in smaller and more uniform bubbles.

For the range of Weber numbers tested with the addition of surfactant (0.75 to 81.06), bubble detachment as well as effective bubble displacements was observed for all the conditions tested. An increase in liquid viscosity slowed down the detachment process, resulting in larger bubbles. Bubble detachment was observed for the Weber numbers ranging from 0.74 to 37.12. However,

the bubbles were never effectively displaced from the near injector area for Weber numbers < 4. Bubble formation under quiescent liquid conditions in microgravity is illustrated in Figure 1. The present experimental results highlight the differences observed between bubbles formed in gas injection from free-standing tubes and those formed when the gas is injected from a plate-orifice.

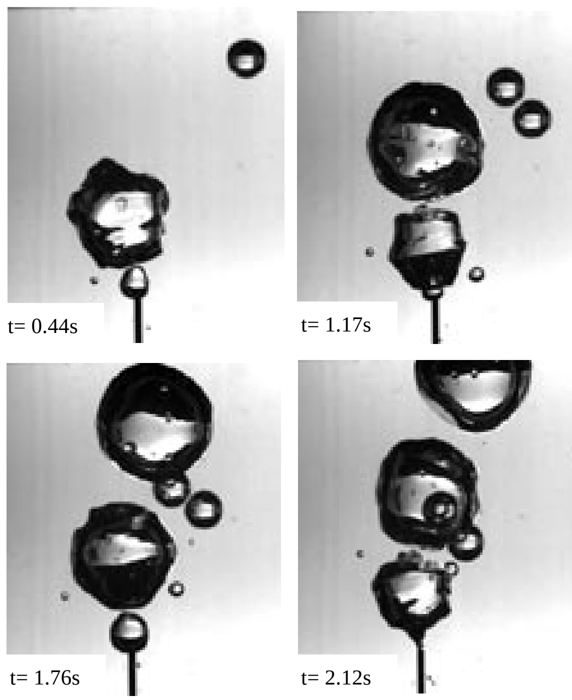

Fig. 1 Bubble formation in quiescent liquid in microgravity, We = 3.02

Resonant Interactions, Multi-frequency Forcing, and Faraday Wave Pattern Control

Mary Silber, Jeff Porter, and Chad M. Topaz
Department of Engineering Sciences & Applied Mathematics
Northwestern University
Evanston, IL 60208 USA

ABSTRACT

Standing surface waves form on a layer of fluid when it is subjected to a sufficiently strong periodic acceleration in the vertical direction. There have been numerous theoretical and experimental investigations of pattern formation in this so-called Faraday wave system in the last 15 years or so, in part because it exhibits patterns not seen in other systems (rhombic and triangular patterns, quasipatterns, superlattice patterns, localized structures akin to oscillons, etc.). Hence it provides a versatile framework in which to develop and test our general understanding of the nonlinear pattern formation process in hydrodynamic systems. However, this versatility comes at some cost. Specifically, many of the more exotic patterns are only realized when the periodic forcing function contains more than one frequency component; the introduction of nonsinusoidal periodic forcing functions leads to a large control parameter space that is difficult to fully characterize. For example, there is an increase from 2 parameters (frequency and amplitude) to 5 parameters in the next simplest case of two-frequency forcing (frequencies, amplitudes and relative phase).

We report on research that helps explain the role of each of the forcing function parameters in the pattern formation process. We focus on resonant triad interactions and their contribution to the weakly nonlinear pattern formation process for two-frequency forced parametrically excited surface waves. Our analysis highlights the effects of weakly broken time translation and time reversal symmetries that result in the weak forcing and damping case. We determine scaling laws for the resonant triad interactions with the forcing frequency ratio. We also find that the relative phase of the two forcing terms can have a dramatic effect on the nonlinear interactions. We confirm our predicted scaling by numerically calculating coefficients for the resonant triad amplitude equations from the quasipotential formulation of gravity-capillary waves due to Zhang and Vinals. Our theoretical results explain a number of recent experimental results, in particular the origin of various superlattice patterns. It also suggests how one might design periodic forcing functions to control pattern selection. We present examples showing how we may control nonlinear resonant triad interactions by an appropriate choice of three frequencies, with appropriate phases, for the forcing function.

Progress in Modeling Nonlinear Dendritic Evolution in Two and Three Dimensions, and Its Mathematical Justification

P.I.: S. Tanveer*, Co-PI: M. R. Foster

The Ohio State University
*420 Math Tower
231 W. 18th Ave.
Columbus, Ohio 43210
614 292 5710 (voice), 614 292 1479 (fax)
tanveer@math.ohio-state.edu
foster.9@osu.edu

We report progress in three areas of investigation related to dendritic crystal growth. Those items are noted below.

1. **Selection of tip features dendritic crystal growth**

   It is to be recalled that crystalline anisotropy is essential for prediction of tip-features in microscopic solvability theory[1]. However, the strong dependence of tip-features on surface energy anisotropy in the limit as anisotropy tends to zero is not quite consistent with experimental observations[2]. In some systems (see explicit examples in reference 3) which are nearly structurally unstable, for example dendritic crystal growth and Hele-Shaw flow, small perturbations can cause unexpectedly large effects, and cross-over in the scaling results. Through formal asymptotic calculation, we have investigated[4] the effect of kinetic undercooling in a two-dimensional symmetric model symmetric model of dendritic crystal growth, with surface energy and anisotropy included. We notice that even for small undercooling, there is a lower threshold of surface energy anisotropy beyond which kinetic undercooling effects become important. We are presently considering such effects for three-dimensional models.

2. **Investigation of nonlinear evolution for two-sided model**

   For time evolving dendritic crystal growth, we are investigating how small disturbances on a nearly parabolic interface shape nonlinearly evolve away from the tip. It is to be noted that we have previously considered this problem[5] for one-sided two-dimensional model, and were able to understand the chaotic nature of evolution in terms of complex singularities and related interfacial distortions. We are now generalizing this approach in a way that does not require complexification, but relies on derivation of parameter free-inner nonlinear integro-differential equations that are valid near a spatially localized disturbance[6]. Parametric scaling dependencies have come as bi-products of this approach. Our earlier work made heavy use of conformal mapping[5]. Since it is not restricted to the use of conformal mapping, this current procedure is especially promising for three-dimensional dendrites. We expect that we will be able to determine more precisely the details of the coarsening process for these two-sided models.

3. **Rigorous mathematical justification**

Dendritic crystal growth theory is riven by conflicting claims, so one important aspect of this investigation is rigorous mathematical justification for our procedures. Some investigators seek to justify their mathematics by agreement between theory and experiment, even when the calculations are not based on sound mathematics. For instance, there are scenarios for describing tip-selection based on marginal stability[7] and its variants[8] that are at odds with microscopic solvability.

Therefore, it is necessary to settle some of the mathematical issues once for all. We are in the process of developing tools for rigorous mathematics to accomplish just that. In the first rigorous study of its kind, we have shown[9,10] that the predictions of microscopic solvability are indeed valid for the mathematically related problem of steady fingers in a Hele-Shaw cell. Dendritic crystal growth involves very similar, though more complicated, integro-differential equations. We anticipate similar results for dendritic growth.

Bibliography

1 D.A. Kessler, J. Koplik & H. Levine, *Advances in Physics* **37**, 255 (1988)

2 M.E. Glicksman & S.P. Marsch, *The dendrite*, in Handbook of Crystal Growth, edited by D.T.J. Hurle (Elsevier, New York, 1993), Volume 1.

3 S. Tanveer, *J. Fluid Mechanics* **409**, 273 (2000)

4* S. Tanveer, The effect of kinetic undercooling on tip-selection in 2-D dendritic crystal growth in the small surface energy anisotropy limit, in preparation (2002)

5 M. D. Kunka, M. R. Foster & S. Tanveer, Dendritic crystal growth for weak-undercooling. II. Surface energy effects on nonlinear evolution, *Phys. Rev. E.* **59**, 673 (1999)

6* M. R. Foster & S. Tanveer, Nonlinear evolution of localized disturbances in a 2-D symmetric and 3-D axisymmetric model for dendritic crystal growth, in preparation (2002)

7 S. Langer & H. Muller-Krumbhaar, *Acta Metall.* **26**, 1697 (1978).

8 J.J. Xu, *Eur. J. Appl. Maths* **2**, 105 (1991).

9* X. Xie & S. Tanveer, Rigorous Results in Steady Finger Selection in Viscous Fingering*, *Archives for Rational Mechanics*, to appear (2002)

10* S. Tanveer & X. Xie, Analyticity and Nonexistence of Classical Steady Hele-Shaw Fingers*, *Comm. Pure & Applied Mathematics*, to appear (2002)

* **supported at least in part by NAG3-2700**

Thermal Convection in Two-Dimensional Soap Films

Jie Zhang and X.L.Wu
Department of Physics and Astronomy
University of Pittsburgh, Pittsburgh, PA 15260

Thermal convection in a fluid is a common phenomenon. Due to thermal expansion, the light warm fluid at the bottom tends to rise and the cold, heavier fluid at the top tends to fall. This so-called thermal convection exists in earth atmosphere and in oceans. It is also an important mechanism by which energy is transported in stars. In this study we investigate thermal convection in a vertical soap film. Two aluminum cylinders, one at the top and one at the bottom, separated by about 2 cm are used to control the temperature at two constant values, as shown:

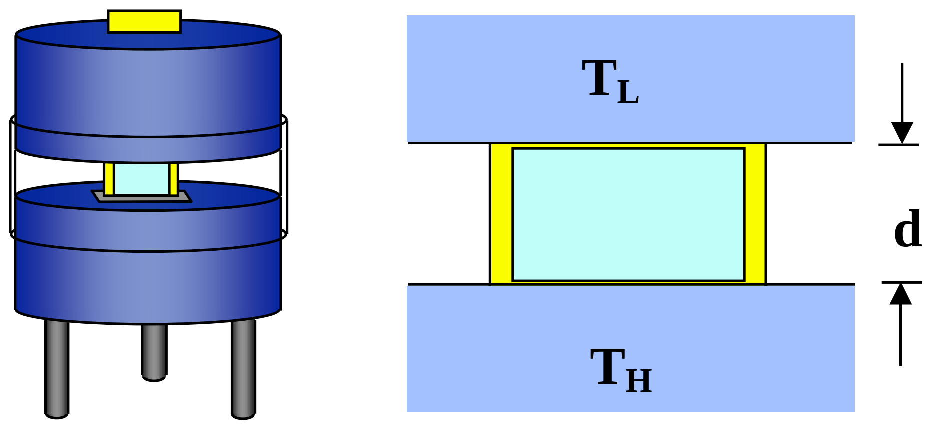

The film is suspended inside a thin metallic frame to improve transverse heat conduction. The aqueous film is made stable by using a small amount of surfactant (1.5 %). At the steady state, the film is typically several microns in thickness, with a uniform thickness gradient due to the gravitational stratification. Thus, thermal convection in the soap film is a double diffusive system, with temperature and 2D mass density forming two diffusive fields.

At a sufficiently large temperature gradient, fluid flow becomes turbulent as delineated below by a shadow graph technique. Here the temperature gradient is about 50 ^{o}C. One observes a frequent emission of thermal plumes at the bottom of the sample along with a large-scale circulation. To study the thermal turbulence quantitatively, power spectra of the temperature field are measured by a thermal radiation detector. This noninvasive technique allows small temperature variations to be measured with a high accuracy and with a time rate of ~100 Hz. Our main observation shows that the temperature power spectrum scales as a power law $P(f) \sim f^{-\alpha}$, with $\alpha=1.4$ for medium temperature gradients and $\alpha=1.0$ for large temperature gradients, where f is the frequency. The latter case ($\alpha=1.0$) suggests that the temperature field can behave like a passive scalar, similar to dispersion of a dye in a turbulent field. Our preliminary observation seems to suggest that the crossover between the two different behaviors is marked by the onset of the large-scale circulation. Currently we are concentrated on measuring the velocity field simultaneously with the temperature field. These later measurements will shed new light on the intricate interactions between the temperature and velocity fields.

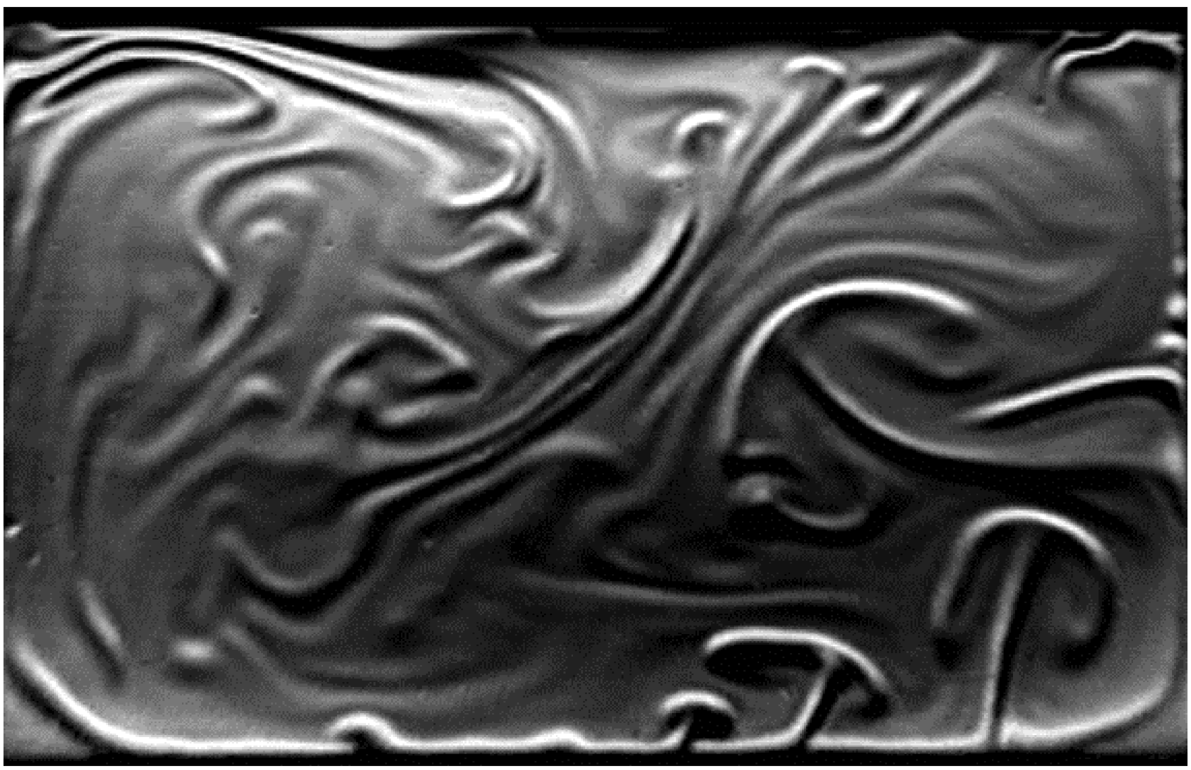

Exposition Session
Guest Posters

AN OBSERVATION OF FILM THICKNESS AND LOCAL PRESSURE IN UPWARD AND DOWNWARD ANNULAR TWO-PHASE FLOW IN MICROGRAVITY, HYPERGRAVITY AND NORMAL GRAVITY

Kamiel S. Gabriel* and Devon L. Manz
Microgravity Research Group, University of Saskatchewan, Saskatoon, S7N 5A9, Canada

ABSTRACT

The phenomenon of two-phase flow in a near weightless environment (or microgravity) is becoming increasingly important. Two-phase flow loops are used in advanced spacecraft thermal management systems and also occur during the transfer of cryogenic propellants. On earth, two-phase annular flow is common in power plants and many chemical processing plants. The liquid film along the tube wall plays a large role in mass and momentum transfer, featuring a complex wave structure. It is the wave structure phenomenon relating to the pressure and film thickness time trace that is the current interest in this investigation.

Film thickness and local pressure time trace measurements were taken in normal (earth gravity) and microgravity (μ-g) conditions during the 29th and 30th Annual European Space Agency parabolic flight campaign operated by Novespace in Bordeaux, France. A high sampling rate and measurement accuracy are essential for a sufficient representation of the film thickness. The parallel wire conductance probe, initially used by deJong (1999), measures the electrical conductance between two wires stretched across the flow. Annular flow film is highly dynamic and hence the film thickness and associated local pressure fluctuate rapidly. The instruments require high frequency response and minimum damping. The Druck PDCR 900 pressure transducer has a frequency response quoted by the manufacturer to be 0 to 20000 Hz. Local pressure taps were placed in the same horizontal plane as the film thickness probes, perpendicular to the wires. It is essential that the local pressure measurement not interfere with the film phenomena, and as such the measurements were made at the tube wall.

An investigation into upward and downward annular flow at earth's gravity was made by Ariyadasa (2002) in a 9.925 mm diameter tube. The primary interest of this investigation was the relationship between the pressure and the film thickness. An investigation was made by Moe (1991) that examined the film thickness and pressure time traces in a horizontal flow. Moe observed the relationship between pressure peaks and film thickness peaks in a horizontal flow and indicated that the pressure differential might be enough to exert a significant force on the waves. Webb and Hewitt (1975) observed the pressure peaks that accompanied and lagged the film thickness peaks. They concluded that the time delay exists because of interaction with the exit condition of the system.

Based on the time traces of the film thickness and localized pressure obtained from available data, the relationship between the film thickness and the pressure under the wave appear to indicate some correspondence. Comparison of the time traces consisted of considering the film thickness greater than one standard deviation from the mean over the 4 or 8 second window. In

* Formerly K.S. Rezkallah

this region, if the film thickness time trace was increasing or decreasing as the local pressure was increasing or decreasing, the relationship was observed. Classification using nearly 100 microgravity, hypergravity and normal gravity annular flow data points was performed.

A typical film thickness and local pressure time trace for an upward annular flow at normal gravity conditions are featured in figure 1a. The liquid superficial velocity is 0.24 m/s and the gas superficial velocity is 20 m/s. Featured in figure 1b, is a flow image in the same tube diameter.

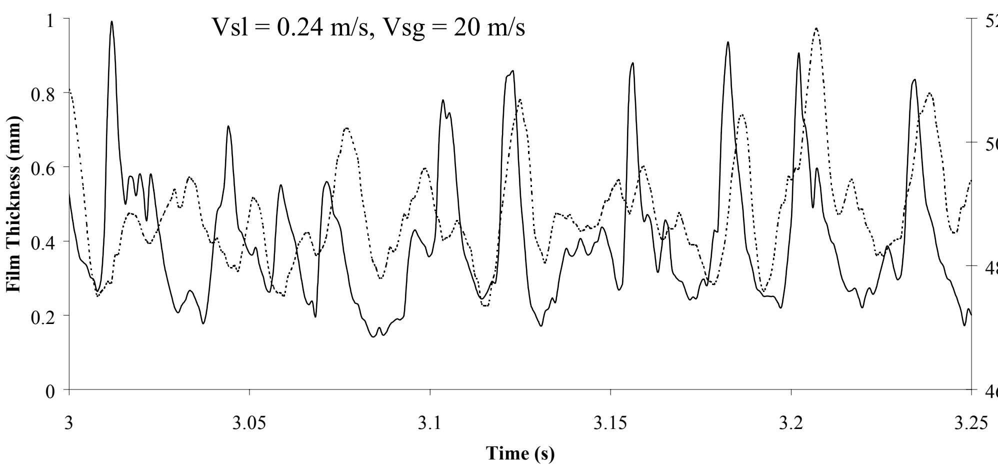

(a) **(b)**

Figure 1: (a) Film thickness (solid line) and local pressure (broken line) time traces at normal gravity; (b) Annular flow image at normal gravity (Vsl = 0.24 m/s, Vsg = 19.5 m/s, P = 99.3 kPa)

1. Ariyadasa, Umesh (2002). An Investigation of Film Thickness and Pressure in Upward and Downward Annular Two-Phase Flow. M.Sc. Thesis, University of Saskatchewan, Canada.
2. deJong, Pieter (1999). An Investigation of Film Structure and Pressure Drop in Microgravity Annular Flow. M.Sc. Thesis, University of Saskatchewan, Canada.
3. Moe, J. (1991). Long-wave disturbances in stratified two-phase pipe flow, phase-interface phenomena in multiphase flow. In Hewitt, G.F., Mayinger, F., and Riznic, J.R. (Eds.), Phase-interface phenomena in multiphase flow, pp. 58. Hemisphere Publishing Corporation, New York.
4. Webb, D.R., and Hewitt, G.F. (1975). Downward co-current annular flow. Int. J. Multiphase Flow 2, 35.

PHOTOINDUCED CAPILLARY MOTION OF DROPS AND BUBBLES

Bezuglyi B.A., Ivanova N.A.
Tyumen State University, Liquid Microgravity Technology Laboratory
Semakova, 10, Tyumen, 625003, Russia, e-mail: nivanova@utmn.ru

ABSTRACT

Bubbles and drops are inhering in many liquid processes on Earth (microfluidics, MEMS technology, flows through porous media etc.) and in space laboratory under μg conditions (preparation composite materials, degassing of liquefied matter, recycling of waste material). They could have affected these processes significantly. Therefore the study of behavior these capillary objects is necessary in order to develop the efficient methods of manipulation of them in situ.

The best solution of such problem is the use of surface forces, which are aroused when the surface tension locally is departed from its equilibrium value as a result of thermal, concentration or electrical perturbations at interface,

$$\nabla\sigma = \sigma'_T\big|_{C,\varphi} \nabla T + \sigma'_C\big|_{T,\varphi} \nabla C + \sigma'_\varphi\big|_{C,T} \nabla \varphi$$

Among the known methods of control of surface tension the most promising is the thermal one. However, the generation of motion of capillary objects by the thermal gradients imposed in liquid bulk (or along solid substrate) by conduction is a passive method, which requires large amount of energy.

In this paper the new method of generation of motion of bubbles and drops in microchannels or Hele-Show cells are reported. This method based on photoinduced solutocapillary convection discovered by Bezuglyi [1,2].

This motion can be caused through simultaneously acting thermocapillary (TC) and solutocapillary (SC) forces, which are induced by a light beam at the interface of the bubbles and drops. A competition between these two forces takes place. A criterion which measures the importance of surface tension gradient, $(\nabla\sigma)_C = \sigma'_C \nabla C$, related to concentration gradient against surface tension gradient, $(\nabla\sigma)_T = \sigma'_T \nabla T$, caused by thermal gradient is a dimensionless number $CT = (\nabla\sigma)_C / (\nabla\sigma)_T$. If $CT > 1$, then the capillary motion is caused by SC forces. When $CT < 1$, drops and bubbles move due to TC forces.

The behavior of the gas bubble of various diameter in a thin layer (10 – 100 μm) of solution tensioactive substance in a high volatile solvent sandwiched between two glass plates and the growth of drops within bubbles under light radiation have been studied. Continuous and intermittent motions of bubbles for numbers $CT < 1$ and $CT > 1$, respectively, were revealed. First, the division of kidneylike bubble [3] in irradiated region was demonstrated. It was found, that the rate of drop growth within bubble is increased when the diameter of bubble is decreased.

[1] B. Bezuglyi, PhD Thesis. Moscow State University. Moscow 1983.
[2] B. Bezuglyi, Proc. Int. Aerospace Congress, Moscow, Russia. (1995) 261
[3] B. Bezuglyi, A. Fedorets, N. Ivanova, First conference of the International Marangoni Association, Abstracts, Sept. 12-16, Giessen, Germany, (2001) 80.

OBSERVATIONS OF CONFINEMENT OF A PARAMAGNETIC LIQUID IN MODEL PROPELLANT TANKS IN MICROGRAVITY BY THE KELVIN FORCE

John Kuhlman[+], Donald D. Gray[*], Austin Barnard[#], Jennifer Hazelton[#], Matthew Lechliter[#], Andrew Starn[#], Charles Battleson[#], Shannon Glaspell[#], Paul Kreitzer[#], and Michelle Lechliter[#]
West Virginia University, Morgantown, WV 26506

[+]Professor, and [#]Undergraduate Student, Dept. of Mechanical and Aerospace Engineering
[*]Associate Professor, Dept. of Civil and Environmental Engineering

INTRODUCTION

The magnetic Kelvin force has been proposed as an artificial gravity to control the orientation of paramagnetic liquid propellants such as liquid oxygen in a microgravity environment. This paper reports experiments performed in the NASA "Weightless Wonder" KC-135 aircraft, through the Reduced Gravity Student Flight Opportunities Program. The aircraft flies through a series of parabolic arcs providing about 25 s of microgravity in each arc. The experiment was conceived, designed, constructed, and performed by the undergraduate student team and their two faculty advisors.

Two types of tanks were tested: square-base prismatic tanks 5 cm x 5 cm x 8.6 cm and circular cylinders 5 cm in diameter and 8.6 cm tall. The paramagnetic liquid was a 3.3 molar solution of $MnCl_2$ in water. Tests were performed with each type of tank filled to depths of 1 cm and 4 cm. Each test compared a pair of tanks that were identical except that the base of one was a pole face of a 0.6 Tesla permanent magnet. The Kelvin force attracts paramagnetic materials toward regions of higher magnetic field. It was hypothesized that the Kelvin force would hold the liquid in the bottom of the tanks during the periods of microgravity. The tanks were installed in a housing that could slide on rails transverse to the flight direction. By manually shoving the housing, an identical impulse could be provided to each tank at the beginning of each period of microgravity. The resulting fluid motions were videotaped for later analysis.

RESULTS

As summarized in Table 1, positive results (more liquid was confined to the bottom of the magnet tank than in the non-magnet control tank) were obtained in 86 out of 89 tests. For 3 tests with relatively large impulses, the magnetic and non-magnetic results were comparable. No negative results were observed. As expected, the Kelvin force was much more effective in controlling the liquid in the shallower liquid cases.

Table 1. Summary of results.

Case	Tank	Depth	# tests	# positive	# negative	# inconclusive
1	Prism	1 cm	27	27	0	0
2	Cylinder	1 cm	18	18	0	0
3	Prism	4 cm	26	26	0	0
4	Cylinder	4 cm	18	15	0	3
Total			89	86	0	3

In every one of the Case 1 tests, the magnet held the liquid interface essentially flat after the initial sloshing transient quickly damped out. In the control tanks, the liquid quickly moved to the top of the tank in 23 cases. In the remaining 4 tests, the interface tilted 1-6 cm, eventually reaching the top of the tank in 3 tests. Figure 1 shows an example of the Case 1 results. The tank with the magnet is on the left of the image.

Among the Case 2 tests, 6 had no input impulse. In these the magnet held the liquid with an essentially flat interface, while in the control tanks the liquid moved to the top in 3 tests and exhibited a tilting interface in 3 tests. For 1 test in which multiple input impulses set up a swirling motion, the magnet tank showed a smaller amount of the liquid at the top of the tank than the control tank. In 5 tests with impulse, the magnet held the liquid with a flat interface, while the liquid either moved to the top of the tank or tilted significantly from a horizontal position in the control tests. For the remaining 6 tests approximately half of the liquid remained in the bottom of the tank for the magnet tanks, while essentially all of the liquid moved to the top in the control tanks. Figure 2 is a Case 2 image; the magnet is visible below the right hand tank.

In Case 3, there were 17 tests in the which magnet allowed the interface to tilt noticeably, but kept the liquid from reaching the top of the tanks, and 9 in which the tilting was followed by some of the liquid moving to the top of the tank near the test's end. In the control tanks, there were 17 tests in which the bulk of the liquid moved quickly to the top of the tank, and usually moved back down to the bottom of the tank, with the cycle repeating one or more times. In the remaining 9 control tank tests, most of the liquid would move to the top of the tank and stay there for most of the parabola. Figure 3 is a Case 3 image; the magnet is below the right hand tank.

In the Case 4 tests, there were 6 with no input impulse. For 4 of these tests the magnet tank showed a tilted interface that never reached the top of the tank, while for 2 some liquid eventually went to the top of the tank. Of the no-impulse control tank cases, 4 had more liquid go to the top of the tank, while 2 had an interface that tilted more than for the corresponding magnet tanks. For the 3 tests in which multiple input impulses set up a swirling motion, the magnet cases showed a smaller amount of the liquid at the top of the tank than the controls. In 6 additional tests an average of 65% of the liquid was near the tank bottom for the magnet tanks compared with an average of 30% for the controls. In 3 tests there was no significant difference between the magnet and control tanks. Figure 4 is a Case 4 image; the magnet tank is on the left.

Fig. 1. Sample image for Case 1.

Fig. 2. Sample image for Case 2.

Fig. 3. Sample image for Case 3.

Fig. 4. Sample image for Case 4.

Session 5:
Biological Fluid Physics
(Biological Fluid Mechanics and Biological Self Assembly)

ASSEMBLY OF COLLOIDAL MATERIALS USING BIOADHESIVE INTERACTIONS

Daniel A. Hammer, Amy L. Hiddessen, Valeria Tohver, and John C. Crocker
Departments of Bioengineering and Chemical Engineering, University of Pennsylvania, Philadelphia, PA 19104

David A. Weitz
Department of Physics and DEAS, Harvard University, Cambridge, MA 02139

ABSTRACT

We have pursued the use of biological crosslinking molecules of several types to make colloidal materials at relatively low volume fraction of colloidal particles. The objective is to make binary alloys of colloidal particles, made of two different colloidal particles coated with complementary biological lock-and-key binding molecules, which assemble due to the biological specificity. The long-term goal is to use low affinity lock-and-key biological interactions, so that the colloidal systems can anneal to form crystalline states.

We have used a variety of different surface chemistries in order to make colloidal materials. Our first system involved using selectin-carbohydrate (sialyl-Lewis^x) interactions; this chemistry is derived from immune system. This chemical interaction is of relatively low affinity, with time-scales for dissociation of several seconds. Furthermore, the adhesion mediated by these molecules can be reversed by the chelation of calcium atoms; thus assembled structures can be disassembled reversibly. Our second system employed avidin-biotin chemistry. This well-studied system is of high affinity, and is generally irreversible on a laboratory time-scale. Thus, we would expect selectin-carbohydrate interactions at high molecular density and avidin-biotin interactions to give kinetically-trapped structures; however, at low densities, we would expect significant differences in the structure and dynamics of the two materials, owing to their very different release rates.

We have also begun to use a third chemistry – DNA hybridization. By attaching single stranded DNA oligonucleotide chains to beads, we can drive the assembly of colloidal materials by hybridization of complementary DNA chains. It is well known that DNA adenosine-thymine (A-T) and guanine-cytosine (G-C) bases hybridize pairwise with a Gibbs free energy change of –1.7 kcal/mol per base; thus, the energy of the assembly can be modulated by altering the number of complementary bases in the DNA chains.

Using these different crosslinking molecules, we have assembled colloidal materials from different-sized colloidal particles, A and B. In the first sets of experiment, we used high densities of adhesion molecules, and 0.96 micron (A) and 5.5 micron (B) diameter particles. The high density of adhesion molecules means that the structures are kinetically trapped in non-equilibrium configurations. The structure of the suspension can be varied by changing the number ratio of the two types of colloidal particles, N_A and N_B, where A is the smaller particle. With carbohydrate-selectin or avidin-biotin interactions, large N_A/N_B leads to the formation of colloidal micelles, with the large center B particle surrounded by many smaller A particles (see Figure 1). As the ratio N_A/N_B decreases, the structures become more extended, approaching the formation of macro-Rouse polymers – extended linear chains where A beads are connected with intervening small B linkers.

When the structures are made with selectin-carbohydrate interactions, the chelation of calcium using EDTA can cause the structures to disassemble entirely. Also, the addition of EDTA prior to the mixing of the suspension can prevent the structures from forming.

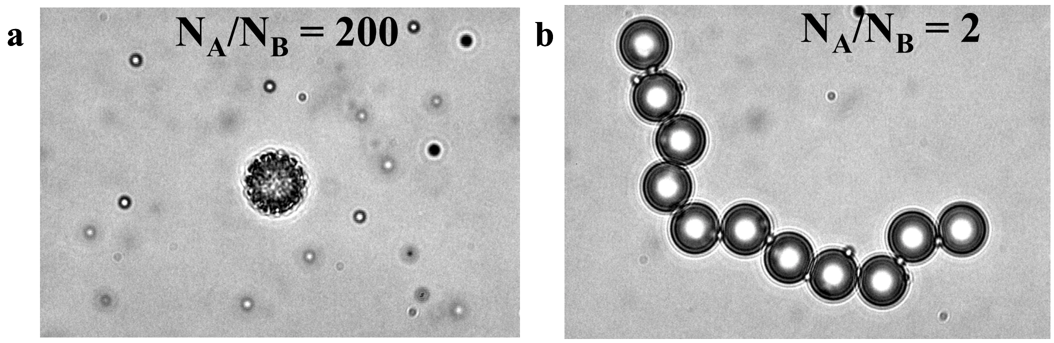

Figure 1. Assembly of colloidal structures using biotin-avidin interactions. At high densities of N_A/N_B (A), a large B particle is surrounded by many A particles. At low densities of N_A/N_B (B), extended chains are formed.

When the density of selectin-carbohydrate molecules is decreased, the binding of small A beads to the central B particle becomes transient. The time-scale for release of A particles from the surface of the central B particle is an increasing function of the molecular density. The density of molecules on the A particles can be changed by the concentration of molecular incubation, and verified with flow cytometry. The time scale of release of many particles can be tracked, and compared to a simple probabilistic binding model for molecular dissociation. The decay of bound (docked) particles can be fit to determine the intrinsic binding dissociation constants. The uni-molecular dissociation constant for sialyl-Lewis^x/E-selectin interactions determined this way is approximately 1 sec^{-1}, which corresponds to the off rate measured separately for this interaction by other laboratories.

We have also been measuring the rheology and assembly of resultant colloidal suspension using micro-rheometry. This has involved bulk rheological measurements, as well as the dynamics of colloidal assembly using confocal microscopy (where the smaller bead species, A, is fluorescent, and its position is tracked with time). At 10 % total volume fraction, and a bead ratio N_A/N_B = 10, colloidal materials assembled using avidin-biotin interactions exhibit a characteristic shear thinning behavior over a wide range of shear stresses. A long-term goal is to compare the time-constants for shear thinning behavior as a function of the density and strength of the biological molecules.

Finally, we have made significant progress in assembling small aggregates of colloidal particles that are crosslinked by DNA hybridization. Avidin-coated particles were coated with 30 base pair DNA sequences (a and b) that had 20 bp overlapping sequences. The sequences were made with biotin at the 5' end and the fluorescent dye Cy5 at the 3' end. The presence of the oligonucleotide strands on the beads was verified by fluorescence flow cytometry. Since the hydbridization of DNA depends on temperature and the length of overlap of the DNA bases, we will explore the effect of temperature and chain length on the ability for assemble stable colloidal structures using DNA hybridization with different lengths of chain overlap.

Acknowledgement: Authors wish to acknowledge support from the NASA Fluid Physics program. Requests for information and reprints should be addressed to Daniel A. Hammer, Department of Bioengineering, University of Pennsylvania, Philadelphia, PA 19104, hammer@seas.upenn.edu.

MICROGRAVITY EFFECTS ON TRANSVASCULAR TRANSPORT AND VASCULAR CONTROL

M. Kim, M. Civelek, K. Ainslie, J. Garanich, N.R. Harris, J.M. Tarbell
Departments of Bioengineering and Chemical Engineering, The Pennsylvania State Univerity, University Park, PA, USA

ABSTRACT

Introduction: Microgravity alters transvascular pressure differential and transmural flow across blood vessel walls. We have hypothesized that changes in transmural flow alter fluid shear stress on vascular smooth muscle cells (SMC) and this in turn affects the state of contraction or "tone" of SMC. Since the cardiovascular system relies on SMC contraction in arterioles in response to changes in pressure ("myogenic response") to regulate blood flow to tissue beds which in turn affects transvascular exchange, we have investigated the effects of fluid flow shear stress on SMC contraction using both in vitro and in vivo models.

In Vitro Studies: Primary rat aortic SMC were expanded in cell culture flasks containing DMEM + 10% FBS. Then the cells were "starved" (maintained in DMEM, no FBS) in culture flasks for two to three days and then on quartz slides at sub-confluent density for two more days prior to experiments that were also run serum-free. SMC starving was necessary to induce the contractile phenotype. To study cell contraction in response to shear stress, sub-confluent cells on quartz slides were exposed to defined levels of steady shear stress in a parallel plate flow chamber for 30 minutes while being photographed under a microscope with a video camera. Reduction in cell area was interpreted as cell contraction and quantified in terms of percent area reduction. Intra-cellular calcium (Ca^{2+}) was imaged under flow in the parallel plate chamber using the calcium sensitive dye fura-2.

Cells in the contractile phenotype that were exposed to 25 dyne/cm^2 shear stress decreased their area significantly within 3 minutes and by more than 30% after 30 minutes. The threshold for contraction was about 7 dyne/cm^2. To our surprise, this contraction response was not accompanied by a response of intracellular Ca^{2+}. Additional experiments in calcium free media and with an intracellular calcium chelator also displayed a significant contraction response to shear stress confirming that shear-induced contraction is not mediated by intracellular Ca^{2+}. Additional pharmacological experiments suggested that the shear-induced contraction is mediated primarily through a Rho-kinase intracellular signaling pathway. In contrast, cells in the proliferative phenotype (maintained in serum) did not contract in response to shear stress but did display a marked intracellular Ca^{2+} response to shear.

In Vivo Studies: Fourteen male Wistar rats were anesthetized and the right carotid artery was cannulated to monitor systemic blood pressure, and for systemic injection of a mixture of bovine serum albumin (BSA) and 70 kD Ficoll in nine of the experiments. The BSA-Ficoll mixture was

used to increase plasma osmotic pressure which reduces transmural flow (J_v) and shear stress on SMC. The small intestine was exteriorized surgically and the mesentery was draped over a glass coverslip which was mounted on the stage of an inverted microscope. The mesentery was observed through a x40 objective (Nikon Plan Apo, 0.95 N.A.) using a 100-W halogen light source, and brightfield images were captured with a color camera and recorded for image analysis of vessel diameter. Arterioles having a baseline diameter of 20-30 microns were occluded with a glass micropipette to initiate a myogenic response. This technique has been performed previously for the hamster cheek pouch [1], where arteriolar pressure upstream of the occluder increased by 22.5%. Following the baseline occlusion, a mixture of dialyzed BSA and Ficoll was injected to increase the osmotic pressure, then a second occlusion was performed. After release of the second occlusion, maximal dilation of the arteriole (D_{max}) was obtained by exposure to papaverine to estimate % tone of the baseline diameter. The value of J_v normalized to the surface area S (J_v/S) was monitored during each occlusion by measuring the decreasing distance between the micropipette and the upstream red blood cells as described previously [2].

Baseline arteriolar tone ($1-D/D_{max}$) and J_v/S were well correlated, with tone increasing from 2% at J_v/S = 0.002 micron/sec up to 8% at J_v/S = 0.013 micron/sec. Although this is consistent with our hypothesis that J_v may control myogenic tone, it is also possible that both factors are related by hydrostatic pressure, an increase of which would be expected to increase both myogenic tone and transmural flow. To further investigate our hypothesis, we compared the myogenic response prior to and following infusion of the BSA-Ficoll osmotic solution. The osmotic solution attenuated J_v by ~50% relative to autologous plasma and reduced the myogenic constriction of arteriolar diameter by ~60%. The occlusion-induced increase in hydrostatic pressure was likely similar for the two data sets (osmotic solution and autologous plasma solution), based on the observation that the arteriole diameter was stretched initially by the same amount for both data sets.

Discussion: The in vitro results show that an increase in fluid shear stress causes SMC to contract in a calcium-independent manner suggesting that increased fluid shear stress on SMC associated with increased transmural flow may drive the myogenic response in arterioles. The in vivo results, which show that a reduction in transmural flow induced by an osmotic solution reduces the myogenic response, are consistent with the in vitro results. These experiments support a new hypothesis for the mechanical basis of the myogenic response that invokes fluid shear stress. The new hypothesis has important implications for vascular control and fluid shift in microgravity since transmural flow is altered by microgravity.

References

1. Lombard, J.H., Duling, B.R. (1977). *Circ. Res.*, vol. 41(3), pp. 365-373.
2. Harris, N.R., Benoit, J.N., Granger, D.N. (1993). *Am. J. Physiol.*, vol. 265, pp. H1623-H1628.

Principal Investigator: John M. Tarbell, Bioengineering Department, The Pennsylvania State University, University Park, PA 16802. email: jmt@psu.edu; tel. 814-863-4801; fax 814-865-7846.

Capillary instabilities in the microgravity environment

David Halpern
Department of Mathematics
University of Alabama
Tuscaloosa AL 35487,

James B. Grotberg
Biomedical Engineering Department
University of Michigan
Ann Arbor, MI 48109

ABSTRACT

The lung consists of a network of bifurcating tubes that are coated with a thin viscous film. In the case of disease, the liquid film can form a meniscus which plugs the tube, thus obstructing gas exchange. The formation of the liquid meniscus is due to capillary driven instabilities which arise in the lining causing it to close up. Airflow can also be obstructed if the airway tube collapses in on itself. This occurs when the elastic forces of the tube are not large enough to sustain the negative fluid pressures inside the tube caused by surface-tension, and the tube collapses. Closure of the airway can be due to either, or a combination of, these mechanisms. In any case the instability is dependent on the surface tension of the liquid lining and the presence, or lack of, surfactants.

Premature babies, whose lungs have not developed sufficient surfactant to maintain the surface tension of the lung at a sufficiently low level for healthy functioning, are especially predisposed to problems caused by airway closure. In such cases, the patients can be treated with high frequency ventilation machines or surfactant replacement therapy or both Adults also are treated with ventilators for a variety of pulmonary conditions which can involve airway closure. For mechanical ventilation, the frequency of the breathing cycle, as well as the tidal volume, are two control parameters at the disposal of the clinician. Little is known, however, of the effect that these two parameters can have on the occurrence of airway closure. Indeed, if airways can be kept open by using some given machine frequency or amplitude, thus causing mechanical perturbations to the unstable interface, then this would important in the treatment of such patients.

In normal gravity, airway closure tends to occur in the lower regions of the lung, due to the weight of the lung above, and at the end of expiration when the lung volume, and hence airway radii, are smallest. The transient blockage of gas exchange in the affected tubes occurs in only part of the lung, the other portions remaining open. In the microgravity environment, airway closure is a potentially significant issue since ventilation and airway closure are more homogeneous, leaving less of the lung to be open during end expiration. Prevention of airway closure in this setting may be useful.

We model the phenomenon of airway closure by considering the stability of a thin film coating the inner surface of a rigid cylindrical tube. An oscillatory air (core) flow exerts

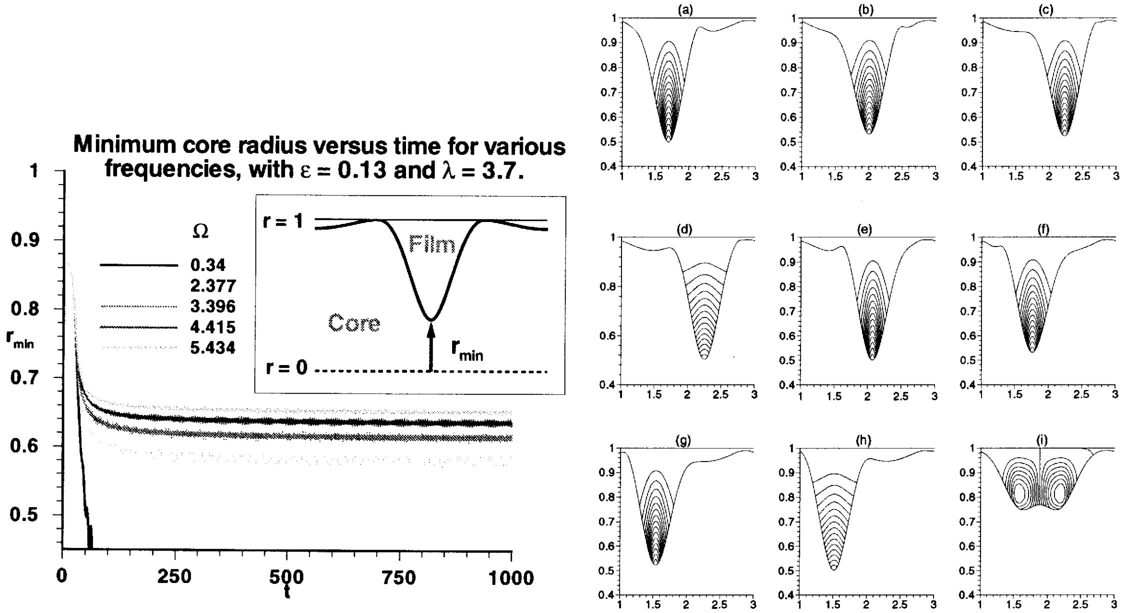

Figure 1: Left panel:Minimum core radius versus time for different values of the frequency parameter Ω for fixed amplitude λ and unperturbed film thickness ϵ. For sufficiently large frequency, closure is prevented since $r_{\min}$ does not approach zero. Right panel: Profiles of air-liquid interface and streamlines at different times during a cycle once an asymptotic state has been reached. The bulge deposits fluid to the film behind it as it moves from one side of the domain to the other, and picks up fluid from the film during the parts of the cycle when it reverses direction.

tangential and normal stresses on the air-liquid interface. The core flow is determined independently of the film flow by assuming that the core perceives the highly viscous film as a rigid boundary. We also consider the effects of a surfactant monolayer present at the air-liquid interface. Lubrication theory is used to derive an evolution equation for the position of the air-liquid interface which includes the effects of the core flow. This equation is coupled to a surfactant transport equation. Scaling analysis reveals several dimensionless parameters involving the frequency and amplitude of the periodic core pressure gradient, the thickness of the film, the tube radius, the viscosities of the fluids, the surface tension and surface-tension gradients due to the presence of the surfactant. When the core is passive, closure is possible provided the ratio of the unperturbed film thickness to tube radius exceeds a certain critical value. For the non-zero frequency case, it is shown that the core flow can stabilize the capillary instability and prevent closure. We find that there is a critical frequency above which closure does not occur, and that this critical frequency increases as the amplitude of the core flow decreases. An example of our computations is shown in figure 1.

THE IMPORTANCE OF INTERFACIAL STRESSES DURING PULMONARY AIRWAY REOPENING IN MICROGRAVITY

D.P. Gaver, A.M. Bilek, K.C Dee
Department of Biomedical Engineering, Tulane University, New Orleans, LA, USA

ABSTRACT

Pulmonary airway closure is a potentially dangerous event that can occur in microgravity environments and may result in limited gas exchange for flight crew during long-term space flight. Repetitive airway collapse and reopening subjects the pulmonary epithelium to large, dynamic, and potentially injurious mechanical stresses. During ventilation at low lung volumes and pressures, airway instability leads to repetitive collapse and reopening. During reopening, air must progress through a collapsed airway, generating stresses on the airway walls, potentially damaging airway tissues. The normal lung can tolerate repetitive collapse and reopening. However, combined with insufficient or dysfunctional pulmonary surfactant repetitive airway collapse and reopening produces severe lung injury. Particularly at risk is the pulmonary epithelium. As an important regulator of lung function and physiology, the degree of pulmonary epithelial damage influences the course and outcome of lung injury. Two companion studies, an experimental investigation and computational fluid dynamic simulation, are presented that address the hypothesis that the mechanical stresses associated with airway reopening inflict injury to the pulmonary epithelium.

Experimental Investigation

A parallel plate chamber lined with pulmonary epithelial cells was constructed as an idealized model of a collapsed segment of an airway where the walls are held in opposition by a viscous fluid. A fetal rat pulmonary epithelial cell line (CCL-149, ATCC) was cultured to confluence on a small (1 cm^2), square region of the upper plate. The narrow channel was filled a model airway lining fluid. Phosphate buffered saline including 0.1 mg/mL $CaCl_2$ and $MgSO_4$ (PBS) was used to model a surfactant-deficient airway lining fluid. A surfactant-containing airway lining fluid was approximated using Infasurf (ONY, Inc.) diluted to 1 mg/mL phospholipid concentration in PBS. Airway “reopening” was generated by the steady progression of a semi-infinite bubble of air down the length of the channel using a constant rate infusion pump (7 or 70 mL/min). For the control, slides were soaked in PBS for 5 minutes. A digital camera mounted above the channel collected sequential overhead images of the progressing bubble, which were used to calculate bubble velocity. Once removed from the apparatus, the slide was incubated with 1.2 μM Ethidium homodimer-1 (Eth-1) and 1.2 μM calcein AM (Molecular Probes). For each slide, the number of injured cells was recorded as the average number of Eth-1 stained nuclei counted in fluorescence microscopic images.

Fluid Dynamic Simulations

The bubble and parallel-plate flow chamber was modeled as a semi-infinite bubble progressing within a Hele-Shaw cell. In this model the walls were separated by a distance $2H$, with the semi-infinite bubble progressing in the x-direction with tip velocity U. The surface

tension, γ, was constant. The capillary number, $Ca = \mu U/\gamma$, representing the relative importance of viscous to surface tension effects on the bubble determines the dynamic response of the system. Stokes equations, $\nabla \mathbf{P} = \mu \nabla^2 u$ and $\nabla \bullet u = 0$, were solved using the boundary element method. The interfacial stress condition applied at the air-liquid interface was $|\sigma \bullet \hat{n}| = \gamma \kappa \hat{n}$, where $\sigma = -P\mathbf{I} + \mu(\nabla u + \nabla u^T)$ was the stress tensor, $\hat{n}$ was the unit normal, and κ was the interfacial curvature. For a given Ca, the system was simulated until a steady-state meniscus had developed and the stress-field and bubble geometry were determined.

Three potentially injurious components of the stress cycle associated with bubble progression – the shear stress, the shear stress gradient, and the pressure gradient – were analyzed. Regression relationships describing the behavior of these components as a function of Ca were determined for very small Ca ($5 \times 10^{-4} \leq Ca \leq 2 \times 10^{-3}$). Additionally, the thickness of the thin film deposited by bubble progression was estimated. Dimensionless values for the experimental flow conditions were extrapolated from the regression equations and redimensionalized.

Results and Discussion

For each condition the average number of injured cells per square centimeter was measured (Table 1). The control showed few injured cells. For the saline-occluded channels, bubble progression at both velocities produced significantly increased numbers of injured cells when compared to the control. The slow velocity resulted in a 66-fold increase in the number of injured cells and the fast velocity produced a 20-fold increase. The addition of Infasurf to the occlusion fluid reduced the number of injured cells to a level similar to the control. These results support the hypotheses that mechanical stresses associated with airway reopening injure pulmonary epithelial cells and that pulmonary surfactant in the normal lung protects the epithelium from injury due to airway reopening.

The stress component that best agrees with the experimentally observed trauma is the maximal pressure gradient (Table 1). Pressure gradients create a force imbalance on the cell membrane over the length of the cell. For a low profile, predominately flat cell or region of a cell, the non-uniformly distributed load can depress region of the cell stretching the membrane. For high profile cells or regions of a cell, such as the protrusion cause by the nucleus, where the normal forces of the cell surface are nearly opposite, a pressure gradient will pinch that region. The pinching can tear the membrane at the base of the protrusion or force fluid upward rupturing the top surface of the cell.

Table 1: Measured and calculated parameter values for the experimental conditions

Fluid	Q (mL/min)	Trauma (10^3 injured cells/cm^2)	γ (dyn/cm)	U (cm/s)	Ca $\times 10^{-3}$	$(\tau_s)_{max}$ (dyn/cm^2)	$(d\tau_s/dx)_{max}$ (dyn/cm^2/μm)	$(dP/dx)_{max}$ (dyn/cm^2/μm)	f (μm)
Control		0.60 ± 0.22							
PBS	7	39.80 ± 8.76 *†	70	0.27 ± 0.01	0.0386	15.5	0.209	6.65	1.3
PBS	70	12.04 ± 5.91 *†	70	2.70 ± 0.33	0.3857	34.3	0.211	3.36	6.0
Infasurf	7	0.80 ± 0.17	25	0.27 ± 0.02	0.1080	7.9	0.075	1.75	2.6
Infasurf	70	1.03 ± 0.74	25	2.42 ± 0.26	1.0800	17.5	0.077	0.88	11.9

PBS = Phosphate Buffered Saline (with Ca^{++} and Mg^{++}), Infasurf = 1mg/mL in PBS, Q = infusion rate, γ = surface tension, U = velocity, Ca = capillary number, $(\tau_s)_{max}$ = maximum shear stress, $(d\tau_s/dx)_{max}$ = maximum shear stress gradient, $(dP/dx)_{max}$ = maximum pressure gradient, f = film thickness, Note: H = 0.085 cm, * Significantly greater than control ($p < 0.01$), † Significantly greater than Infasurf for the same velocity ($p < 0.01$)

PROTEIN VIRIAL COEFFICIENTS FROM SIZE EXCLUSION CHROMATOGRAPHY

Seth Fraden[A], Joshua Bloustine, Viatcheslav Berejnov
Martin Fisher School of Physics, Brandeis University

ABSTRACT

An improved method is presented for measuring protein virial coefficients from retention time measurements in size exclusion chromatography (SEC). Second virial coefficients for the self-interaction of lysozyme have been determined by analyzing the concentration dependence of the partition coefficient obtained from SEC studies on silica beads. Our SEC results show agreement with virial coefficients obtained by light scattering.

It is well known in the standard practice of size exclusion liquid chromatography (SEC) that the solute retention time depends sensitively on the solute's excluded volume. It has also been realized that the thermodynamic non-ideality resulting from any excluded volume leads to a *concentration* dependence of the retention time[1], and that such dependence can be utilized to quantify the second osmotic virial coefficient, B_2 by $\mathrm{Ln}\,(\frac{K_D}{K_o}) = 2B_2\frac{N_A}{M_w}C_i(1-K_D)$. Here K_D and K_0 are the SEC distribution coefficients for finite and zero concentration, respectively, M_w the solute molecular weight and N_A Avogadro's number. Second virial coefficients are often reported as $A_2 = B_2\frac{N_A}{M_w^{\ 2}}$.

Winzor et al's[1] measurements of B_2 employed frontal elution liquid chromatography. Although frontal chromatography allows one to fix the solute concentration in the column directly, it requires a large amount of protein ($\approx 2.5g$) and (prohibitively) long experiment times (≈ 2 days). We extend their method to modern SEC, which necessitates a consideration of the solute concentration in the column. This adaptation drastically reduces the amount of protein ($\approx 25mg$) and time needed (≈ 2 hours) to measure B_2 by SEC. We show that our results for B_2 from SEC compare quantitatively well to light scattering measurements, and that SEC can track the evolution of B_2 from positive to negative values.

In the above discussion the crucial parameter C_i represents the solute concentration in the *mobile* phase of the migration zone, not the *injected* concentration, C_{nj}. Therefore one must relate C_i to measurable parameters. One measures the mass of solute molecules in the migration zone (m_{zone}) by integrating the concentration as a function of time curve (the peak) over the zone width (V_{zone}). Because the fraction of molecules in the mobile phase is V_{ret}/V_{Total} one has $C_i = \frac{m_{zone}}{V_{zone}}\frac{V_{Total}}{V_{ret}}$ where V_{Total} is the total volume and V_{ret} is the protein retention time.

[A] Address: 415 South St. MS 057, Waltham, MA 02454
fraden@brandeis.edu, fax: 781.736.2915, tel: 781.736.2888

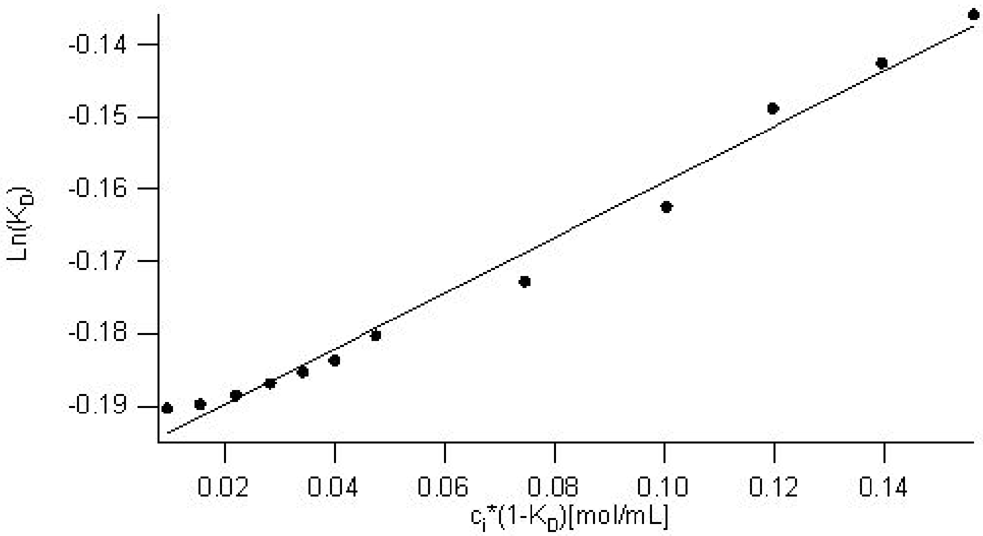

Lysozyme
Buffer: Sodium Acetate 0.05M pH 4.7
Concentration dependent distribution coefficient

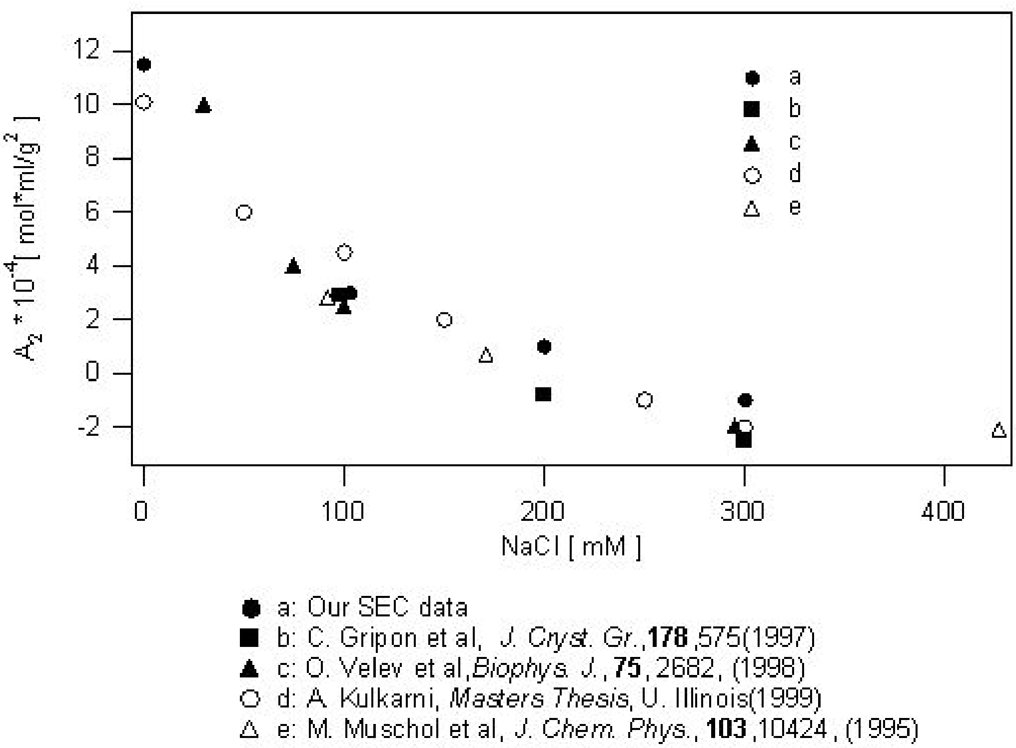

---

[1] D.J. Winzor et al, *Biophys. Chem.*, **9**,47 (1978)

MICRO-FLUID DYNAMICS IN AN EVAPORATING SESSILE DROPLET: APPLICATION TO DNA OPTICAL GENE MAPPING

Hua Hu, Lei Li, and Ronald Larson
Dept. of Chemical Engineering, Univ. of Michigan

ABSTRACT

The flow field proposed by a drying, sessile droplet has been used by Jing, et al. (1998) to stretch and adhere DNA molecules to derivatized glass substrate, as a preparation for optical gene analysis using restriction enzymes. We have carried out experimental, analytical, and numerical analysis of the flow field in an evaporating droplet, and combined this flow field with a Brownian dynamics analysis of polymer deformation to predict the conformations of DNA molecules adhered to the substrate in this flow. We have compared these predictions to experimental observations and measurements of the DNA configurations, obtaining excellent agreement. The results indicate that combined hydrodynamic/Brownian dynamic analyses can be used to design flows for micro-manipulation of DNA, for gene analysis.

The flow fields in the evaporating droplet, obtained from a finite element analysis and from an analytic lubrication analysis are similar qualitatively. However there are some quantitative differences that can be traced to the boundary condition at the air-fluid interface, which reduces to a zero axial gradient in radial velocity in the case of the lubrication approximation, but which does not quite hold in the numerical analysis, due to the radial gradient in evaporation rate. The analytic flow field is then combined with a Brownian dynamics method to predict the stretching and deposition of DNA molecules to a glass substrate treated with 3-aminopropyltriethoxysilane (APTES) to induce irreversible adsorption of DNA In the Brownian dynamics simulation, the DNA molecule is represented as a bead-spring chain, with parameters chosen from known elastic and hydrodynamic properties of lambda-phage DNA. Any bead coming into contact with the substrate due to a combination of flow and Brownian motion is "frozen" to the surface.

An image of DNA molecules adhered to the treated glass substrate is shown in Fig. 1. Fig. 2 analyzes the distribution of stretch length and orientation angle, relative to the radial flow direction, from many such images, and compares the results to the predictions of the Brownian dynamics simulations. The agreement is very good, indicating that analysis of DNA molecular dynamics and surface adhesion in complex flows is now possible. We are extending this work to flow in a channel, and to electrostatic manipulations of DNA molecules, with the aim of developing tools for manipulation of DNA single molecules in microfabricated devices. Such devices are of growing interest in the biomedical community and for space applications, including space flight.

Reference: Jing J., J. Reed, J. Huang, X. Hu, C. V. Clarke, J. Edington, D. Housman, T. S. Anantharaman, E.J. Huff, B. Mishra, B. Porter, A. Shenker, E. Wolfson, C. Hiort, R. Kantor, C.

Aston, D. C. Schwartz, "Automated high resolution optical mapping using arrayed, fluid-fixed DNA molecules," Proc. Natl. Acad. Sci. USA **95**, 8046-8051 (1998).

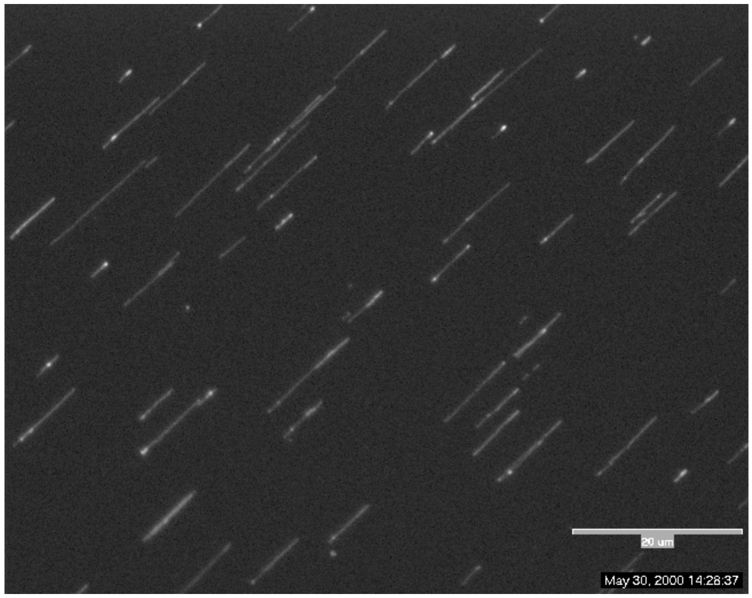

Fig. 1. Image of DNA adhered to substrate following drying droplet flow

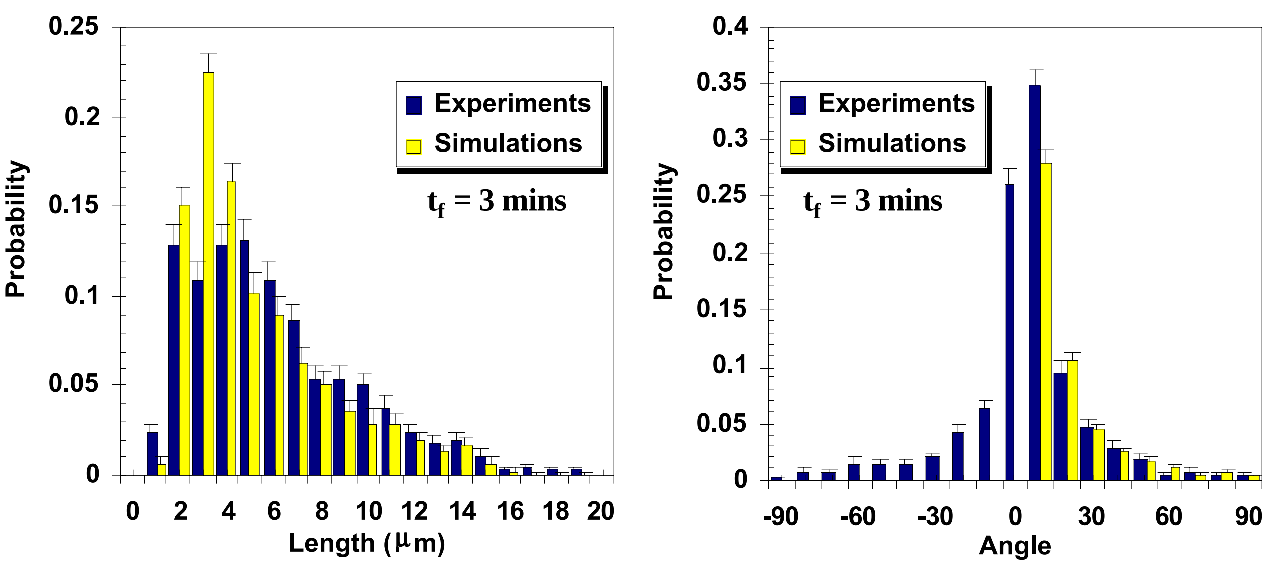

Fig. 2 Distribution of stretch and of orientation of lambda-phage DNA molecules resulting from drying droplet flow, under "fast" drying conditions

NON-INVASIVE HEALTH DIAGNOSTICS USING EYE AS A "WINDOW TO THE BODY"

RAFAT R. ANSARI
NASA Glenn Research Center
Mail Stop 333-1, 21000 Brookpark Road
Cleveland, OH 44135
Tel: 216-433-5008, Fax: 216-977-7138, E-mail: rafat.r.ansari@grc.nasa.gov

ABSTRACT

As a "window to the body", the eye offers the opportunity to use light in various forms to detect ocular and systemic abnormalities long before clinical symptoms appear and help develop preventative/therapeutic countermeasures early. The effects of space travel on human body are similar to those of normal aging. For example, radiation exposure in space could lead to formation of cataracts and cancer by damaging the DNA and causing gene mutation. Additionally, the zero-gravity environment causes fluid shifts in the upper extremities of the body and changes the way blood flows and organ system performs. Here on Earth, cataract, age-related macular degeneration (AMD), diabetic retinopathy (DR), and glaucoma are major eye diseases and are expected to double in next two decades. To detect, prevent, and treat untoward effects of prolonged space travel in real-time requires the development of non-invasive diagnostic technologies that are compact and powerful. We are developing fiber-optic sensors to evaluate the ocular tissues in health, aging, and disease employing the techniques of dynamic light scattering (cataract, uveitis, Alzheimer's, glaucoma, DR, radiation damage, refractive surgery outcomes), auto-fluorescence (aging, DR), laser-Doppler flowmetry (choroidal blood flow), Raman spectroscopy (AMD), polarimetry (diabetes), and retinal oximetry (occult blood loss). The non-invasive feature of these technologies integrated in a head-mounted/goggles-like device permits frequent repetition of tests, enabling evaluation of the results to therapy that may ultimately be useful in various telemedicine applications on Earth and in space.
Acknowledgements: NASA-NIH and NASA-FDA Interagency Agreements, and John Glenn Biomedical Engineering Consortium. Collaborators: Manuel B. Datiles, MD and J. Samuel Zigler, Ph.D., (NEI/NIH), Michelle M. Chenault, Ph.D., (FDA), J. Sebag, MD (Doheny Eye Institute), Luigi Rovati, Ph.D., (University of Modena, Italy), Martial Geiser (Institute for Research in Ophthalmology, Switzerland), Marco F. Cabrera, Ph.D., (CWRU), Fabrice Moret (NCMR/HEVs), and James F. King (QSS/NASA).

Session 6:
Dynamics and Instabilities

CONTAINERLESS RIPPLE TURBULENCE

Seth Putterman and William Wright
Physics Department, University of California Los Angeles CA 90095

Walter Duval and Charles Panzarella
NASA Glenn Research Center, Cleveland OH

ABSTRACT

One of the longest standing unsolved problems in physics relates to the behavior of fluids that are driven far from equilibrium such as occurs when they become turbulent due to fast flow through a grid or tidal motions. In turbulent flows the distribution of vortex energy as a function of the inverse length scale [or wavenumber 'k']of motion is proportional to $1/k^{5/3}$ which is the celebrated law of Kolmogorov. Although this law gives a good description of the average motion, fluctuations around the average are huge. This stands in contrast with thermally activated motion where large fluctuations around thermal equilibrium are highly unfavorable. The problem of turbulence is the problem of understanding why large fluctuations are so prevalent which is also called the problem of "intermittency".

Turbulence is a remarkable problem in that its solution sits simultaneously at the forefront of physics, mathematics, engineering and computer science. A recent conference [March 2002] on "Statistical Hydrodynamics" organized by the Los Alamos Laboratory Center for Nonlinear Studies brought together researchers in all of these fields. Although turbulence is generally thought to be described by the Navier-Stokes Equations of fluid mechanics the solution as well as its existence has eluded researchers for over 100 years. In fact proof of the existence of such a solution qualifies for a 1M$ millennium prize.

As part of our NASA funded research we have proposed building a bridge between vortex turbulence and wave turbulence. The latter occurs when high amplitude waves of various wavelengths are allowed to mutually interact in a fluid. In particular we have proposed measuring the interaction of ripples [capillary waves] that run around on the surface of a fluid sphere suspended in a microgravity environment.

The problem of ripple turbulence poses similar mathematical challenges to the problem of vortex turbulence. The waves can have a high amplitude and a strong nonlinear interaction. Furthermore, the steady state distribution of energy again follows a Kolmogorov scaling law; in this case the ripple energy is distributed according to $1/k^{7/4}$. Again, in parallel with vortex turbulence ripple turbulence exhibits intermittency [Wright et al Science 278, 1609 (97)].

The problem of ripple turbulence presents an experimental opportunity to generate data in a controlled, benchmarked system. In particular the surface of a sphere is an ideal environment to study ripple turbulence. Waves run around the sphere and interact with each other, and the effect of walls is eliminated. In microgravity this state can be realized for over 2 decades of frequency.

Wave turbulence is a physically relevant problem in its own right. It has been studied on the surface of liquid hydrogen [Brazhnikov et al] and its application to Alfven waves in space is a source of debate.[P. Goldreich]. Of course, application of wave

turbulence perspectives to ocean waves has been a major success of V. E. Zakharov. [Kolmogorov Spectra of Turbulence, Springer, Berlin 1992].

The experiment which we plan to run in microgravity is conceptually straightforward. Ripples are excited on the surface of a spherical drop of fluid and then their amplitude is recorded with appropriate photography. A key challenge is posed by the need to stably position a 10cm diameter sphere of water in microgravity. Two methods are being developed. Orbitec is using controlled puffs of air from at least 6 independent directions to provided the positioning force. This approach has actually succeeded to position and stabilize a 4cm sphere during a KC 135 segment. Guigne International is using the radiation pressure of high frequency sound. These transducers have been organized into a device in the shape of a dodecahedron. This apparatus 'SPACE DRUMS' has already been approved for use for combustion synthesis experiments on the International Space Station.

A key opportunity presented by the ripple turbulence data is its use in driving the development of codes to simulate its properties. A head start on this aspect of the project is being developed at NASA Glenn Research Center.

Phase separation, density fluctuations, and boiling near the liquid-gas critical point

John Hegseth, Ana Oprisan, and Arun Roy
Department of Physics, University of New Orleans, New Orleans, LA 70148
Telephone: 504-280-6706, FAX: 504-280-6048, E-mail: jhegseth@uno.edu

Vadim S. Nikolayev, Carole Lecoutre, D. Beysens, and Y. Garrabos
CEA and CNRS, ICMCB, Université de Bordeaux

ABSTRACT

A pure liquid-gas mixture is one of the simplest examples of a soft-matter system. In fact, when co-existing gas and liquid phases of pure fluid are heated to their critical point, large-scale density fluctuations make the fluid extremely compressible (to external forces), expandable (to heating), slows the diffusive transport, and decreases the surface tension. In principle these properties and others either diverge to infinity or converge to zero at the critical temperature. These properties lead to some very unusual behavior: large density gradients at the laboratory scale, a large mechanical response to heating, and perfect wetting of a solid wall by the liquid phase (zero contact-angle). We have further simplified this system by performing experiments in weightlessness (Mir spaces station). By controlling the fluid's temperature, these properties may be varied over large ranges in a single sample. When the fluid is driven out of equilibrium by a fast temperature quench from the single-phase (supercritical fluid) state into the two-phase state, we have observed universal growth laws of minority domains (gas bubbles) during phase separation. Prior to this quench we have also observed density fluctuations using optical microscopy near the critical point. When heat is applied to a liquid-gas mixture, we have observed a spectacular spreading of a gas bubble along a hot solid wall as well as gas bubble over-heating (where the interior of a gas bubble gains a higher temperature than the heating wall). Although this gas phase over-heating appears to violate the second law, it is really a transient our-of-equilibrium effect. Inside of these unusual bubbles we also have observed unusually large variations in liquid wetting film thickness that often appear to evolve into spreading contact lines on the sapphire wall when heat is applied.

We have observed coarsening and growth of minority domains (gas bubbles) in SF_6 near its liquid-gas critical point. Phase separation in our constant density samples was induced in our constant volume cells by temperature quenches in weightless conditions (Mir station), while visualizing density fluctuations and domain growth using optical microscopy. The optics of the formation of the density fluctuation images will be discussed. The well-known statistics of the density fluctuations provide natural space and time scales for domain growth. Previous experiments have documented two morphologies and two associated growth laws with a sharp transition between the two. This transition appears to be controlled by the minority volume fraction. While the slow, $t^{1/3}$ growth, for disconnected morphologies, is understood as a diffusion process, the fast growth, t^1 growth, for connected domains, is less well-understood. We will discuss several shallow quenching sequences at the critical density (±0.02%) and slightly off-critical where we have observed fast linear growth.

When a coexisting liquid-gas mixture of a single species fluid is heated into a single phase a complex transport and interfacial processes occurs in the two-phase fluid. This process, that is often called boiling, is important in many applications because of the large heat transfer that it facilitates. In the weightless environment of an orbiting space craft, the buoyancy force and all of the complications it causes is negligable. The perfect wetting by the liquid phase (zero contact-angle) near the critical temperature, T_C, will be replaced by liquid-gas-solid contact lines with a zero degree contact angle when a wetted wall dries from evaporation.

In this presentation, we also report on the behavior of a single bubble in a thin constant mass cell in several experiments where the cells are filled with fluid very close to the liquid-gas critical density and heated. These thin cells produce a considerable constraint on the bubble and allow the entire bubble to be observed as the heat is applied. Our experiments have recorded two types of behavior depending on the initial conditions and the constraints on the bubble. The first behavior is characterized by vigorous gas spreading over much of the heating copper side-wall near T_C, when the system's temperature, T, is increased at a constant rate past T_C. This behavior occurs when the bubble is free to move in the cell and is initially in contact with the highly conductive side-wall. We identify this behavior with the boiling crisis near the critical point, i.e., a reaction of the fluid to the heating surface where the heating surface becomes covered with gas. A likely mechanism for this spreading is revealed near the critical point by an analysis of the critical anomalies: the vapor recoil from evaporating fluid pushes the fluid near the liquid-gas-solid contact line at the edge of the bubble.

No gas bubble spreading is observed in the second type of behavior that occurs when a piston and temperature sensors, present inside of the cell, prevent the bubble from moving and touching the side-wall. This case did reveal that as the liquid-gas mixture is heated toward the critical point, gas phase over-heating is observed. Previously this gas phase over-heating was only observed when the temperature was quenched in a thick cell. Here, we have observed overheating in a thin cell when the temperature is ramped. More interestingly, this over-heating effect persists and increases when the temperature is ramped into the single-phase supercritical fluid state, where the liquid becomes high-density fluid and the gas become low-density fluid.

In both cases large distortions in the liquid wetting layer inside the bubble is also observed at lower T. The film distortions were sometimes continuous, appearing to be similar to a refracting (converging) lens. By ray tracing the shadow of a defocused grid through the cell and the film, we modeled this film shape as an ellipse. This showed that these films were much thicker than films typically found on Earth, by more than an order of magnitude. This large film thickness allows an explanation of the over-heating in this thin cell that is consistent with a previous explanation for thick cells. Other film structures appear as lines of almost discontinuous film thickness changes that propagate away from the bubble's edge into the bubble. We conclude that these are spreading contact lines. These spreading contact lines are usually observed near the region where the bubble touches the copper side-wall and they are also highly correlated with cell heating events. The zero contact-angle for these contact lines implies that an external stress is applied to create a large curvature change at these lines. Once again the vapor-recoil force is a good candidate for the cause of this additional stress.

STRATIFIED TAYLOR-COUETTE FLOW WITH RADIAL GRAVITY

John Hart, Dan Ohlsen
Program in Atmospheric and Oceanic Sciences, Univeirsity of Colorado, Boulder, CO 80309

Randall P. Tagg
Department of Physics, University of Colorado, Denver, CO 80217

Patrick D. Weidman
Department of Mechanical Engineering, University of Colorado, Boulder, CO 80309

ABSTRACT

An experiment to study stratified Taylor-Couette flow with radial, or cross-stream, gravity is being developed. The experiment uses ferromagnetic fluid (ferrofluid) and a unique stacked-magnet configuration to generate a strong (3 to 10 g) radial gravity field. In the microgravity environment this experiment will permit laboratory study of a wide range of stability, transitional, and turbulent flow problems in a simple re-entrant geometry. Important fundamental situations that can be implemented include thermal convection in a "vertical" shear flow, stably stratified shear flows, and stably or unstably stratified centrifugal (spiral) instabilities. Figure 1 (below) shows a sketch of the experiment, which also illustrates the basic-state flows expected in the terrestrial laboratory.

The linear stability problem for an axially and azimuthally invariant mean flow consisting of the exact analytically determined fields

$$\mathbf{V} = [\,0, V_m(r), W_m(r)\,],\quad T = T_m(r)$$

has been solved numerically for the terrestrial case with both g_e and $g_m(r)$ present, and for the microgravity case where g_e is negligible. Modifications to the usual Taylor-Couette modes are found, along with new disturbance modes arising from the radial magnetic gravity.

In order to carry out meaningful experiments with this system, an effective visualization method for the opaque ferrofluid is required. Ultrasonic Doppler Velocimetry has been used to measure the velocity distributions in ferrofluid for a simple mechanically forced un-heated configuration. The experimental results are in good agreement with direct numerical simulations of the axisymmetric (2D) steady flow, suggesting that UDV is a very promising tool for studying circulations in this medium.

Other issues, such as determining the significance of non-Newtonian fluid effects, and predicting the nature of motions driven directly by magnet field imperfections (in height), have been studied theoretically, and will be summarized as time permits.

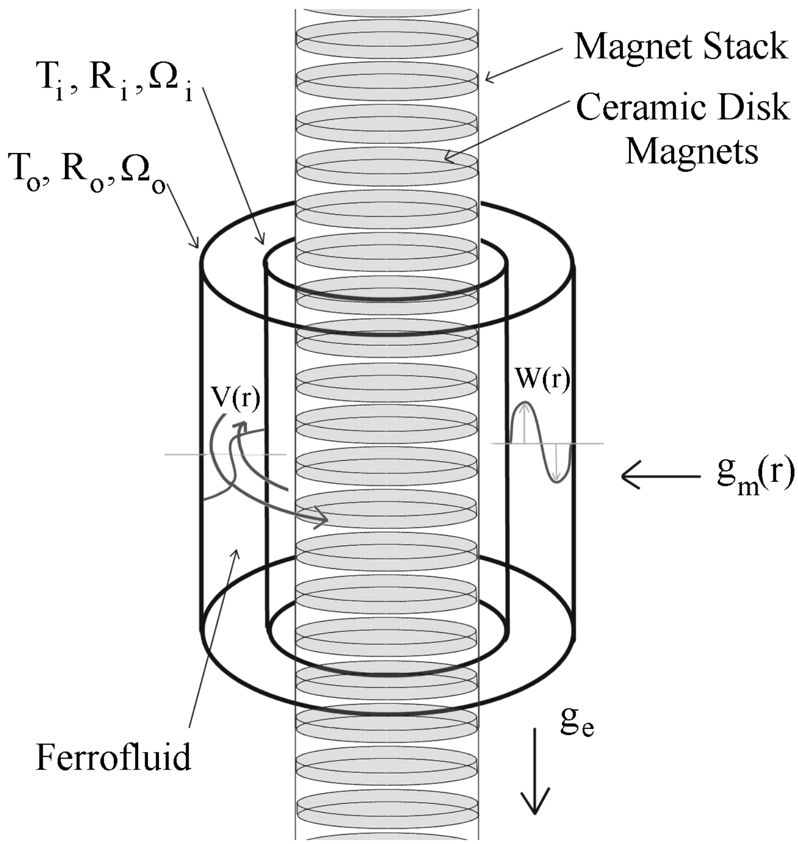

Figure 1. Stratified Taylor-Couette Flow. Radial gravity is achieved from the magnetization of the ferrofluid by the magnetic field created by a stack of high intensity disk magnets. The absolute magnitude of the **B**-field is almost exactly uniform in axial height z, and independent of azimuthal angle θ. This leads to a strong inwards-directed magnetic gravity $g_m(r)$. Flows are driven by differential rotation of the inner and outer walls that turn at rates Ω_i and Ω_o respectively, and by imposing either positive or negative radial thermal gradients across the annular gap via thermal baths at temperatures T_i and T_o.

PI: John E. Hart, Program in Atmospheric and Oceanic Sciences, Stadium 255UCB, University of Colorado, Boulder, CO 80309. hart@tack.colorado.edu 303-492-3524 (fax) 303-492-4248 (Lab).

AN EXPERIMENTAL INVESTIGATION OF INCOMPRESSIBLE RICHTMYER-MESHKOV INSTABILITY

J. W. Jacobs[†]
University of Arizona

C. E. Niederhaus
NASA Glenn Research Center

ABSTRACT

Richtmyer-Meshkov (RM) instability occurs when two different density fluids are impulsively accelerated in the direction normal to their nearly planar interface. The instability causes small perturbations on the interface to grow and eventually become a turbulent flow. It is closely related to Rayleigh-Taylor instability, which is the instability of a planar interface undergoing constant acceleration, such as caused by the suspension of a heavy fluid over a lighter one in the earth's gravitational field. Like the well-known Kelvin-Helmholtz instability, RM instability is a fundamental hydrodynamic instability which exhibits many of the nonlinear complexities that transform simple initial conditions into a complex turbulent flow. Furthermore, the simplicity of RM instability (in that it requires very few defining parameters), and the fact that it can be generated in a closed container, makes it an excellent test bed to study nonlinear stability theory as well as turbulent transport in a heterogeneous system. However, the fact that RM instability involves fluids of unequal densities which experience negligible gravitational force, except during the impulsive acceleration, requires RM instability experiments to be carried out under conditions of microgravity.

This experimental study investigates the instability of an interface between incompressible, miscible liquids with an initial sinusoidal perturbation. The impulsive acceleration is generated by bouncing a rectangular tank containing two different density liquids off a retractable vertical spring. The initial perturbation is produced prior to release by oscillating the tank in the horizontal direction to produce a standing wave. The instability evolves in microgravity as the tank travels up and then down the vertical rails of a drop tower until hitting a shock absorber at the bottom. Planar Laser Induced Fluorescence (PLIF) is employed to visualize the flow. PLIF images are captured by a video camera that travels with the tank. Figure 1 is as sequence of images showing the development of the instability from the initial sinusoidal disturbance far into the nonlinear regime which is characterized by the appearance of mushroom structures resulting from the coalescence of baroclinic vorticity produced by the impulsive acceleration. At later times in this sequence the vortex cores are observed to become unstable showing the beginnings of the transition to turbulence in this flow. The amplitude of the growing disturbance after the impulsive acceleration is measured and found to agree well with theoretical predictions. The effects of Reynolds number (based on circulation) on the development of the vortices and the transition to turbulence are also determined.

[†] Address: Department of Aerospace and Mechanical Engineering, University of Arizona, Tucson, AZ 85721; e-mail: jwjacobs@u.arizona.edu; phone: (520) 621-8459; fax: (520) 621-8191.

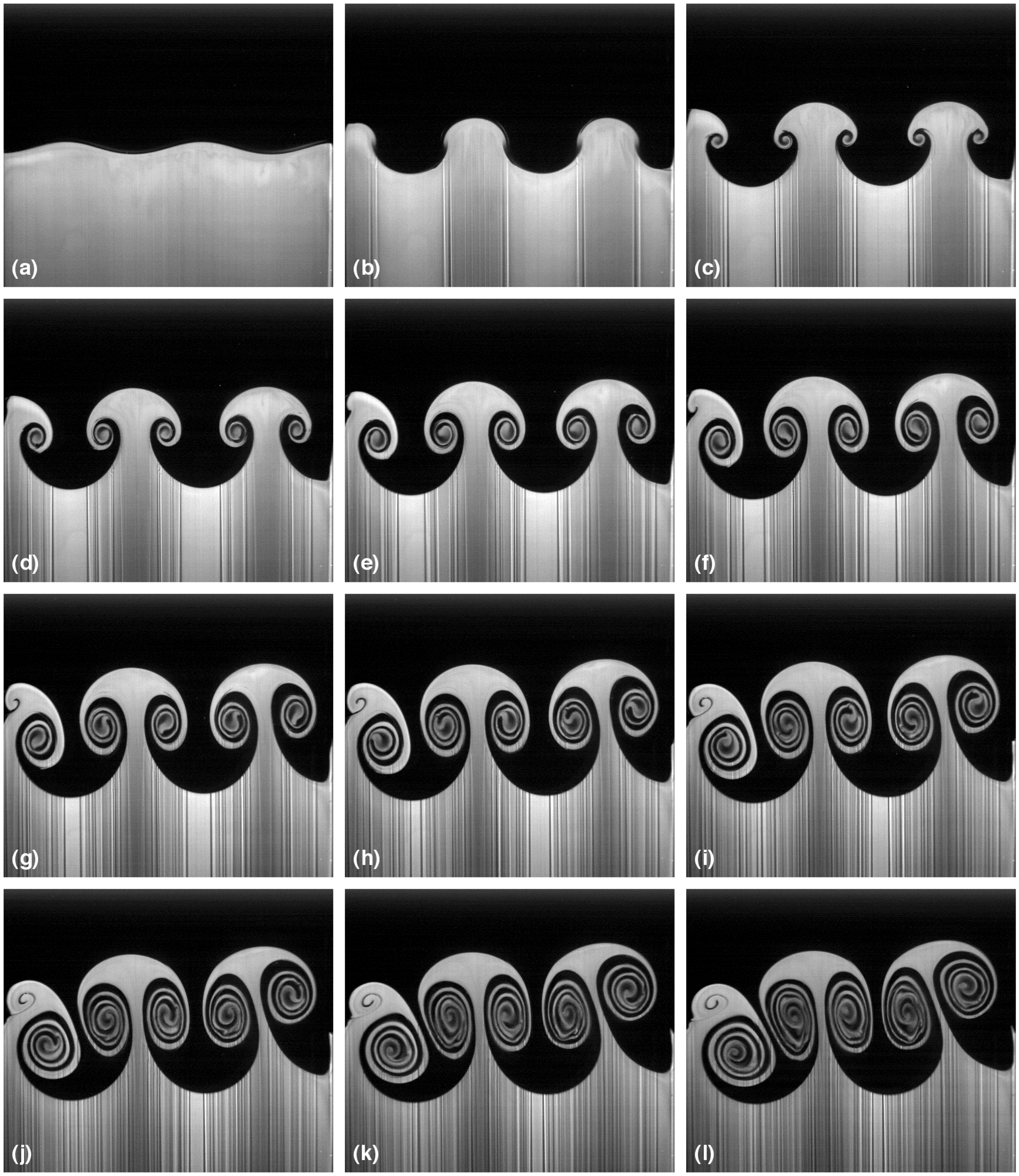

Figure 1. A sequence of images from an experiment showing the development of the RM instability. The initial sinusodial perturbation inverts (due to the acceleration direction) and then evolves into a mushroom pattern that is nearly symmetrical due to the moderate density difference (Atwood number of 0.15). At late times and high Reynolds number (2400 for this experiment based on circulation), an instability develops in the vortex cores, as can be seen beginning in (i). Times relative to the midpoint of spring impact are (a) –28 ms, (b) 88 ms, (c) 172 ms, (d) 255 ms, (e) 339 ms, (f) 422 ms, (g) 505 ms, (h) 589 ms, (i) 672 ms, (j) 756 ms, (k) 839 ms, and (l) 906 ms.

THE USE OF PULSATILE FLOW TO SEPARATE SPECIES

R. Narayanan, Professor
Department of Chemical Engineering
University of Florida

Aaron M. Thomas, Assistant Professor
Department of Chemical Engineering
University of Idaho

ABSTRACT

The removal of carbon dioxide from air is important in producing a habitable environment for the self-supporting space stations of the space program. Pulsatile flow is a novel way to help in the partial separation of different species from air by using a purely mechanical method. The advantage of this is that no chemicals are needed. Pulsatile flow also has the advantage that it can handle large volumes. While it is not expected that this process will replace existing methods of separation, it can surely be used as a means to assist in the overall separation process, possibly as a precursor to conventional methods. This work specifically focuses on the physics of pulsatile flow and its effect on the mass transfer of species and the separation that can be achieved. From the theoretical model that predicts the mass transfer and separation of species, we provide a physical explanation of the phenomena predicted by the models. If two dilute species are present in a carrier, the mass transfer of the faster diffusing species may be higher, lower, or the same as the slow diffusing species. This depends on the time constants associated with the system and the ability of a species to remain in the fast moving portion of the flow field. The difference in the mass transfer of each species can lead to a separation that can be used in a number of processes including the removal of carbon dioxide from the air. This phenomenon is modeled in an open tube geometry and in the annular space between two concentric cylinders. Further, in annular pulsatile flow, the effect of the inner cylinder being off center from the outer cylinder on the mass transfer and separation is also analyzed. Experiments were also conducted to verify the validity of the models and the viability of pulsatile flows as a separations procedure.

PHYSICS OF THE FLUID FLOW--MASS TRANSPORT INTERACTION

Picture a tube with a gas occupying a reservoir at each end. One of the reservoirs can be considered to hold a pure gas called the carrier while the other is a mixture of the carrier gas with a dilute amount of a single species as shown in Fig. 1 According to Fick’s law for dilute species, the non-interacting particles will move from the mixture to the carrier gas from high to low concentration in a process involving pure molecular diffusion. Now, suppose that the fluid in the tube oscillates with no net flow from one reservoir to the other. This, for example, can be achieved with a piston. In the first half of a cycle of the piston stroke, a nearly parabolic flow profile is produced in the tube, provided that the frequency is not large. This in turn causes radial concentration gradients. The dilute species then diffuses from the core of the tube to the boundary. In the second half of a cycle, the flow profile is reversed and the species moves from the boundary to the core where the concentration of the species is small compared to itw value at the boundary. In the first half of the next cycle of the piston stroke, the species that is in the fast moving core of the tube is convected down the tube and again radially diffuses

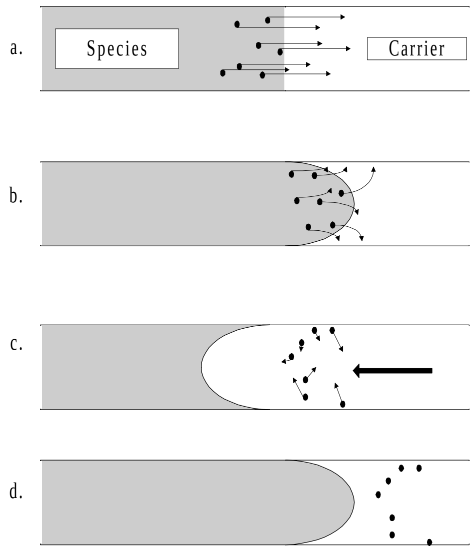

Figure 1. Dispersion mechanism for dilute species in pulsatile flow.

towards the wall of the tube. The species thus proceeds to move in this zigzag fashion down the tube giving a higher transport of it than by pure molecular diffusion, yet with no net flow between the two reservoirs. If another non-interacting dilute species were added to the mixture, the time constants of the system become very important due to the differing diffusion coefficients of the species, the frequency of oscillation, and the kinematic viscosity of the fluid. These different time constants can give rise to a separation of species due to the periodic flow. It is the relationship of the different time constants that govern the mass transfer for each species as well as an analysis of the mass transfer and separation of species for different geometries that are the focus of this research.

References:

a) Aaron M. Thomas, and R. Narayanan, Periodic flow and its effects on the mass transfer of a system and separation of species, Physics of Fluids, Vol 13, p 859, (2001.)

b) Thomas, A and Narayanan, R., " The Mechanism for Enhanced Mass Transfer in Oscillatory Flow- Comparison Between Wall Driven and Pressure Driven Flows", in press , Int. J. Heat and Mass Transfer, (2002)

c) Thomas, A. and Narayanan R., " The use of pulsatile flow to separate species", in press N.Y. Acad. Sciences (2002)

PARTICLE PROXIMITY SENSORS: A NOVEL TECHNIQUE FOR VISUALIZING PARTICLE DEPOSITION IN SUSPENSION FLOWS

M. Yoda, B. C. Bailey and U. C. Andresen
G. Woodruff School of Mechanical Engineering, Georgia Institute of Technology

ABSTRACT
Efficient fluid reclamation is a critical technology for manned space exploration. Centrifugal filtration, where non-colloidal particles are deposited on filter fibers due to inertial impaction or direct interception, is a promising candidate for mechanical separation in variable gravity environments. Understanding how fluid inertia characterized by shear-based Reynolds number affects deposition is therefore critical in designing fluid reclamation systems for microgravity environments.

This work will develop "particle proximity sensors," or non-intrusive optical diagnostic techniques for directly visualizing where and when non-colloidal particles deposit upon, or contact, solid surfaces. Essentially, any particle near the surface will scatter light at a different wavelength from that scattered by particles in the bulk suspension. The particles next to the surface can then be easily isolated using a wavelength filter. The technique exploits the pH sensitivity of fluorophores and uses an applied electric potential to create a pH gradient next to the surface of interest.

The particle proximity sensors require aqueous chemistries. We have therefore developed and characterized a new *aqueous* model suspension system of polymethyl methacrylate (PMMA) particles suspended in a ternary mixture of the salt ammonium thiocyanate (NH_4SCN), water and glycerin. The model suspension has a refractive index n = 1.4867, a density ρ = 1.19 g/cm^3, a viscosity μ = 4.99 cP at 22°C—giving a kinematic viscous four times that of water—and a pH of 4.5. Transmission measurements using both polydisperse and nearly monodisperse PMMA particles (diameters ranging from 106–212 μm and 75–90 μm, respectively) show that a 5% volume fraction suspension has an optical transmission through 1 cm of suspension that is 80% of that for the same solution without particles at 22.5°C when illuminated at 488 and 514.5 nm.[1] The optical transmission of this suspension is comparable to that of a suspension system used by other researchers for laser-Doppler velocimetry studies[2]. This aqueous system is less hazardous than previous model systems based on organic solvents and halogenated hydrocarbons. It is, with its relatively low viscosity, also useful for higher Reynolds number studies, including turbulent suspension flows.

---

1 Bailey, B. C. and Yoda, M. (2001) An aqueous density- and refractive-index matched suspension system. Submitted to *Experiments in Fluids*

2 Lyon, M. K. and Leal, L. G. (1998) An experimental study of he motion of concentrated suspensions in two-dimensional channel flow. Part I. Monodisperse systems. *J. Fluid Mech.* **363**, 25–56

Fluorescein in aqueous solution fluoresces at pH values above 6. The aqueous suspension is dyed with *O*(1 μM) disodium fluorescein. A weak electric current (*O*(10 μA)) is applied across the suspension with the solid surface of interest as the cathode, creating a higher pH layer (due to depletion of protons by the cathode) next to the surface. The fluorescein then fluoresces only in this "boundary layer" region, whose thickness can be adjusted from *O*(0.1–1 mm) by adjusting the applied current. A particle illuminated by light from an argon-ion laser at 514.5 nm scatters light at 514.5 nm in the bulk fluid, and light at longer (about 520–600 nm) wavelengths in the fluorescent region next to the surface. The flow is imaged from the side or through the surface of interest using a nearly transparent layer of indium tin oxide on glass as the electrode. Preliminary experimental results characterizing the effect of a solid surface (*i.e.*, wall) at varying orientation on a single sedimenting particle will be presented using this technique.

We plan to also use particle proximity sensors to study inertial particle impaction upon a single filter fiber in centrifugal filtration, or a cylinder immersed in a simply sheared suspension. To this end, a plane Couette suspension flow facility to study simply sheared suspensions has been designed and built. Based upon a previously used apparatus for single-phase Newtonian fluid studies, the facility uses an endless belt stretched over and driven by two large rollers and a contraction at both ends of the test section to minimize end effects. The temperature-controlled suspension is confined inside the belt by a layer of heavy immiscible fluid at the bottom of the test section. Preliminary results on the rotation rate of a circular cylinder immersed in a simply sheared suspension in this new facility at various shear-based Reynolds number will be presented and compared with previous numerical and experimental results for a cylinder immersed in a single-phase fluid.

This ground-based project is a first step towards "heavy" and "light" suspension flow experiments in microgravity. Considering the current limitations of computational techniques in non-Stokesian, many-particle suspension simulations and our inability to decouple inertial and buoyancy effects upon Earth, microgravity environments present a unique opportunity to isolate and study the effects of differential particle-fluid inertia. In addition, particle proximity sensors could be a valuable diagnostic technique in studying several multiphase flow problems of importance in manned space exploration, such as dust deposition on solar arrays and seal degradation in dusty environments.

PI:	Minami Yoda
Mailing address:	School of Mechanical Engineering
	Georgia Institute of Technology
	771 Ferst Dr., NE
	Atlanta, GA 30332–0405
E-mail address:	minami.yoda@me.gatech.edu
Fax number:	(404) 894-8496
Phone number:	(404) 894-6838

Effects of Gravity Modulation on the Convective Instabilities of a Horizontal Double-Diffusive Layer

Wen-Yau Chen, Cho Lik Chan, and C. F. Chen
University of Arizona
Aerospace and Mechanical Engineering Department
Tucson, AZ 85721

ABSTRACT

Linear stability analysis of a horizontal double-diffusive layer under gravity modulation is performed. The steady part of the gravity is in the vertical direction while the oscillating part of the gravity is arbitrary. In the absence of gravity modulation, two modes of instabilities are possible, they are steady finger and oscillatory diffusive modes. The gravity modulation excites synchronous and quasi-periodic modes in the case of steady finger convection. In the oscillatory diffusive case, synchronous, quasi-periodic and subharmonic modes are found.

We consider a horizontal fluid layer of thickness D stratified by a stable constant solute gradient characterized nondimensionally by the solute Rayleigh number $R_S = g_0 \beta \Delta S D^3 / \kappa \nu$ in which $\beta = \rho^{-1} \partial\rho / \partial S$, κ and ν are thermal diffusivity and kinematic viscosity of the fluid, ΔS is the difference in solute concentration across the layer maintained constant by the rigid diffusive upper and lower boundaries, and g_0 is the steady gravity field. The lower boundary is maintained at a temperature ΔT higher than that of the upper boundary. Instability occurs when the thermal Rayleigh number $R_T = g_0 \alpha \Delta T D^3 / \kappa \nu$ in which $\alpha = -\rho^{-1} \partial\rho / \partial T$ exceeds its critical value. Under steady gravity, the instability onsets in the oscillatory mode and the oscillation frequency, σ, depends on the wave number of the perturbation. Now, if the fluid layer is subjected to gravity modulation in the form $g = g_0 \vec{k} + g_1 \cos(\Omega t) \vec{e}$. Resonance may occur when Ω is some multiple of σ. Such resonance effects are the focus of our investigation. Also $\vec{k}$ is the unit vector in the vertical direction and $\vec{e}$ is the unit vector of the oscillating gravity direction.

We investigate the linear stability of such a system under gravity modulation based on the set of equations derived by Terrones and Chen (1993). The method of analysis according to Floquet theory is carried out with a double series expansion, Galerkin and Chebyshev, as used by Chen and Chen (1999) for convection in a vertical slot under gravity modulation. Numerical results are obtained for a liquid metal with Pr = 0.01, Le = 3333, $g_1 / g_0 = 0.2$, and an initial $R_S = -3200$ [one of the examples given by Terrones and Chen (1993)]. Three modes, synchronous, quasi-periodic and subharmonic, were excited by gravity modulation. The subharmonic mode corresponds to the resonance and has the most destabilizing effect. The critical Rayleigh number versus modulation frequency for different directions of the oscillating part of the gravity is shown in Figure 1. The resonance effect is found to be increasing with angle (θ = 0 corresponds to horizontal and 90^{o} means vertical). The maximum reduction in the critical thermal Rayleigh is 86%.

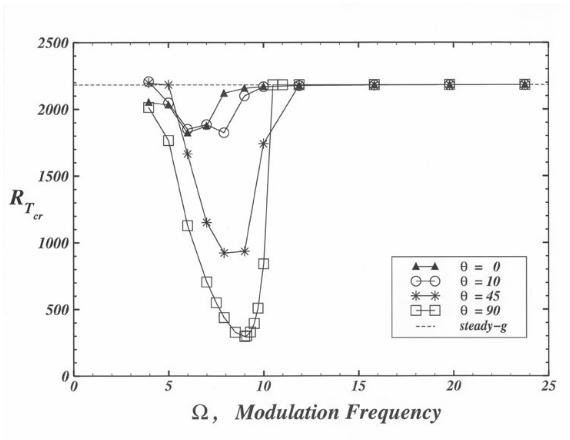

Figure 1. Resonance Curve vs Modulation Frequency

We also investigate the effect of gravity modulation on the steady finger instability case. Only synchronous and quasi-periodic modes exist. The results presented in Figure 2 corresponds to Pr = 7 Le = 100 $g_1/g_0 = 0.4$, and an initial $R_S = 100$. The gravity modulation has a small destabilizing effect on the onset of steady finger convection.

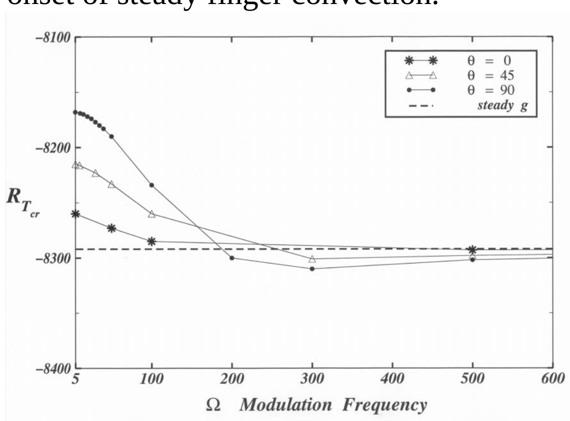

Figure 2. Critical Rayleigh Number versus Modulation Frequency

In this investigation, we found that resonance occurs only in the diffusive regime with modulation frequency being approximately twice the natural frequency. The destabilizing effect is most pronounced when the gravity modulation is in the same direction of the steady gravity vector. In the finger convection regime, gravity modulation causes slight destabilizing effect at low modulation frequencies.

References

Chen, W. Y. and Chen, F., 1999, “Effect of Gravity Modulation on the Stability of Convection in a Vertical Slot,” *J. Fluid Mech.* **345**: 327-344.

Terrones, G. and Chen, C. F., 1993, “Convective Stability of Gravity-Modulated Doubly Cross-Diffusive Fluid Layers,” *J. Fluid Mech.* **255**: 301-321.

Author Index

REPORT DOCUMENTATION PAGE

Form Approved
OMB No. 0704-0188

1. AGENCY USE ONLY (*Leave blank*)

2. REPORT DATE
August 2002

3. REPORT TYPE AND DATES COVERED
Technical Memorandum

4. TITLE AND SUBTITLE
Sixth Microgravity Fluid Physics and Transport Phenomena Conference
Abstracts

5. FUNDING NUMBERS
WU–101–58–0A–00

6. AUTHOR(S)
Bhim Singh, compiler

7. PERFORMING ORGANIZATION NAME(S) AND ADDRESS(ES)
National Aeronautics and Space Administration
John H. Glenn Research Center at Lewis Field
Cleveland, Ohio 44135–3191

8. PERFORMING ORGANIZATION REPORT NUMBER
E–13063

9. SPONSORING/MONITORING AGENCY NAME(S) AND ADDRESS(ES)
National Aeronautics and Space Administration
Washington, DC 20546–0001

10. SPONSORING/MONITORING AGENCY REPORT NUMBER
NASA TM—2002-211211

11. SUPPLEMENTARY NOTES
Abstracts of a conference cosponsored by the NASA Office of Life and Microgravity Sciences and Applications and the Fluid Physics and Transport Phenomena Discipline Working Group and hosted by NASA Glenn Research Center and the National Center for Microgravity Research on Fluids and Combustion, Cleveland, Ohio, August 14–16, 2002. Responsible person, Bhim Singh, organization code 6712, 216–433–5396.

12a. DISTRIBUTION/AVAILABILITY STATEMENT
Unclassified - Unlimited
Subject Category: 34 Distribution: Nonstandard

Available electronically at http://gltrs.grc.nasa.gov
This publication is available from the NASA Center for AeroSpace Information, 301–621–0390.

12b. DISTRIBUTION CODE

13. ABSTRACT ***(Maximum 200 words)***

The Sixth Microgravity Fluid Physics and Transport Phenomena Conference provides the scientific community the opportunity to view the current scope of the Microgravity Fluid Physics and Transport Phenomena Program, current research opportunities, and plans for the near future. The conference focuses not only on fundamental research but also on applications of this knowledge towards enabling future space exploration missions. A whole session dedicated to biological fluid physics shows increased emphasis that the program has placed on interdisciplinary research. The conference includes invited plenary talks, technical paper presentations, poster presentations, and exhibits. This TM is a compilation of abstracts of the papers and the posters presented at the conference. Web-based proceedings, including the charts used by the presenters, will be posted on the web shortly after the conference.

14. SUBJECT TERMS
Fluid dynamics; Fluid physics; Fluid mechanics; Microgravity; Reduce-gravity; Heat transfer; Multiphase flow; Complex fluids

15. NUMBER OF PAGES
298

16. PRICE CODE

17. SECURITY CLASSIFICATION OF REPORT	18. SECURITY CLASSIFICATION OF THIS PAGE	19. SECURITY CLASSIFICATION OF ABSTRACT	20. LIMITATION OF ABSTRACT
Unclassified	Unclassified	Unclassified	